Compréhansion des mécanismes de destructuration de la matière cellulosique après prétraitement et de son aptitude à libérer un substrat carbone fermentescible dans un bioprocédé

Tuan Le

THÈSE

En vue de l'obtention du

DOCTORAT DE L'UNIVERSITÉ DE TOULOUSE

Délivré par:

Université Toulouse 3 Paul Sabatier (UPS)

Cotutelle Internationale avec:

Hanoi University of Science and Technology (HUST)

École doctorale et Discipline ou spécialité:

ED SEVAB, Ingénieries microbienne et enzymatique

Présentée et soutenue par

Tuan LE

Le 10 mai 2017

Titre:

INVESTIGATION OF PHYSICAL MECHANISMS DURING DECONSTRUCTION OF PRETREATED LIGNOCELLULOSIC MATRIX AND ITS ABILITY TO LIBERATE A FERMENTABLE CARBON SUBSTRATE IN A BIO-PROCESS

JURY

KRULL Rainer (Pr.), Institute of Biochemical Engineering, GER.	Rapporteur
DE LEON Rizalinda L. (Pr.), University of the Philippines Diliman, PHI.	Rapporteur
PHI Quyet Tien (D.) Vietnam Academy of Science and Technology, IBT, VN.	Rapporteur
ROUX Gilles (Pr.), Université Paul Sabatier, FR.	Président
ANNE-ARCHARD Dominique (CR CNRS), IMFT, FR.	Examinateur
LE Thanh Ha (Pr.), School of Biotechnology and Food Technology, HUST, VN.	Examinateur
COMA Véronique (MdC), LCPO, Université de Bordeaux, FR.	Invité
RECORD Eric (DR INRA), BBF, Université de Marseille, FR.	Invité

Ecole doctorale: ED SEVAB
Unité de recherche: LISBP (INRA UMR792, CNRS UMR5504, INSA de Toulouse)

Directeur(s) de Thèse:
Dr. Luc FILLAUDEAU (DR INRA), LISBP, FR. Directeur de thèse
Prof. Kim Anh TO (Pr.), SBFT, HUST, VN. Directrice de thèse

LE Tuan

"*Investigation of physical mechanisms during deconstruction of pretreated lignocellulosic matrix and its ability to liberate a fermentable carbon substrate in a bioprocess"*

Universities and PhD Schools :

Université Paul Sabatier, Toulouse, France

ED Sevab, Ingénieries microbienne et enzymatique

Hanoi University of Science and Technology (HUST) Hà Noï, Viet Nam

School of Biotechnology and Food Technology (SBFT)

Laboratories:

LISBP, Laboratoire d'Ingenierie des Systemes Biologiques et des Procédés (INRA UMR792, CNRS UMR5504, INSA), Toulouse, France

CRDB, Center for Research and Development in Biotechnology (HUST), Hà Noï, Viet Nam

What do you think about you bring about.

- Bob Proctor -

REMERCIEMENTS

J'adresse mes plus sincères remerciements au *Laboratoire d'Ingénierie des Systèmes Biologiques et des Procédés (LISBP - Toulouse)* et au *Centre de Recherche et Développement de Biotechnologie (CRDB - Hanoi),* les deux laboratoires où ce travail a été réalisé. Je remercie egalement le *Laboratoire de Chimie des Polymères Organiques (LCPO - Bordeaux)* et *Universite Waterloo* pour les cooperations scientifiques.

Je voudrais exprimer mes gratitudes au *Bureau des Affaires Internationales* (HUST-VN) pour la bourse Techno 1, Erasmus Mundus

Je tiens a remercie Carole Molina-Jouve et Stéphane Guillouet, les chefs de l'EAD8 et Claude Maranges, le directeur de l'école doctorale SEVAB, d'avoir autorisé le déroulement de ma these au sein de l'équipe.

Je remercie chaleureusement le jury pour la participation à ma soutenance et à l'evaluation de mon travail réalisé aucours de ces trois années. Vos commentaires et suggestions ont largement contribués à la finalisation de mon manuscrit.

Je souhaite a remercie vivement M. Eric Record d'avoir participé dans tous mes deux comite de suivi de these avec ses valuables conseils scientifiques.

Mes remerciements vont egalement adressés Mme. Veronique Coma non seulement pour les analyses chimiques réalisées au sein du LCPO mais aussi pour les discussions scientifiques pendant mes trois années de thèse.

Je remercie Mme. Dominique Anne-Archard pour les aides surtout pendant ma redaction the thèse et des publications. Malgre la distance, tu es toujours disponible pour les longues discussions par email. Tes visions scientifiques, tes corrections tres detailles ont largement contribue a ce travail.

Je souhaite témoigner mes remerciements profonds à Professeur TO Kim Anh, ma directrice de thèse, qui a encadré cette recherche depuis les premiers instants. Sa pédagogie, sa vision de recherche scientifique ont largement contribué à l'évolution de ce travail.

Je tiens à remercier mon co-directeur de thèse, M. Luc Fillaudeau. Tu n'es non seulement mon encadrant scientifique mais aussi mon grand ami et mon prof de la langue francais «vivant». Sans toi, ce travail n'aurait jamais fini. Merci d'avoir partagé avec moi les moments les plus difficiles quand le reacteur n'a pas voulu tourner ou quand le logiciel a été planté pour plusieurs fois. Je garde toujours dans ma tête la phrase que tu m'avais dit l'autrefois, que les poblemes viennent seulement lorsqu'on travaille et la personne qui ne rencontre jamais les problemes c'est quelqu'un qui travaille pas.

Mes remerciements s'adressent également à tous l'equipe EAD8 pour les experiences et connaissances que vous m'avez partagés. Je tiens a remercier M. Eric Lombard qui avait assurré mon stockage des substrates extrudeés et qui avait intervenu chaque fois que j'ai rencontré une probleme technique. Je remercie Xavier Cameylere pour les discussions portant sur l'enzymo. Merci Sandrine Alfenore, tu m'as montre comment faire pour rendre le stockage de frigo en bon ordre. Merci Florence Leray pour les analyses HPLC.

Je remercie chaleureusement l'equipe de recherche du laboratoire de Fermentation (CRDB) pour leurs soutiens, leurs aides, leurs encouragements, leurs conseils et aussi pour les innombrables discussions. Merci Bach et Thao pour les repas que vous m'avez préparés lorsque j'etais en manip toute la nuit.

Enfin, je souhaite remercier sincèrement tous mes amis et ma famille, ceux qui m'ont toujours supporté.

SCIENTIFIC VALORIZATION & COMMUNICATIONS

Publications

- Le Tuan, Anne-Archard Dominique, Coma Veronique, Cameleyre Xavier; Lombard Eric, To Kim Anh, Pham Tuan Anh, Nguyen Tien Cuong, Fillaudeau Luc. Using in-situ viscosimetry and morphogranulometry to explore hydrolysis mechanisms of filter paper and pretreated sugarcane bagasse under semi-dilute suspensions. Biochemical Engineering Journal, 127:9-20, 2017. (http://dx.doi.org/10.1016/j.bej.2017.07.006 ,1369-703/ © 2017.)
- Le Tuan, Anne-Archard Dominique, Coma Véronique, Cameleyre Xavier, Lombard Eric, To Kim Anh, Pham Tuan Anh, Nguyen Tien Cuong and Fillaudeau Luc. In-situ viscometry during hydrolysis of lignocellulosic materials by single and cocktail enzymatic activities: from material impact to viscosity overshoot. 16ème Congrès de la Société Française de Génie des Procédés (SFGP), 11 - 13 July 2017, Nancy, France. Récents Progrès en Génie des Procédés, Numéro 110 – 2017 ISSN: 1775-335X; ISBN: 978-2-910239-85-5, Ed. SFGP, Paris, France, 5.27-1-5.27.8. (proceeding).
- 1 paper submitted to BEJ (under work)
- 1 paper submitted to Applied Rheology (under work)

International communications

- Fillaudeau Luc, Manon Yannick, Kraiem Hazar, Timoumi Asma, Nguyen Tien Cuong , Le Tuan, Anne-Archard Dominique, Bideaux Carine, Gorret Nathalie, Molina-Jouve Carole. Characterization of mycelial transition of Yarrowia lipolytica during oxidative cultures: comparison of optical methods and their limitation, impact of morphology on rheological behavior. 2nd Braunschweig International Symposium on Pharmaceutical Engineering Research SPhERe, TU Braunscheig, Germany, September 06 to 08th, 2017.
- Le Tuan, Anne-Archard Dominique, Coma Véronique, Cameleyre Xavier, Lombard Eric, To Kim Anh, Pham Tuan Anh, Nguyen Tien Cuong and Fillaudeau Luc. In-situ viscometry during hydrolysis of lignocellulosic materials by single and cocktail enzymatic activities: from material impact to viscosity overshoot. 16ème Congrès de la Société Française de Génie des Procédés (SFGP), 11 – 13 July 2017, Nancy, France. Récents Progrès en Génie des Procédés, Numéro 110 – 2017 ISSN: 1775-335X; ISBN: 978-2-910239-85-5, Ed. SFGP, Paris, France, 5.27-1-5.27.8. (oral presentation).
- Le Tuan, Anne-Archard Dominique, Coma Veronique, Cameleyre Xavier, Lombard Eric, To Kim Anh, Pham Tuan Anh, Nguyen Tien Cuong and Fillaudeau Luc. Using in-situ viscosimetry and morphogranulometry to explore hydrolysis mechanisms of filter paper and pretreated sugarcane bagasse under semi-dilute suspensions. Ref: 71761. Topic 6 - Applied Biotechnology (integrated in ECAB4) - Bio-based Economy: Biorefineries. 10th World Congress of Chemical Engineering, 11th European Congress of Chemical Engineering and 4th European Congress of Applied Biotechnology (WCCE10+ECCE11+ECAB4). October 1st – 5th, 2017, FIRA, Barcelona, Spain. (oral presentation+ abstract).
- Nguyen Tien Cuong, Anne-Archard Dominique, Coma Véronique, Cameleyre Xavier, Lombard Eric, To Kim Anh, Le Tuan and Fillaudeau Luc. Hydrolysis of high concentration lignocellulose suspensions with a cumulative feeding strategy: rheometry and morphogranulometry. 10th European Symposium on Biochemical Engineering Sciences and 6th International Forum on Industrial Bioprocesses ESBES-IFIBiop 2014, Lille Grand Palais, 6th to 11th September 2014, Lille, France. (oral presentation).

- Fillaudeau Luc, To Kim Anh and De Leon Rizalinda, Cameleyre Xavier, Lombard Eric, Goma Gérard, Pham Tuan Anh, Nguyen Tien Cuong, Le Tuan, Cao Xuan Bach, Le Duy Khuong, Ngo Duy Sa, Lao Marco. HTMS BioAsie project: Bioprocess intensification: challenges related to transfer limitation./Areas of Interest (AOI): Biomass and Renewable Energies. BIO/ICT-Asia Workshop, 30-31 May 2016, Kuala Lumpur, ©2016 ICT — Bio Asia 2016. (Poster presentation + abstract).
- Fillaudeau Luc, To Kim Anh and De Leon Rizalinda, Cameleyre Xavier, Lombard Eric, Goma Gérard, Pham Tuan Anh, Nguyen Tien Cuong, Le Tuan, Cao Xuan Bach, Le Duy Khuong, Ngo Duy Sa, Lao Marco. HTMS BioAsie project: Bioprocess intensification: challenges related to transfer limitation./Areas of Interest (AOI): Biomass and Renewable Energies. BIO/ICT-Asia Workshop, 30-31 May 2016, Kuala Lumpur, ©2016 ICT — Bio Asia 2016. (Poster presentation + abstract).
- Timoumi Asma, Nguyen Tien Cuong, Le Tuan, Anne-Archard Dominique, Bideaux Carine, Cameleyre Xavier, Lombard Eric, Molina-Jouve Carole, To Kim Anh, Gorret Nathalie and Fillaudeau Luc. Optical methods and their limitation to characterize the morphology and granulometry of complex shape biological materials. Journées Internationales de Biotechnologie 2016 (JIB 2016), – Port El Kantaoui, Sousse, Tunisie – 18 to 22 December 2016 Session: Biotechnologie Industrielle (BIO5; BIO21-23) (Oral presentation by L. Fillaudeau)

Communications

- Le Tuan, To Kim Anh, Fillaudeau Luc. Investigation of physical mechanisms during deconstruction of pretreated lignocellulosic matrices. Workshop 2017 of the young scientists in Environment Research Faculty of Environment (FOU), Halong University – 23rd February 2017. (Oral presentation)
- Le Tuan, To Kim Anh, Fillaudeau Luc. Investigation of physical mechanisms during deconstruction of pretreated ligno-cellulosic matrixes: from pure enzymatic activity to cocktail (Presentation 8). Bioprocess intensification: challenges related to transfer limitation. 2nd workshop at CRDB / SBFT-HUST (Hanoi, VN), 26-30th June 2016.
- Fillaudeau Luc, Nguyen Tien Cuong and Le Tuan. Hydrolysis of pretreated lignocellulosic matrixes: focus on physical insight. HTMS BioAsie project. Bioprocess intensification: challenges related to transfer limitation 1st workshop at LISBP (Toulouse, FR), 23-26th June 2015, Toulouse, France.
- Fillaudeau Luc, Nguyen Tien Cuong and Le Tuan. Transfers limitation in bioprocess: Why physical approaches have some meaningful effect for white biotechnology development? Bio Asie frame-work Meeting at HUST – SBFT, Hà Nôi, Viet Nam – 07 to 9th April 2015. (oral presentations).

Presentation issued from HTMS BioAsie network can be downloaded from http://bioasie.hust.edu.vn/en/events/workshop-seminar/symposium

FINANCIAL ACKNOWLEDGEMENTS

This work was supported by TECHNO 1 & 2 – Erasmus Mundus Program (European Commission, project managed by UPS - Toulouse) and HTMS BioAsie project (funded by Ministry of Foreign Affairs and International Development, MAEDI, BIO-Asie program, N° 34082NF). It participated in the ANR Grant ProBio3-Investissement d'Avenir under the contract number ANR-11-BTBR-0003.

WORKING SCHEDULE

Period	Laboratory	Actions	Funding
02/2014 – 07/2015	LISBP, Toulouse, France	Inscription ED SEVAB and HUST (sandwich) Bibliographic analysis and experiments 1st thesis committee (Nov 2014)	Techno 2, Erasmus Mundus
08/2015 – 01/2016	CRDB, HUST, Hanoi, Vietnam	2nd thesis committee (Oct 2015) Data treatment Oral presentation, 1st Bioasie-HTMS workshop	HUST
02/2016 – 06/2016	LISBP, Toulouse, France	Oral presentation, 2nd Bioasie-HTMS workshop. Experiments, data analysis.	BioAsie-HTMS
07/2016 - present	CRDB, HUST, Hanoi, Vietnam	Data treatment and thesis writing. Communications: scientific articles and international congress. Thesis defense 10/05/2017	BioAsie-HTMS

ABSTRACT

Lignocellulosic biomass consists of several agriculture and industrial by-products that can be used as raw material for several bioprocesses to obtain range of products. Among lignocellulosic sources, the pulp & paper industry is appropriated for modern bio-refining thank to pulp with low lignin content and free of inhibitory compounds. Besides, sugarcane bagasse is a very promising feedstock because of its simple chemical composition and its abundancy especially in tropical countries. In the bioconversion of lignocellulose, enzymatic hydrolysis is a crucial step that allows the transformation of cellulosic and hemicellulosic fibers into fermentable carbon sources. The lack of knowledge about physical limitations and hydrolysis mechanisms, especially at high dry matter content, stands as the main barrier which forbids the scale-up of bio-refinery processes. Thus, the efficient and sustainable use of lignocellulosic resources is currently a major challenge and need to be investigated.

In this context, this PhD focused on the enzymatic hydrolysis of lignocellulose by both physical and biochemical approaches. The strategy consisted in carrying out and in analyzing the hydrolysis reactions under different operating conditions with semi-dilute suspensions. Then, obtained results were used to develop a hydrolysis strategy for concentrated suspensions. Different methodologies, *in-* and *ex-situ* analyses, were implemented and provided complementary results. From physical approach, analyses consisted in rheological behavior of suspensions as well as the morpho-granulometry of particles. The study was carried out on a reference substrate, Whatman paper, and on two industrial substrates, paper pulp and sugarcane bagasse. The strategy aimed to investigate different stakes: (i) evolution of rheological behaviors and the morphological properties of suspensions, (ii) hydrolysis mechanisms during the degradation of substrates, (iii) impact of substrate composition and structure on solubilization and hydrolysis kinetics, (iv) quantification of the contribution of single enzyme and enzyme mixture activities by multi-scale physical approaches and (v) control and optimization of feeding parameters for fed-batch process in order to access to concentrated suspension.

Chapters 1 and 2 of this document are devoted to a research bibliographic and presentation of materials and methods. The third chapter presents obtained results and discussion in three sections. The first one is a study of the properties of different enzymes and substrates, in particular, the determination of semi-dilute and concentrated regime. Subsequently the enzymatic hydrolysis at semi-dilute regime is presented to highlight the hydrolysis mechanisms (fragmentation, solubilization, solvation and agglomerate separation) in relationship with enzyme mixtures and dosages. Finally, results in concentrated regime are discussed in the final section. A fed-batch strategy is proposed to hydrolyze real lignocellulosic substrates (paper pulp, sugarcane bagasse) at high dry matter content. Chapter 4 presents the conclusion and perspectives of this work. The main results are:

- Characterization of rheological behaviors and morpho-granulometric properties of lignocellulosic substrates and suspensions. The modeling of suspension viscosity as a function of shear-rate and concentration was performed.
- Roles of single enzyme activities as well as the synergy of enzyme mixtures were pointed out through physical approach.
- Impacts of particle size and shape distributions on suspension viscosity during enzymatic hydrolysis were quantified.
- Power law index was monitored revealing the evolution of rheological behavior under enzyme actions.
- Kinetics of solubilization (viscosity –time) and hydrolysis (substrate – time) were analyzed and modeled in batch and fed-batch mode.

- With SCB suspension, viscosity overtakings were observed during the first stage of hydrolysis at low enzyme/substrate ratio (≤ 10 FPU/g cellulose). Phenomenon was quantified and explained by particle size and shape analyses.
- A rational definition of the critical feeding rate for fed-batch hydrolysis was proposed. Results showed more than 65% glucose yield for fed-batch hydrolysis of SCB and PP at final concentration 100 to 140 gdm/L (10 and 14% w/v).
- Uniqueness viscosity-time (μ-t) curves were demonstrated with FP and PP at different operating conditions from batch to fed-batch, from low to high enzyme/substrate ratios.
- Substrate rheological properties showed important effect on energy consumption for mixing during fed-batch hydrolysis

Keywords: lignocellulose, sugarcane bagasse, paper pulp, enzyme cocktail, single enzyme activity, rheometry, viscometry, morphometry, granulometry, size distribution, batch, fed-batch.

RESUME

La biomasse lignocellulosique comprend les sous-produits agricoles et industriels pouvant être utilisés comme matière première dans des bioprocédés variés destinés à produire des molécules d'intérêt énergétique ou chimique. Ces ressources lignocellulosiques, peuvent notamment être fournies par l'industrie papetière qui est particulièrement adaptée pour les bio-raffineries modernes car elle est en capacité de produire en grande quantité un substrat ayant une faible teneur en lignine et sans composés inhibiteurs. La bagasse de canne à sucre est également un substrat prometteur par sa composition chimique simple et son abondance dans les pays tropicaux. Lors de l'utilisation de ces substrats, l'hydrolyse enzymatique constitue une étape cruciale permettant la transformation des fibres de cellulose en une source de carbone fermentescible. Si les aspects biochimiques de cette étape d'hydrolyse font l'objet de nombreuses recherches et de développements, les réactions sous haute teneur en matière sèche font apparaître des limitations physiques qui sont beaucoup moins étudiées et analysées mais constituent des verrous scientifiques et technologiques qui freinent actuellement l'utilisation de cette ressource abondante et durable.

Ce travail s'inscrit dans ce contexte et propose l'étude de cette étape d'hydrolyse enzymatique de la lignocellulose en s'intéressant conjointement aux aspects biochimiques et physiques de façon à aller vers une compréhension et une maîtrise des transferts (de masse, de chaleur) dans les réactions à forte concentration en substrat. La stratégie adoptée a consisté à réaliser et analyser des réactions d'hydrolyse sous différentes conditions opératoires en travaillant dans un premier temps sur des concentrations intermédiaires (suspension semi-diluée), c'est-à-dire en introduisant, mais de façon limitée, les complexités dues aux interactions entre particules/fibres de lignocellulose. Les résultats obtenus sont ensuite utilisés pour élaborer une stratégie adaptée aux fortes concentrations. Les aspects physiques analysés sont essentiellement le comportement rhéologique du milieu réactionnel ainsi que la morpho-granulométrie des objets en suspension. Différentes métrologies, tant *in-situ* que *ex-situ*, ont été mises en œuvre et apportent des résultats complémentaires. Les études ont été menées sur un substrat de référence, le papier Whatman, et deux substrats à vocation industrielle: la pâte à papier et la bagasse de canne à sucre. La stratégie d'étude porte sur les aspects suivants: (i) le suivi de l'évolution des comportements rhéologiques et des propriétés morphologiques des suspensions au cours de l'hydrolyse, (ii) l'étude des mécanismes d'hydrolyse lors de la dégradation des substrats, (iii) l'étude de l'impact de la composition et de la structure des substrats sur les cinétiques de solubilisation et d'hydrolyse, (iv) la quantification de la contribution des différentes activités enzymatiques, seules ou en mélange par une approche physique multi-échelle et (v) le contrôle et l'optimisation des conditions d'alimentation dans un procédé discontinu alimenté (fed-batch) afin d'atteindre des conditions de milieu concentré.

Les chapitres 1 et 2 de ce document sont consacrés à une étude bibliographique du sujet et à la présentation des matériels et méthodes mis en œuvre. Le troisième chapitre présente les résultats obtenus et leur analyse. Il est constitué de trois sections: tout d'abord une étude des propriétés des différents enzymes ou cocktail d'enzymes utilisés, des substrats retenus et des suspensions avec, notamment, la détermination des régimes semi-dilués et concentrés. Ensuite sont présentées et analysées les hydrolyses effectuées en milieu semi-dilué. Les mécanismes d'hydrolyse (fragmentation, solubilisation, hydratation et séparation des agglomérats) sont étudiés pour diverses concentrations et divers enzymes/cocktails. Enfin les résultats en milieu concentré sont présentés dans une dernière section. Une stratégie fed-batch est proposée afin d'hydrolyser les substrats lignocellulosiques réels (pâte à papier, bagasse) en condition de haute teneur en matière sèche. Le chapitre 4 présente la conclusion et les perspectives de ce travail.. Les principaux résultats pouvant être mis en avant sont:

- La caractérisation du comportement rhéologique et des propriétés morpho granulométrie des substrats et des suspensions lignocellulosiques. La viscosité des suspensions en fonction de la vitesse de cisaillement et de la concentration a été modélisée.
- Le rôle des activités enzymatiques individuelles et la synergie entre elles sont signalés par l'approche physique.
- L'impact de la distribution de taille et de formes des particules sont quantifiés.
- L'indice de la loi en puissance (Loi d'Ostwald–de Waele) a été étudié au cours de l'hydrolyse et démontre l'évolution des comportements rhéologiques sous les actions enzymatiques.
- Un phénomène d'«overtaking» (augmentation passagere) de la viscosité a été observé pendant la première étape d'hydrolyse à faible ratio enzyme/substrat (≤ 10 FPU/g cellulose). L'overtaking est ensuite quantifié et expliqué par les analyses de taille et de forme des particules.
- Une définition rationnelle de la vitesse d'ajout pour l'hydrolyse en mode discontinu alimenté (fed-batch) est proposé. Les résultats montrent plus de 65% de rendement glucose pour les hydrolyses (fed-batch) de la bagasse et de la pâte a papier de 100 à 140 gdm/L.
- Une courbe unique traduisant la relation entre viscosité et temps adimensionnels est obtenue quelques soient les conditions d'hydrolyse avec la bagasse et la pâte a papier.

Mot clés: lignocellulose, bagasse de canne à sucre, pâte à papier, cocktail enzymatique, activité enzymatique individuelle, rhéométrie, viscométrie, morphométrie, granulométrie, distribution de taille, discontinu (batch), discontinu alimenté (fed-batch).

TOM TẮT

Sinh khối lignocellulose bao gồm các phụ phẩm nông nghiệp và công nghiệp, có thể sử dụng làm nguyên liệu cho các quá trình sinh học để sản xuất ra nhiều sản phẩm phong phú. Trong các nguồn nguyên liệu lignocellulose, nguồn bột giấy của ngành công nghiệp giấy rất phù hợp với công nghệ biorefinery nhờ vào hàm lượng lignin thấp và không chứa chất ức chế. Đại diện cho nguồn phụ phẩm công nghiệp, bã mía là nguồn nguyên liệu triển vọng của các nước nhiệt đới với thành phần hóa học đơn giản và trữ lượng dồi dào. đặc biệt là ở. Trong quá trình biến đổi sinh học của lignocellulose, công đoạn thủy phân là bước quan trọng, cho phép chuyển hóa cellulose và hemicellulose thành nguồn cơ chất cho lên men. Việc thiếu kiến thức về các giới hạn vật lý cũng như cơ chế quá trình thủy phân ở điều kiện nồng độ cơ chất cao là rào cản lớn cho nâng cấp quy mô các quy trình chuyển hóa sinh học tạo sản phẩm. Do đó, việc sử dụng có hiệu quả và bền vững nguồn sinh khối lignocellulose hiện là thách thức lớn và cần được nghiên cứu chi tiết.

Trong bối cảnh trên, luận án này tập trung vào nghiên cứu quá trình thủy phân cơ chất lignocellulose dựa trên hai hướng tiếp cận vật lý và hóa sinh nhằm. Chiến lược nghiên cứu bao gồm nhiều bước. Bước đầu tiên là thực hiện phản ứng thủy phân tại các điều kiện khác nhau ở nồng đô cơ chất thấp. Kết quả thu được từ bước này là tiền đề cho bước thứ hai, là phát triển một phương thức thủy phân phù hợp cho nồng độ cơ chất cao. Các khía cạnh vật lý được quan tâm phân tích là đặc tính lưu biến nội, ngoại vi và các phân tích về hình thái, kích thước hạt của cơ chất lignocellulose trong quá trình thủy phân bằng enzyme. Các thí nghiệm được tiến hành trên cơ chất đối chứng, giấy Whatman, và cơ chất thực tế, bột giấy và bã mía tiền xử lý. Luận án này tập trung nghiên cứu các vấn đề sau: (i) biến đổi đặc tính lưu biến và hình thái của huyền phù lignocellulose, (ii) cơ chế thủy phân cơ chất lingocellulose, (iii) ảnh hưởng của thành phần và cấu trúc nguyên liệu đến quá trình hòa tan và động học thủy phân cơ chất, (iv) lượng hóa vai trò của các enzyme đơn lẻ hoặc hỗn hợp thông qua đánh giá các thông số vật lý ở các mức độ khác nhau và (v) phương thức điều khiển và tối ưu các thông số của quá trình fed-batch thủy phân cơ chất ở nồng độ cao.

Chương 1 và 2 của luận án này giới thiệu phân tích tài liệu tổng quan cũng như vật liệu và phương pháp sử dụng trong nghiên cứu. Chương 3 trình bày các kết quả và phân tích thông qua 3 mục. Mục 1 là nghiên cứu về đặc tính của enzyme và cơ chất, đặc biệt là xác định giá trị giới hạn của nồng độ cơ chất từ thấp (semi-dilute) đến cao (concentrated) dưới góc nhìn của cơ học chất lưu. Tiếp đó, các phân tích trong quá trình thủy phân tại nồng độ cơ chất thấp được trình bày ở mục 2. Cuối cùng, mục 3 thảo luận về các kết quả thu được khi thủy phân cơ chất thực (bột giấy, bã mía tiền xử lý) ở nồng độ cơ chất cao bằng phương pháp thủy phân fed-batch. Chương 4 tổng kết lại các kết luận và triển vọng của nghiên cứu này.

Một số kết quả chính từ luận án này:

- Đặc trưng hóa các tính chất lưu biến và hình thái phần tử của cơ chất và huyền phù lignocellulose. Mô hình hóa sự phụ thuộc của độ nhớt dung dịch vào nồng độ cơ chất và ứng suất cắt.
- Chỉ ra vai trò của enzyme đơn lẻ và tính hiệp đồng của hệ enzyme thông qua các phân tích vật lý nội, ngoại vi.
- Định lượng ảnh hưởng của phân bố kích thước và hình thái phần tử đến độ nhớt dung dịch trong quá trình thủy phân.
- Giám sát biến đổi của chỉ số cấu trúc chỉ ra biến đổi đặc tính lưu biến của dung dịch trong quá trình thủy phân.

- Động học quá trình hòa tan (độ nhớt – thời gian) và thủy phân (glucose – thời gian) được phân tích và mô hình hóa
- Ghi nhận hiện tượng tăng độ nhớt trong giai đoạn đầu thủy phân bã mía ở tỉ lệ enzyme/cơ chất thấp (≤ 10 FPU/g cellulose). Hiện tượng này được định lượng và giải thích thông qua phân tích hình thái và kích thước phần tử.
- Đề xuất tốc độ bổ sung cơ chất khuyến cáo cho quá trình thủy phân fed-batch. Kết quả cho thấy quá trình đạt được hiệu suất glucose trên 65% trên nguyên liệu bã mía và bột giấy ở nồng độ cơ chất 100 đến 140 g chất khô/L.
- Chứng minh mô hình duy nhất biểu diễn mối tương quan độ nhớt – thời gian cho bột giấy và giấy lọc ở các điều kiện thủy phân khác nhau: gián đoạn, liên tục, nồng độ enzyme biến đổi.

Từ khóa: sinh khối lignocellulose, bã mía, bột giấy, cocktail enzyme, enzyme đơn lẻ, cơ học chất lưu, hình thái phần tử, phân bố kích thước, thủy phân gián đoạn, thủy phân liên tục.

TABLE OF CONTENTS

LIST OF FIGURES

LIST OF TABLES

ABBREVIATIONS

AVCU	Avicel unit
BAG	Sugarcane bagasse
CBU	Cellobiose unit
CLD	Chord length distribution
CMC	Carboxymethyl cellulose
CS	Corn stover
DLS	Diffraction light scattering
DM	Dry matter
DNS	3,5-Dinitrosalicylic acid
DP	Degree of polymerisation
E	Enzyme
EnXU	Endo-xylanase unit
FBRM	Focus Beam Reflectance Measurement
FP	Fiter paper
FPU	Filter paper unit
Glc	Glucose
HM	Humid matter
IU	International unit
Lig	Lignin
Man	Mannose
MG	Morpho-granulometry
Np	Power number
PP	Paper-pulp
PSD	Particle size distribution
Re	Reynolds number
S	Substrate
SSF	Simultaneous saccharification and fermentation
TIS	Total insoluble solid
WP	Whatman paper
Xyl	Xylose

SYMBOLS

γ	Surface free energy	$(N.m^{-1})$
$\dot{\gamma}$	Shear rate	(s^{-1})
$\dot{\gamma}^*$	Complex shear rate	(s^{-1})
ϕ	Volume fraction	(/)
ϕ_c	Critical volume fraction	(/)
$\phi_{v\text{-}max}$	Maxima volume fraction	(/)
$\phi_{v\text{-}eff}$	Effective volume fraction	(/)
$[\eta]$	Intrinsic viscosity	(/)
φ	Heat flux	(W)
λ	Wavelength	(nm)
ω	Angular velocity	$(rad.s^{-1})$
ρ	Density	$(kg.m^{-3})$
ρ_s	Substrate density	$(kg.m^{-3})$
ρ_w	Water density	$(kg.m^{-3})$
μ	Viscosity	(Pa.s)
μ_0	Initial viscosity	(Pa.s)
μ_∞	Final viscosity	(Pa.s)
μ_s	Suspendant viscosity	(Pa.s)
μ_{rel}	Relative viscosity	(/)
μ^*	Dimensionless viscosity	(/)
τ	Shear stress	(Pa)
τ_0	Yield stress	(Pa)
τ^*	Complex shear stress	(Pa)
θ	Angle contact	(°)
ν	Kinetic viscosity	$(m^2.s^{-1})$
ν_s	Settling velocity	$(m.s^{-1})$
ξ	Ionisation energy	(mV)
ΔG	Gibbs free energy	$(N.m^{-1})$
C*	Critical substrate concentration	$(gdm.L^{-1})$
Cm	Mass concentration	$(gdm.L^{-1})$
Cp	Specific heat mass capacity	$(J.K^{-1}.kg^{-1})$
CrI	Crystallinity	(%)
$d_v(0.1)$	Particle diameter for 10 % population	(µm)
$d_v(0.5)$	Particle diameter for 50 % population	(µm)
$d_v(0.9)$	Particle diameter for 90 % population	(µm)

D[4,3]	Mean volume diameter	(µm)
D_{CE}	Circle equivalent diameter	(µm)
D_{SE}	Spherical equivalent diameter	(µm)
F_{xy}	Force	(N)
g	Gravity	($m.s^{-2}$)
G’	Elastic modulus	(Pa)
G”	Viscous modulus	(Pa)
G*	Complex modulus	(Pa)
l_c	Chord length	(µm)
m_s	Substrate weight	(g)
N	Mixing rate	(round per second)
P	Power consumption	(W)
Q*	Critical substrate flow rate	($gdm.h^{-1}$)
t	Time	(h)
t*	Dimensionless time	(/)
$t_{0.25}$	Time for 75% reduction in viscosity	(/)
T	Temperature	(°)
V_s	Substrate volume	(L)
V_{sup}	Supernatant volume	(L)
V_{tot}	Total volume	(L)
W	Water content	(%)
W_{SL}	Total surface energy (solid-liquid)	($N.m^{-1}$)

GENERAL INTRODUCTION

Today, facing the risk of depleting fossil, namely coal and oil fuel, and in addition to the pollution of environment caused by greenhouse gases (GHG), every country is planning for its roadmap for alternative and clean energy sources, especially, for liquid fuel substituent. Solar and wind energies were developed and can partially respond to energy need but they appear inappropriate for domestic or airplane transportation. In this context, biofuels are seen as a promising solution to reduce both the dependence on the fossil energy and reducing GHG. Bioethanol can be produced from either starch-based (first generation) or cellulosic feedstock (second generation). The 1st generation of biofuel obtained from starch and sugar feedstock was used to reduce the petrol dependency and control fuel price. However, it is not the optimal solution due to food security concerns. The complementarity and competing uses of bioresources to meet food needs in the first instance, and also those for energy, chemistry and bioresource materials stand as a major stake for future generation (**Figure 0-1**). Therefore, scientific and technical research turned to the 2nd generation obtained from lignocellulose biomass, which is able to resolve the biggest problem of the first one: food security. In addition, biomass offers several advantages such as abundancy, renewability (recycling carbon) and non-polluting process.

Scientific and technical literature as well as reports from national and international institutes (International Renewable Energy Agency IRENA, International Energy Agency IEA, National Research Laboratory on Energy NREL, Union des Industries Chimiques UIC, Pôle interministériel de Prospective et d'Anticipation des mutations économiques PIPAME, Agence De l'Environnement et de la Maitrise de l'Energie ADEME...) provide the overview and potential of biorefineries. The most important and recent (2014-2016) documents are:

- *Process design and economics for the conversion of lignocellulosic biomass to hydrocarbons: dilute-acid and enzymatic deconstruction of biomass to sugars and catalytic conversion of sugars to hydrocarbons* (Report NREL/TP-5100-62498). It described the potential conversion process to hydrocarbon products by conversion of lignocellulosic derived hydrolysate. Materials, energy balance, capital and operating costs were documented in detail (Davis, Tao et al. 2015).
- *Global Bioenergy - Supply and demand projections. A working paper for REmap 2030*. (IRENA). Global Renewable Energy Roadmap (Remap 2030) is a project developed by IRENA to double the share of renewables in the global energy mix by 2030. The report gave an overview of the current biomass demand and bioenergy market situation. The estimation of future bioenergy demand and technologies to realize sustainable bioenergy growth were discussed (Nakada, Saygin et al. 2014).
- *IEA bioenergy Task42 on biorefineries, coproducing fuels, chemicals, power, and materials from biomass*. (IEA) The objective of this Task is to assess the worldwide position and potential of the biorefinery concept. It provides an insight for new competitive, sustainable and safe manufacture of transportation fuels from biomass (Bell, Schuck et al. 2014).
- *Etudes économiques, prospective: Benchmark européen sur les plateformes chimiques, quels sont les leviers pour améliorer la compétitivité des plateformes françaises? (European benchmark of chemical platform, what are the lever arms to improve the competitiveness of French platforms?)* (PIPAME). This report presents the essential elements of benchmark methodology, main force and weakness of French chemical platforms and recommendation for improving competitiveness (Rico, Hugon et al. 2014).

Figure 0-2 clearly reflects this trend in scientific research with the keyword "biorefinery book" from Google online searching tool (Jan 2016).

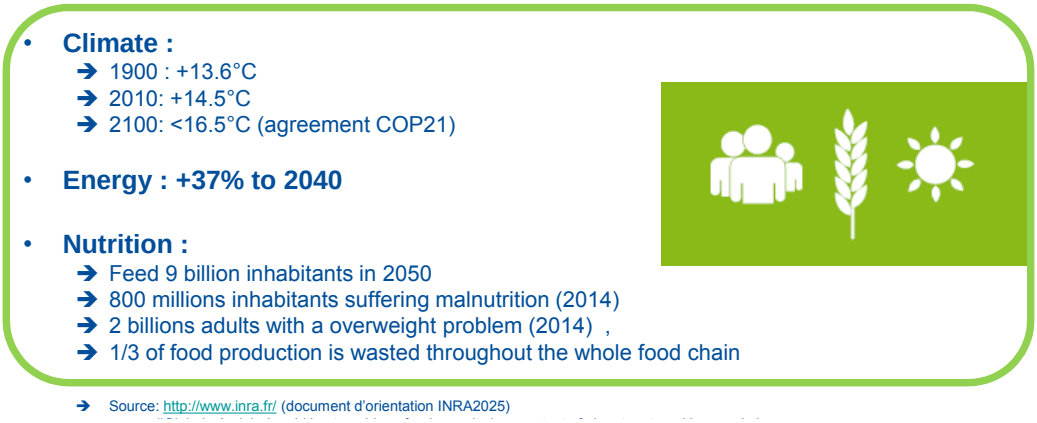

Figure 0-1. Facing to challenges, the key figures ((Vilotte, Houllier et al. 2016))

Figure 0-2. Scientific books in the domain of biomass energy, result from Google search (January 2016, key word "biorefinery book").

The process of bioethanol production from lignocellulose contains 3 mains steps: (i) the pretreatment of raw material to increase its accessibility, (ii) the hydrolysis by enzymatic biocatalysts in order to release fermentable carbon source and (iii) the biotransformation through microbial biocatalyst (cell culture) in order to produce molecules of interest (biofuel and the likes). All steps are determinant to achieve a competitive and viable bio-refinery. Focusing on the hydrolysis step, great progress in enzyme optimization and production were achieved in the recent decade mainly due to "omics" technologies (ex. genomic, proteomic), computational design of enzymes and high throughput screening method. However, these researches were limited at lab scale (molecular biology) and limitation due to up-scaling and intensification scale was not yet considered. Beyond, the bio-refinery must operate at high concentration of raw material to achieve an economic viability. This strict prerequisite imposes a considerable constraint particularly on the physicochemical and bio-catalytic steps, whose overall aim is to produce high quality, fermentable sugar syrups, but is essential to be compatible with industrial criteria regarding maximum reactor volumes, energy and water consumption and wastewater management. Bioprocess control under high dry matter content from pilot up to industrial scales forces to solve not only biochemical problem but also

physical/mechanical limitation occurring at both macroscopic and microscopic scales. Among the main barriers reducing hydrolysis efficiency, limitations in heat, mass and momentum transfers are crucial. Thus the rheological behavior of suspensions, the morphology of fibers and particles and the mechanisms of disaggregation, disintegration and solubilization appear as determinant steps for an efficient bioprocess.

In Vietnam, an agricultural country with a limited fossil carbon reserve (gas and petrol), biofuel production can first, solve the energy requirement and second, open a new way to valorize the agricultural by-products. Through the statistical report of Ministry of Agriculture and Rural Development (MARD) of Vietnam (http://www.mard.gov.vn/Pages/statisticreport.aspx?TabId=thongke), the total cultivation area of rice in Vietnam was 7.8 MHa (2016). The rice straw is absolutely the most important lignocellulosic resources of the region. Vietnamese researches have focused on bioethanol production from this substrate and a national policy sustains its emergence. However, rice straw is not the best feedstock to privilege because of its high silica concentration (Pandey, Soccol et al. 2000) which represents an inhibitor of microbial cell activity during oxidative and fermentative cultivation. In addition, the widespread of rice straw over the cultivated area limits its harvesting and industrial scale processing. By contrast, sugarcane bagasse indicates several advantages: a simple chemical composition with high percentage of cellulose (up to 47 % w/w), an existing collect of substrate and a centralized industrial processing (sugarcane mill). Statistically, the Vietnamese production of sugarcane ranged between 15 and 17 millions of tons/year since 2010, reached recently 17.2 millions of tons in 2016 (MARD annual report). According to Ceraueira et al. (2007), the amount of bagasse is approximately 28 % of sugarcane plant, it means around 5 millions of tons of bagasse are generated per year in Vietnam. This by-product stands as a realistic feedstock for biofuel production.

In Europe, the pulp and paper manufacturing sector is energy and raw materials intensive, with high capital costs and long investment cycles. The industry has an excellent track record in resource efficiency and innovation. Thanks to its knowledge of wood fiber, the pulp and paper industry is at the forefront of developing innovative products alongside more traditional products. It is a pioneer in making the EU low-carbon bio-economy an industrial reality. According to statistic data by RISI (Resource Information Systems Inc. provides information and data for the global forest products industry, http://www.risiinfo.com/), main producing countries of paper and paperboard, not including pulp, in the world have produced around 400 million tons (77.4 million tons in Europe) in 2014. The pulp and paper industry (Vallette and De Choudens 1987) is able to provide a tried and tested industrial model for the processing of lignocellulosic biomass into pre-treated cellulosic pulps. The pulp product of this industry is appropriate for modern bio-refining thank to its low lignin content and free of inhibitory compounds Nevertheless the enzymatic hydrolysis of paper-like pulps are subjected to the same constraints as other pulps obtained via alternative methods such as steam explosion or dilute acid hydrolysis. Therefore, the better scientific understanding and ultimately the technical mastering of these critical biocatalytic reactions, which involve complex matrices at high solids content, is currently a major challenge that must be met in order to facilitate the intensification of bio-refining operations.

My PhD work integrates in the scientific collaboration network between five establishments (laboratory, institute and university) (**Figure 0-3**). The contribution of each establishment is correlated to their own specificity and domain of competency. LISBP is dedicated for the physical measurement (rheological, viscometry, particle distribution …) and the process development. IMFT participates in the rheological approach on lignocellulosic suspension. LCPO carried out the analysis of substrate composition and structure, as well as the identification of intermediaries. Finally, CRDB (SBFT, HUST, Hanoi) is responsible for the

organosolv pretreatment of raw material (sugarcane bagasse) and biochemical investigations. This work also takes part in the BioAsie HTMS project (http://www.bioasie.hust.edu.vn) which creates an international network implying three partners from three countries: France, Vietnam and Philippines.

Figure 0-3. Scientific network associated with PhD

Considering the context and challenges, our research focuses on the enzymatic hydrolysis of pretreated sugarcane bagasse and paper pulp for the production of biofuel. The scientific questions are illustrated in **Figure 0-4**. Firstly, the rheological properties of lignocellulosic suspension are investigated in relationship with substrate properties (structure, composition, concentration) and lignocellulolytic enzymes (from single up to cocktail). Secondly, from observed phenomenon during enzymatic digestion and base on the appropriated analytical methods, we scrutinize the mechanisms of reaction and try to explain how the degradation was. Thirdly from these results, we intend to identify the physical limitation of high solid loading process to propose the strategy to hydrolyze biomass at high dry matter condition through fed-batch mode. The ultimate goal of this study is to maximize the production of mono sugar (glucose, xylose) by enzymatic hydrolysis in term of yield and concentration.

Corresponding to the scientific questions, the approach and research strategy is clearly defined. The mechanisms during deconstruction of pretreated lignocellulosic biomass are specifically investigated under "favorable" conditions with different enzymes preparations. This is then followed by the evaluation of up-scaled hydrolysis in fed-batch mode. Thus, this study is divided in two mains parts:

- Part 1: Investigation of physico-chemical properties of dilute fibers suspensions during enzymatic hydrolysis. This first step is dedicated to the understanding of hydrolysis mechanism in relation to single up to cocktail activities.
- Part 2: Identification of limit in operating conditions at high solids loading for various fed-batch strategies. The aim of this phase will be to raise the solid concentration as high as possible while maintaining a good hydrolysis yield.

In this study, three lignocellulosic substrates are selected: milled filter paper (FP) for the reference, extruded hard wood paper pulp (PP) and extruded pretreated sugarcane bagasse (SCB) for the real materials. The substrate concentrations vary from semi-dilute regime (1.5% w/v for FP, 3% w/v for PP and SCB) to concentrated conditions (up to 14% w/v). In order to

evaluate the mechanism of the hydrolysis related to single enzyme activities and their own roles in the cellulase family, 6 commercial enzymes are selected from Novozymes, Sigma Aldrich and Megazymes. Enzyme dosages range between 0.3 and 25 FPU/g cellulose. All experiments are carried out in a 2 L bioreactor (working volume 1.3 L) equipped with a home-made agitation system consisting two impellers. Both *in*- and *ex-situ* analysis (rheological, particle size, particle shape and biochemical) are conducted and enable a multilateral investigation of the hydrolysis.

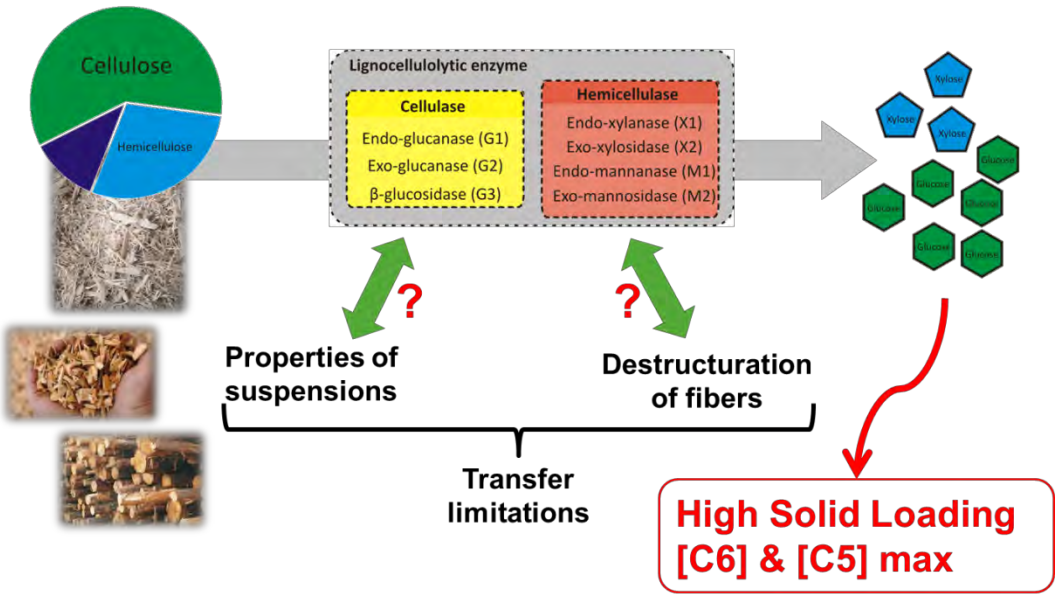

Figure 0-4. Context and scientific questions

This PhD manuscript is structured around four chapters:

- Chapter 1 is a bibliography review. It firstly presents basic knowledge about lignocellulose and lignocellulolytic enzymes. Secondly, the methodology for construction of a working database (publications, thesis …) is presented. Finally, this database is quantitatively and qualitatively analysed.
- Chapter 2 gives a detailed description about materials (substrates, enzymes and experimental setup) and analytical methods (physical and biochemical). The research strategy is specifically detailed at the end of this chapter.
- Chapter 3 is dedicated to results and discussions. This chapter is divided in three sub-chapters that correspond to (i) the characterization of materials, (ii) the enzymatic hydrolysis in dilute condition and batch mode and (iii) the enzymatic hydrolysis up to concentrated conditions though fed-batch strategy.
- Chapter 4 is a conclusion of this work. It not only summarizes the main achievements but also points out the most important issues to be investigated in the future researches.

1 BIBLIOGRAPHY

In this chapter, the bibliography is specifically scrutinized. The first sub-chapter is dedicated for the properties of lignocellulosic substrates and its degradation by enzymes. It is then followed by the second sub-chapter that focuses on the related publications under both physical and biochemical approaches. In this second sub-chapter, the methodology of database construction is described. Different steps to analyze the database are performed, from quantitative to qualitative. Final conclusion highlights the general research trend in the world as well as identifies the lacks of knowledge.

1.1 LIGNOCELLULOSIC BIOMASS AND ENZYMES

Lignocellulosic biomass and enzymes are two main subjects in this study. Lignocellulose is a generic term for describing the main constituents in plants a matrix of cellulose, hemicelluloses and lignin. The degradation of lignocellulose by biochemical way requires the actions of several single enzyme activities. The structure and properties of lignocellulose are described in this part. Afterwards, common knowledge about lignocellulolytic enzymes is reported. Finally, different ways to calculate hydrolysis yields are also explored.

1.1.1 Lignocellulosic biomass

Lignocellulosic biomass represents one of the most abundant and renewable resource in the world. It chemical composition contains three principal fractions: cellulose, hemicellulose and lignin (**Figure 1-1**). The proportion of these constituents may significantly vary between biomass types. In general, cellulose is the main component accounting for 25-50 % in dry weight basis. Cellulose is the fraction of interest in lignocellulosic biomass; it gives glucose (C6 sugar) through enzymatic bioconversion and various molecules through microbial bioconversion. The valorization of hemicellulose fraction was considered more recently due to specific microorganisms to consume xylose (C5 sugar) (Giovanni, Eleonora et al. 2011). Lignin is an undesired fraction for bioconversion and contributes to the strong chemical and mechanical resistance of lignocellulosic matrices. At present time, the elimination of lignin fraction by fractionation or degradation is a mandatory step before enzymatic and microbial bio-catalytic conversion. Besides, the valorization of lignin was considered recently. The compositions of several lignocellulosic biomasses are depicted in **Table 1-1**.

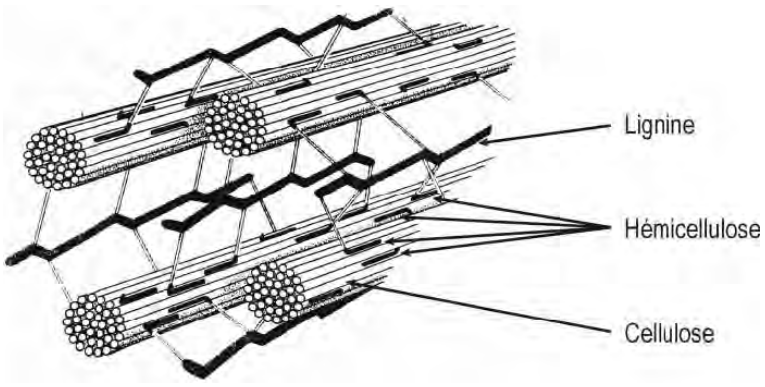

Figure 1-1. Structure of lignocellulosic biomass (Joseleau, Comtat et al. 1992)

Sugarcane bagasse is the accumulated lignocellulosic residue during the production of sugar. The chemical composition of sugarcane bagasse can be varied between varieties and geographic zone.

Table 1-1. Chemical composition of some lignocellulosic biomasses (Xu, Singh et al. 2009)

	Cellulose	Hemicellulose	Lignin
Soft wood	40-55 %	24-40 %	18-25 %
Hard wood	45-50 %	25-35 %	25-35 %
Straw	30-43 %	22-35 %	15-23 %
Sugarcane bagasse	40-55 %	25-40 %	5-25 %
Herb	25-40 %	35-50 %	10-30 %

In general, cellulose is the main composition of sugarcane bagasse that accounted for more than 40 %. Because of the low ash content in chemical composition comparing to other lignocellulosic biomasses such as rice straw (17.5 %) or wheat straw (11 %), sugarcane bagasse is therefore one of the most promising feedstock for usage in bio-refinery (Pandey, Soccol et al. 2000). For centenaries, sugarcane was the major crop cultivated in many tropical area countries over the world such as Brazil, Thailand, China, India (Soccol, Vandenberghe et al. 2010). According to Kim and Dale (2004), the global production of sugarcane is 328.10^9 Kg, corresponding to around 180.10^9 Kg of dry sugarcane bagasse. This resource can be utilized and could produce about 51 GL of bioethanol. Thus, the bioconversion of sugarcane bagasse to bioethanol has been considered since longtime (Gottschalk, Oliveira et al. 2010, Carvalho, Sousa et al. 2013, Zhao, Dong et al. 2013)

Table 1-2. Chemical composition of sugarcane bagasse through different studies.

References	Cellulose	Hemicellulose	Lignin	Extractives	Ashes
(Pandey, Soccol et al. 2000)	50 %	30 %	17.6 %	-	2.4 %
(Mosier, Wyman et al. 2005)	42.1 %	23.6 %	23.7 %	-	-
(Singh, Varma et al. 2009)	25-45 %	28-32 %	15-25 %		
(Rocha, Gonçalves et al. 2012)	45.5 %	27 %	21.1 %	4.6 %	2.2 %

1.1.1.1 Cellulose

Cellulose is one of the principal constituent of cell wall, it is water insoluble and resistant to physical and biochemical degradation. It is a polymer of glucose, linked between them by β-(1,4) glucosidic links. Cellulose can be considered as a polysaccharide of high polymerization degree, varying from 7000 to 15000 (Fengel and Wegener 1983). The cellulose chains are condensed by hydrogen bonds to form micro-fibrils. There are two types of structural zones: crystalline zones consisting of crystalline celluloses and non-ordered zones consisting of amorphous celluloses (Brown 1999). **Figure 1-2** represents the chemical structure of cellulose. In the bioconversion of lignocellulosic material, cellulose is the most valuable fraction, producing glucose that can be fermented into different products.

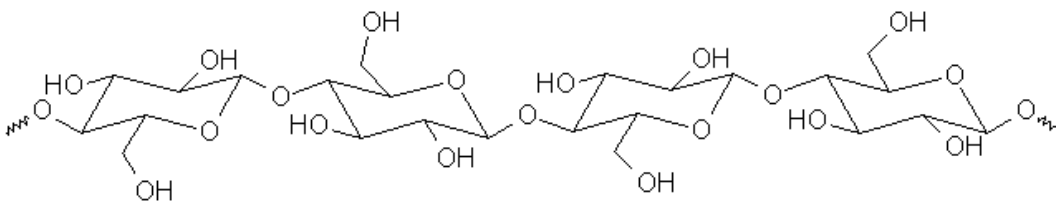

Figure 1-2. Structure of cellulose (Gardner and Blackwell 1974).

1.1.1.2 Hemicellulose

Hemicellulose is the second principal constituent of lignocellulose. It is a complex and ramified polymer with a degree of polymerization from 70 to 200 depending on biomass type. In the structure of hemicellulose, there are several types of pentose and hexose such as xylose, arabinose, glucose, mannose and galactose. Among these mono-sugars, xylose or arabinose are the two main constituents corresponding to two types of hemicellulose from hard and soft wood. Hexoses represent minor proportion in hemicellulose. For hard wood, β-D-xylopyranose is the principal unit, linked between them by β-(1,4) glucoside links. Following (Hồ 2006), the structure of hemicellulose is very dependent of the wood type however several common properties can be pointed out:

- The principal chain is form by β-(1,4) links.

- Xylose is the dominant constituent.

- Most frequent positions for substitution are C_2 and C_3.

- The secondary chain consists of simple molecules such as di- or tri-saccharides. Due to these residues, hemicellulose is able to link with other polysaccharides and lignin.

- Hemicellulose is easier to be hydrolyzed than cellulose.

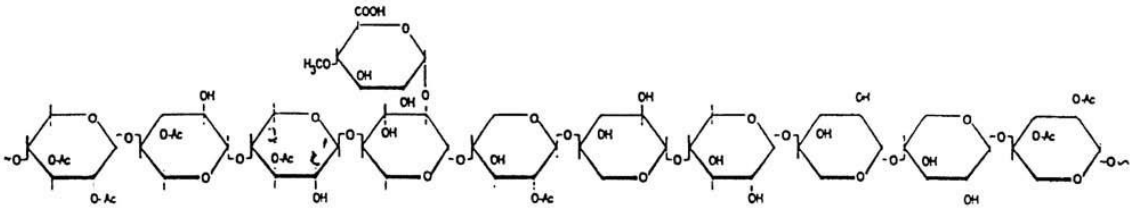

Figure 1-3. Acetyl-4-O-methyl-glucuronoxylan.

For soft wood, there are two types of hemicellulose (Hồ 2006)

- Acetyl-4-O-methyl-glucuronoxylan: a polymer with principal chain formed by β-D-xylopyranoses linked between them by glycosides-(1,4) links. In the structure of this hemicellulose, 70% of hydroxyl group at position C_2 and C_3 are substituted by acetyl and 10% of these groups are linked to acid 4-O-methyl-D-glucoronic

- Glucomannan: a co-polymer of β-D-glucopyranose and β-D-mannopyranose linked between them by glycoside (1,4) links.

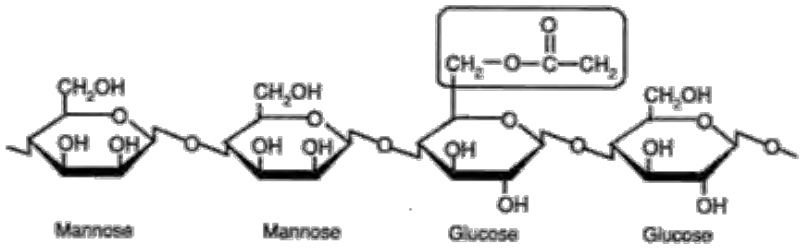

Figure 1-4. Structure of glucomannan.

For hard wood, there are also two type of hemicellulose (Hồ 2006)

- Galactoglucomannan: a polymer from D-mannopyranose and D-glucopyranose linked between them by glycoside-(1,4) links. The ratio between galactose/glucose/mannose in galactoglucomannan is approximately estimated to 1/1/3 or 0.1/1/3 for wood which is either

rich or poor in galactose content. Hemicellulose with high galactose content is water soluble while hemicellulose with low galactose content is soluble in alkaline condition. It is also reported that hydroxyl group in position C_2 and C_3 are sometimes substituted by acetyl group.

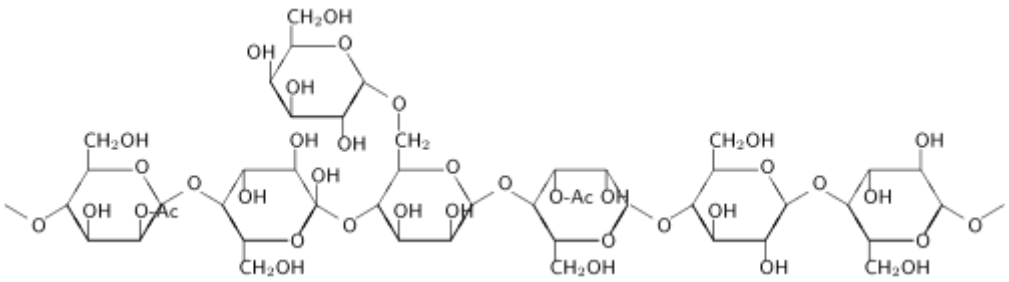

Figure 1-5. Galactoglucomannan.

- Arabinoglucuronoxylan: a polymer of xylose constituted by glucoside-(1,4) links. In the structure of this hemicellulose, the principal chain is substituted by the group 4-O-méthyle-α-D-glucuronic and α-L-arabinofuranoses at position C_2 or C_3.

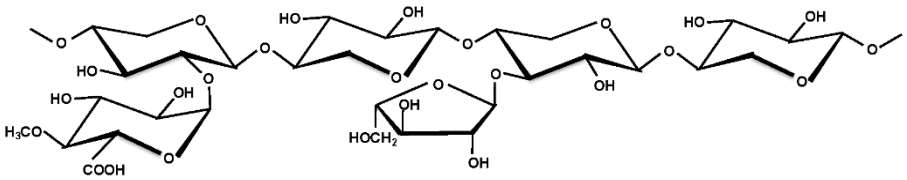

Figure 1-6. Arabinoglucuroxylan.

Hemicellulose is always the first fraction to be degraded during the destructuration of lignocellulosic material. It liberates minor amount of glucose and principally xylose or mannose depending on the type of biomass. Xylose can be used for xylitol conversion or pentose fermentation to produce various molecules of interest.

1.1.1.3 Lignin

Lignin is a complex and hydrophobic macromolecule. In nature, lignin is closely linked to cellulose and hemicellulose in the plant cell walls to form a complex matrix. It is constituted by three units of phenyl-propene: guaiacyl (G), syringyl (S), et p-hydroxyphenyl (H). These three units are linked by C-C and C-O links, mainly of type aryl-glycerol, aryl-aryl or diaryl-ether.

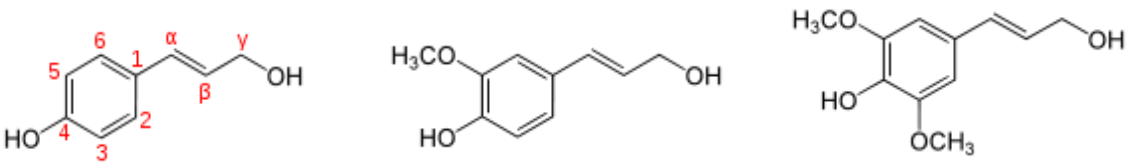

Unit H Unit G Unit S

Figure 1-7. Three units of lignin.

Lignin can be divided in two major types: guaiacyl lignin and guaiacyl-syringyl lignin (Gibbs 1958). Guaiacyl lignin is principally product of polymerization from coniferylic alcohol and guaiacyl-syringyl lignin is formed by guaiacyl and syringyl with a low quantity of p-hydroxyphenyl (Fengel and Wegener 1983). Guaiacyl lignin is the major constituent of soft

wood and guaiacyl-syringyl lignin is the major component of hard wood. It is reported that lignin from soft wood is more resistant to alkaline extraction than that from hard wood. In addition, guaiacyl lignin limits the swelling of fiber, that make the material more resistant to enzymatic digestion than syringyl lignin (Ramos, Breuil et al. 1992).

Published studies have shown that all types of lignin are not homogeneous in their structure, it appears to consist of ultra-structural (amorphous) zones and structured zones of oblong shape and globule (Novikova, Medvedeva et al. 2002). The chemical structure of native lignin is essentially changed under severe temperature and acid conditions, by a steam pretreatment for example. At reaction temperatures higher than 200ºC, lignin is agglomerated into small particles and separated from cellulose (Tanahashi, Takada et al. 1982).

Lignin is non digestible by mammalian and other animal enzymes, but some fungi and bacteria can biodegrade this polymer. White rot fungi are known since long time ago for its ability to degrade lignin. However, the mechanism of biodegradation is not fully understood because it depends on structure and origin of lignin.

In the structure of lignocellulosic matrices, due to the entanglement between cellulose, hemicellulose and lignin, the enzymatic accessibility is reduced to a minimal level (Odier and Artraud 1992). Then, a pretreatment step is required to eliminate lignin before further bioconversion.

1.1.2 Lignocellulolytic enzymes

Lignocellulosic substrate can be totally degraded by synergetic action of multiple enzymes. Corresponding to the three main constituents of lignocellulosic material, at least three enzymatic cocktails are required.

For the digestion of cellulose, three main enzymes are well known for their actions (Goyal, Ghosh et al. 1991, Lynd, Weimer et al. 2002, Rabinovich, Melnik et al. 2002). Firstly, endo-1,4-β-glucanase (EC 3.2.1.4) or 1,4-β-D-glucan 4-glucanohydrolase: this enzyme attacks randomly cellulose chain in amorphous regions, breaks 1,4-β-glucan links and generally produces oligosaccharides of different degree of polymerization. The action of endo-glucanase is reported as dominant for liquefaction as it strongly reduces viscosity of the substrate suspension (Szijártó, Siika-aho et al. 2011). Secondly, exo-1,4-β–D-glucanase (EC 3.2.1.74) contains 2 activities: i) 1,4-β-D-glucan glucohydrolase which liberates D-glucose from 1,4-β-D-glucan and slowly hydrolyze D-cellobioses; and ii) 1,4-β-D-glucan cellobiohydrolase which liberates cellobiose from longer poly- and oligosaccharides. Cellobiohydrolase are divided in two types that attack the chain from reducing and non-reducing ends. Finally, β-D-glucosidase (EC 3.2.1.21) cleave the glyosidic bonds of cellobiose and oligosaccharides (from non-reducing terminal), releasing glucose which is the final product of enzymatic hydrolysis reaction of cellulose chain. The conversions of cellulose into glucose and cellobiose are presented as **Eq. 1-1** and **Eq. 1-2**.

$$(C_6H_{10}O_5)_n + nH_2O \xrightarrow{cellulase} nC_6H_{12}O_6 \qquad \textit{Eq. 1-1}$$

$$C_{12}H_{22}O_{11} + H_2O \xrightarrow{\beta\text{-}glucosidase} 2C_6H_{12}O_6 \qquad \textit{Eq. 1-2}$$

The digestion of hemicellulose can be performed by various enzymes corresponding to the chemical composition of hemicellulose in the substrate. Two categories of enzymes can be listed for this reaction; one catalyzes the hydrolysis of principal hemicellulose chain (xylanase, mannanase) and the other attacks the substitution group. Endo-1,4-xylanase (EC 3.2.1.8) degrades the linear polysaccharide beta-1,4-xylan into xylose. Mannanase or β-D-mannosidase

(EC 3.2.1.25) catalyzes the hydrolysis of terminal, non-reducing β-D-mannose residues in β-D-mannosides. It is noticeable that hemicellulases have been found to facilitate the total hydrolysis of biomass (Himmel, Ding et al. 2007). Synergistic action of xylanase and mannanase can improve the hydrolysis efficiency of cellulose from softwood (Várnai, Huikko et al. 2011). This can be explained by the fact that hemicellulose is the easiest fraction to hydrolyze in lignocellulosic matrix. Actions of hemicellulase enzymes may open the fiber structure and make the substrate to be more accessible by cellulase. Hydrolyses of main components of hemicellulose are described by **Eq. 1-3** to **Eq. 1-7**.

$$(C_5H_8O_4)_n + nH_2O \xrightarrow{\textit{Endo-1,4-xylanase}} 2C_5H_{10}O_5 \qquad \textit{Eq. 1-3}$$

xylan — xylose

$$(C_5H_7O_3 - OOC - C_5H_9O_5)_n + 2nH_2O \xrightarrow{\textit{Endo-1,4-xylanase}} nC_5H_{10}O_5 + nC_5H_9O_5 - COOH \qquad \textit{Eq. 1-4}$$

glucoroxylan — xylose — glucoronicacid

$$(C_{10}H_{18}O_9)_n + nH_2O \xrightarrow{\textit{Endo-1,4-xylanase}} nC_5H_{10}O_5 + nC_5H_{10}O_5 \qquad \textit{Eq. 1-5}$$

arabinoxylan — xylose — arabinose

$$((C_6H_{10}O_5)_{16} - (C_6H_{10}O_5)_{10})_n + 26nH_2O \xrightarrow{\textit{mannanase}} 16nC_6H_{12}O_6 + 10nC_6H_{12}O_6 \qquad \textit{Eq. 1-6}$$

glucomannan — mannose — glucose

$$(C_6H_{10}O_5 - C_5H_8O_4)_n + 2nH_2O \xrightarrow{\textit{endo-β-1,4-glucanase}} nC_6H_{12}O_6 + nC_5H_{10}O_5 \qquad \textit{Eq. 1-7}$$

xylo-glucan — glucose — xylose

For the most undesirable fraction, three enzyme are able to degrade lignin are lignine-peroxydase (LiP), manganesse-peroxydase (MnP) and laccase (Lac) (Kuhad, Singh et al. 1997, Leonowicz, Matuszewska et al. 1999). Different from cellulolytic and hemicellulolytic enzymes, these three enzymes catalyze the degradation of lignin by oxidation mechanism. LiP, MnP and Lac belong to oxydoreductase family. Among these three enzymes, laccase (EC 1.10.3.2) is the most studied for application in bioethanol production due to the fact that LiP and MnP required H_2O_2 as electron acceptor for their enzymatic reaction. As for laccase, it requires oxygen as a second substrate for its enzymatic reaction that makes the application of laccase less complicate compared to LiP and MnP. The broad range of substrate is another advantage of this enzyme. Laccase can be produced by some insects and bacteria. Among them, laccase from fungi (*Botritis cinerea*, *Pycnoporus cinnabarus* and *Trametes versicolor)* are the frequently used thanks to its high activities.

1.1.3 Calculation of hydrolysis yield

From a biochemical standpoint, the overall efficiency of enzymatic hydrolysis is evaluated by the bioconversion rate of substrate (cellulose, hemicellulose) into final product (glucose, xylose). As lignocellulase enzyme is a mixture of several activities, the contribution of each individual activity can be considered taking into account the measurement of other component like cellobiose for exo-glucanase.

The quantification of final product has been reported in literature. Reducing sugar determined by dinitrosalicylic acid (DNS) method (Goyal, Ghosh et al. 1991) can be used for the estimation of hydrolysis yield (Peng and Chen 2011). More precise, the hydrolysis yield

can also be calculated based on the monomer sugar that are liberated following enzymatic digestion such as glucose, xylose, arabinose, galactose, … This analysis is generally performed by HPLC analysis with various protocols and instruments (column, detector) (Lynd, Weimer et al. 2002). It is clear that, the most popular method to determine hydrolysis yield is related to the quantification of glucose concentration. The calculation of hydrolysis yield for bioconversion of cellulose is proposed by National Renewable Energy Laboratory (NREL) as follow

$$Yield_{cellulose}\,(\%) = \frac{[Glc] + 1.0526 \cdot [Cello]}{1.111 \cdot F_{cellulose} \cdot [Ini.Sol]} \cdot 100 \qquad \textit{Eq. 1-8}$$

with $[Glc]$: glucose concentration in the supernatant ($g.L^{-1}$); $[Cello]$: cellobiose concentration in the supernatant ($g.L^{-1}$); $F_{cellulose}$: concentration of cellulose in the substrate (g cellulose/g dry matter); [Ini.Sol]: concentration of initial solid in the reaction ($g.L^{-1}$). Coefficients (1.111 and 1.0526) are related to stoichiometric equation regarding the molecular weight of cellulose, glucose and cellobiose respectively (**Eq. 1-1** and **Eq. 1-2**).

To simplify, the yield can be calculated from only glucose concentration as below

$$Yield_{cellulose}\,(\%) = \frac{0.9 \cdot Glc_{produced}\,(g)}{Cellulose_{initial}\,(g)} \cdot 100 \qquad \textit{Eq. 1-9}$$

For hemicellulose, because of its complex chemical composition, it is difficult to propose a unique equation to calculate the hydrolysis yield. However, considering only the main components of hemicellulose – xylan (for hard wood) or mannan (for soft wood) - the hydrolysis yield could be calculated as below:

$$Yield_{Xylan}\,(\%) = \frac{0.88 \cdot Xyl_{produced}\,(g)}{Xylan_{initial}\,(g)} \cdot 100 \qquad \textit{Eq. 1-10}$$

$$Yield_{Mannan}\,(\%) = \frac{0.9 \cdot Man_{produced}\,(g)}{Mannan_{initial}\,(g)} \cdot 100 \qquad \textit{Eq. 1-11}$$

where Xyl is the quantity of obtained xylose (g); Man is the quantity of obtained mannose (g), $Xylan_{initial}$ and $Mannan_{initial}$ are the quantities of initial xylan and mannan (g). Coefficients (0.88 and 0.9) are related to stoichiometric equation regarding the molecular weight of xylan, glucomannan, xylose and mannose (**Eq. 1-3** and **Eq. 1-6**).

1.2 DATABASE CONSTRUCTION AND ANALYSIS

The successive steps associated to this bibliographic research are summarized in **Figure 1-8**. Firstly, the keywords were defined in order to associate the different subjects of our study: (i) lignocellulosic biomass, (ii) pre-treatment process, (iii) lignocellulolytic enzyme and (iv) physical properties. By associating several keywords, profiles are proposed. Secondly, the selected databases were identified from commercial scientific databases focusing on biotechnology and process engineering. The fields and period of interrogation (title, topic…) were selected. Thirdly, alternative databases (PhD thesis, scientific books and documents) by electronic library were scrutinized. Fourthly, a working database was built after quick analyses of all extracted documents by skimming its keywords and abstracts. Finally, this working database was analyzed from quantitative and qualitative stand point.

Three scientific databases dealing with biology, physics, chemistry, energy, environment, agriculture science and technology were selected. Database access was provided by CNRS

(http://www.inist.fr/?-Portails-) WoS and Science Direct are the most used in engineering science (worldwide editor) and one additional databases was added: Engineering Village for environmental and energy science.

- **Engineering village (editor: Elsevier):**
  Address: https://www.ebscohost.com/academic/greenfile
- **Web of Science ® Core collection (editor: Thomson-Reuter):**
  Address: https://webofknowledge.com/
- **Science Direct (editor: Elsevier):**
  Address: http://www.sciencedirect.com/

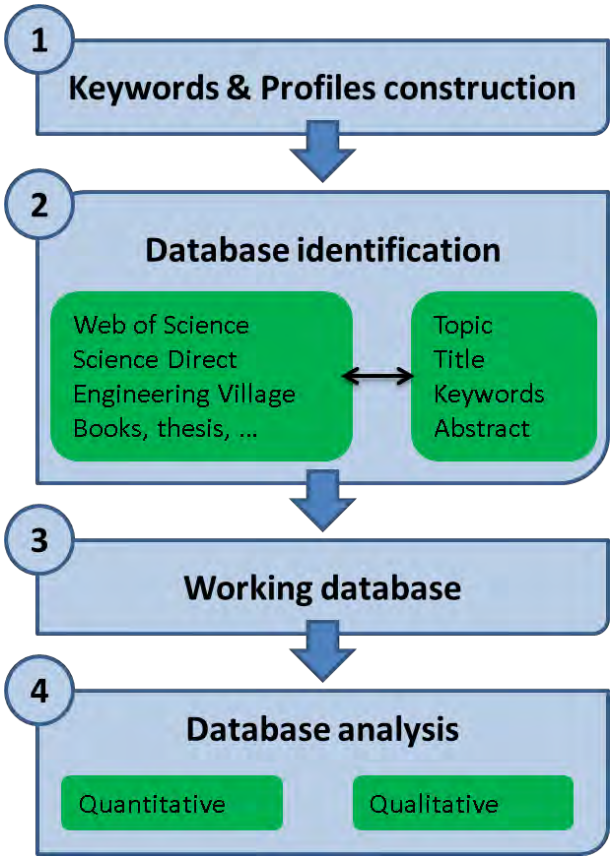

Figure 1-8. Diagrammatic illustration for the methodology of bibliographic research

Starting from PhD title "*Investigation of **physical mechanisms** during **deconstruction** of **pretreated lignocellulosic matrix** and its ability to liberate a fermentable carbon substrate in a bio-process*", 3 "key" terms were pointed out. Our bibliographic investigation was driven by these terms. In the first step, 4 groups of key words have been determined related to "*physical mechanisms*", "*deconstruction*" and "*pretreated lignocellulosic matrix*"

- Group 1 (**G1 PHY**) = rheo* *OR* visco* *OR* newt*
- Group 2(**G2 LIG**) = lignocellulo* *OR* bagasse* *OR* "pulp paper"
- Group 3 (**G3 PRE**)= pretreatment *OR* organosolv
- Group 4 (**G4 HYD**)= hydrolys* *OR* enzym* *OR* bioconver* *OR* biocatalys*

In addition, considering the goal of this study which was to investigate the hydrolysis mechanisms of single and cocktail enzymatic activities and to go towards high dry matter content, two groups of keywords were then created

- Group 5 (**G5 ENZ**)= cellulase *OR* *glucanase *OR* hemicellulase *OR* xylanase *AND NOT* (production *OR* characterization *OR* *bleach*)
- Group 6 (**G6 HDM**)= "high dry matter" *OR* "high solid*" *OR* "high consistency"

Secondly, from the 6 initial groups of key-words, 6 profiles were defined by combining these groups in order to find and filter publications and to extract the most pertinent ones. Detailed information about the construction of profiles is presented in **Figure 1-9**. Profile 1 revealed the publications that mention physical approach on lignocellulosic biomass. Profile 2* can be considered as a more restricted version of Profile 1 with the participation of G3 in addition. Profile 3 and 4* indicated the physical and biochemical (kinetics) approaches on hydrolysis of lignocellulosic biomass, respectively. Profile 5 presented our interest in the role of single up to cocktail enzyme activities on lignocellulosic substrate by physical standpoint. Finally, profile 6 specifically focused in the publications that deal with hydrolysis at high dry matter content

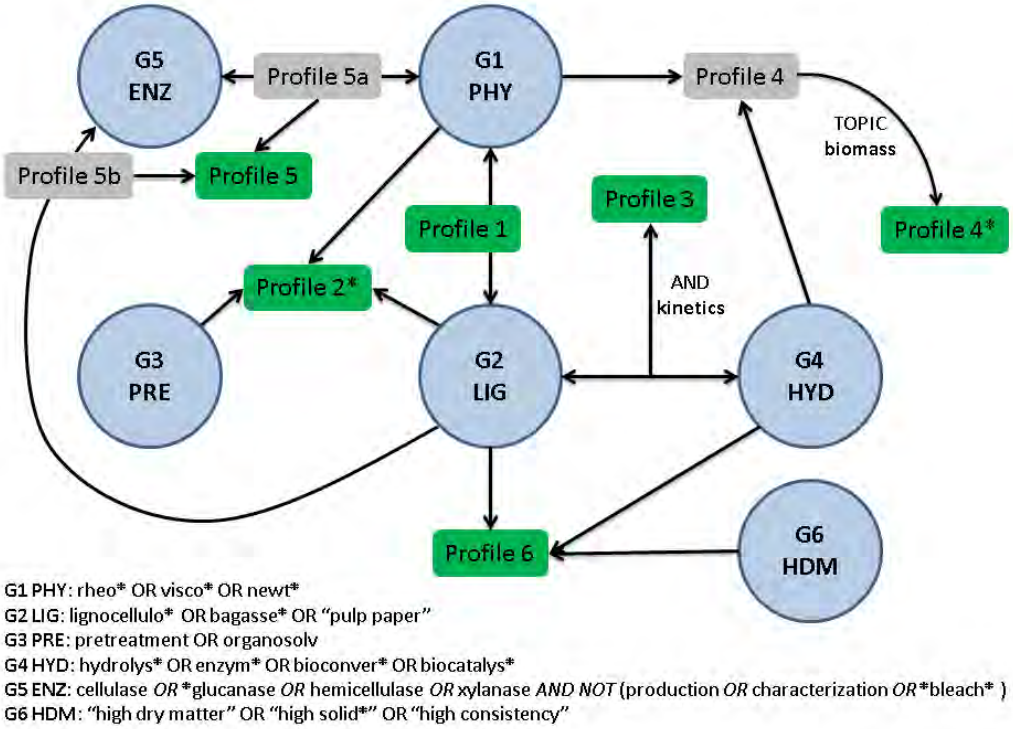

Figure 1-9. Structuration of profiles from generated groups.

Finally, all papers resulting from this research on three databases were collected. A pre-selection step was performed by skimming in the title, keys words and then abstract of these publications. From several hundreds of initials papers, approximately 47 were selected by evaluation of title and abstract. These 47 articles were closely related to this study and provided information about substrates properties (biochemical, rheological), enzymatic hydrolysis, impact of pretreatment and rheological approach.

Final reference database consisted of 47 most pertinent and multiple related publications. We performed an automatic follow of our most-interested key word profile in Web of Science online database and notifications were sent monthly whenever new publications match with the key words. This allowed to regularly updating our working database along the PhD. The final review of working database was performed in summer 2016 when all experiments has been done. Recent publications relating to the research were added and the database was extended to more than 50 pertinent papers from more than 200 authors. The total number of publications in our database is 130 by Jan 2017.

The analysis of bibliography was performed after the working database has been established. This consists of two principal steps

- A quantitative analysis to report the annual number of publication per key word profile that allows understanding the global research trend in the world. In addition, statistical analysis highlight the lignocellulose material that is the most interested. More important, this helps to identify "strong" research group in the domain (by number of publication per year per group or laboratory). Subsequently, we are able to track the progress of these research groups and to orient our research goal in order to not overlap with others.
- A qualitative analysis to explore the contents of each pertinent paper. In this step, scientific results as well as methodology and approaches were analyzed. Information from articles was extracted and summarized using EndNote and Office Excel software.

1.3 OVERVIEW AND TREND (QUANTITATIVE ANALYSIS)

Figure 1-10 provides information about the number of publication in database WoS between 1984 and 2013 for the four keyword groups G1, G2, G3, G4. Clearly, a same increasing tendency is observed in all key word groups.

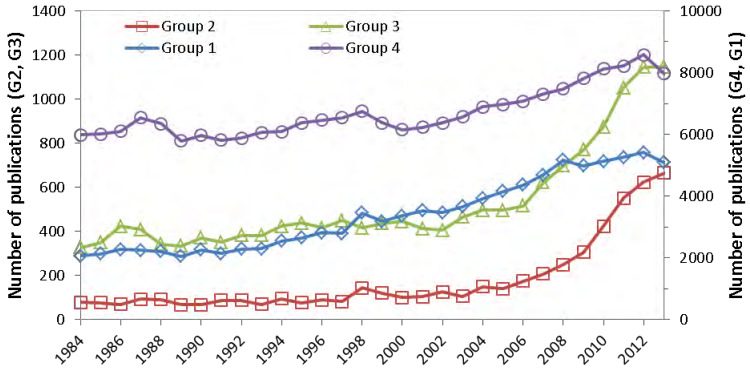

Figure 1-10. Number of publications since 1984 by group of key word (database WoS) with Group 1 = rheo* OR visco* OR newt* , Group 2 = lignocellulo* OR bagasse* OR "pulp paper", Group 3 = pretreatment OR organosolv and Group 4 = hydrolys* OR enzym* OR bioconver* OR biocatalys*.

According to the line graph, the total number of publication on the rheological field (G1) and enzyme/hydrolysis field (G4) tended to increase regularly apart from some variation, reached respectively around 5500 and 8500 publications in 2012. As for G2 (lignocellulose matrix) and G3 (pretreatment), the trend revealed a similar tendency in the first two decades then followed by a sharp grow and a peak reached in 2012: around 700 related publications for G2 (≈3 fold increase in 10 years) and 1100 publications for G3. It can be explain by the attention given to pretreatment of the lignocellulosic biomass that just appeared in the 20 recent years in the need of new energy source. This is also related to the changes from 1st to 2nd generation of bioethanol. Searching result from database Science Direct and Engineering Village was not shown.

Following the graph in **Figure 1-11,** the cumulated number of publications in the last 20 years for the different profiles was illustrated. From all database, 140 papers were identified. It was interesting that, despite the same level before 1993, profile 4* that is related to physical approach of enzymatic hydrolysis of biomass, contributed the highest number of publications

(48/140) counted until 2014. This figure demonstrated the advent of a new research strategy concerning hydrolysis of biomass by enzymes: not only on the point of view bio-chemical but also to approach the phenomenon by physical analysis. The physical parameters, such as rheological behavior of lignocellulosic suspensions or viscosity evolution during enzymatic hydrolysis played an important role and strongly affected the final bioconversion yield.

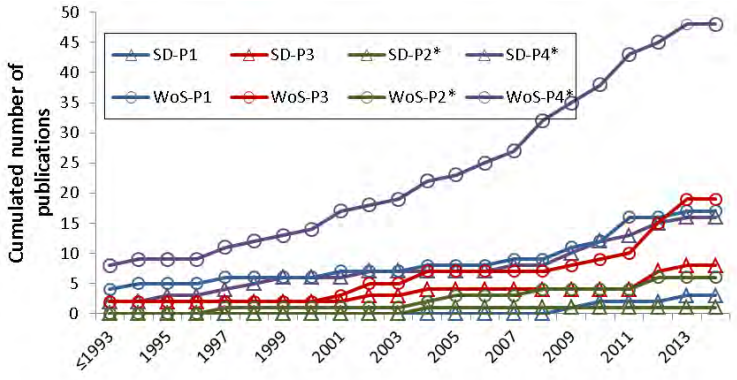

Figure 1-11. Cumulated number of publication since 1984 by profile and database with SD: Science Direct, WoS: Web of Science, P1 = G1 AND G2, P2* = G1 AND G2 AND G3, P3 = G2 AND G4 AND "kinetics", P4* = G1 AND G4 AND TOPIC(biomass).

Figure 1-12 represents the repartition of all publications by country. Statistically, with 35.6 % of all publication, USA has left China (12.3 %) and Brazil (10.5 %) far behind. The others country that took part in the competition were left with the modest number of publication in this domain.

In term of laboratory, the biggest contributor was NREL (National Renewable Energy Laboratory - USA) followed by UFRJ (Federal University of Rio de Janeiro) and Lund University, VTT Research Center and University Helsinki. The majority of publications during this period were from USA, with 9/25 from NREL.

Table 1-3 illustrates the statistic of publication by biomass type arranged in 4 mains categories: academic, agriculture byproduct, wood and paper industry and others. It is clearly observed that there were a huge number of lignocellulosic materials that has been studied. This may be related to the geographic position of each country that is suitable for specific crops. Among these biomasses, many publications in the domain aimed to valorize corn stover and sugarcane bagasse. Paper pulp and avicel were also focused.

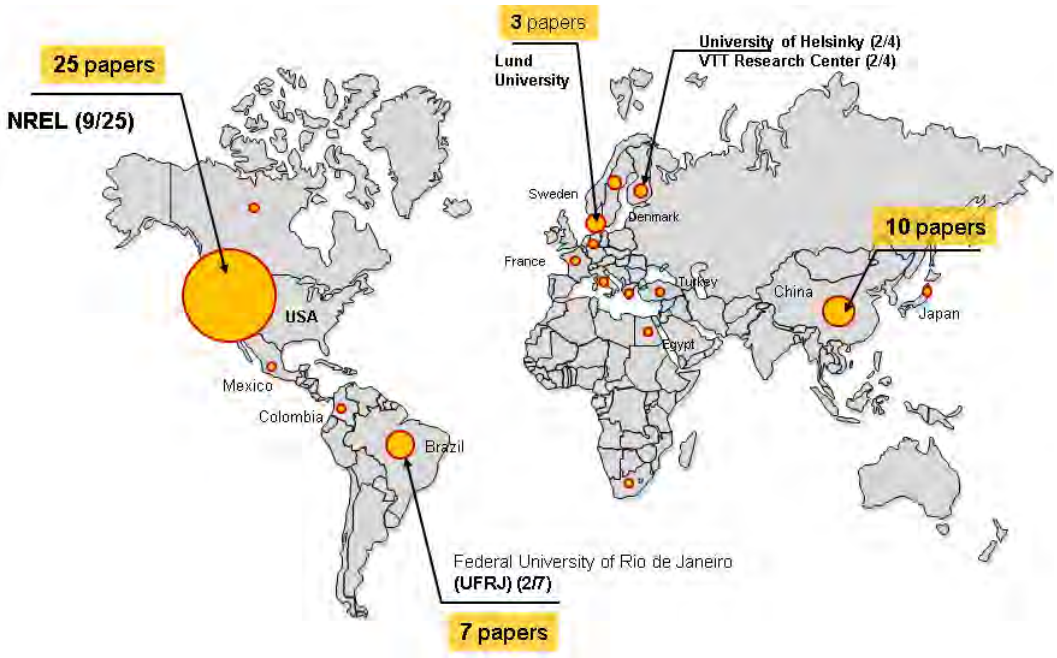

Figure 1-12. World publications by research groups, period 1991-2016.

Table 1-3. Number of publication by biomass types, period 1991-2016..

Biomasse type	Academic	Avicel (microcrystalline-cellulose)		6
		NFC (nano- fibril cellulose)		1
		Xylan		2
		Filter paper		**4**
	Agriculture by-product	CS: corn stove		10
		Bagasse	**SCB: sugar cane**	**10**
			AB: agave	1
			SSB: sweet sorghum	1
			RS: rice	1
		Straw	BS: barley	1
			WS: wheat	4
	Wood & paper industry	**Paper pulp**		**5**
		SD: sawdust		2
		Wood & wood chip		2
	Others plants	AD: arundo donax		2
		SG: switch grass		3

Corn is the main agriculture plant in America (especially in USA and Brazil). Following the statistic of United States Department of Agriculture (USDA), the corn production of USA in 2013/2014 was 353.74 million metric tons (MMT), accounted 35.8% of the worldwide production (988.57 million metric tons). With a chemical composition of 35-40% cellulose (Mosier, Wyman et al. 2005), corn stove is showing a good perspective for future feedstock for

lignocellulosic bioethanol production. This also explained why all researches from NREL (USA) were carried out on pretreated corn stover.

As for sugarcane bagasse, the advantages that made it promising for future application are

- High percentage in cellulose, usually 43 - 47 %w/w with a simple chemical composition (probably cellulose, hemicellulose, lignin) without any metallic compound (silica, rice straw) or high DP organic compound (latex, rubber wood)
- Sugarcane was collected from sugar factories. At the end of the process, bagasse was stored in the factory and can be used for bioprocess without any extra cost for collecting.
- Sugarcane bagasse is an abundant lignocellulosic resource. It is the principal crop in many countries around the word especially Brazil and South Asia country.

The researches on bioethanol production from lignocellulose showed an increasing trend in term of quantity, leading by countries where the lignocellulosic resource is abundant. Among lignocellulosic resources, corn stover and sugarcane bagasse were the most investigated feedstocks until now. This may be assumed by the advantages in chemical composition of these materials as well as its abundant quantity. From the number of publication per key word profile, it was clearly found that the physical approach is a new approach to investigate the enzymatic hydrolysis of lignocellulosic materials.

1.4 ENZYMATIC HYDROLYSIS OF LIGNOCELLULOSIC MATERIAL

Hydrolysis is a key step in the process of 2nd generation bioethanol production that allows the bio-conversation of lignocellulosic material (almost cellulose and hemicellulose) into fermentable sugars (glucose, xylose). For many years, the aim of research on enzymatic hydrolysis of lignocellulosic material was the high cellulose – glucose conversion yield. At the moment, with the persistent efforts in enzyme engineering for new generation of lignocellulolytic cocktail and in optimization of pretreatment process, the hydrolysis yield reached more than 80 % for some specific substrates (sugar cane bagasse, corn …). Although, in order to improve process viability, the enzymatic hydrolysis have to be performed at high concentration of raw material to provide higher end product concentration for the later fermentation. However, process at high solids loading, more challenges such as mixing, transfer limitation, end-product inhibition will be appeared. It is important to control those factors in order to achieve pertinent hydrolysis yield at high dry matter content.

From the working database, publications were analyzed and specific informations were extracted. Three principal points of interest were focalized

- Specific and dedicated reactor and mixing system to investigate the hydrolysis of lignocellulosic suspension
- Hydrolysis strategies and their performances
- Rheological approach during hydrolysis

In addition, most pertinent publications related to SCB and PP were summarized and presented in **Table 1-5**.

1.4.1 Reactor and mixing system

Poor mixing capacity might lead to limitation in transfers (momentum, mass, heat) and in enzyme and substrate distribution that negatively affect process efficiency. The first problem to solve in the process at high insoluble solids loading is mixing capacity of reactor system.

Usually, at lab scales, shake flasks are used to hydrolyze substrate at low solids loading (< 10 %w/w). Under concentrated conditions (superior to 15 %w/w solid loading), the flask

becomes ineffective and clearly inappropriate to hydrolyse of lignocelluloses substrates (Jørgensen, Vibe-Pedersen et al. 2007, Hodge, Karim et al. 2008, Roche, Dibble et al. 2009a). A poor mixing capacity, a limitation in mass transfer, a heterogeneous enzyme distribution and a local hydrolysis are commonly reported. Unfortunately, there were no standard rules to design bioreactor dedicated to high dry matter hydrolysis. Many research group in all around the world proposed their own models either horizontally or vertically to ensure bulk fluidity and homogeneity (Rosgaard, Andric et al. 2007, Kristensen, Felby et al. 2009, Roche, Dibble et al. 2009a, Roche, Dibble et al. 2009b, Matsakas and Christakopoulos 2013). Currently, the most promising systems are: (i) cylindrical horizontal or vertical reactor placed on rotating shaft and working at low angular velocity and (ii) stirred reactor equipped with singular and home-made impellers. A short description of original device is developed hereafter.

1.4.1.1 Horizontal rotating or rolling bioreactors

Matsakas and Christakopoulos (2013) studied the liquefaction of pretreated sweet sorghum bagasse at 18 % w/v with a reactor vertically placed drum and a rotating shaft which rotate at 7 rpm and was programmed to shift every minute. Promising cellulose – glucose conversion rate (65 %) was received after 24 h hydrolysis using Ctec2.

A rotating shaft systems but with a horizontally five-chambered reactor was also used in the research on the hydrolysis of steam pretreated wheat straw by Denmark researchers Jørgensen, Vibe-Pedersen et al. (2007) **Figure 1-13A**. This reactor consisted of a horizontally placed drum divided into five separate chambers, each 20 cm wide and 60 cm in diameter. A horizontal rotating shaft mounted with three paddlers in each chamber was used for mixing and agitation. A 1.1 kW motor was used as drive and the rotation speed could be controlled between 2.5 and 16.5 rpm. The direction of rotation was programmed to shift twice per minute between clock and anti-clock wise. A water-filled heating jacket on the outside enabled the control of the temperature up to 80 ºC but no cooling system was installed. Enzymatic hydrolyses were carried out from 20 to 40 % w/w substrate content using this reactor. Final results showed the cellulose conversions rate ranged between 30 and 50 % after 96h, depending on initial solids loading content. Two years later, another group from Denmark, Kristensen, Felby et al. (2009) used the same reactor at rotational speed approximately 6 rpm to hydrolyze filter paper at 20 % w/w initial solids content. Final result showed a yield of 38.6 % conversion after 48 hours of hydrolysis.

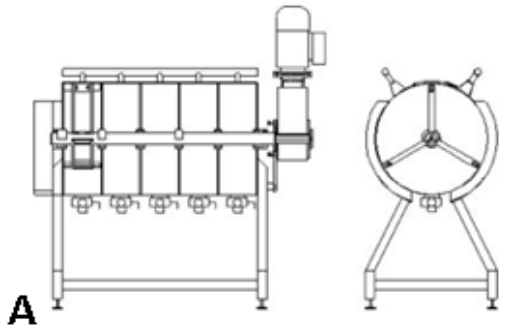

Five-chambered reactor (Jørgensen, Vibe-Pedersen et al. 2007, Kristensen, Felby et al. 2009)

Roller bottle reactor (RBR) (Roche, Dibble et al. 2009a, Roche, Dibble et al. 2009b)

High-solid bioreactor (HSBR) (Roche, Dibble et al. 2009b)

Figure 1-13. Illustration for horizontal bioreactors reported from the literature.

From United State, other types of reactor using roller polypropylene bottle horizontally rotated (RBR - **Figure 1-13B**) and horizontally rotating paddles (HSBR - **Figure 1-13C**) were reported (Roche, Dibble et al. 2009a, Roche, Dibble et al. 2009b) with a promising yield. For RBR type, it consisted of a 2 L wide-mouth polypropylene bottles (Thermo Fisher Scientific, Inc.,Waltham,MA). These roller bottle reactors (RBRs) were rotated horizontally using a modified three deck Roller Apparatus (Bellco Biotechnology, Vineland, NJ). The roller apparatus was encased by a custom built incubator heated via a steam-to-air heat exchanger. For HSBR type, it consisted of a 5 L horizontally mounted reactor vessel with eight paddles and wiper blades mounted on a horizontal rotating shaft. The wiper blades clear the wall of the reactor to enable mixing at high-solids concentrations. Temperature control was achieved by using an external resistance heating pad. The entire reactor was insulated to minimize heat loss. Both reactors working at low mixing speed (≤ 20 rpm) achieved around 70 % conversion yield of cellulose from dilute acid pretreated corn stover at 20 % w/w solids loading. It is important to notice that, up-scaling the experiment in rotated rolling bottles from 125 mL to 250 mL and 2 L, the enzymatic saccharification reactions are not appreciably different in term of conversion yield.

It is interesting to point out from these publications that the horizontal mixing or shaking system which requires very low rotational speed but provides promising performances. However, the energy required for mixing was not mentioned in these studies. In addition, the *in-situ* rheological investigation during enzymatic hydrolysis using these reactors seems to be difficult to establish.

1.4.1.2 Vertical stirred bioreactors

In parallel with the studies on horizontal reactor previously discussed, vertical stirred bioreactor was also investigated since 2007 by a Denmark group (Rosgaard, Andric et al. 2007). In their study, 6 custom-made impeller systems each using three sets of three-winged blades which were distributed along a rod connecting to the motor running at 57 rpm equipped in 2 L bottle. The whole system was incubated in a water bath at 50 ºC to carry out the hydrolysis experiments of pretreated barley straw up to 15 % w/w dry matter. The enzyme dosages were 7.5 FPU/g DM of Celluclast 1.5L (cellulase cocktail) and 13 CBU/g DM of NS 188 (β-glucosidase). Final glucose yield achieved was 80 % after 72 hour hydrolysis.

Stirred bioreactor was also reported in the research of Palmqvist and Lidén (2012). In this study, the hydrolysis of steam pretreated arundo donax and spruce chips (10 – 20 %w/w) were carried out in a 3 L bioreactor (Belach Bioteknik, Stockholm, Sweden) with an inner diameter of 14 cm, at a working weight of 1.5 kg. The reactor was equipped with an anchor impeller with

a diameter of 13 cm and a blade width of 2 cm. The reactor was equipped with a strong motor (down-geared fivefold) able to measure the torque on the stirrer shaft which allowed monitoring of torque and power input throughout hydrolysis. At enzyme loading 0.1 g/g water insoluble content, their results reported approximately 30 % conversion yields for both substrates after 48 hours of hydrolysis at constant impeller speed (10 rpm)

Peg-mixer systems (**Figure 1-14**) manufactured by the Pulp and Paper Research Institute of Canada (Pointe Claire, QC) was used for hydrolysis of organosolv pretreated poplar at high consistency (Zhang, Qin et al. 2009). The horizontal peg mixer has a working volume of 9000 mL and approximately 800 g (oven dried weight) substrate was used for batch hydrolysis under the conditions of temperature 50 ºC, pH 4.8 and enzyme dosage 20 FPU (celluclast 1.5L) + 80 CBU (Novozym 188) per gram of cellulose in the substrate. The mixing speed was set at 20 rpm and hydrolysis time was 96 h. The final cellulose conversion rate achieved 85 % at 20 % w/w initial solids loading. More recently, stirred reactor using peg-mixer systems were investigated. Caspeta, Caro-Bermudez et al. (2014) designed a double jacket mini-bioreactor with a vertical peg-mixer for hydrolysis agave bagasse organosolv-pretreated (**Figure 1-15**). The reaction temperature was maintained at 50 ºC by water circulation. At mixing speed 150 rpm, the result showed 90 % conversion yield at 20 % w/w solids loading. it was observed that at loading of raw material increased up to 30 % w/w, a glucose yield of 70 % was recognized. Comparing to other reactor types that previously discussed in **§0**, the conversion yields were really impressive for peg-mixer systems. Both studies of Caspeta and Zhang reached over 70 % bioconversion rate for different substrates. This can be assumed for the high enzyme loading (20 FPU/g cellulose in both cases) but the contribution of impeller design cannot be negated. Unfortunately, rheological approach was not considered through these studies. The biochemical analysis, in this case, was not able to quantitatively describe the contribution of impeller design during enzymatic hydrolysis.

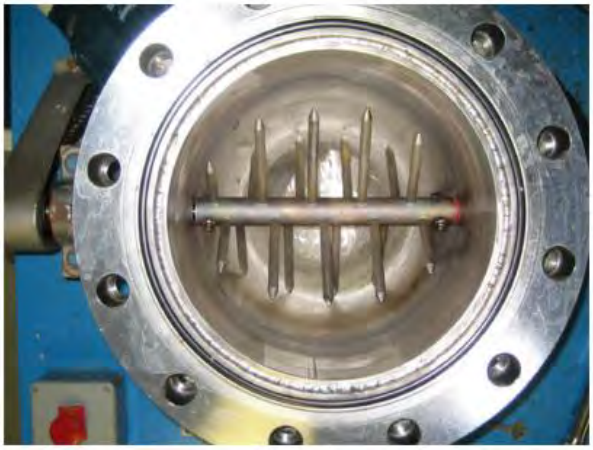

Figure 1-14. The inner chamber of the laboratory peg mixer (Zhang, Qin et al. 2009)

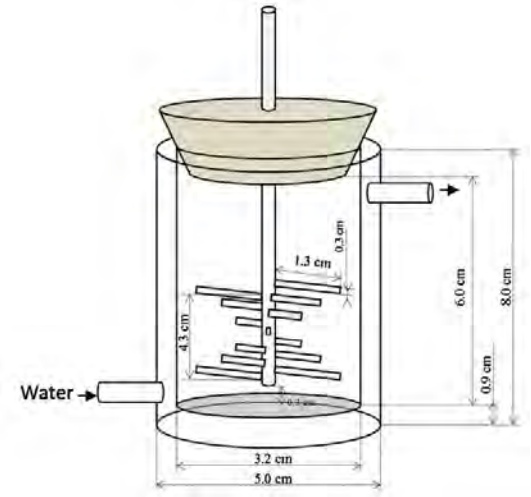

Figure 1-15. Peg-mixer bioreactor (Caspeta, Caro-Bermudez et al. 2014)

Other impeller design for hydrolysis of lignocellulose was reported by Correa, Badino et al. (2016a). Their system consisted of a homemade 3 L working volume stirred tank reactor with four baffles (D = 0.160 m; H = 0.370 m). A motor (Model ARB71A6-E2260, Voges, Brazil) was used to ensure the mixing by two Elephant Ear impellers. This configuration was selected for the best performance in sugarcane hydrolysis experiments carried out in batch mode by Correa, Badino et al. (2016a). Fed-batch enzymatic hydrolysis (Correa, Badino et al. 2016) were done to explore the use of their systems and the cellulose conversion yield ranging from

40 to 55 % at final solid loading 20 % w/v with different feeding strategies of enzyme and substrate was reported. From our standpoint, the original point of this configuration is the way that author design their impellers. The Elephant Ear up-pumping impeller located at the bottom of reactor enables to avoid the substrate decantation during experiment. In parallel, the top Elephant Ear impeller (down pumping) ensures the homogenization of suspension in the upper region of the reactor. The combination of two impellers clearly reflects the effort to improve mixing capacity at concentrated condition.

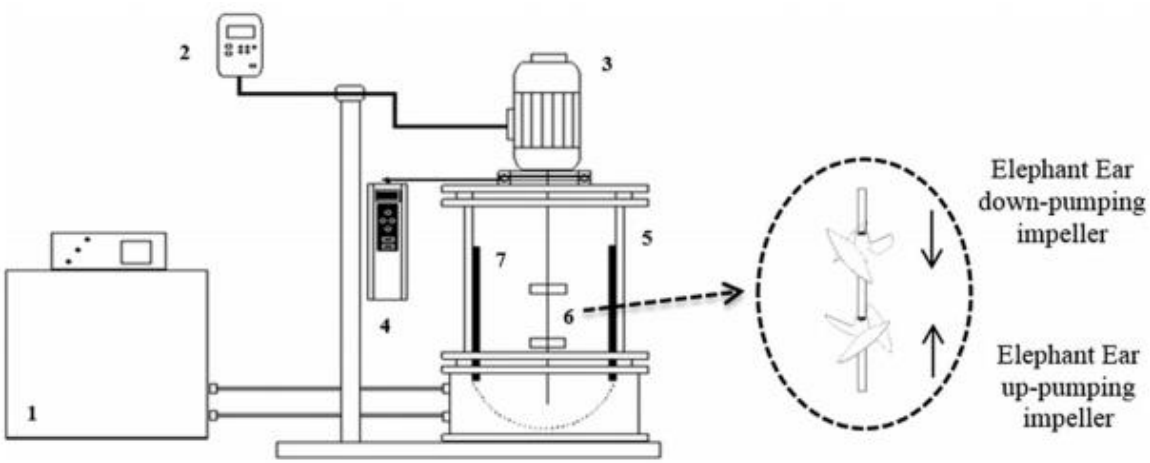

Figure 1-16. Stirred bioreactor with elephant ear impeller from Correa, Badino et al. (2016)

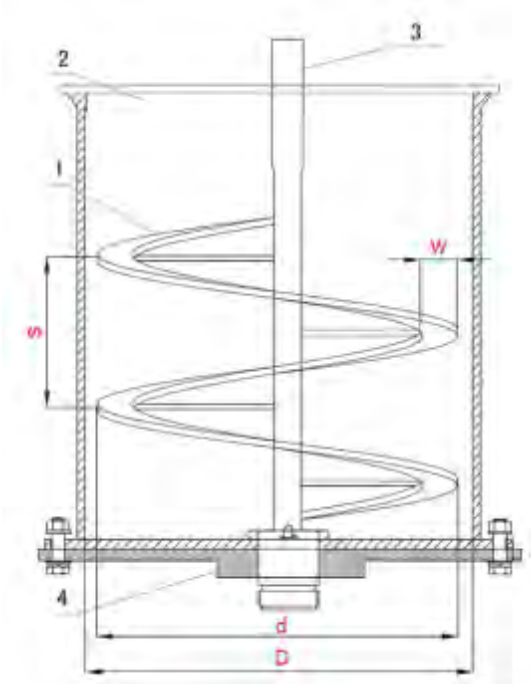

1: single helical ribbon impeller

2: material inlet

3: agitating shaft for driving the helical ribbon impeller

4: material outlet

d and D: the outer and inner diameters of the helical impeller

w: the thickness of the helical impeller

s: the pitch size of the helical impeller

Figure 1-17. Schematic diagram of the mock-up reactors from Zhang, Zhang et al. (2014)

By rheological approach, the reactor design was investigated in the research of Zhang, Zhang et al. (2014) for the pretreatment of corn stover slurries. Their three reactors at different scales were made using PMMA polymer material. The helical ribbon impeller was welded on the central shaft, and the motor was mounted on the top of the impeller to form axial upwelling flow (**Figure 1-17**). The torque meter HX-901 (Huaxin Mechanical and Electrics Co., Beijing,

China) was installed for the measurement of agitation torque. In the three reactors, 150 g, 1.50 kg, and 15.0 kg of corn stover (dry base) was charged and the torque was recorded every 5 s at desired agitation rate in the range of 50 – 100 rpm. Two year after their first publication, this rheological approach was continuously used for the study of corn stover and wheat straw at extreme high substrate loading condition (Hou, Zhang et al. 2016). It is interesting to note that the rheological methodology used by Zhang, Zhang et al. (2014) and Hou, Zhang et al. (2016) was exactly similar with ours (Nguyen, Anne-Archard et al. 2013): suspension viscosity (μ) was calculated from *in-situ* torque measurement and imposed mixing rate through a power consumption curve that reflects the one to one relation between power number (Np) and Reynold number (Re). Even when the reactor from this study was designed for pretreatment process, its use for enzymatic hydrolysis will be always possible. The biggest advantage in this configuration is the ability of *in-situ* viscometry measurement that provides additional information to evaluate and optimize the process efficiency.

1.4.2 From hydrolysis strategies to bioconversion yields

From the biochemical standpoint, the main constraint when working at high substrate loading is the inhibition effect of end product on cellulase activities. Recent works proved the inhibition effect of glucose, cellobiose and ethanol on endo-glucanase, cellobio-hydrolase and β-glucosidase (Z, X et al. 2004, Kristensen, Felby et al. 2009, Miao, Chen et al. 2012). The importance of β-glucosidase in the cellulase mixture was also investigated on switchgrass pretreated by different techniques (Pallapolu, Lee et al. 2011). It was reported that the effect of β-glucosidase supplementation was discernible only at the early phase of hydrolysis where accumulation of cellobiose and oligomers was significant. Until now, studies aim to optimize enzyme loading ratio in order to minimize the accumulation of end products (cellobiose and others oligomers) and further increase cellulose to glucose conversion yield.

1.4.2.1 Impact of substrate

Following bibliographic research, it seems that the role of each factor influencing glucose yield is not clearly understood and strongly depends on the biomass type. Palmqvist and Lidén (2012) investigated the effects of an increase in water insoluble content at constant mixing speed (N = 10 rpm) using a bioreactor equipped with an anchor impeller. At the same enzyme loading ratio of 0.1 g Cellic Ctec2 per gram water insoluble solid, it was found that an increase in solids loading of arundo donax from 10 to 20 % w/w resulted in a decrease in final glucose conversion yield. However, for spruce, it was unexpectedly that the similar experiments revealed an improvement in glucose yield at higher concentration of initial solids. The interaction between enzyme loading and solids loading for hydrolysis of specific lignocellulosic substrate is thus needed to be investigated.

1.4.2.2 Operation conditions

Figure 1-18 illustrates the enzyme loading ratio (at FPU/g cellulose) at specific solids loading of batch hydrolysis. It is clearly seen that, most research from the last decade focused on hydrolysis at average amount of enzyme (below 20 FPU/g cellulose). Statistically, 63.8 % of experimentales points of the figure **Figure 1-18** was localised in the zone of 3 - 25 FPU/g cellulose for a solids loading of 10 to 20 % w/w. In some studies, the enzyme loading ratio were slightly higher and reached well under 25 FPU/g cellulose (Dunaway, Dasari et al. 2010, Carvalho, Sousa et al. 2013). At 10 - 20 % solid loading, all publications showed the interest to hydrolysis with low enzyme concentration (from 5 to 10 FPU/g cellulose). Even in some research, where authors tried to work with extra-high solids loading (until 40 % w/w dry matter), the ratio of enzyme is maintained at a low level, around 7.5 FPU/g cellolose (Dasari

and Berson 2007, Kristensen, Felby et al. 2009) and even lower (Jørgensen, Vibe-Pedersen et al. 2007).

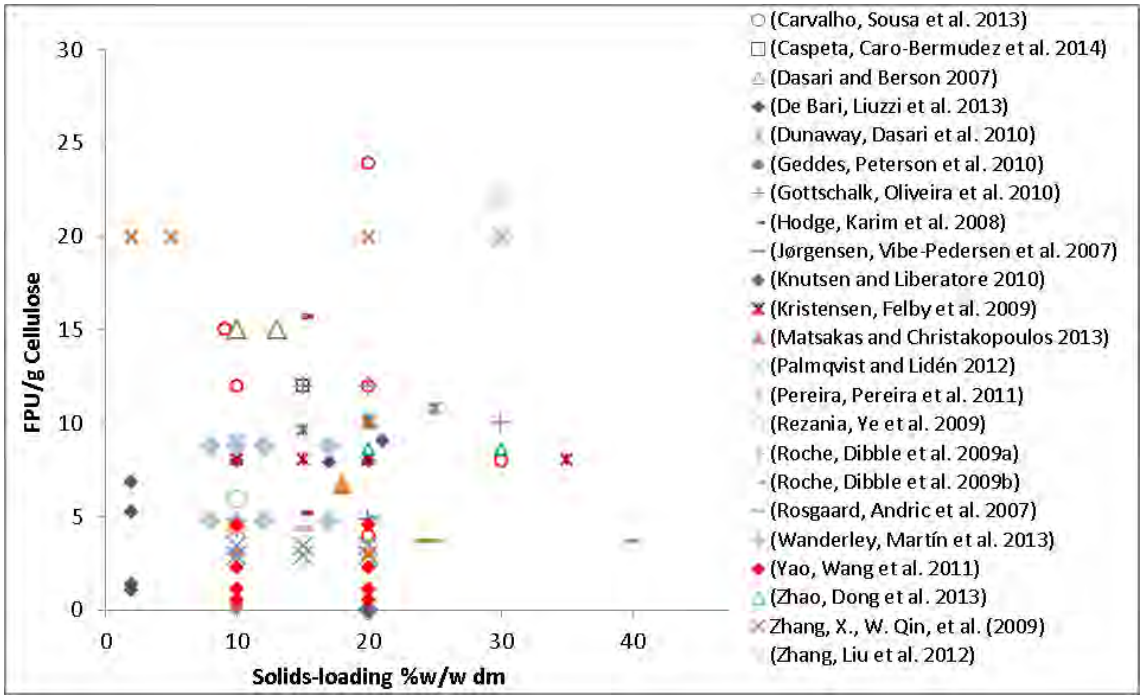

Figure 1-18. Enzyme and solid loading from literature.

Fed-batch is known as the best strategy to increase final solid loading. By adding substrate periodially during enzymatic digestion, fed-batch mode allows slurry to be liquefied before substrate adding, which maintains the suspension viscosity that avoid transfer limitations. Several strategy was investigated and based on feeding interval as well as feeding quantity (substrate feeding & enzyme feeding). The fed-batch strategies for different substrates are summarized in **Table 1-4**.

Feeding strategy was used in the research of Zhang, Liu et al. (2012) on wheat straw and SCB: the enzymatic hydrolysis started at 9 % w/v initial solid content and then 8 %, 7 % and 6 % w/v solid was fed at 8, 24, 48 h respectively. Lu, Wang et al. (2010) studied the fed-batch hydrolysis of wheat straw at initial substrate concentration 15 % w/v. This was then followed by two adding step of 7.5 %w/v to reach final substrate concentration equal to 30 %. It is observed that, for fed-batch up to ≥ 20 % solid loading, most proposed strategies consisted of an initial substrate loading that was always higher than the subsequent added quantities. It may be due to the fact that final product (mainly glucose) was accumulated in the suspension that slowdown enzymatic reaction rate.

It is interesting that the fedding strategy was investigated not only for substrate but also for enzyme. Through the analysis presented in **Table 1-4**, enzyme was totally added at the beginning of hydrolysis or partially fed with substrate. Theoretically when all enzyme is added at t = 0 h, the enzymatic digestion will progressed at higher rate corresponding to the higher ratio E/S. Then during enzymatic reaction, if the hydrolysis rate can compensate the increasing in substrate concentration by feeding, the reaction might be maintained at equilibre state of [S] under hypothesis of negligible enzyme degradation or denaturation. However, this ideal equilibre state was not reported by any author. On the other hand, considering the loss in enzyme activity, mainly due to irreversible absorption on lignin or protein denaturation, enzyme was fed with substrate in order to maintain high reaction rate. It was reported that this strategy resulted in lower final glucan conversion compared to the first strategy (all enzyme added

initially) for the hydrolysis of pure cellulose fibers (Cardona, Tozzi et al. 2015). Previously, Rosgaard, Andric et al. (2007) stated similar glucose conversion yield achieved from barley straw for both strategies but confirmed better liquefaction (by monitoring suspension viscosity) achieved in strategy 1 at the first stage of hydrolysis.

In these publications, most authors did not provide any explaination for the choice of substrate quantity in each feeding step. No scientific approach to control fed-batch hydrolysis is reported until 2015. Cardona, Tozzi et al. (2015) seems to be the first group who proposed control of the process flow based on the real yield stress monitoring to clearly identify the feeding point as well as feeding quantity . The approach was purely rheological and consisted in a on-line measurement instrument (magnetic reasonance imaging in this case) that monitored the suspension yield stress during enzymatic digestion (**Figure 1-19**). Biomass was added until the yield stress reached or exceeded specific value depending on substrate properties and equipement used (15 Pa and 100 Pa for Solka-Floc C100 and 200EZ fibers, respectively). Once the slurries are hydrolyzed, new feeding step will be started when yield stress reachs a steady state. This control loop was repeated until the end of hydrolysis.

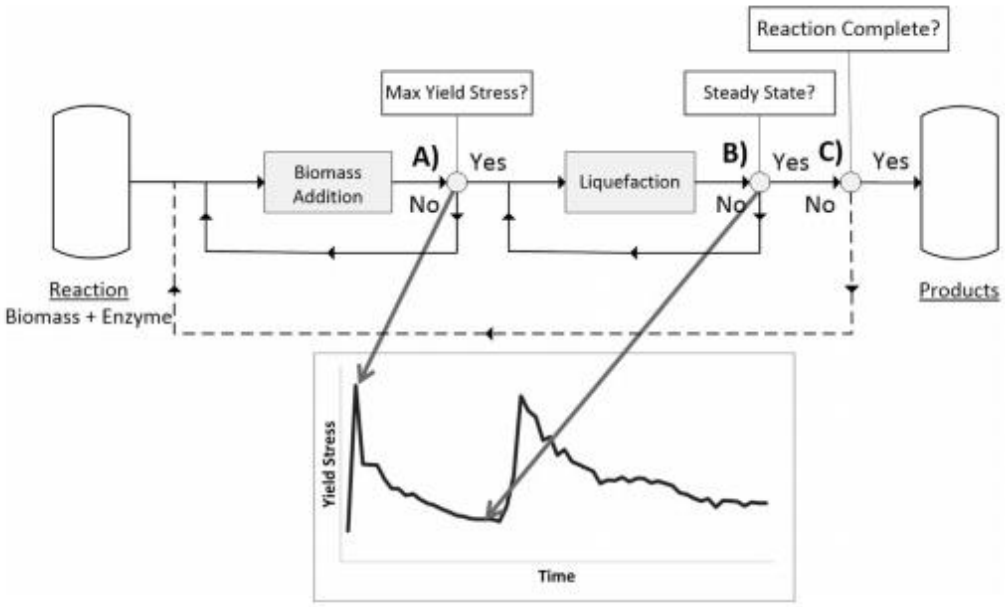

Figure 1-19. Fed-batch process control scheme proposed by Cardona, Tozzi et al. (2015)

Table 1-4. Operating conditions for fed-batch hydrolysis

Substrate	Substrate feeding strategy (% w/v)	Total solids & total time	Enzyme dosage	Enzyme feeding strategy	Notes	Ref
SCB	3 equal feds (6.67 %) at 0h, 12h, 36h	20 % (216h)	10FPU/gDM	with substrate feeding	Similar efficiency for two strategies	(Zhao, Dong et al. 2013)
	3 equal feds (6.67 %) at 0h, 12h, 48h	20 % (216h)	10FPU/gDM	with substrate feeding		
SCB	8% + 1% every 12h	17 % (120h)	10FPU/gC	not specified	Highest glc production at 12 hours feeding interval V = 100 mL	(Wanderley, Martín et al. 2013)
	8% + 1% every 24h	12 % (120h)	10FPU/gC	not specified		
	8% + 1% every 48h	10 % (120h)	10FPU/gC	not specified		
SCB	10 % + 5 % (1h) + 5 % (2h)	20 % (96h)	10FPU/gDM	initial time	Enzyme feded with substrate showed best final glucose yield.	(Correa, Badino et al. 2016)
	5 % + 5 % (0.5h) + 5 % (1h) + 5 % (2h)	20 % (96h)	10FPU/gDM	initial time		
	5 % + 5 % (2h) + 5 % (12h) + 5 % (24h)	20 % (96h)	10FPU/gDM	initial time		
	5 % + 5 % (2h) + 5 % (12h) + 5 % (24h)	20 % (96h)	10FPU/gDM	with substrate		
Recycled aper	5 % + 3 % (24h) + 2 % (48h)	10 % (72h)	15FPU/gDM	with substrate feeding	Fed-batch hydrolysis and SSF	(Ballesteros, Oliva et al. 2002)
Corn stover	15 % + 5 % (2h)	20 % (96h)	20FPU/gDM	with substrate feeding	103.3g/L glucose at solid loading 30% w.v (72.5% conversion yield)	(Lu, Wang et al. 2010)
	15 % + 10 % (2h)	25 % (96h)	20FPU/gDM	with substrate feeding		
	15 % + 7.5 % (2h) + 7.5 % (4h)	30 % (96h)	20FPU/gDM	with substrate feeding		
Corn stover	12 % (initial)	25% (288h)	10.7FPU/gC	with substrate feeding	Reactor 7L	(Hodge, Karim et al. 2009)
	15 % (initial)	30% (188h)				
Barley straw	5 % + 5 % (6h) +5 % (24h)	15 % (72h)	7.5FPU/gDM	initial time	Stronger μ reduction when all enzyme added at t=0h but similar glucose yields for two strategies.	(Rosgaard, Andric et al. 2007)
	10 % + 5 % (24h)	15 % (72h)	7.5FPU/gDM	initial time		
	5 % + 5 % (6h) +5 % (24h)	15 % (72h)	7.5FPU/gDM	with substrate feeding		
	10 % + 5 % (24h)	15 % (72h)	7.5FPU/gDM	with substrate feeding		
Wheat straw	9 % + 8 % (8h) + 7 % (24h) + 6 % (48h)	30 % (144h)	9.6FPU/gDM	initial time	Final glucose yield ~40%	(Zhang, Liu et al. 2012)
SCB	9 % + 8 % (8h) + 7 % (24h) + 6 % (48h)	30 % (144h)	9.6FPU/gDM	initial time	Final glucose yield ~55%	
Solka-Floc 200EZ	16.9 % + substrate fed whenever yield stress > 100 Pa	30.7 % (12h)	4.3FPU/gDM	initial time	10L bioreactor All enzyme initial resulted in higher glucan conversion yield (47% versus 40%)	(Cardona, Tozzi et al. 2015)
SolkaFloc C100	8.7 % + substrate fed whenever yield stress > 15 Pa	19.3 % (12h)	5FPU/gDM	initial time		
SolkaFloc C100	8.7 % + substrate fed whenever yield stress > 15 Pa	19.3 % (12h)	5FPU/gDM	with substrate feeding		

1.4.2.3 Glucose conversion yields

In term of hydrolysis yield, there is no general tendency reported from bibliography. Depending on type of biomass and hydrolysis conditions, final yields can be very different. **Figure 1-20** illustrates the cloud of point (glucose yield – enzyme loading) by solids loading range from 10 to 20 % w/w for diferent lignocellulosic biomass at different hydrolysis conditions. It is clearly seen that, up to 20 % w/w dry matter, High glucose yields can be reached around 80 % or even higher in many publications. Unfortunately, there were no common strategy or operating conditions that can be pointed out from these "best performances" studies.

In term of lignocellulosic substrate and pretreatment, ethanosolv pretreated agave bagasse (Caspeta, Caro-Bermudez et al. 2014), dilute acid pretreated corn stove (Roche, Dibble et al. 2009a), organosolv pretreated poplar and hard wood paper pulp (Zhang, Qin et al. 2009) and formilin pretreated sugar cane bagasse (Zhao, Dong et al. 2013) were reported with approximately 80 % glucan conversion rate under different hydrolysis conditions.

In term of enzymes, Caspeta, Caro-Bermudez et al. (2014) used a mixture of NS50013 and NS50010 from Novozymes at enzyme loading ratio ranged between 5 and 30 FPU/g solid and supplemented by 10 – 60 CBU/g solid. Their results showed final yields from 70 % to well under 90 % after 72 h hydrolysis. In the research of Roche, Dibble et al. (2009a), Spezyme-CP and GC220 were used for enzymatic hydrolysis of concentrated corn stover slurries (from 15 to 30 %w/v) at low enzyme loading (10 – 12 FPU/g cellulose). The best performances among all experiments in this study were 82 and 86 % conversion rate for Spezyme-CP and GC220, respectively. Another enzyme combination, Celluclast 1.5 L (20 FPU/g cellulose) and Novozyme 188 (80CBU/g cellulose) was tested (Zhang, Qin et al. 2009). This showed 84 % glucose yield after 96 h hydrolysis of hard wood paper pulp. Finally, the very promissing results recently came from the study of Zhao, Dong et al. (2013). Using a enzyme cocktail named C2 from Novozymes at 10 FPU/g solid, the final glucose conversion yields reached approximately 72 and 80 % after 196 and 144 h at solid loading 30 and 20 % w/v, respectively.

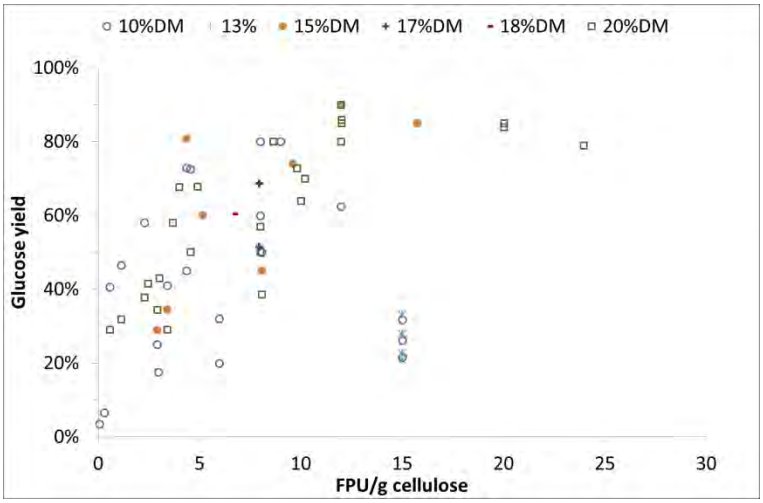

Figure 1-20. Cellulose to glucose conversion yield by enzyme loading at batch hydrolysis.

Regarding fed-batch hydrolysis, it is reported that most published researchs did not achieved good efficiency with fed-batch strategy compared to batch hydrolysis. **Figure 1-21** summarise the glucose yields extracted from several researchs on various biomass types and enzymes for fed-batch hydrolysis (Rosgaard, Andric et al. 2007, Hodge, Karim et al. 2008, Zhang, Qin et al. 2009, Roche, Dibble et al. 2009b, Geddes, Peterson et al. 2010, Zhao, Dong et al. 2013, Caspeta,

Caro-Bermudez et al. 2014). For most of listed work, the glucose yield varied from 30 to under 80 % depending on operating conditions (enzyme loading, solid loading, hydrolysis time). Zhang, Liu et al. (2012) reached approximatly 60 % glucose conversion from alkali-pretreated wheat straw after the first feeding with all enzyme added at the beginning. However, glucose conversion decreased with each successive feeding, reaching finaly nearly 40 % by 144 h and at 30 % final solid concentration. Also from this research, similar fed-batch strategy was applied on pretreated sugarcane bagasse. The cellulose conversion rate was nearly 40 % after the first feeding but it increased up to more than 55 % at the end of hydrolysis. Hodge, Karim et al. (2009) reported more than 80 % cellulose conversion after 7 days fed-batch hydrolysis at 10.7 FPU/g cellulose, final solid loading 25 % w/w. The long hydrolysis reaction time may be the reason for this high efficiency. Zhao, Dong et al. (2013) got better hydrolysis yield: 86.1 % of glucan conversion in fed-batch hydrolysis of organosolv pretreated sugarcane bagasse at final concentration 30 % w/w solids (3 equals substrate feeding).

Considering scale-up challenges for industrial applications, the strategy of fed-batch hydrolysis need to be rationally defined by taking into account hydrolysis yields, kinetics and energy consumption. Even in the research of Zhao and co-worker (the best one with 86.1 % glucose yield), experiments were conducted in shake flask at laboratory scale. Physical limitations of momentum, mass and heat transters as well as heterogeneous distributions of enzyme and substrate will become more and more significant when working at larger scale. In order to completely understand the factors influencing hydrolysis yield in fed-batch mode and to establish an efficient process control for fed-batch hydrolysis, research on both biochemical and physical approaches must be considered.

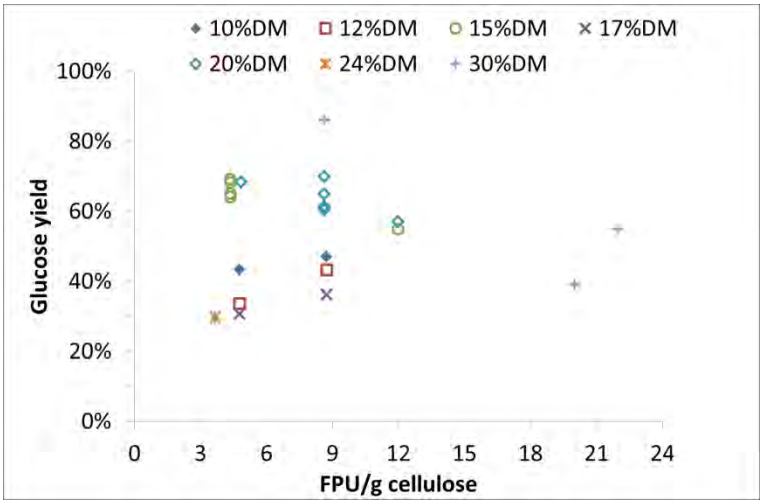

Figure 1-21. Cellulose to glucose conversion yield by enzyme loading at fed-batch hydrolysis.

1.4.3 Rheological approach on enzymatic hydrolysis

During enzymatic hydrolysis, an adequate mixing is required to ensure appropriate contact between lignocellulosic enzymes and cellulose and/or hemicellulose chains and also heat transfer. In order to understand the mixing phenomenon and to overcome the mass, heat and momentum transfer limitations, a physical approach of monitoring the enzymatic hydrolysis process is necessary. Among the physical properties to be studied, rheological behavior and particle morphology were considering as the most interested parameters from the recent decade. The rheological properties of lignocellulosic suspension before and during enzymatic hydrolysis will be summarized and presented hereafter.

1.4.3.1 Rheological properties of lignocellulosic suspension

Lignocellulosic suspensions are reported to behave as non-Newtonian fluids. Pimenova and Hanley (2003) observed a decrease in suspension viscosity of corn stover (10, 20 and 30 %) when increasing shear rate, that indicates shear-thinning properties. It is also reported that suspension viscosity strongly depends on applied shear rate for concentrated condition (30 %) but seems to be constant at dilute condition (5 %). This shear-thinning behavior is frequently modeled by a Power law $\mu = K \cdot \dot{\gamma}^{n-1}$, where μ is the suspension viscosity, n the power-law index (/) and K the consistency (Pa.s^{-n}). Shear-thinning behavior corresponds to power-law index strictly less than 1. Power law parameters for corn stover suspensions were also pointed out in this research, indicating an increasing trend with increased substrate concentration. Knutsen and Liberatore (2009) also stated the strong shear thinning properties of pretreated corn stover slurries, ranged from 5 to 17 % insoluble solid content. Similar conclusion on various lignocellulosic materials can be found easily from the literature (Rezania, Ye et al. 2009, Pereira, Pereira et al. 2011, Nguyen, Anne-Archard et al. 2013). Following bibliographic research, the lignocellulosic slurries were frequently described by the power law model for non-Newtonian fluids (Pimenova and Hanley 2004, Derakhshandeh, Hatzikiriakos et al. 2010, Dunaway, Dasari et al. 2010) even if extended models from the power law model can be proposed (Sisko, Cross, Powell-Eyring, Carreau…)

A viscoplastic behavior is often identified as concentration reaches the semi-dilute regime, but it is also observed in dilute regime. Viscoplastic fluids, also called yield stress fluids, do not flow when submitted to stress less than a threshold (yield stress). In a first approach, they can be considered as solid below this threshold. The relation between yield stress and other factors was well described for some specific biomass; especially dilute acid pretreated corn stove slurries. At 4 % w/w dilute acid pretreated corn stove, the yield stress of suspension was 820 - 980 Pa.s (Knutsen and Liberatore 2010). By increasing the volume fraction from 10 % to 30 % Dibble, Shatova et al. (2011) witnessed a raise on yield stress by approximately 100 folds. Similar tendency was also reported earlier (Roche, Dibble et al. 2009b). Particle size also affects the rheological properties of suspension. Following the study of Viamajala, McMillan et al. (2009), slurries containing larger particles exhibit higher yield stress than those containing smaller particles at the same solids concentration. Dibble, Shatova et al. (2011) compared mechanical and chemical pretreatments leading to similar particle size distributions (PSD). Their results revealed that the yield stress of suspension was not affected by mechanical pretreatment whereas it decreased with chemical one. On the other hand, Dasari and Berson (2007) found that smaller particles sizes lead to smaller suspension viscosity. It is interesting that the enzymatic conversion of cellulose to glucose was also boosted when hydrolyzing suspension of smaller particles. Dibble, Shatova et al. (2011) observed that the slurries with smaller mean particle diameters due to pretreatment are more digestible than their larger counterparts. However, mechanical size reduction on the same size scale does not increase enzymatic digestibility.

1.4.3.2 Suspension viscosity during enzymatic hydrolysis

The evolution of apparent viscosity of the suspension during enzymatic hydrolysis was observed in many works. Dunaway, Dasari et al. (2010) investigated the changes in viscosity during enzymatic saccharification of dilute acid pretreated corn stove slurries at high solids loading (10 - 25 % w/w dry matter) by Spezyme-CP. Their results showed that viscosity decreases dramatically in the first 8 hours. On steam pretreated sugarcane bagasse, after 5 hours of hydrolysis at 10 % w/w solids loading using Cellulase-W mixed with Novozyme 188, Geddes, Peterson et al. (2010) observed a drop by 88 % in relative viscosity. Similar viscosity trend was also reported in other publication for various substrates and operating conditions

(Pereira, Pereira et al. 2011, Nguyen, Anne-Archard et al. 2013, Correa, Badino et al. 2016). From all published works, the evolution of viscosity during hydrolysis can be divided in 2 phases with different velocities: i) a rapid decrease at the beginning of enzymatic reaction and ii) a steady state until the end of hydrolysis. The collapse in suspension viscosity was reported in parallel with the evolution in particle size distribution (Nguyen, Anne-Archard et al. 2013). However, the mechanisms of reaction to explain this evolution of suspension viscosity were not largely investigated. Understanding these mechanisms is necessary for optimization of process for high efficiency.

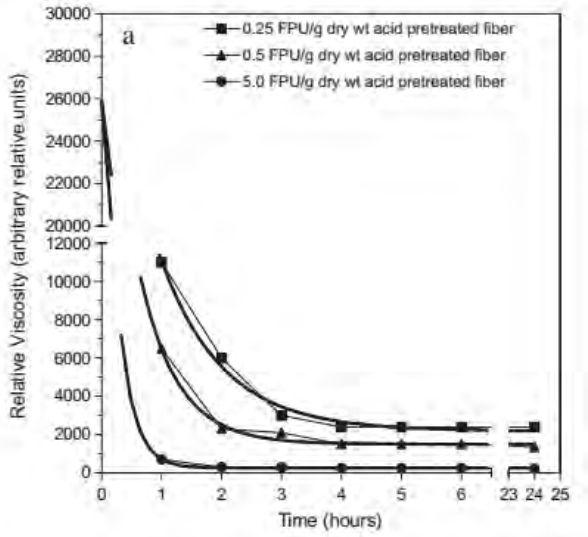

Figure 1-22. Evolution of suspension viscosity during enzymatic hydrolysis of sugarcane bagasse (from Geddes 2010)

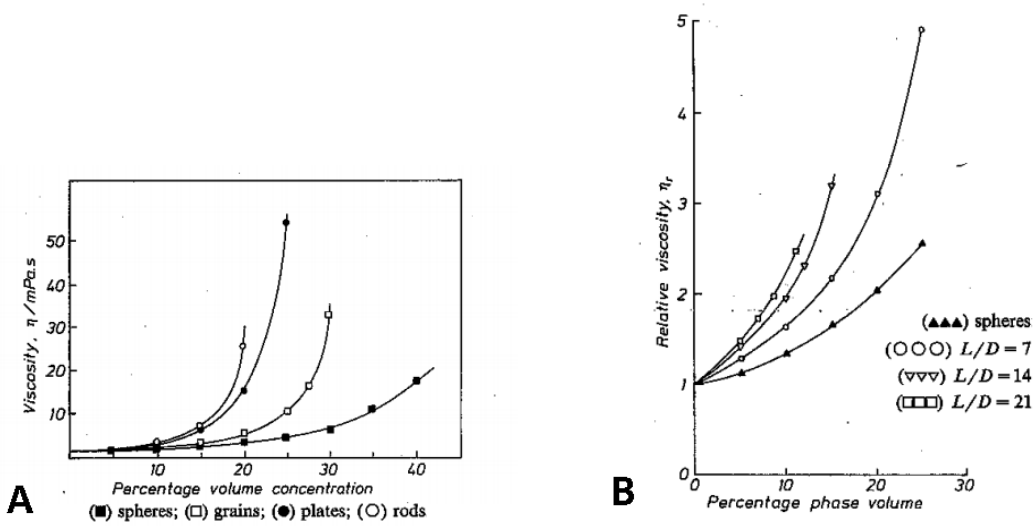

Figure 1-23. Dependence of the viscosity of glass particle suspensions of various shape from Clarke 1967 (A) and various length/diameter ratios (L/D) from Giesekus 1983 (B).

Suspension viscosity depends on several factors related to particle properties or operation conditions. The relative viscosity of suspension has been studied for more than 100 years (Barnes, Hutton et al. 1989, Quemada 2006). It has been observed that the rheological properties of these suspensions depend on the substrate concentration, the imposed mixing rate (related to shear rate) and the fiber properties (size, shape).

At given substrate concentration, suspension viscosity is affected by particle size and shape distribution. As the ratio length to diameter (L/D) growths, suspension became more viscous. Giesekus (1983) studied the dependence of glass fiber suspension viscosity on length/diameter (L/D) ratios (**Figure 1-23B**). This study revealed that the relative viscosity rose as the L/D proportion increased, or in other words, a suspension of longer fibers will possess higher viscosity than a suspension of shorter ones, all other things being equal. For lignocellulosic suspension that contains large amount of long and ramified fiber, as the fiber length growth, the interaction between particles will be strongly enhanced and consequently suspension viscosity rise. During enzymatic hydrolysis, long cellulosic fibers may be broken into shorter ones due to action of endo-glucanase. This mechanism, theoretically, will cause a decrease in suspension viscosity.

On the other hand, it was also reported that for all type of particle shape, an increase in particle volume fraction or substrate concentration led to a drastic rise in suspension viscosity. For glass fibers, both Clarke (1967) and Giesekus (1983) reported the strong dependency of suspension viscosity on particle volume fraction (**Figure 1-23**). Recently, results on academic particle (glass fiber) were confirmed on real lignocellulosic suspension. Nguyen, Anne-Archard et al. (2013) investigated the rheological properties of three cellulosic suspensions: microcrystalline cellulose (MCC), Whatman paper (WP), paper pulp (PP - hard and soft wood) at different substrate volume fraction. It was reported that suspension viscosities of WP and PP drastically increased with the rise in substrate volume fraction. Critical concentration points, indicating the change between dilute, semi-dilute and concentrated regimes were also pointed out. Similar conclusion was also revealed from the research on dilute acid pretreated corn stove: higher solids loading lead to higher viscosity of suspension (Dunaway, Dasari et al. 2010). The work of Knutsen and Liberatore (2009) revealed that from 10 %w/w to 25 %w/w of pretreated corn stover, viscosity of suspension were 100 to 1000 fold the water one. During the enzymatic digestion, cellulosic fibers (insoluble) were converted into glucose (soluble). This bioconversion led to a decrease in substrate concentration that theoretically will lead to a decrease in suspension viscosity.

Focusing on sugarcane bagasse and paper pulp, **Table 1-5** summarizes the most pertinent research on enzymatic hydrolysis of these lignocellulosic resources from the last 15 years. It was observed that authors paid more attention to chemical composition than physical criteria, namely particle size (and/or particle shapes). There were only three articles reporting influence of particle size of substrates and one of them monitored the change in particle size during enzymatic hydrolysis. As previously mentioned, particle shape and size distribution may significantly affect suspension viscosity. The investigation of these parameters is then important to understand liquefaction mechanisms. In parallel with traditional biochemical analysis, it was found that physical analyses were performed in several publications. Two main factors, suspension viscosity and yield stress were largely investigated. Beyond, the modeling of suspension viscosity was also treated in one publication. This trend reflected the important role of physical approach on enzymatic hydrolysis, especially the evolution in particle size and shapes and its relationship with both biochemical and rheological parameters such as viscosity and hydrolysis yield.

In addition with particle shape and substrate concentration, others factors may contribute to the evolution in suspension viscosity. Generally, by increasing the shear rate (which is roughly proportional to the mixing rate), the decrease in viscosity of whole suspension depends on the type of substrate. The change in suspension temperature may also affect suspension viscosity. However, during enzymatic hydrolysis, these parameters were usually controlled at constant values. The rheological approach on enzymatic hydrolysis needs to be carried out taking in consideration all of these parameters.

1.5 CONCLUSION

Lignocellulosic biomass is clearly a promising feedstock for bioprocess because of its abundancy and renewability. Among many lignocellulosic materials, sugarcane bagasse, corn stover and paper pulp were mentioned in the majority of publications. Through the bibliography research, the enzymatic hydrolysis of lignocellulose was investigated by both biochemical and rheological approaches. Rheological behavior of suspensions and high solid loading condition were two principal subjects of these publications.

From a rheological standpoint, the properties of initial lignocellulosic suspensions were investigated. Factors influencing suspension viscosity and yield stress were pointed out and deeply described. However, concerning enzymatic hydrolysis, the mechanisms of reaction needs to be deepened by additional works, crossing biochemical and physical analysis. It is important to note that, the role of single enzyme activities in liquefaction of lignocellulosic suspension was mentioned only in the work of Szijártó, Siika-aho et al. (2011). That is a lack of knowledge of the hydrolysis process in which enzymes play a crucial role and catalyze the bioconversion of lignocellulosic materials into molecules of interest (fermentable sugars). By understanding the role of single enzyme activities, the cocktail can be optimized in terms of composition in order to improve hydrolysis efficiency.

Our purpose in this study was to investigate the bioconversion of lignocellulosic materials during enzymatic hydrolysis using multi scale analysis techniques. Sugarcane bagasse, paper pulp and filter paper were selected as raw materials for enzymatic digestion. The reaction was followed by rheological, morpho-granulometrical and biochemical analyses, including both in- and ex-situ methods. The aim of this thesis will focus on three principal points:

- Mechanisms of enzymatic liquefaction and bioconversion.
- Role of single cellulase activities in the enzymatic hydrolysis.
- Fed-batch hydrolysis to reach high solid loading and good efficiency.

Highlights from bibliography

- A limited number of scientific works investigates the hydrolysis under high-solid content.
- No trend and rational identification of optimal E/S ratio.
- Fed-batch appears as a promising way to raise solid loading and to optimize transfer
- No rational definition of fed-batch strategy was explored (fed flow-rate magnitude, continuous, fed-batch or cumulative add strategy).
- Rheological behaviors of cellulose fiber suspensions appear as shear-thinning and sometimes visco-plastic (non-Newtonian).
- No generic approach to describe the evolution of rheology and morphology during hydrolysis.

Table 1-5. Summary of identified researchs works on enzymatic hydrolysis of SCB and PP (2000-2016).

Ref	Material								Hydrolysis						Biochemical		Physical		
	Biomass	D	L	M	Composition				Solids	Mix	T	pH	t	Enzyme	Yield glucose		μ	Yield stress	Notes
		μm	mm	%	G %	X %	L %	A %	%w/w	rpm	°C	/	h		%	g/L		Pa	
(Cao and Tan 2002)	PP-SW	/	/	/	92.8	/	/	0.09	3	175	50	7	2	In-house			x		Viscosity (cm^3/g)
(Prior and Day 2008)	SCB (AFEX)				41.7	20.4	22.6	/	1w/v	100	50	4.8	72	SpezymCP N188		~7.5	/	/	Synergy
(Zhang, Qin et al. 2009)	PP-HW	/	/	/	80.1	9.6		/	20	20	50	4.8	96	In-house Celluclast 1.5L, N188	84	144	/	/	Hydrolysis in shaked flask
(Geddes, Peterson et al. 2010)	SCB (StE)	/	/	/	59.3	8.7	/	/	10	200	55	5	6	Cellulase W, N188	3.5-17.6	/	x	/	< 77 % reduce in μ
(Gottschalk, Oliveira et al. 2010)	SCB (StE)	/	/	/	48.4	10.3	34	/	20	200	50	4.8	72	Mix, in-house	68.4	/	/	/	Feed-batch sub+enz
(Pereira, Pereira et al. 2011)	SCB (StE)	/	/	/	43.6	8.75	33.75	/	10	200	50	4.8	36 0 22	In-house enzyme	45 / /	22	/ x x	/ / /	 Shear rate 1/100s Shear rate 1/100s
(Várnai, Huikko et al. 2011)	PP-SW	/	/	/	69.1	13.8	< 1	/	1	250	45	5	12	IH pure	30-90		/	/	Yield calculated on reducing sugar
(Zhang, Liu et al. 2012)	SCB (NaOH)	/	/	/	68.6	24.3	6.52	/	30	120	50	5	144	A1500	55	125.97	/	/	
(Nguyen, Anne-Archard et al. 2013)	PP-HW	x	x	74	75	19	/	/	1-3	150	40	4.8	24	A1500	x	x	x	/	Suspension properties
(Neto, Dos Reis Garcia et al. 2013)	SCB (various)	< 420	/	/	/	/	/		3	100	50	4.8	10-72	ATCC 26921, N188			/	/	Kinetics parameters
(Wanderley, Martín et al. 2013)	SCB (StE)	/ /	/ /	/ /	47.7 87.3	8.9 6.9	34.3 5.7	/ /	8	150	50	4.8	120	Celluclast 1.5L, N188	/ /	17 39	/ /	/	
(Zhao, Dong et al. 2013)	SCB-OS	/ /	/ /	/ /	86.2	6.99	8.78	/ /	30 20	200 200	50 50	/ /	196 144	CTec2 (Novozyme)	~72 ~80	~215 ~150	/ /	/	Batch Batch
(Carvalho, Sousa et al. 2013)	SCB (StE)	/	/	/	88.2	7	5.37	2	6.54	250	50	4.8	50	A1500	x	x	/	/	
(Sánchez, Quintana et al. 2015)	Bleached SCB	27	0.956	/	78.5			/	3	/	40	/	/	No	/	/	/	~20 Pa	Carreau-Yasuda model
(Liu, Xu et al. 2015)	SCB (Alkaline)	/	/	/	60.1	25.5	8	/ / /	9 12 15	150	50	5	96	CTec2	 80.4	 75.5	x x x	/ / /	viscosity final 0.04 Pa.s
(Mesa, López et al. 2016)	SCB (OS)	/	/	/	44.5	20.7	18	1.3	10w/v	150	50	4.8	24	C-1.5L, N188	11.8-22.1	/	/	/	Economic evaluation
(Correa, Badino et al. 2016)	SCB (StE)	/	/	/	43.1	12.4	28.8	5.7	10w/v	470	50	4.8	96	CTec2	60-75	/	x	/	Viscosity ~3.5mPa.s (0h) to ~1mPa.s (96h)

D: Mean diameter (μm); L: Length (mm);M: % moisture; G %: %Glucose, X %: % Xylan; %L: % lignin, %A: %Ash; T: temperature (°C),t: time (h); μ: viscosity (Pa.s); / not mentioned ; x : mentioned

2 MATERIALS & METHODS

2.1 EXPERIMENTAL SET-UP

The experimental set-up includes a double jacket glass bioreactor (d = 130 mm, H = 244 mm, V = 2.0 L) equipped with a home-designed impeller system associated with several in-situ sensors (temperature, pH, rotation speed, torque, FBRM). The first impeller consists of three inclined blades (diameter: 73.5 mm, angle: 45°, h = 38 mm) located at 75 mm height from the bottom to ensure mixing. The second one is a close bottom mixer including 2 large blades (diameter: 120 mm, h = 22 mm) to avoid substrate decantation. The impeller shaft is connected to a viscometer (Viscotester HaakeVT550, Thermo Fisher Scientific, ref: 002-7026) that ensures the mixing at specific rotation speed as well as in-situ torque measurements. The temperature was controlled by water circulation (combined cryostat Haake DC30-K20, Thermo Fisher Scientific) through the water jacket of the bioreactor. The viscometer and the cryostat were controlled by original software from Haake (RheoWin Job Manager) that also ensured real-time data recording (temperature, torque, mixing rate). The pH of suspension was controlled and auto adjusted by a Biostat-B (Sartorius Stedim Biotech) via an home-designed software created on LabView environment. In addition, a focused beam reflectance sensor (FBRM-G400-Mettler Toledo) was located inside the reactor in order to measure the in-situ distribution of particle chords.

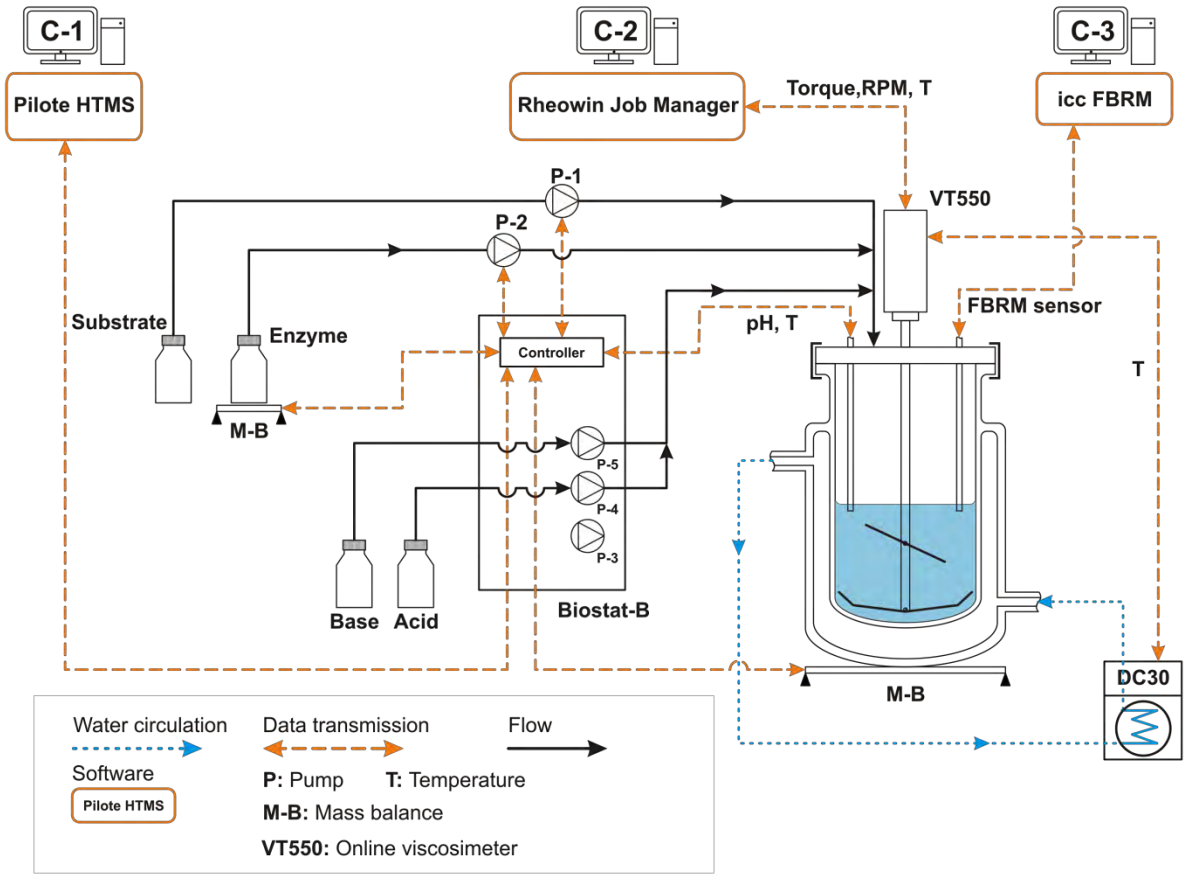

Figure 2-1. Process and instrumentation diagram (PID) of experimental set-up.

To ensure the feeding of enzyme, our systems consist in two- and four-channel pumps. Motors speed range is 0.5 to 10 rpm for the Watson Marlow 403U/VM4 (4 channels) and 2.5 to 50 rpm for the Watson Marlow 403U/VM2 (2 channels). The system is designed for flows from 0.001 to 17 mL/min depending on motor speed, diameter of the used flexible and the

properties of enzymes (principally viscosity). For substrate feeding, an Archimedean pump was used. The pump drive, pump head and pump hopper are illustrated in **Appendix 6**. The Archimedean screw is fixed on the rotating part of the pump drive. It consists of a screw (a helical surface surrounding a central cylindrical shaft) inside a hollow pipe. The screw is turned by the pump drive. As the shaft turns, the bottom end scoops up a volume of the matrix. The matrix will slide up in the spiral tube, until it finally pours out from the top of the tube and feeds the bioreactor system. Two screws are available for the experimentation: one "classical" and one shaft less screw. A global description of the whole systems is illustrated in **Figure 2-1**.

- Sampling procedure

For all enzymatic hydrolysis experiments, sampling were performed with a 7 mm flexible connected to a 50 mL syringe with a unique protocol **Figure 2-2**. The sample was then distributed in falcons and eppendorf. The inactivation of enzyme was carried out by using pH or temperature shocks depending on the ulterior analysis. For physical and dry matter analysis, the enzymatic activities were inactivated by 0.1 mL of sodium hydroxide 10 N. For biochemical analysis, the inactivation was ensured by heating the sample up to 95ºC and maintaining for 20 min. Samples after inactivation were stored at frozen until analyzed. To minimize the risk of changes in fiber properties during storage, samples for physical analysis are considered in priority.

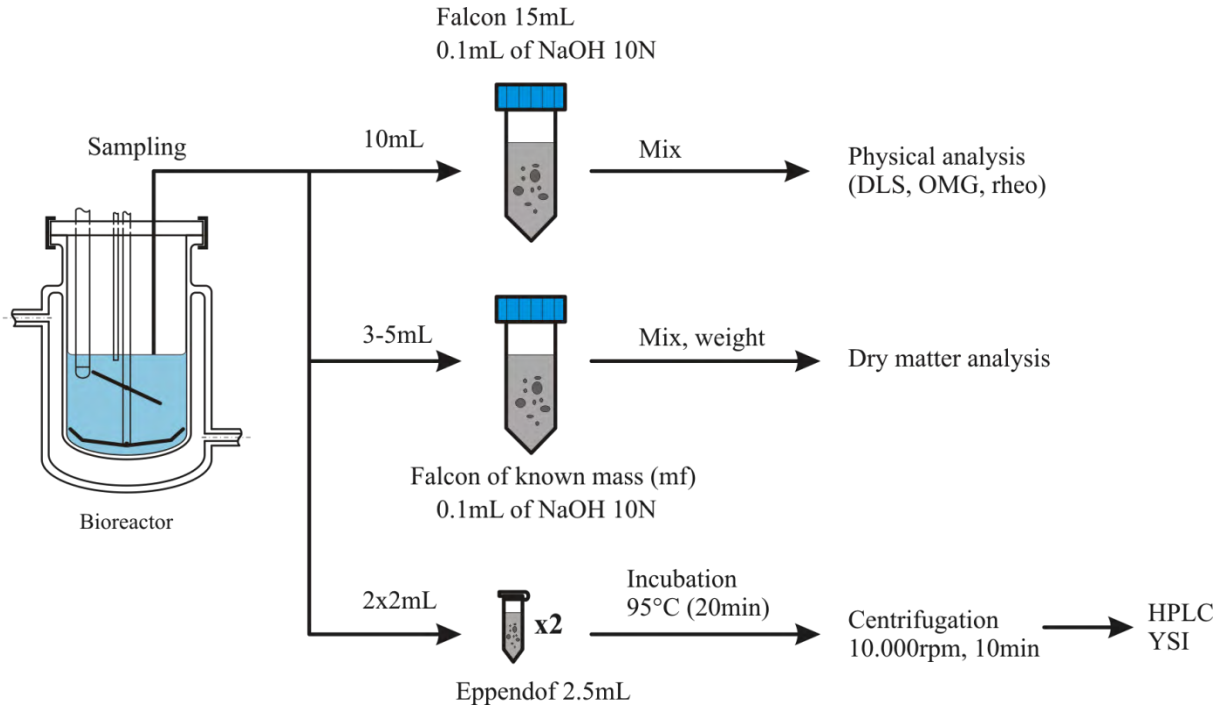

Figure 2-2. Protocol of sampling during enzymatic hydrolysis.

2.2 SUBSTRATES AND ENZYMES

2.2.1 Lignocellulose matrixes

Three matrixes with different chemicals and physical properties were selected corresponding to a reference substrate (Whatman paper Nº 1), an industrial feedstock (hard wood paper pulp) and an agricultural by-product (sugarcane bagasse).

Whatman paper Nº1, FP (Whatman International Ltd., Maidstone, England, Cat No 1001 090) is milled using a Bosch MKM6003 mill at 720 rpm Milled filter paper was stored in plastic zip bag at room temperature.

Hardwood paper-pulp, PP (type FPP31), after extrusion (Extruder Prism TSE24MC, 400 mm failure, Thermo Electron Corp, extrusion line: 7/8 mixing, 1/8 shear stress) was received from Tembec Co. (Saint-Gaudens, France). Raw paper pulp was stored in freezer (-18 °C). Before used, material was defrosted, then extruded to homogenize particle size (Extruder Eurolab 16, 400 mm failure, extrusion line: 25 L/D 18/25 conveying, 7/25 shear stress). Extruded paper pulp was stored at 4 °C until use.

The raw sugarcane bagasse was collected from Lam Son sugar factory (Thanh Hoa, Viet Nam). Organosolv pretreated bagasse (SCB) was produced by CRDB (Center for Research and Development in Biotechnology) associated with SBFT-HUST (School of Biotechnology and Food Technology, Hanoi University of Science and Technology, Vietnam). The organosolv process consists of a thermo-chemical pretreatment of bagasse using formic acid (10 % w/v, 70 – 80 % formic acid, 120 °C, 1 h), followed by a deformylation of bagasse by diluted NaOH 10 % at 80 °C, and washing with water to neutral pH. At LISBP, pretreated sugarcane bagasse was extruded in order to homogenize particle size (Extruder Eurolab 16, 400mm failure, extrusion line: 25 L/D 18/25 conveying, 7/25 shear stress) then stored at 4 °C until use.

All matrixes were characterized for composition (in partnership with LCPO, Bordeaux University, France - the analysis was performed using FibertecTM following the Van-Soest method (Van-Soest 1963)), moisture, density, morpho-granulometry, surface properties (in partnership with Dept Chem Eng, Waterloo University, Canada – method described in **§2.4.2**). Suspensions were analyzed for particle size distribution and rheological properties.

2.2.2 Enzymes

Several enzymes from single up to cocktail enzymatic activities were selected for hydrolysis in this study. All enzyme products were ordered from commercial producer. The full listing of enzyme products is presented in **Table 2-1**

Cellic® CTec2 from Novozyme, Serial 0139 batch VCN10002 is a commercial cocktail enzyme which is lignocellulolytic complex, containing several activities such as endo-glucanase, exo-glucanase, β-glucosidase and hemicellulase. Protein concentration of Ctec2 is 64.8 ± 4.7 mg/mL analyzed by Bradford method (Bradford 1976) using Bovine Serum Albumin as standard.

E-Celan from Megazymes, lot #130501 is a highly purified endo-β-glucanase from *Aspergillus niger*. Detail information about E-Celan is presented in **Appendix 1.**

E6412 from Sigma Aldrich, lot #SLBF4539 is a recombinant cellobiohydrolase I from *Hypocrea jecorina,* expressed in corn. Enzyme is provided in liquid form, dissolved in sodium acetate and ammonium sulfate solution, containing 0.02 % sodium azide.

49290 from Sigma Aldrich, lot #BCBM881V is a β-glucosidase from almonds. Enzyme is provided in lyophilized powder form.

X2753 from Sigma Aldrich, lot #SLBC5352V is a recombinant endo-xylanase from *Thermomyces lanuginosus* produced by submerged fermentation of a genetically modified *A. oryzae*. Enzyme is provided in powder form.

Multifect-Xylanase from Genecor is a genetically modified strain of *Trichoderma reesei*. Enzyme is provided in liquid form.

Table 2-1. Enzyme products used in this study

Enzyme	Product	Enzyme specifications
Lignocellulase	Cellic Ctec2 (Novozymes)	t_{opt} = 45 - 50 ºC

		pH_{opt} = 5.0 - 5.5
Endo-glucanase (E 3.2.1.4) G1	E-CELAN (Megazyme)	t_{opt} = 60 ºC (stable < 50 ºC) pH_{opt} = 4.5 (stable 4 - 10)
Exo-glucanase (EC 3.2.1.91) G2	E6412 (Sigma Aldrich)	t_{opt} = 45 ºC (stable < 37-50 ºC) pH_{opt} = 5-6 (stable 4 - 10)
Beta-glucosidase (EC 3.2.1.21) G3	49290 (Sigma Aldrich)	t_{opt} = 37 ºC (stable range not specified)
Endo-xylanase	X2753 (Sigma Aldrich)	not specified
Xylanase	Multifect-Xylanase (Genecor)	t_{opt} = 55 ºC (stable 50 - 60 ºC) pH_{opt} = 5.0 (stable 3.5 – 6.5)

(*) Information presented in this table is collected from producer's site and/or specification sheets.

2.3 BIOCHEMICAL ANALYSIS

The biochemical analysis includes the measurement of water content, the dosage of glucose by YSI, the dosage of mono and disaccharide by HPLC and the measurement of enzymatic activities and thermal stability. Detailed protocols are presented.

2.3.1 Water and dry matter content

The water content of substrate and hydrolysate were determined by drying at high temperature and atmospheric pressure. The mass differences before and after drying is the water content in the sample. Empty metal cups were numbered, drilled overnight in an oven at 105 °C. Mass were then quantified with a precision balance (Sartor IUs ED224S, 0.005-230g ± 0.1mg). These masses were noted m_{cup}. During enzymatic hydrolysis, a quantity of sample (m_s) was filtered through a Whatman No1 filter paper of known weight (m_{fp}) then washed by ≈10 mL distilled water. This filter paper containing the sample was placed in the numerated cup then dried all in the oven at 105 °C until constant mass (quantified with a precision balance). This final weight was noted m_{fin}. Water content (W) and dry matter (DM) were calculated following **Eq. 2-1** (accuracy ± 0.5 %):

$$W(\%) = \frac{m_s + m_{fp} + m_{cup} - m_{fin}}{m_s} \times 100 \qquad \textit{Eq. 2-1}$$

$$DM(\%) = 100 - W$$

2.3.2 Glucose (YSI)

Glucose concentration was checked in the supernatant along enzymatic hydrolysis by Analyser YSI model 27A (Yellow Springs Instruments, Yellow Springs, Ohio, sampling volume is equal to 25 µL) (Ehrhardt, Monz et al. 2010, Pereira, Pereira et al. 2011, Wang, Post et al. 2012). This machine uses an immobile enzyme (glucose-oxidase) fixed on a membrane to produce peroxide from glucose:

$$C_6H_{12}O_6 + O_2 \xrightarrow{glucose-oxydase, H_2O} HOCH_2(CHOH)_4COOH + H_2O_2$$

The oxidation of peroxide on a platinum electrode liberates these electrons which induce an electric current proportional to glucose concentration. The machine will measure this electric current and bring the glucose concentration in $g.L^{-1}$. The range of result varies between 0-2.5 $g.L^{-1}$ ± 2 % and between 2.5-9.0 $g.L^{-1}$ ± 5 %.

2.3.3 Mono and disaccharides (HPLC)

Mono and di-saccharides were analyzed using a high-performance liquid chromatography (HPLC, Agilent Technologies, 1200 series). Measurements were performed on an Aminex HPX-87P column (Aminex®HPX-87P column #1250098, Bio-Rad Laboratories, Richmond, CA-detection range 0.1 - 50 g/L) with micro-guard Carbo-P refill cartridges #1250119 (both from Bio-Rad). This column was reported in the literature for the good quantification of glucose (Ghose 1987, Ghose and Bisaria 1987, De Bari, Viola et al. 2002, Cara, Moya et al. 2007) Separation was carried out at flow rate 0.5 mL/min, column temperature 60 °C using HPLC grade water (LiChrosolv, Merck) as mobile phase and refractive index detector (Shodex RI 101). All samples were centrifuged at 10.000 rpm for 10 min then filtered through 0.22 µm filter before injection into the column. Calibration curves were established with standard solutions of cellobiose, glucose, xylose, arabinose, galactose, and mannose with concentration ranging between 0 to 1 g/L. The lower and upper LOD are equal to 0.01 and 1 g/L respectively and the LOQ is equal to 0.036 g/L. The retention times of these compounds are presented in **Table 2-2**:

Table 2-2. Retention time of composes may be present in hydrolyzed suspension.

Compound	Retention time (± 0.03 min)
Cellobiose	12.99
Glucose	15.54
Xylose	17.17
Galactose	18.76
Arabinose	21.33

2.3.4 Enzyme analysis

Lignocellulase cocktail is generally consists of several different activities such as cellulase, hemicellulase and lignin degrading enzymes. In our framework, the measurement of enzyme activities was performed only for the following:

Cellulase:

- Saccharifying cellulase or filter paper activity (FPU)
- Endo-glucanase (G1)
- Exo-glucanase (G2)
- Cellobiase (G3)

Hemicellulase:

- Endo-xylanase (X1)
- Exo-β-xylosidase (X2

The enzyme activities were characterized following IUPAC standard methods (International Union of Pure and Applied Chemistry, http://www. IUpac.org/publications/pac/). The thermostability of commercial cocktail Ctec2 was investigated at 40 and 50 ºC.

2.3.4.1 Cellulase and hemicellulase activities

Cellulase and hemicellulase catalyze the hydrolysis reaction of cellulose and hemicellulose into monomers (glucose, xylose, mannose …). The analyses of enzyme activities are based on well-known protocol for cellulase (Ghose 1987) and for hemicellulase activities (Ghose and Bisaria 1987). By definition, one unit of activity (1 IU) is equals to the amount of enzyme that

convert corresponding substrate and forms 1 µmol.min^{-1} of product (glucose, xylose or reducing sugar depend on each enzyme). The activity can be normalized by the enzyme volume (IU/ mL) or amount of enzyme protein (IU/mg protein). Especially for cellobioase (β-glucosidase) activity, the definition was based on 2 µmol.min^{-1} of product instead of 1 µmol.min^{-1} due to the fact that the break of one cellobiose gives two molecules of glucose.

The conditions for enzymatic reaction and corresponding substrate for each activity are shown in **Table 2-3**

Table 2-3- Summary of measurement conditions and substrates for enzymatic activities.

Unit	Substrates	Time (min)	T (°C)	V_{buffer} (mL)	V_{enzyme} (mL)	Measurement
FPU	1 strip 1 x 6 cm ≈ 50 mg Whatman filter paper N°1	60	40/50	1	0.5	RS
CMCU	2 % carboxymethyl-cellulose sodium salt (DS: 0.65 - 0.9) dissolved in buffer.	30	40	0.5	0.5	RS
AVCU	2 % avicel (Sigma) dissolved in buffer.	30	40	0.5	0.5	RS
CBU	15mM cellobiose in buffer.	30	40	0.5	0.5	Glucose
EnXU	1 % Xylan (from Beech wood - Sigma) dissolved in buffer.	30	40	0.5	0.5	RS
ExXU	9 mM Methyl β-D-xylopyranoside in buffer.	30	40	0.5	0.5	RS

The buffer used in this protocol was 0.05M sodium citrate pH 4.8
RS: Reducing sugar

The enzymatic reactions were carried out at specific conditions (T, pH, duration, substrate concentration) and products (glucose or reducing sugar) were quantified accordingly. For each activity, at least two different dilutions (d_1, d_2) of enzyme were made and the sugar amount (mg/reaction) released slightly less and more than the critical point (**Table 2-4**). From d_1 and d_2 the critical amount of sugar per reaction S_s was interpolated which enables to estimate the critical dilution d_c. The principle of this method is illustrated in **Figure 2-3**

Table 2-4- Critical points for enzymatic assays

Activities	S_c (mg/reaction)	Activities name
Cellulase	2.0	FPU
Endo glucanase	0.5	CMCU
β-glucosidase	0.5	CBU
Exo glucanase	0.5	AVCU
Endo Xylanase	1.0	EnXU
Exo β xylosidase	0.2	ExXU

S_c: critical mg of sugar released per reaction.

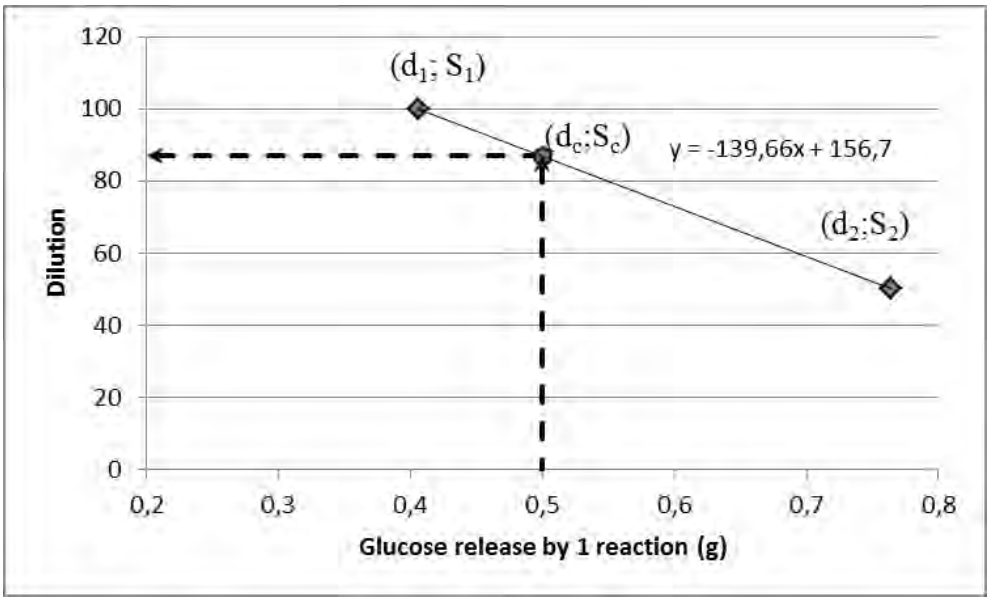

Figure 2-3: Example: determination of d_c in case of S_c = 0.5. d_1 and d_2 are two experimental points, d_c is deduced by interpolation.

Enzyme activities were calculated following **Eq. 2-2** with the obtained value of $\mathbf{d_c}$

$$U/mL = \frac{S_c \cdot d_c \cdot 1000}{MW \cdot t \cdot V_e} \qquad \textit{Eq. 2-2}$$

Where:

1000: conversion factor from mol to µmol of sugar released

S_c: amount of glucose released in one enzymatic reaction (mg)

V_e: volume of enzyme in the reaction (mL)

MW: molecular weight of sugar product equivalent (180 for glucose, 150 for xylose)

t: duration of the reaction (min)

For CBU, the enzyme activity U/mL should divided by 2 due to the definition of 1 CBU = 2 µmol.min^{-1} glucose released.

2.3.4.2 Thermal stability and dependency of enzymatic activities

The Michaelis-Menten kinetic model and the Arrhenius equation were used to characterize thermodynamic of enzyme.

The Arrhenius equation describes temperature effects on the reaction rates:

$$k(T) = Ae^{-E_a/RT} \qquad \textit{Eq. 2-3}$$

Where T is the absolute temperature (K), A is the pre-exponential factor (min^{-1}), R is the gas constant (8.314 kJ.mol^{-1}), and E_a is the activation energy (kJ.mol^{-1}). The Michaelis–Menten equation describes reaction rate as a function of substrate and enzyme concentrations (Davies and Henrissat 1995):

$$E + S \underset{k_{-1}}{\overset{k_1}{\rightleftharpoons}} ES \xrightarrow{k_{cat}} E + P \qquad \textit{Eq. 2-4}$$

$$v(T,[S]) = k_{cat}(T) \cdot \frac{[E_o][S]}{K_m(T) + [S]} \qquad \textit{Eq. 2-5}$$

Where: *E:* Enzyme, *S*: Substrate, *ES*: complex enzyme-substrate; *P*: Product, k_1, k_{-1}, k_{cat}: rate constants of formation of ES complex, dissociation of ES complex and product formation respectively. For enzymatic reaction at high substrate concentration $[S] \gg K_m$ (or $[S] \approx K_m(T) + [S]$) and in considering Arrhenius equation, **Eq. 2-5** can be simplified by:

$$k_{cat}(T) = \frac{v(T)}{[E_o]} = Ae^{-E_a/RT} \qquad \textit{Eq. 2-6}$$

From **Eq. 2-6** we obtains then

$$lnk_{cat} = -\frac{E_a}{R} \cdot \frac{1}{T} + lnA \qquad \textit{Eq. 2-7}$$

Where $v(T) = \frac{dC}{dt}$ [mol.L^{-1}.s^{-1}]; [E_0] [g protein. mL^{-1}] or [E_0] = [mL enzyme. mL^{-1}]

$$k_{cat} = \frac{v(T)}{[E_o]} = [mol.L^{-1}.s^{-1}] \qquad \textit{Eq. 2-8}$$

The enzyme unit (U) is defined as the amount of the enzyme that catalyzes the conversion of 1 µmol of substrate per minute (Simha 1952, Elwyn T. Reese 1968). One katal is defined as the amount of enzyme that converts 1 mol of substrate per second, so

$$1\ U = \frac{10^{-6}}{60} katal \qquad \textit{Eq. 2-9}$$

Or:

$$U = k_{cat}(T) \cdot \frac{10^{-6}}{60} \qquad \textit{Eq. 2-10}$$

Knowing enzymatic activities at different temperatures, it is possible to calculate activation energy (E_a) and pre-exponential factor (A) by plotting linear equation between ln(k_{cat}) and (1/T).

2.4 PHYSICAL AND PHYSICO-CHEMICAL ANALYSIS

2.4.1 Densimetry

2.4.1.1 Densimetry of fluids

The density of fluids was determined by a densimeter Mettler Toledo DE40 (10^{-4} to 3 g.cm^3 ± 10^{-4} g.cm^{-3}; 4-90 °C ± 0.05 °C). This device is based on the measurement of an induced mechanical oscillation on a "U" tube. A magnet is fixed on the tube "U" vibrating at different frequencies depending on the density range of the fluid contained in the tube. The oscillation period T of the system changes as a function of the total mass of the system ("U" tube + fluid within the tube). The internal volume of the tube is constant and defined for a given temperature;

the period of oscillation of the system is directly related to the density of the fluid contained in the tube. The relationship between density and oscillation period is given by **Eq. 2-11**

$$\rho_{sam} = \left(\frac{K}{4\pi^2 V_{cell}}\right) \cdot T^2 + \left(-\frac{m_{cell}}{V_{cell}}\right) \qquad \textit{Eq. 2-11}$$

In this equation, K ($g.s^{-2}$) is a constant of the cell, m_{cell} (g) and V_{cell} (mL) are the weight and the volume of the cell, T (s) is the oscillation period and ρ_{sam} ($g.mL^{-1}$) the sample density.

Before sample measurement, the machine was calibrated with air and distilled water at desired temperature (20, 30 and 40 °C). The sample was injected slowly in tube U with a syringe. Sample volume necessary is approximately 2 - 5 mL. The tube is rinsed with 3 - 5 mL of sample before measurement.

2.4.1.2 Densimetry of substrates

The density of substrates was determined by gravimetry-volume method (proportion of substrate volume and added water volume in a volumetric flask). This density corresponds to the suspended matrix, including its initial water content (if applicable). It was used to calculate the volume fraction, even though other definitions can be proposed. It characterizes raw matter and emanates directly from the industrial process.

Firstly, the empty and dry flask (Flask Duran, type A, 100 ± 0.1 mL, 20 °C) was weighted (Sartor IUs ED822CW, 0.5 – 820 g ± 0.01 g). A quantity of substrate (7 different quantities ranging from 5 to 30 g) was added in each flask. Secondly, distilled water was injected slowly in the flask. Before the flask volume was reached, it was gently manually shacked to avoid air bubbles and ensure the water distribution in substrate. All measurements were realised at ambient temperature (20 °C ± 2). The substrate density (± 5 %) was calculated with **Eq. 2-12**

$$\rho_s = \frac{m_s}{V_s} = \frac{m_1 - m_0}{V_{tot} - V_w} \qquad \textit{Eq. 2-12}$$

$$V_w = \frac{m_2 - m_1}{\rho_w^{20}}$$

with ρ_s and ρ_w^{20} : apparent density and water density at 20 °C, respectively ($g.\ mL^{-3}$).

m_s, m_0, m_1, m_2: mass of substrate, empty flask, flask before and after water added respectively (g).

V_s, V_{tot}, V_w: volume of substrate, flask and water added respectively (mL).

The linear regression of m_s versus V_s enables to quantify the value of ρ_s (**Figure 2-4**)

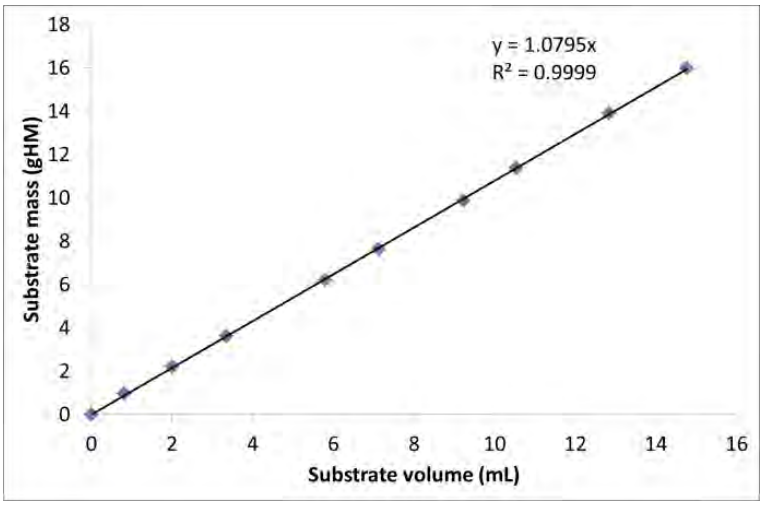

Figure 2-4. Example of ρ_s identification for SCB.

It is necessary to calculate the intrinsic density ρ_{DM} considering the dry matter as reference. We define then

- Dry matter content $DM = {m_{DM}}/{m_s}$ ***Eq. 2-13***
- Water content $W = {m_w}/{m_s}$ ***Eq. 2-14***
- Apparent density $\rho_s = {m_s}/{V_s}$ ***Eq. 2-15***
- Intrinsic density $\rho_{DM} = {m_{DM}}/{V_{DM}}$ ***Eq. 2-16***

where m_s; m_w and m_{DM} are masse of humid substrate, water and dry matter content, respectively ($m_s = m_w + m_{DM}$).

$$V_s = V_w + V_{DM}$$

$$\leftrightarrow \frac{m_s}{\rho_s} = \frac{m_w}{\rho_w} + \frac{m_{DM}}{\rho_{DM}}$$

$$\leftrightarrow \frac{1}{\rho_s} = \frac{m_w/m_s}{\rho_w} + \frac{m_{DM}/m_s}{\rho_{DM}}$$

Replace W and DM from **Eq. 2-13** and **Eq. 2-14** we obtains then

$$\frac{1}{\rho_s} = \frac{W}{\rho_w} + \frac{DM}{\rho_{DM}}$$

$$\leftrightarrow \rho_s = \left(\frac{W}{\rho_w} + \frac{DM}{\rho_{DM}}\right)^{-1}$$

$$So\,\rho_{DM} = DM \cdot \left(\frac{1}{\rho_s} + \frac{W}{\rho_w}\right)^{-1} \qquad \textit{Eq. 2-17}$$

2.4.2 Surface free energy (Contact angle measurement – Partnership with UW)

Adhesive forces between a liquid and a solid cause a liquid drop to spread across the surface. Cohesive forces within the liquid cause the drop to ball up and avoid contact with the surface. The contact angle (θ) is the angle at which the liquid–vapour interface meets the solid–liquid interface. The contact angle is determined by the resultant between adhesive and cohesive forces. As the tendency of a drop to spread out over a flat, solid surface increases, the contact angle decreases. Thus, the contact angle provides an inverse measure of wettability. The mechanical equilibrium of a liquid drop on a solid surface is determined by the balance of the three surface tension forces acting at the liquid-solid-vapour contact line. The mechanical equilibrium is represented by the well-known Young's equation.

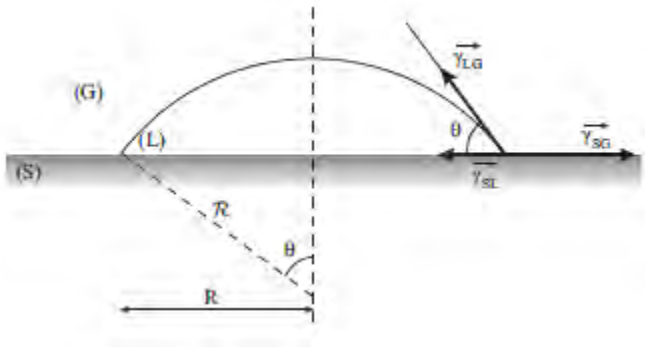

Figure 2-5: Three phases system assuming a spherical drop interface (Soulies, Pruvost et al. 2013).

$$\gamma_{SG} + \gamma_{SL} \cdot \cos(\pi) + \gamma_{LG} \cdot \cos(\pi - \theta) = 0$$
$$\gamma_{LG} \cdot \cos(\theta) = \gamma_{SG} - \gamma_{SL} = \gamma_S - \gamma_{SL} - \pi_E \qquad \textit{Eq. 2-18}$$

With γ_S, γ_L, γ_G: surface free energy of solid, liquid and gas, γ_{SG}, γ_{LG}, γ_{SL}: surface free energy of interfaces (solid-gas, solid-liquid and liquid-gas) ($N.m^{-1}$), θ: contact angle (°), π_E: equilibrium spreading pressure (adsorbed vapour of liquid on solid) ($N.m^{-1}$).

The Dupré's equation amounts to a conservation of total energy in a reversible process of adhesion and cohesion of two phases. The work of adhesion is expressed by:

$$W_{SL} = \gamma_{SG} + \gamma_{LG} - \gamma_{SL} \qquad \textit{Eq. 2-19}$$

The combination of the Young and Dupré's equations results in:

$$W_{SL} = \gamma_{LG} \cdot (1 - \cos(\theta)) \qquad \textit{Eq. 2-20}$$

In this way, the two unknowns (γ_{SG} and γ_{SL}) of the original Young's equation can be reduced to only one, W_{SL}.

Quiroga, Costa et al. (2010) provided a method to analyse the energy of surfaces from contact angles which does not require detailed knowledge of the surface compositions of solids. Quiroga, Costa et al. (2010) considered that the total surface tension of a solid or a liquid can be decomposed into components corresponding to the specific types of intermolecular interactions.

$$\gamma = \gamma^d + \gamma^p + \gamma^i + \ldots \qquad \textit{Eq. 2-21}$$

where d, p, and i stand for the dispersion, polar and induction interactions. A large number of terms can follow afterwards as indicated by the dots. This division of the surface tension into components allowed the work of adhesion to be expressed as follows:

$$W_{SL} = 2 \cdot \sqrt{\gamma_S^d \cdot \gamma_L^d} + 2 \cdot \sqrt{\gamma_S^p \cdot \gamma_L^p} + 2 \cdot \sqrt{\gamma_S^i \cdot \gamma_L^i} + \ldots \qquad \textit{Eq. 2-22}$$

In order to estimate the surface free energy components of solid surface, contact angles of several liquids are measured (liquids whose surface tension components have already been determined). The surface tension components of the solid are determined by combining **Eq. 2-20** and **Eq. 2-22** as follows:

$$W_{SL} = \gamma_{LG} \cdot (1 - \cos(\theta)) = 2 \cdot \sqrt{\gamma_S^d \cdot \gamma_L^d} + 2 \cdot \sqrt{\gamma_S^p \cdot \gamma_L^p} + 2 \cdot \sqrt{\gamma_S^i \cdot \gamma_L^i} + \ldots \qquad \textit{Eq. 2-23}$$

The induction components of the surface free energies of solids and liquids are generally negligible in comparison with the two other terms. Thus, for all practical purposes, it is sufficient to account for the dispersion and polar terms only.

In our conditions, dispersive and polar contributions are considered. Gibbs (or total) energy is then given by the relation:

$$\Delta G_{TOT} = \Delta G^d + \Delta G^p \qquad \textit{Eq. 2-24}$$

With $\Delta G^d = -W_{SL}^d = \gamma_{SL}^d - \gamma_S^d - \gamma_L^d$

and $\Delta G^p = -W_{SL}^p = \gamma_{SL}^p - \gamma_S^p - \gamma_L^p$ *Eq. 2-25*

Thermodynamically, if ΔG_{TOT} is positive, the adhesion is disadvantaged (repulsion) and reciprocally, if ΔG_{TOT} is negative, the adhesion is advantaged (attraction). The total free energy of interaction is the sum of the electrostatic free energy, ΔG_{TOT} and non-electrostatic.

Contact angle measurements enable to measure surface free energy of materials and consequently to determine the total surface energy. A Drop shape, analyser DSA100 (Krüss GmbH, Germany) was used at room temperature in a static mode. The measurement was digitally recorded and the videos analyzed with the software DSA1 V1.9 - 03 9 (Krüss GmbH, Germany). Two analysis methods were considered for low contact angle values: Tangent method 1 and Young-Laplace method (sessile drop) (Krüss GmbH, 2004). The initial contact angle and the change over time (at least ten seconds) were recorded for a drop of liquid deposited on the compact of a given material. The mean contact angle and the standard deviation were then obtained by summarizing values issued from 12 liquid drops per specimen (aberrant data were removed); depending on how well the drop shape is fitted by the method. With Tangent 1 method, the complete profile of a sessile drop was fitted to a general conic section equation. The derivative of the equation at the baseline gives the slope at the three-phase contact point and thus the contact angle. With Laplace Young method, the profile of a sessile drop in the region of the baseline was fitted to the rational function ($y = a+bx+cx^{0.5}+d/\ln(x) +e/x^2$). From the fitted parameters the slope of the three-phase contact point at the baseline was first determined and used to determine the contact angle. This function has been selected from numerous theoretical simulations.

Contact angle measurements were conducted with milled and compacted materials and using two liquids: water and diiodomethane. For each given material, three experiments were realized: water contact angle on milled and unmilled material, diiodomethane contact angle on

unmilled material. Each experiment was carried out on 12 samples in order to estimate the error associated with the measurement. The surface energy properties of the liquids are summarized in **Table 2-5**

Table 2-5. Surface energy properties of water and di-iodomethane.

Liquid	Total surface energy (σ_{tot}, mN/m)	Dispersive component (σ_{tot}, mN/m)	Polar component (σ_{tot}, mN/m)
Water (W)	72.8	21.8	51.0
Diiodomethane (D)	50.8	50.8	0.0

A preliminary preparation of the samples involved a milling and compaction steps. An ultra-centrifugal mill ZM200 (Retsch GmbH, Germany) and 0.08 mm sieve with trapezoid shaped holes (part # 03.647.0231) were used to mill the materials. A dischargeable KBr pellet die (International Crystal Laboratories, USA) at room temperature was used to compact 0.2 g of substance as suggested for pigment specimens in ASTM D7490–08 (American Society for Testing and Materials, 2008). The KBr mould is 13 mm in diameter and a 4 ton pressure was applied for 30 s, followed by a 60 s 7 ton load (7000 kg/132.73 mm^2 = 517.19 MPa) in a press Model #3925 (Carver Inc., USA). The compacts are then fixed onto a microscope object slide (Pearl 7101, T& Q Industries, China) with double sided tape (137-2C, Scotch, Canada) and stored in a desiccator (Nalgene, Sybron Corporation, USA) until testing. In order to minimize the potential humidity absorbed by the samples, the compaction and the contact angle measurement were always carried out the same day.

2.4.3 Rheometry

Through the literature, there are no standard methods for the analysis of flow behavior for lignocellulosic suspensions, especially due to the complex rheological properties. Lignocellulosic suspension usually contains particles of broad size and shape distribution which are deformable. It presents several difficulties for rheological measurement such as rapid decantation, mixing required to maintain the homogeneity…In order to overcome these challenges, the rheological properties of suspension were characterized following two methods: i) *in-situ* viscometry that allows real-time monitoring of suspension viscosity during enzymatic hydrolysis and ii) *ex-situ* rheometry with oscillation measurement condition that enable analysis of suspension yield stress as well as viscous and elastic modulus.

2.4.3.1 Ex-situ rheometry

Samples taken from hydrolysis were analyzed with a Mars III rheometer (Thermo Scientific, torque measured range: 10^{-8} – 0.2 N.m, with oscillation: 3.10^{-8} < C < 0.2 N.m, rotation speed range: 10^{-7} – 4500 rpm, frequency: 10^{-6} – 10^{2} Hz,). The experimental strategy and data acquisition were performed using the software RheoWin Job Manager. Rheometry for these suspensions was realized with serrated plates (35 mm). The measurement protocol consists of two steps:

- An oscillatory shear flow at a fixed frequency f = 1 Hz (equivalent to ω = 6.283 rad/s with increasing shear stress amplitude τ = 0.001 to 0.3 Pa, measurement gap 1 mm (SCB) and 1.5 mm (FP and PP), T = 20 °C. This step allows the determination of linear domain of the suspension.
- A scan at constant shear stress, chosen in the linear domain determined in step (i) and varied frequency f = 0.5 Hz to 20 Hz ((equivalent to ω = 3.142 rad/s to 125.7 rad/s), measurement gap 2 mm, T = 20 °C.

For hydrodynamic identification of the reactor, Newtonian (water, Marcol oil, glycerol) and non-Newtonian homogeneous fluids (glucose-xanthan and sucrose-xanthan: 640 $g.L^{-1}$ glucose and 947 $g.L^{-1}$ sucrose) were used. Viscosity and rheological behavior for all these test fluids were measured with a cone and plate system (60 mm diameter, 2° angle) and for shear rate varying from 10^{-2} to 10^{3} s^{-1} at two different temperatures, 20 °C and 40 °C. The characteristics of these fluids are presented in **Table 2-6**.

Table 2-6. Density and rheological behavior of used fluids.

Fluid	Newtonian	Non-Newtonian		Density ($kg.m^{-3}$) (20/40 °C)
	μ (Pa.s) (20/40 °C)	n (/) (20/40 °C)	K ($Pa.s^n$) (20/40 °C)	
Distilled water	10^{-3}/6.5.10^{-4}	-	-	998.2/992.2
Marcol oil	0.01/5.4.10^{-3}	-	-	827.6/811.9
Glycerol	1.20/0.25	-	-	1261.1/1255.0
Glucose-Xanthan 0.04 %	-	0.65/0.69	0.12/0.07	1237.3/1229.5
Glucose-Xanthan 0.1 %	-	0.45/0.50	0.51/0.34	1237.7/1229.7
Sucrose-Xanthan 0.04 %	-	0.74/0.75	0.70/0.36	1236.5/1226.5

2.4.3.2 In-situ rheometry

2.4.3.2.1 Principe of in-situ viscosity measurement

- *Establishment of power consumption curve*

Ex-situ rheological characterizations were limited by the number of samples and the substrate properties, predominately decantation and flocculation of material. To overcome these problems, an in-situ viscometry was conducted throughout hydrolysis. This method is based on the real-time monitoring of torque and establishment of power consumption curve during suspension mixing (Nguyen, Anne-Archard et al. 2013). Reynolds number (Re) and Power number (N_p) were defined as

$$N_p(/) = \frac{P}{\rho \cdot N^3 \cdot d^5} \qquad \textit{Eq. 2-26}$$

with $P(W) = 2 \cdot \pi \cdot \omega \cdot M$

$$Re(/) = \frac{\rho \cdot N \cdot d^2}{\mu} \qquad \textit{Eq. 2-27}$$

Where d(m) is the mean diameter of the mixing systems, N(rps) is the mixing rate, ρ(kg/m^3) is the volumetric mass of the dissolved material and M(N.m) is the measured torque. In laminar regime, the linear relationship between Re and Np can be illustrated by

$$N_p(/) = K_p \cdot \frac{1}{Re} \qquad \textit{Eq. 2-28}$$

Where Kp is a constant that depends only on impeller shape and geometry for any Newtonian fluid. In pure turbulent regime and for Newtonian fluids, the dimensionless power number Np is assumed to be independent of mixing Reynolds number and equal to a constant, (N_{p0}). Several model fluids were tested: distilled water, glycerol and Marcol 52 oil as Newtonian fluid references; xanthan 0.04 % - 0.1 % prepared in saturated solution of glucose or saccharose as

reference for non-Newtonian fluids. From experimental data, a semi-empirical model or Churchill model (**Eq. 2-29**) including laminar and transition regions were considered for the reference curve with a one-to-one relationship between Np and Re (Churchill 1977). Experimental results on our system gave Np_0 = 0.017, α = 0.75 and Kp = 115.2.

$$N_p(/) = \left[\left(\frac{K_p}{Re}\right)^{\alpha} + {N_{p0}}^{\alpha}\right]^{\frac{1}{\alpha}} \qquad \textit{Eq. 2-29}$$

From the power consumption curve, reference values, $Re_{crit\text{-}1}$ and $Re_{crit\text{-}3}$ were identified as leading to a 15 % deviation of Np (**Eq. 2-29**) from laminar (Np = Kp/Re) and turbulent (Np = Np_0) models, respectively. In addition, $Re_{crit\text{-}2}$ = 642 was identified by the intersection of laminar and turbulent models.

In the non-Newtonian case, a generalized mixing Reynolds number has to be defined as the viscosity is not a constant. The well-known Metzner and Otto concept (1957) was used: an equivalent viscosity μ_{eq} is defined as the Newtonian viscosity leading to the same power number. Metzner and Otto (1957) showed that the equivalent shear rate $\dot{\gamma}_{eq}$ associated to this viscosity (through the rheological behaviour of the fluid) is proportional to the rotation frequency, then introducing the Metzner-Otto parameter Ks:

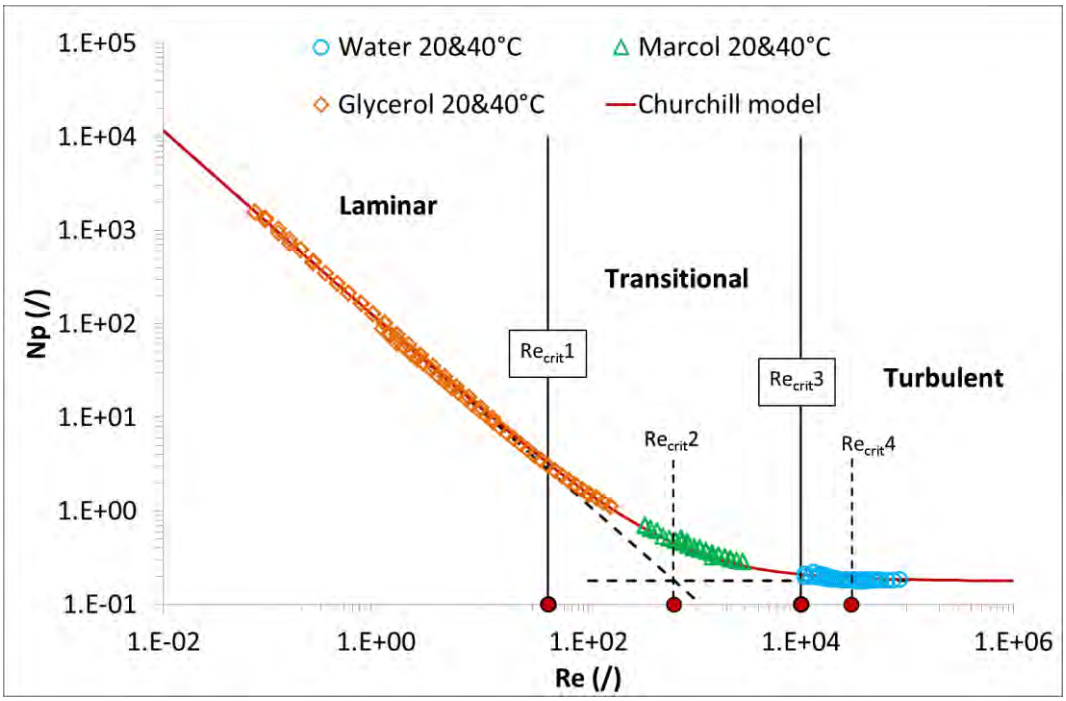

Figure 2-6. Power consumption curve, Np-Re of experimental set-up

$$\dot{\gamma}_{eq} = K_s \cdot N \qquad \textit{Eq. 2-30}$$

For the shear-thinning fluids described by a power-law, $\mu = k \cdot \dot{\gamma}^{n-1}$, this leads to the generalized Reynolds number:

$$\mathrm{Re}_g = \frac{\rho \cdot N^{2-n} \cdot d^2}{k \cdot K_s^{n-1}} \qquad \textit{Eq. 2-31}$$

Ks is a constant depending only on the geometry of both reactor and impeller. The concept can be extended to the transition region using a power equation (Jahangiri, Golkar-Narenji et al. 2001). Xanthan solutions (0.04 %; 0.1 %; 0.4 %) in glucose solution (650 $g.L^{-1}$) and in sucrose solution (943 $g.L^{-1}$) were used to determine the proportionality constant Ks. The corresponding value of the shear rate, $\dot{\gamma}_{eq}$, was extracted from the rheogram of the Xanthan solutions. Rieger and Novak's approach (Yang, Zhang et al. 2010) was used to determine the value of Ks: **Eq. 2-30** with the generalized Reynolds number Re^* is written in a similar form:

$$N_p \cdot Re^* = K_P(n) \qquad \textit{Eq. 2-32}$$

With $\mathrm{Re}^* = \frac{\rho \cdot N^{2-n} \cdot d^2}{k}$ and $K_P(n) = K_P \cdot K_s^{n-1}$.

The value of Ks is directly deduced from the linear regression $Ln[K_p(n)] = f(n-1)$ using the previously determined Kp value. This leads to Ks ≈ 38.5 (/).

- *Use of power consumption curve and extended Metzner and Otto concept.*

The in-situ viscometry was conducted throughout hydrolysis in order to estimate the suspension viscosity and to establish the rheogram.

During experiments, the torque measurement used in conjunction with the power consumption curve, allowed the determination of a Reynolds number, and then of the viscosity. This procedure is valid as long as the power consumption curve allows a one to one correspondence between Np and Re. This is true in the laminar and transition regimes. However, precision decreases when Reynolds number increases as variations of Np are weaker and weaker until a roughly constant value for Np in the turbulent regime. For this reason, viscosity calculus using **Eq. 2-33** was limited to $Re < Re_{crit\text{-}4} = 30000$ (beyond this value, Np was almost constant) even if between $Re_{crit\text{-}4}$ and $Re_{crit\text{-}3}$, viscosity calculus was poorly reliable (± 200 %). Detailed methodology was previously described (Nguyen, Anne-Archard et al. 2013) and all critical Re were illustrated in **Figure 2-6**.

$$\mu(Pa.s) = \frac{\rho \cdot N \cdot d^2}{Re} \qquad \textit{Eq. 2-33}$$

To establish the suspension rheogram, it is mandatory to identify the equivalent shear rate, $\dot{\gamma}_{eq}$. This was only possible in laminar regime (Metzner and Otto 1957) and extended to the transition regime using a power equation (Jahangiri, Golkar-Narenji et al. 2001). In our case, this interpretation was limited to $Re < Re_{crit\text{-}2}$.

2.4.3.2.2 Identification of power law index

Shear-thinning (or pseudo-plastic) is a term used in rheology to describe non-Newtonian fluids which have a decreasing viscosity when subjected to increasing shear rates. For shear-thinning fluids, the relationship between shear stress and shear rate can be modeled by Ostwald-de Waele (or Power-law) formula:

$$\tau = k \cdot \dot{\gamma}^n \qquad \textit{Eq. 2-34}$$

Where k is flow consistency index ($Pa.s^n$), $\dot{\gamma}$ is the shear rate (s^{-1}) and n is the flow behavior index (dimensionless). By definition, apparent viscosity μ of a fluid can be described by

$$\mu = \frac{\tau}{\dot{\gamma}} \qquad \textit{Eq. 2-35}$$

By replacing τ with the Ostwald formula, we obtain then $\mu = k \cdot \dot{\gamma}^{n-1}$

Following Metzner and Otto (1957), in laminar flow, the relation between equivalent shear stress and rotation speed can be represented by $\dot{\gamma} = Ks \cdot N$ where Ks is a coefficient depending only on systems geometry (for our reactor, Ks = 38.9). The concept can be extended to transitional flow according to Jahangiri, Golkar-Narenji et al. (2001). The viscosity from (**Eq. 2-35**) can be written as

$$\mu = k \cdot (K_s \cdot N)^{n-1} \qquad \textit{Eq. 2-36}$$

In our work, by periodically increasing the rotation speed from 100 rpm (equivalent to N_1) to 125 rpm (equivalent to N_2), it is possible to deduce from **Eq. 2-36** the relationship between viscosity and mixing rate

$$\frac{\mu_1}{\mu_2} = \left(\frac{K_s \cdot N_1}{K_s \cdot N_2}\right)^{n-1} = \left(\frac{N_1}{N_2}\right)^{n-1} \qquad \textit{Eq. 2-37}$$

From the semi-empirical Re – Np equation (**Eq. 2-29**) and for $Re < Re_{crit\text{-}2}$, the relationship between Reynolds number and mixing rate can also be be written.

$$\frac{Re_2}{Re_1} = \frac{N_2^2 \cdot M_1}{N_1^2 \cdot M_2} \qquad \textit{Eq. 2-38}$$

From **Eq. 2-33**

$$\frac{\mu_1}{\mu_2} = \frac{Re_2}{Re_1} \cdot \frac{N_1}{N_2} \qquad \textit{Eq. 2-39}$$

Eq. 2-38 and **Eq. 2-39** lead to

$$\frac{\mu_1}{\mu_2} = \frac{N_2 \cdot M_1}{N_1 \cdot M_2} \qquad \textit{Eq. 2-40}$$

Finally, using **Eq. 2-40** and **Eq. 2-37,** the dependence of torque on mixing rate can be written as

$$\frac{M_1}{M_2} = \left(\frac{N_1}{N_2}\right)^n \leftrightarrow ln\frac{M_1}{M_2} = n \cdot ln\frac{N_1}{N_2} \qquad \textit{Eq. 2-41}$$

Knowing the corresponding torque values (M_1, M_2) for the imposed mixing rate (N_1, N_2), the flow behavior index (n) can be deduced from equation **Eq. 2-41.**

2.4.4 Particle size and morphology analysis

The rheological behavior of the suspension and the fiber particle size and morphology stand out as determinants of the process efficiency. They are the principal elements for the choice of the equipment and the strategy. This section will detail the different methods used to characterize particle size and shape. Two types of measurements were used: in-situ chord length measurement (FBRM) and ex-situ particle size analysis which consist of two methods: laser granulometry and morpho-granulometry.

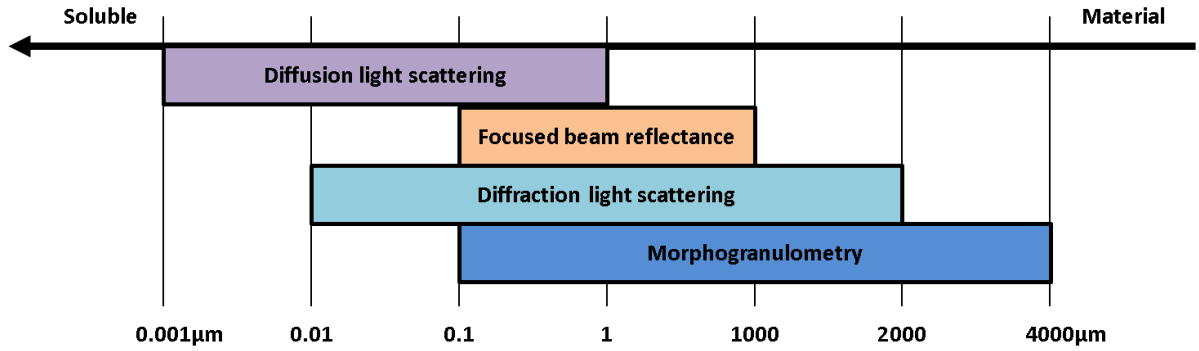

Figure 2-7. Overview of size range associated with identified technics.

Figure 2-7 illustrates the overlapping of size range for the three methods: focused beam reflectance (FBRM), diffraction light scattering (DLS) and optical morphogranulometry (MG). The bioconversion of raw (lignocellulosic) material into final molecule of interest (glucose, xylose) can be illustrated by a reduction of particle size from coarse to fine and soluble molecules. The combination of these three methods allows characterization of particle size between 0.01 and 10000 µm. Each technique presents several advantages and drawbacks associated to its principles, to sample preparation, and to assumptions needed for signal and data treatment and transformation. The three techniques are associated to three different approaches to characterize the particle size and shape.

Table 2-7: Summary of particle size analysis techniques.

Method	FBRM	DLS	MG
Measurement mode	In-situ	Ex-situ	Ex-situ
Wave length	795 nm	632.8 nm 470.0 nm	White light
Sample preparation	None	Dilution	Ultrasound Dilution Sample fixing
Analyse	2D	3D	2D
Measured quantity	l_c, N_c	D_{SE}	D_{CE}
Distribution	Number	Volume	Number

Table 2-7 summarizes the general properties of these techniques. Detailed descriptions for each analysis method as well as common theory are presented in the following. The FBRM allows the monitoring in-situ and in real time of the evolution of chord length during hydrolysis. Not limited by the number of sample, FBRM is a powerful tool for studying the evolution of particle size during reaction. It provides information about number distribution of particle chord length, which is sensible for the fraction of fine population. In the other hand, the DLS measurement's principle, based on volume distribution, highlights the contribution of coarse population. The advantage of both FBRM and DLS methods is simple manipulations that minimizing the measurement error. However, the conversion from raw signal into final data (distribution function) needs to be performed under restriction considering the mathematical model used. The last method, optical morphologranulometry (MG) appears as the most reliable technique as it is based on direct observation of particles under microscopy and requires less

theoretical assumption than FBRM or DLS. In contrast, the disadvantages of MG come from the sample preparation step, which strongly affect measurement results.

2.4.4.1 Theory associated with distribution function and mean diameter definitions

To compare the particle sizes of the various matrices and also to monitor their changes during enzymatic attack, the analysis of distribution profile is used. These distribution profiles can be compared via distribution functions E(x) and cumulative distributions functions F(x) (**Eq. 2-42**). They can be represented as discrete or continuous functions (p_i is the probability corresponding to class i).

	Distribution	Cumulative distribution
Continuous function	$E(x) \cdot dx = \frac{dn}{n}$	$F(x) = \int_0^{\infty} E(x) \cdot dx = 1$
Discrete function	$p_i = \frac{dn}{n}$	$F = \sum_0^{n_c} p_i = 1$

Eq. 2-42

Each distribution function can be characterized by a range of moment and centred moments of order j (**Eq. 2-43**) (Mosier, Wyman et al. 2005, Himmel, Ding et al. 2007, Sánchez, Quintana et al. 2015)

$$\Gamma^i = \int_0^{\infty} x^i \cdot E(x) \cdot dx \quad and \ \Gamma^{i'} = \int_0^{\infty} (x - \bar{x})^i \cdot E(x) \cdot dx \qquad \textit{Eq. 2-43}$$

The function E(x) is characterized by his average value, $\bar{x}$ which is the moment of order 1, Γ^1. The variance σ^2 and the reduced variance $\beta^2 = \frac{\sigma_x^2}{\bar{x}^2}$ correspond respectively to centered moments of order 2; $\Gamma^{2'}$ and $\frac{\Gamma^{2'}}{\bar{x}}$ characterize the dispersion of the distribution curve. The centered moments of order 3, $\Gamma^{3'}$ or $\frac{\Gamma^{3'}}{\sigma^3}$ provides information on the asymmetry of the curve (Skewness). An asymmetric distribution is left when S<0 and is right when S>0. The centered moments of order 4, $\Gamma^{4'}$ or $\frac{\Gamma^{4'}}{\sigma^4}$ allows evaluating the spread of the distribution curve (Kurtosis).

There are various ways to define an "equivalent" diameter for a non-spherical particle that will be reduced to the diameter if the particle is a spherical one (**Table 2-8**). Liu, Xu et al. (2015) have listed thirteen possible ways to define an equivalent diameter of a given particle using sphere as reference. The sphere is chosen as reference because of its unambiguous definition of the diameter. However, most of the particles are not spherical; the knowledge of more than one dimension is required to describe the shape of a particle. The most useful diameter is the diameter of the volume equivalent sphere, d_v, which corresponds to the diameter of the sphere having the same volume as the particle.

Each measurement technique for spherical geometry should give the same result. For irregular shapes, there is an influence of the measurement method, which must then be selected with a particular care.

Table 2-8. Diversity of particle equivalent diameter definitions.

Symbol	Appellation	Definition
d_v	Volume diameter	Diameter of the sphere that has the same volume as the particle: $v_i = \frac{\pi}{6} \cdot d_v^3$
d_s	Surface diameter	Diameter of the sphere that has the same area as the particle: $s_i = \frac{\pi}{4} \cdot d_s^2$
d_p	Perimeter diameter	Diameter of the sphere that has the same perimeter as the projected area of the particle: $p_i = \pi \cdot d_p$
d_c	Falling diameter	Diameter of the sphere that has the same density and the same free-fall velocity of the particle in a fluid at the same density and same viscosity.
d_{St}	Stockes's diameter	Diameter of a sphere freely falling at the same velocity as the particle in a laminar flow (Rep < 0,2).
d_t	Sieving diameter	Side of the smallest square mesh through which the particle can move.
d_F	Feret diameter	The distance between the two parallel planes restricting the object perpendicular to that direction.
d_d	Diffraction diameter	Diameter of the circle that generates the same beam deflection that the particle due to the wave nature of the radiation.

Because of the non-uniform size of particles, the variation of population size is presented as a size distribution. In this work, the frequency distributions or cumulative distributions are used. Most existing techniques give the characterization of distributions based on the number, length, surface or volume of the particles.

Depending on the definition of the classes of particle, four types of distributions are defined (

Table 2-9). Considering the complexity of particle shapes and according to the highlighted properties, it is important to define a mean diameter (and standard deviation describing the width of the distribution around this average trend) for a given particle population. The average diameter is defined as follows:

$$d_{p,q} = \left[\frac{\sum n_i \cdot d_i^p}{\sum n_i \cdot d_i^q} \right]^{1/p-q} \qquad \textit{Eq. 2-44}$$

with n_i: the number of particles of diameter d_i. (Mesa, López et al. 2016).

We note $d_{1,0}$ the number-average diameter, $d_{2,0}$ the quadratic mean diameter, $d_{3,0}$ the cube average diameter, $d_{4,3}$ the mass or volume mean diameter, $d_{3,2}$ the area-average diameter or Sauter diameter...

Table 2-9. Definitions of distributions in number, dimension, surface and volume.

Distribution	Signification	Formula
Distribution in number	Percentage in number associated with each class	$p_{n_i} = \frac{n_i}{\sum n_i}$
Distribution in dimension	Percentage in dimension associated with each class	$p_{d_i} = \frac{n_i \cdot d_i}{\sum n_i \cdot d_i}$
Distribution in surface	Percentage in surface associated with each class	$p_{s_i} = \frac{n_i \cdot d_i^2}{\sum n_i \cdot d_i^2}$
Distribution in volume	Percentage in volume associated with each class	$p_{v_i} = \frac{n_i \cdot d_i^3}{\sum n_i \cdot d_i^3}$

2.4.4.2 Diffraction Light Scattering (DLS)

The volume weighted particle size distribution was determined with diffraction light scattering (Mastersizer 2000 Hydro, Malvern Instruments Ltd. SN: 34205-69, range from 0.01 to 2000 µm). A known volume of suspension (0.5-3 mL) was added in the water circulation loop in order to obtain laser obscuration rates (red λ = 632.8 nm and blue λ = 470.0 nm lights) between 5 % and 40 %. Whole suspension was mixed by a Heidolph magnetic stir at 200 rpm when circulation loop was maintained by a Masterflex L/S model 7553-79 at pump speed 240 rpm (tube Tygon, R, Saint Gobain Plastics, ref: 89120, ID:4.8 mm, AD: 8.0 mm). Analyses are conducted at room temperature (20 °C). Raw signal (scattered light) was converted into a particle size distribution following Mie scattering theory or the Fraunhofer approximation (of Mie theory). The principle of method is described in **Figure 2-8.**

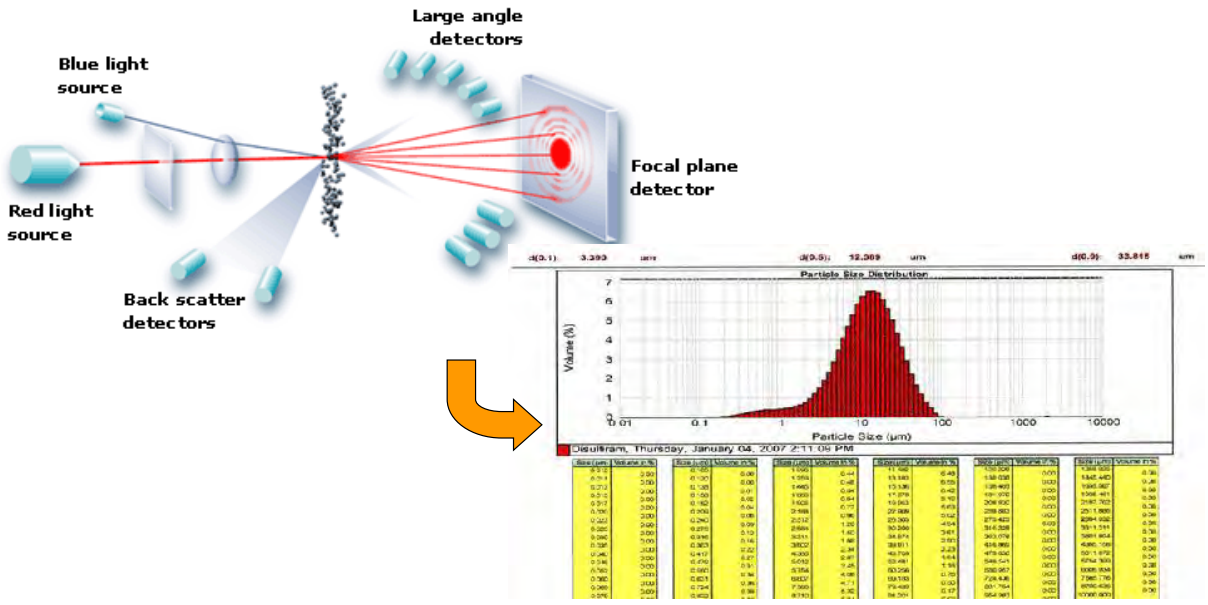

Figure 2-8. Operational principle of laser granulometer – Example of result presentation.

For each sample, analyses were performed for 3 dilution rates and in triplicate. From the average results, a volume weighted particle size distribution (E_v) was calculated by the Mastersizer software. The diameter of a theoretical sphere d_{SE} that has the same volume than the particle was used as the criteria for particle size. Particle size distribution $E_v(d_{SE})$ during enzymatic hydrolysis was weighted by volume fraction (Φ_V) in order to evaluate the impact of solubilization on suspended population. The volume fraction Φ_V was estimated from measured dry matter content and substrate densities. Particle volume diameters $d_v(0.1)$, $d_v(0.5)$, $d_v(0.9)$ indicating the value of diameter corresponding to 10 %, 50 % and 90 % of the population by volume were also investigated. The volume weighted mean diameter D[4,3] was calculated following **Eq. 2-44**.

In addition, the evolution of obscuration rate versus substrate concentration was also considered. It informed about optical properties of particle during enzymatic hydrolysis.

2.4.4.3 Focus Beam Reflectance measurement (FBRM)

Focus beam reflectance measurements enable in-situ quantification and characterization of chord length distribution (CLD). The major advantage of in-situ measurement is that it allows a real time tracking of the evolution of suspension without sampling and preparation steps. In-situ CLD was realized using an FBRM G400 probe (Mettler Toledo, range: 0.1 to 1000 µm). Its principle is illustrated in **Figure 2-9**. A solid-state laser light source (λ = 795 nm) provides a continuous beam of monochromatic light. An intricate set of lenses focuses the laser light to a small spot. This focal spot is carefully calibrated to be positioned at the interface between the probe window and the fluid. Tightly controlling the position of the focal spot is necessary to obtain sensitive and repeatable measurements. A precision electric motor is used to precisely rotate the optics at a constant speed (2 $m.s^{-1}$). The focused beam scans a circular path at the interface between the probe window and the suspension. As the scanning focused beam sweeps across the face of the probe window, individual particles or particle structures (agglomerated or floc) will backscatter the laser light back to the probe. Particles and droplets closest to the probe window will be located in the scanning focused spot and backscatter distinct pulses of reflected light. These pulses of backscattered light are detected by the probe and translated into chord lengths, based on the simple calculation of the scan speed (velocity) multiplied by the pulse width (time); a chord length is simply defined as the straight-line distance from one edge of a particle or particle structure to another edge. Thousands of individual chord lengths are typically measured each second to produce the Chord Length Distribution which is the fundamental measurement provided by FBRM®.

The FBRM probe was directly inserted in the reactor to track changes in particle size and count in real time during enzymatic hydrolysis. Acquisition time for all experiment was chosen equal to 1min, meaning 1 data point was calculated from the average chord count per second during 1min interval. The iccFBRM software treated the raw data by dividing the size range from 0.1 to 1000 µm into 1000 class by logarithm distribution then returned the average value of counts/s for each class. Due to technical limitation, user can only export the pre-classified data with 100 classes ranging from 0.1 to 1000 µm. The number distribution of chord length, $E_n(l_c)$, and the mean chord length, l_c, were calculated following **Eq. 2-45**

$$E_n(l_c)_i = \frac{N_c(i)}{\sum_{i=1}^{100} N_c(i)} \cdot 100\ (\%)$$

$$l_c = \frac{1}{100} \sum_{i=1}^{100} E_n(l_c)_i \cdot M_i \qquad \textit{Eq. 2-45}$$

Where i: class number ($1 < i < 100$), $N_c(i)$: average number of chord counted per second for the class i, M_i: the middle value of size band for class i (µm)

Differently from DLS, the FBRM provides chord length distribution (CLD). The conversion from number weighted CLD into volume weighted PSD is possible under severe assumptions (Nguyen, Anne-Archard et al. 2015). Several modeling approaches for the generation of CLD from known PSD can be found in the literature (Bradford 1976, Rocha, Gonçalves et al. 2012). Furthermore, solutions for the inverse problem of reconstructing a PSD from a CLD using these models have been addressed (Wynn 2003, Worlitschek and Mazzotti 2004, Li and Wilkinson 2005, Giovanni, Eleonora et al. 2011). For lignocellulosic substrates which contain deformable particles of various shapes, dispersed size and high aspect ratio, there are no appropriate model for the conversion of CLD into PSD. Consequently, the number weighted distribution of chord length, $E_n(l_c)$, and the average number of chord counted per second, N_c, will be used as indicators of population evolution. In order to facilitate the comparison between experiments, normalized parameters were defined as the ratio between instant value and initial value at t = 0h.

Normalized mean chord length

$$l_c^*(t) = \frac{l_c(t)}{l_c(t = 0h)} \qquad \textit{Eq. 2-46}$$

Normalized total chord counts

$$N_c^*(t) = \frac{N_c(t)}{N_c(t = 0h)} \qquad \textit{Eq. 2-47}$$

Furthermore, as native measurements are number based, the under-represented classes into widespread population may become non-significant. It will be the case for the largest particles with FP and SCB substrates.

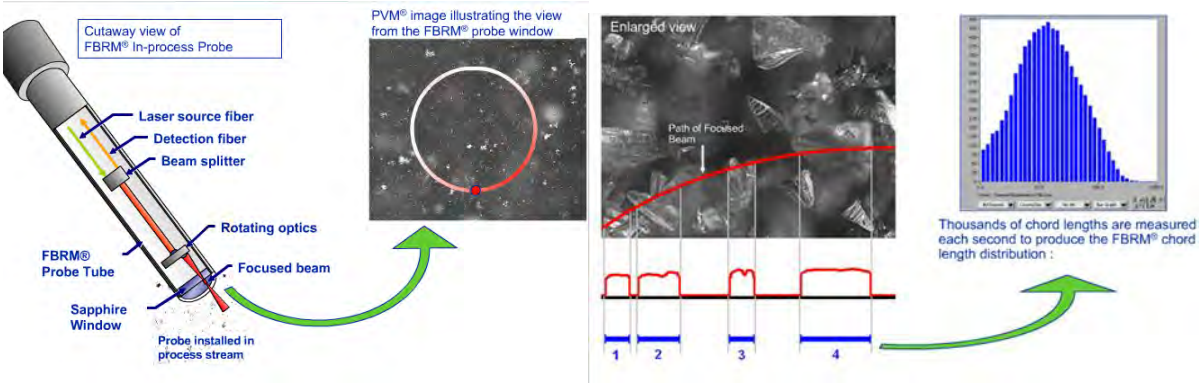

Figure 2-9. Operational principle of FBRM sensor from light signal up to CLD.

2.4.4.4 Optical morpho-granulometry (MG)

The morphologranulometry of lignocellulosic particles in suspensions was analyzed using a mopho-granulometer (Morphologi G3S, Malvern Instruments Ltd. SN: MAL1033756, software Morphologi v8.1.1). This optical device includes a lens (magnification: from x1 to x50, dimension min/max: 0.2/3000 µm), an optical system (Nikon CFI60 Brightfield/Darfield) and a camera (IEEE1394a, FireWireTM, 2592x1544 pixels). Principles of measurement and data encoding are represented in **Figure 2-10** and **Figure 2-11**. The advantages of this method, is definitively a very detailed description of each particle that appears in the observation zone. Post measurement analysis by Morphologi software is capable to provide fully statistical information about particle such as Circle Equivalent diameter, Mean diameter, Length, Width, Perimeter, Area, Aspect ratio (width/length), Circularity, HS Circularity, Convexity, Solidity, Elongation, Major Axis, Max. Distance, SE Volume, Mean Intensity, Intensity Standard Deviation.

Samples were analyzed by "wet" way following a standardized procedure (**Figure 2-13**). Suspensions were firstly treated in ultrasonic water bath for 15 min in order to separate individual particles and agglomerates before dilution using demineralized water from 10 to 40 times depending on substrate concentration. One drop of dilute sample was deposited on a glass slide with cover slip. Nail lacquer was used for fixing the position of cover slip on the glass slide as well as to prevent water evaporation during analysis. The capture of image was then performed by scanning the sample underneath the microscope optics (lens 10×) in dark field mode (illuminated from above), light intensity 90 %, exposure time 400 ms, and single image overlap 40 %. Single captured data was encoded as 8 bits grayscale image. A recomposed image of a surface 1cm×1cm was re-created from all single captures.

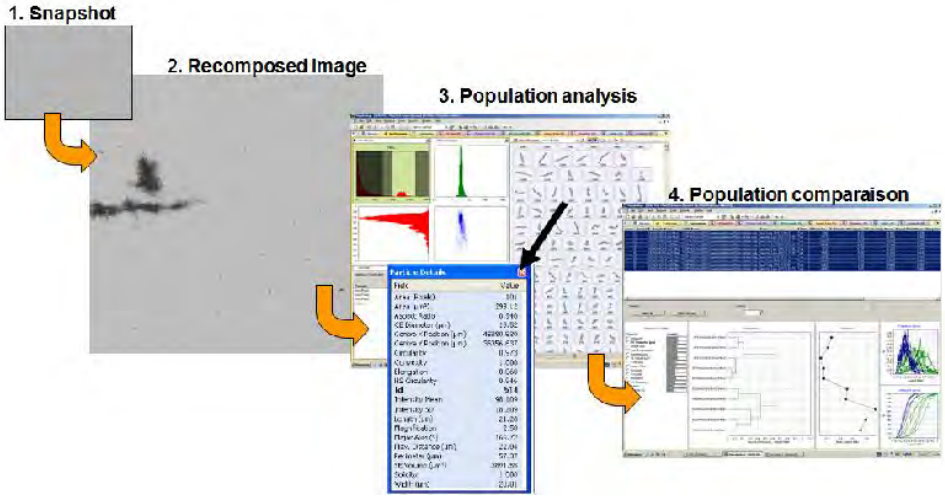

Figure 2-10. Principe and working step with Morphology G3S apparatus.

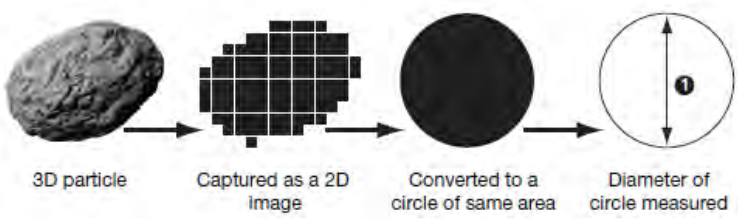

Figure 2-11. Data acquisition and image analysis of Morphology G3S.

Table 2-10. Circularity and HS-circularity of various references shapes.

Shape					
Circularity	1	0.952	0.886	0.835	0.608
HS-circularity	1	0.907	0.785	0.698	0.370

Figure 2-12. Illustration for particles in contact with lightning trace.

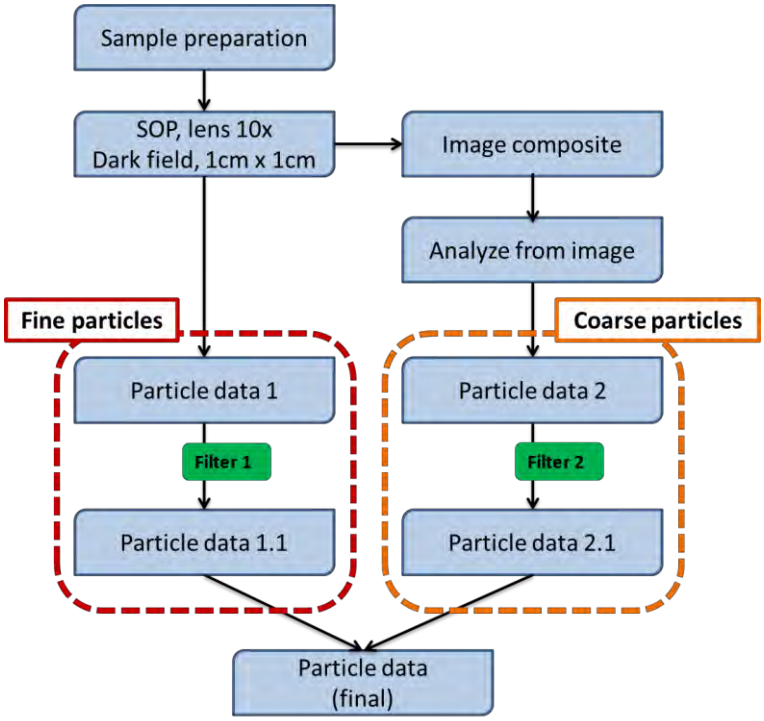

Figure 2-13. Procedure for morphogranulometry analysis using Mastersizer G3S.

Obtained data were treated under Morphologi v8.1.1 software. Firstly, a data filter was applied, particles of Area < 1.25 μm^2 and HS circularity > 0.91 were eliminated. Technical limitation of analytical systems reported a pixel size for 10× lens equals to 0.28 µm, equivalent to an Area equal to 0.078 μm^2. In this work, a particle is defined by minimal dimension of 4 pixels × 4 pixels, equivalent to an Area equal to 1.25 μm^2. In addition, particles having HS circularity ≥ 0.91 are generally sphere-like (**Table 2-10**) which represents lightning trace in halo form. Finally, particles in contact with lightning trace (**Figure 2-12**) were also removed by manually scanning the population. Filtered data was named "*Particle data 1.1*" (**Figure 2-13**)

Due to the fact that, the suspension of FP and PP contain a broad range of particle size from fine to coarse fiber, the analysis using lens 10× was unable to recognize all particles size. The

largest fibers were always omitted when analyzing data with Morphologi software. A second step specifically for coarse particles was then added. It consisted in a statistical analysis of the recomposed image. Statistical data on coarse particles, named "*Particle data 2.1*", were combined with "*Particle data 1.1*" to form a final statistical data of a sample. From the final data, number and surface weighted particle size distribution (E_n, E_s) were calculated using Excel software. The diameter of a theoretical circle that has the same area of the particle (d_{CE}) was used as the criteria for particle size.

The morpho-granulometry analysis presents several advantages but also drawbacks. Firstly, this is a very time-consuming method; the analysis in dark field mode requires an exposure time (≈ 400 ms in present case) for each single capture. An observation of a surface 1 cm by 1 cm on lens 10× took 40 min approximately to be completed. In addition with the time needed for sample preparation and fixing, total analysis time for one sample took around 55 min. This number strongly depends on observation surface, overlap percentage between single capture and lens magnification. Secondly, it seems that fiber's parameters including fiber length and fiber width were not correctly calculated by the Malvern's software. To assess the fiber's length, its "skeleton" is assessed and the length is derived. Effectively this gives the length of the fiber as if it was straightened out. The fiber width is calculated from particle area and fiber length as

$$Fiber\ width\ = \frac{Particle\ area}{Fiber\ length}$$

Several particles showed a value of fiber width superior to fiber total length following Morphologi v8.1.1 analysis. Once the phenomenon was observed, it is suggested that the calculation of fiber length encountered an error, leading to false value of fiber width. In order to ensure reliable results, the interpretation of morphological data is limited to d_{CE} and particle area. All fiber parameters were not taking in consideration.

2.5 METHODOLOGY

2.5.1 Study strategy

Our strategy was based on three scientific questions corresponding to three working packages

i) To investigate the role of single up to cocktail activities in the enzymatic hydrolysis of lignocellulosic biomass.
ii) To understand the hydrolysis mechanisms hiding behind observed phenomena by both physical and biochemical approach.
iii) To investigate the fed-batch hydrolysis at high dry matter content in order to reach better final product concentration and overpass physical limitations.

In the first working package, preliminary experiments and analysis were performed. It represents two sub-parts focusing on experimental systems and raw material. The development and hydrodynamic characterization of working systems is presented previously in **§2.1**. It enables the real time tracking of torque and chord length during enzymatic hydrolysis. The characterization of raw material, which consists in physical and biochemical properties of substrates and suspensions, as well as enzyme analysis will be discussed in **§3.1**.

The purpose of the second working package is to answer two scientific questions: hydrolysis mechanisms and contribution of single activity enzymes. Different levels of observation from macro scale (viscometry and rheometry); micro scale (DLS, FBRM, and MG) and molecular scale (biochemical analysis) sustain this investigation. In-situ viscometry provides information related to the liquefaction mechanisms through analyze of the time-evolution of suspension

viscosity. In parallel, ex-situ rheometry measurements reveal suspension yield stress as well as the evolution of viscous and elastic modulus during enzymatic reaction. In addition, in- and ex-situ granulometry analyze the evolution of particle size and shape during enzymatic hydrolysis. Finally, biochemical approach constitutes the last shard to complete the full overview of implied mechanisms.

The third working package focused on the proposition of a semi-continuous fed-batch strategy to achieve high concentration hydrolysis. For these experiments, a specific screw-pump systems and *Pilote_HTMS* software were developed in order to carry out the adding of substrate. Its allows to run enzymatic hydrolysis at different feeding rate as well as real time data acquisition of process parameters such as pH, temperature and mass balance. Similarly with the hydrolysis in semi-dilute condition, the observation of phenomena was based on the tripode Macro – Micro – Molecular scales with in- and ex-situ analysis.

2.5.2 Characterization of substrates and rheology of suspension

Prior to enzymatic hydrolysis, rheological properties of lignocellulosic suspensions were characterized using our experimental design (**Figure 2-1**). Suspensions at different concentrations (up to 15 gdm/L for FP, 35 gdm/L for PP and 53 gdm/L for SCB) were characterized using different impeller speeds (from 20 to 250 rpm). The experimental protocol is illustrated in **Figure 2-14**.

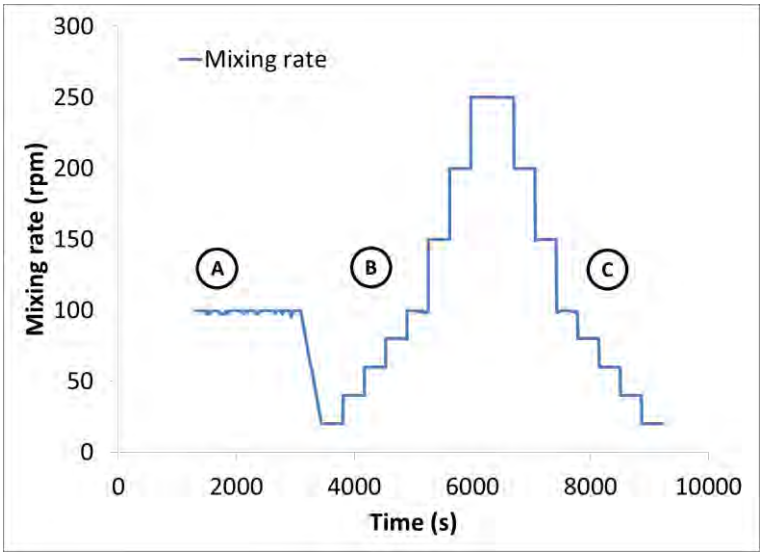

Figure 2-14. Rheological characterization of suspensions. (A) stabilization step, (B) ascending step, (C) descending step.

Lowest concentration of tested suspension (1300 mL) was mixed at 100 rpm, T = 40 °C for approximately 1 hour to obtain homogeneous state. This was then followed by an ascending step of mixing rate, started at 20 rpm and ended at 250 rpm. Finally, a descending step was performed. For each mixing rate at given concentration, the duration of mixing was equal to 300 s with data acquisition every 3 s. At the end of experiment, substrate was added to reach the chosen concentration and the protocol was repeated. Suspension viscosity for a given substrate concentration at specific mixing rate was deduced following described method (**§2.4.3.2.1**) from the mean value of measured torque. The relationships between suspension viscosity and substrate concentration or imposed shear rate (equivalent to mixing rate by Metzner and Otto coefficient – Ks) were then established. For each substrate, the viscosity versus shear rate relation was modeled using a Power law equation and the viscosity versus concentration (for a given shear rate) was modeled using a Krieger-Dougherty or a Simha

relations. Once successfully established, these models allow firstly the prediction of suspension viscosity at specific condition of mixing rate and concentration. It is valuable to design a hydrolysis process at high dry matter content. Secondly, critical concentration points indicating the change between different regimes could be pointed out.

2.5.3 Enzymatic hydrolysis at semi-dilute conditions (batch mode)

Enzymatic reactions were carried out during 24 h at 100 rpm, 40 °C, pH 4.8 ± 0.2 with a total volume equal to 1.3 L. The temperature of reaction in this work is fairly lower than known optimum temperature of cellulase cocktail (50 °C). It results from energy saving considerations together with conditions for the fermentation step which will be further added toward a simultaneous saccharification and fermentation process. The pH was automatically adjusted using diluted sulfuric acid 0.05 N. An antibiotic (1.3 mL of chloramphenicol 50 $g.L^{-1}$) was added to prevent microbial contamination. As mentioned in **§2.5.1**, experiments were proceeded in two steps: batch enzymatic hydrolysis in semi-dilute condition and short duration then semi-continuous feeding strategy for concentrated conditions.

For semi-dilute conditions, these experiments were carried out through three steps: i) the torque control (with water) and substrate adding (**Figure 2-15** phase A and B), ii) homogenization of suspension (**Figure 2-15** phase C) and iii) enzymatic hydrolysis (**Figure 2-15** phase D). In the first step, water at 40 °C was mixed at 100rpm for around 15min to verify the blank torque value of the system. Then substrate was added little by little up to the desired concentration. In the second step, the material was mixed with water at 100rpm for a given duration (2-10hrs depending on substrate properties) in order to reach a homogeneous suspension and a stable torque. In the last step, enzymes were added (at time t = 0) and in-situ measurements (torque, pH, T, chord length distribution) conducted. Experiments were performed at 1.5 % w/v for FP and at 3 % w/v for PP and SCB and from 0.3 to 25 FPU/g cellulose enzymes loading. These concentrations are 1.5 to 2 times higher than the critical concentration beyond which the regime is a semi-dilute one. This choice of semi-dilute regime leads to non-Newtonian behaviors without the full complexity of concentrated regimes due to strong interactions between fibers. In addition, working at very low enzyme loading, hydrolysis kinetic is slowed down that facilitates the observation and the characterization of phenomena. Varying the enzyme to substrate ratio (E/S) enables to investigate rheological behavior and changes in particles size and shapes at differences levels of bioconversion. In the results presentation and knowing the non-Newtonian behavior of suspensions, one specific value of viscosity is chosen to follow the time evolution of hydrolysis, namely the viscosity at 100 rpm (μ_{100rpm}). Moreover the in-situ viscometry was investigated every 30 minutes by considering the repetition of the cycle: (i) mixing at 100 rpm during 28 minutes, (ii) shift at 125 rpm during 1 minute and (iii) linear slowdown to 100 rpm in 1 minute. Data acquisition was adjusted to 1 minute at constant mixing (100rpm) and increased to 10 s in other conditions. Samples (20 mL) were taken at 0 h, 1 h, 2 h, 3 h, 6 h, 12 h, 18 h and 24 h for biochemical and granulometric analysis. Detailed information on experiments at semi-dilute condition is presented in **Table 2-11**.

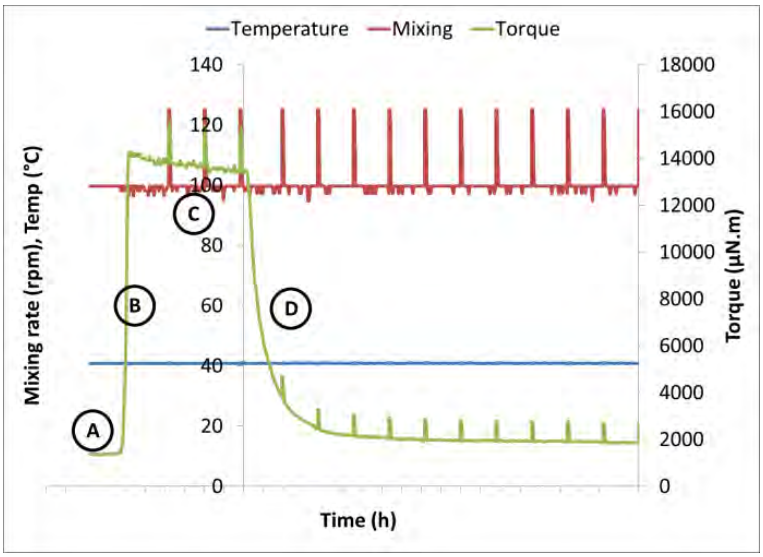

Figure 2-15. Batch hydrolysis scheme. (A) test phrase on water to verify blank value of torque, (B) substrate adding to reach specific concentration, (C) suspension homogeneization and (D) enzymatic reaction.

Table 2-11- Overview of batch hydrolysis at semi-dilute condition.

Enzyme (Dose/g cellulose)	Ctec2 (0.3FPU)	Ctec2 (3FPU)	Ctec2 (25FPU)	G1	G2+G3	G1+G2+G3	X1+X2	X1
WP - 1.5 %w/v	x	xx	x	x	x	x		
SCB - 3 %w/v	x	xx		x	x	x		
SCB - 6 %w/v		x						
PP31 - 3 %w/v	x	xx		x	x	x	x	x

G1: endo-glucanase (E-Celan - Megazymes)
G2: exo-glucanase (E6241 - Sigma)
G3: β-glucosidase (49290 - Sigma)
X1+X2: cocktail Xylanase (Multifect- Genecor)
X1: endo-xylanase pure (X2753 – Sigma)`
Ctec2: cocktail lignocellulose (Novozymes)
xx: experiments in duplicate

2.5.4 Enzymatic hydrolysis at concentrated conditions (fed-batch mode)

For semi-continuous fed-batch hydrolysis, enzymatic reactions were started with 1200 mL water at mixing rate 100 rpm, T = 40 °C, pH 4.8 ± 0.2. Humid substrate and enzyme solution was pumped in to reactor using respectively an ultra-compact multichannel pump, Watson Marlow (ref 403U/VM2 50 rpm, 2 channels) and Masterflex (Thermo Fisher, ref 77521-47) at constant pump speed. The relation between pump speed versus flow rate of both enzyme and substrate was characterized preliminary (**Figure 2-16**). Each experimental point is the mean of 3 - 5 pump tests, each test 2 min for enzyme pump and 5 min for substrate pump.

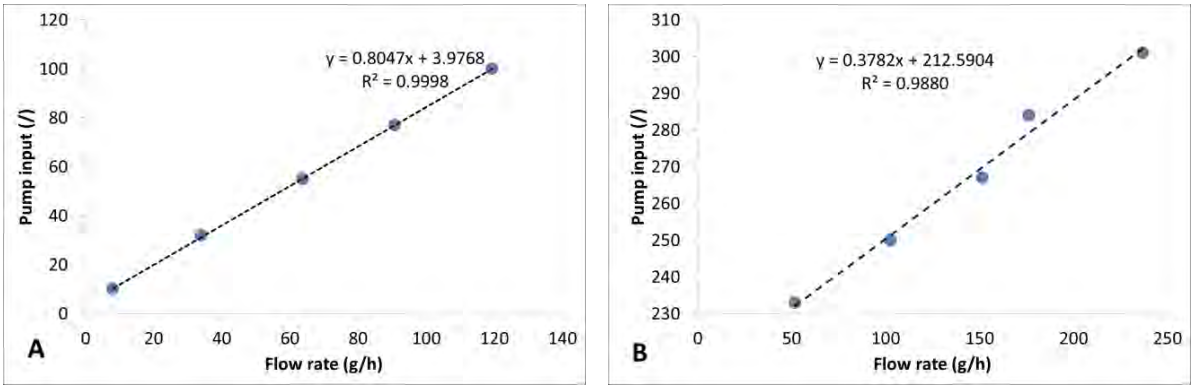

Figure 2-16. Calibration curves for enzyme (A) and substrate (B) pumps established on Ctec2, dillution 10x and sugarcane bagasse.

Torque and in-situ chord length distribution of the suspension were continuously measured and these measurements were used to decide the cycle: when each batch were started or ended. Taking into consideration the technical aspect of currently used viscometer (VT 550 has torque range up to 30. 10^3 µN.m), the upper limit of measured torque was selected at 22.10^3 µN.m ± 10 % and the lower limit represent 25 % of the upper one (**Figure 2-17**). Similar mixing and data acquisition strategies as batch hydrolysis were applied. During enzymatic hydrolysis, samples were periodically taken from the reactor every 1 h at feeding step and 3-12 h at non feeding step for biochemical and morphological analysis. Feed batch hydrolysis was tested only with real lignocellulosic materials (PP and SCB) at different feeding rates and E/S ratios. Final substrate concentration reached between 80 and 140 gdm/L, which was unreachable through batch strategy. **Table 2-12** gave detailed information about semi-continuous fed-batch experiments.

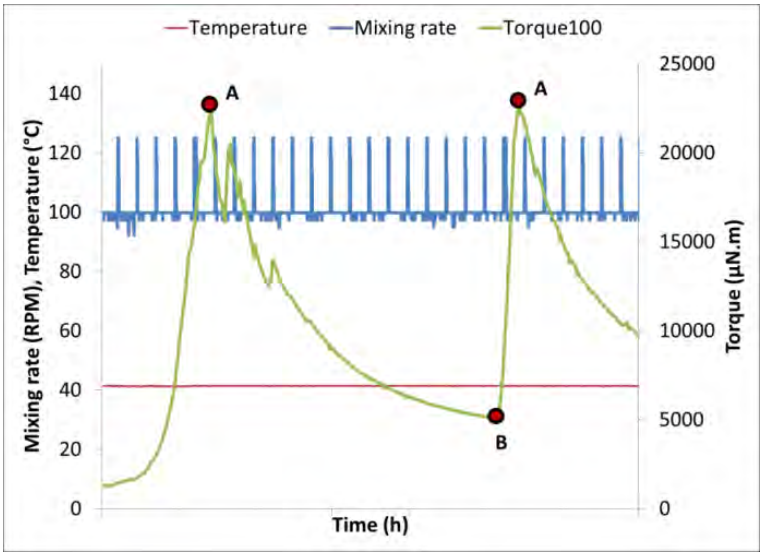

Figure 2-17. Semi-continuous fed-batch mode scheme. (A) upper limit torque, feeding stop when measured torque reachs this point. (B) lower limit torque, feeding start when measured torque decreases to this point.The scheme illustrates only value of torque at 100 rpm, the jump at 125 rpm were identical as batch hydrolysis.

Table 2-12- Overview of semi-continuous fed-batch hydrolysis at concentrated conditions.

Experiment code	PP-1	PP-2	PP-3	SCB-1	SCB-2	SCB-3
E/S ratio (FPU/g cellulose)	3	25	25	3	3	25
Qs (ghm/h)	23.5	23.5	41.9	41.6	23.1	23.4
Final DM	74.7	113.8	99.4	102.4	100.4	140.0

3 RESULTS AND DISCUSSIONS

Corresponding to the research strategy and scientific questions, the experimental part of this study was divided in 4 main work packages (W0 to W4, **Figure 3-1**). The work package W0 corresponded to preliminary experiments aiming to characterize the reactor and mixing system. It was presented in **§2.1** - p60. The results and discussions are structured in three parts corresponding to three mains work packages.

- Part 1 (**§3.1**) reports the physical and biochemical properties of initial substrates and suspensions. Enzyme activities and thermal stability are also presented.
- Part 2 (**§3.2**) provides information about enzymatic hydrolysis at semi-dilute condition through both physical and biochemical points of view in order to reveal appropriated mechanisms hiding behind observed phenomena. In parallel, the mathematical modeling of biochemical and rheological parameters during hydrolysis are scrutinized.
- Part 3 (**§3.3**) presents the enzymatic hydrolysis at high dry matter content (HDM) through semi-continuous fed-batch strategy mode is discussed.

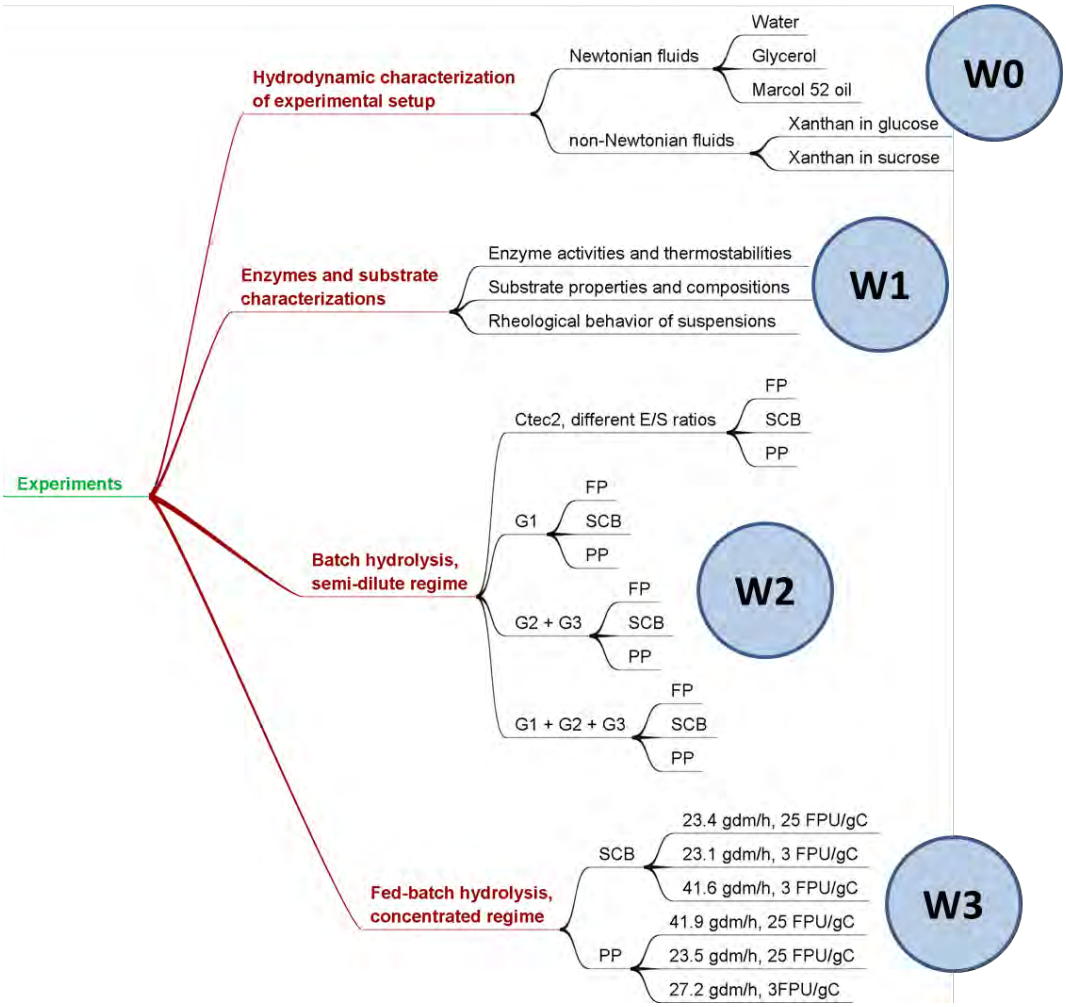

Figure 3-1. Tree diagram describing the experimental plan of PhD. G1: endo-glucanase, G2: exo-glucanase, G3: β-glucosidase, FP: filter paper, SCB: sugarcane bagasse, PP: paper pulp.

The overview on all analysis is represented in **Table 3-1** for experiments at semi-dilute condition and in **Table 3-2** for experiment at high dry matter content. At semi-dilute condition,

nearly all physical and biochemical analysis were performed in- and ex-situ in order to explore the hydrolysis mechanisms. Ex-situ rheology was tested on some experiments for all substrates to compare with in-situ measurements. The optical morpho-granulometry (MG) was unable to apply for PP suspension due to the complexity and poor homogeneity of particles. For experiments at concentrated condition of substrate loading, only vital analysis such as HPLC, in-situ viscometry, DLS and FBRM were carried out. Through hydrolysis at semi-dilute condition, these measurements provided large quantity of data with good reproducibility. Ex-situ rheometry and MG were forbidden due to the strong effect of sample preparation into measurement result.

Table 3-1. Overview of data analysis for enzymatic hydrolysis under semi-dilute condition.

Nº	Substrate	Enzyme	Biochemical (HPLC, YSI)	Rheological		DLS	FBRM	MG
				In-situ	Ex-situ			
01	FP	C-0.3	×	×		×	×	
02		C-3	×	×	×	×	×	×
03		C-25	×	×		×	×	×
04		G1	×	×	×	×	×	×
05		G2+G3	×	×	×	×	×	×
06		G1+G2+G3	×	×	×	×	×	×
07	PP	C-0.3	×	×	×	×	×	
08		C-3	×	×		×	×	
09		C-25	×	×		×	×	
10		G1	×	×		×	×	
11		G2+G3	×	×	×	×	×	
12		G1+G2+G3	×	×	×	×	×	
13		X1	×	×	×	×	×	
14		X1 + X2	×	×	×	×	×	
15	SCB	C-0.3	×	×		×	×	×
16		C-3	×	×	×	×	×	×
17		C-10	×	×			×	
18		C-25	×	×			×	
19		G1	×	×	×	×	×	×
20		G2+G3	×	×		×	×	×
21		G1+G2+G3	×	×		×	×	×
22	SCB 5.3 %	C-3	×	×	×		×	

C: Cellic Ctec 2, G1: endo-glucanase, G2: exo-glucanase, G3: β-glucosidase

0.3, 3, 10, 25: enzyme loading ratios FPU/g cellulose. FP 1.5 % w/v, PP and SCB 3 %w/v.

The strategy of data exploitation is presented in **Figure 3-2**. For three blocks corresponding to biochemical, morphological and rheological analysis, there are three levels of data treatment. First level consists of presenting raw data exported form measurement instrument. For some specific analysis, the raw signal needs to be treated and converted to provide comprehensive data. That is the case of in-situ viscometry where suspension viscosity was calculated from

measured torque and mixing rate. For FBRM, the mean value of chord length and its number weighted distribution was calculated from particle count dividing in 100 classes. For MG analysis, data acquired was the particle encoding in 8 bits grayscale image and it morphological parameters. The number weighted distributions of particles size (d_{CE}) and shape (aspect ratio) were calculated in Microsoft Excel worksheet. In the second level, treated data are deeply discussed and phenomena are modeled using different equation which has been reported from the literature. At the last level, by crossing results from different blocks, we aim to explain hydrolysis phenomena and to reveal the hydrolysis mechanisms.

Table 3-2. Overview of data analysis for enzymatic hydrolysis at concentrated conditions.

Substrate	Feeding rate (gdm/h)	Enzyme (FPU/g cellulose)	Biochemical (HPLC, YSI)	Rheological		DLS	FBRM	MG
				In-situ	Ex-situ			
PP	27.2	3	×	×		×	×	
	23.5	25	×	×		×	×	
	41.9	25	×	×		×	×	
SCB	23.4	3	×	×		×	×	×
	23.1	25	×	×		×	×	×
	41.6	3	×	×		×	×	×

DLS: diffraction light scattering
FBRML focused beam reflectance measurement
MG: optical morphogranulometry

Data analysis is illustrated in **Figure 3-2**. Raw data are divided in three main blocks: biochemical, morphological and rheological. The analysis was performed through three different levels, from raw data treatment up to phenomena characterization and mechanisms.

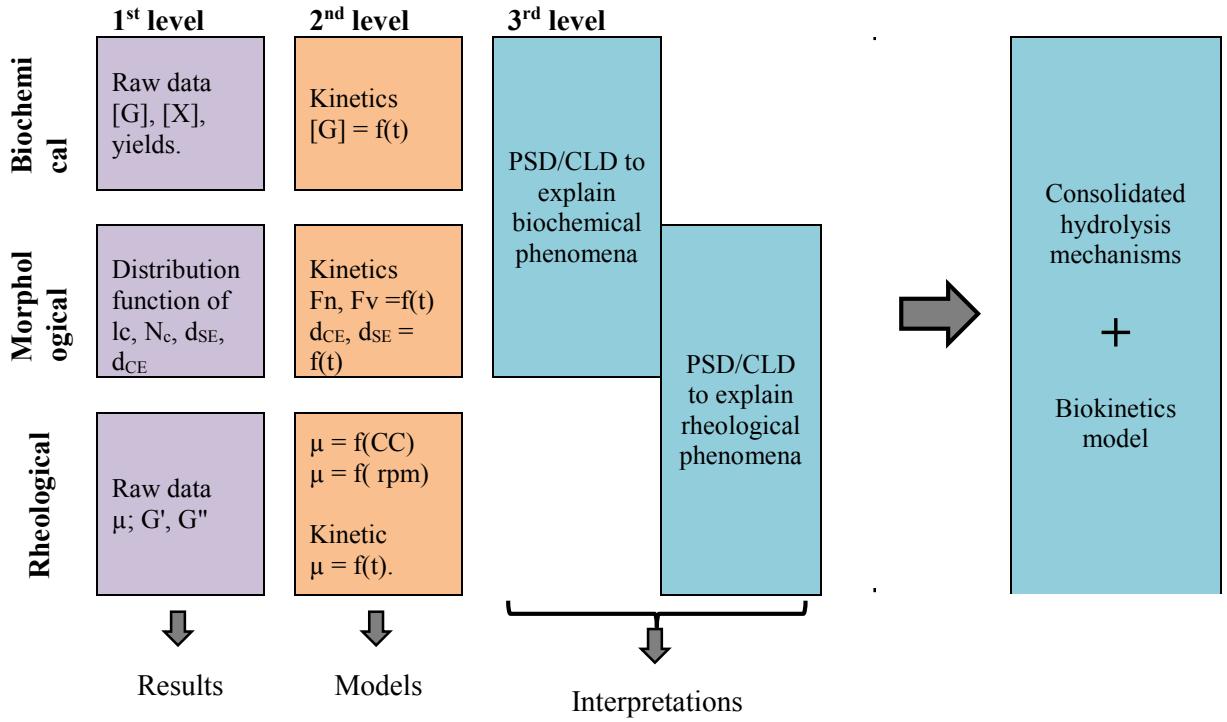

Figure 3-2. Data exploitation strategy.

3.1 R&D: ENZYME ACTIVITY, INITIAL SUBSTRATE AND SUSPENSION PROPERTIES

In a bioprocess, initial properties of materials are important information, which is a guideline for selection and optimization of process parameters and operating conditions. In case of lignocellulosic substrates, several physical and biochemical parameters are measurable and quantifiable such as composition, density of suspension, surface properties, thermal properties, particle size and morphology, rheometry, etc. Among them, density and viscosity are general properties of fluids mechanics which are interested in bioprocess engineering. Lignocellulose suspensions present complex rheological behavior; suspension viscosity stands as a fundamental parameter to design and to configure a mixing device (Samaniuk, Scott et al. 2015, Correa, Badino et al. 2016). In this work, both physical and biochemical properties were scrutinized. Especially, enzymes are also characterized by its activities on specific substrates, as well as the thermal stability and dependency. This first working package aim to investigate substrate properties in order to understand its advantages – inconveniences for an enzymatic hydrolysis process.

3.1.1 Properties of enzymes

3.1.1.1 Enzymatic activities

The measurement of enzymatic activities is crucial step in order to ensure correct enzyme loading dosage. In this study, CTec2 and purified enzymes are measured for activities and results are presented in **Table 3-3.** Through literature, the activities of commercial cocktail Cellic Ctec2 at 50 °C are reported, varying from 127 FPU/ mL (Matsakas and Christakopoulos 2013) to 176 FPU/ mL (De Bari, Liuzzi et al. 2013) and approximately 200 FPU/ mL (Wiman, Palqvist et al. 2011). The considerable difference in activity can be explained by different in tested conditions or in #lot of enzyme. However, authors are in agreement with high CBU activity in Ctec2 (De Bari, Liuzzi et al. 2013, Matsakas and Christakopoulos 2013). The cellulase activity (FPU/ mL) of Ctec2 at 40 °C is lower than reported value from literature. It may due to the different in reaction temperature. Endo-glucanase activity (CMCU) is found in same order of magnitude as De Bari, Liuzzi et al. (2013).

For E-CELAN (endo-glucanase), the measured activity on CMC is nearly 10 times lower than reported by Megazymes (126.7 CMCU/ mL versus ≈ 1200 U/ mL). It can be explained by the difference in substitution degree of substrate using for enzymatic reaction. In the protocol of Megazyme, a CMC 4M (degree of substitution 0.4 - 0.5 equivalent to 4 - 5 carboxymethyl groups per 10 anhydroglucose units) was used whereas following IUPAC method, the enzyme assay in this work was carried out with CMC 7M (degree of substitution 0.65 - 0.9, equivalent to 6.5 - 9.0 carboxymethyl groups per 10 anhydroglucose units). As the degree of substitution increases, substrates (CMC) become less sensible to enzyme, lead to lower value of activity. Through literature review, CMC 7M are generally used to determine endo-glucanase activity. In order to keep a coherent with existed studies, CMC 7M was selected as substrate for endo-glucanase assay.

For exo-glucanase, the measurement of activities was not performed, due to the limit in enzyme quantity. Reported activity by producer is directly used.

For 49290 (β-glucosidase), the measured activities on cellobiose is 7 times lower than reported by Sigma Aldrich on salicin (0.83 CBU/mg versus 6 U/mg). Salicin (hydrolymethyl phenyl-β-D-glucosepyranoside) is an alcoholic β-glucoside while cellobiose contains two glucose molecules linked by β(1-4) bond. As cellobiose contains twice as much glucose as salicin, a CBU is defined as the amount of enzyme to release 2 µmol glucose/min in tested

condition. The difference between in value of β-glucosidase activity might due to the differences in conditions (pH, temperature, substrate concentration and reaction time). Comparing between cellobiose, salicin and p-nitro-phenyl-β-D-glucopyranoside, Breil et al. recommended cellobiose as the only substrate used for the β-glucosidase assay (Breuil, Mayers et al. 1986). In this work, cellobiose was selected as substrate for β-glucosidase assay.

Table 3-3. Activities of single and cocktails enzymes at 40°C, pH 4.8

Enzyme product	C Tec2		E-CELAN	E6412	49290	X2753	Multifect
Activities	(U/ mL)	(U/mg proteins)	(U/ mL)	(U/ mL)	(U/mg)	(U/mg)	(U/ mL)
FPU	103	64,8	n.t	n.t	n.t	n.t	n.t
AVCU	103.5	1,59	n.t	100[(a)]	n.t	n.t	n.t
CMCU	830.1	1,60	126.7	n.t	n.t	n.t	n.t
CBU	3796	12,8	n.t	n.t	0.83	n.t	n.t
EnXU	7407	58,0	n.t	n.t	n.t	26.6	9175
ExXU	n.t	n.t	n.t	n.t	n.t	n.d	0.57

[(a)] data from producer
n.t: not tested
n.d: not detected
Ctec2: 64.8 mgProteins/ mL

3.1.1.2 Thermal stability and dependency

The thermal stability of commercial cocktail Ctec2 was tested at 40 ºC (operating temperature of hydrolysis) and incubation in sodium citrate buffer 0.05M, pH 4.8. The results were reported in **Figure 3-3**. Generally, for both tested activities, FPU and CMCU, commercial cocktail Ctec 2 showed good thermal stability. During approximately 3 days of incubation, the measured activities of FPU and CMCU varied in the rage of ± 15 % around initial value. At tested condition, the loss in activities is negligible.

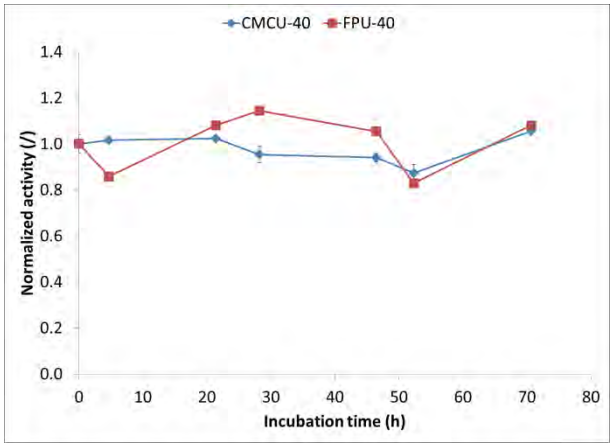

Figure 3-3. Thermal stability of Ctec2 at 40°C

Activation energy (E_a) and pre-exponential factor (A) of commercial cocktails Ctec2 were calculated following the method described in **§2.3.4.2**. Results are summaries in **Table 3-4**.

Wang et al. (Wang, Post et al. 2012) reviewed 39 scientific papers for activation energy of cellulolytic and ligninolytic activities, reporting an average E_a equal to 42 and 37 $kJ.mol^{-1}$ for

β-glucosidase and cellulase respectively. For mixture NS50013(cellulase) + NS50010 (β-glucosidase) from Novozymes, an activation energy equal to 46 $kJmol^{-1}$ on steam pretreated wheat straw was recognized (Radeva, Valchev et al. 2012). Compare to value from literature, it is clear that Ctec2 shows nearly two fold lower in activation energy. The Arrhenius equation states that, the rate of the reaction will increase with the decrease in E_a. Due to the fact that filter paper (> 99 % cellulose) and purified cellobiose was selected as substrate for enzyme assay, it is coherent when both cellulase and β-glucosidase in Ctec2 show significant low value of activation energy.

Table 3-4- The value of E_a and A for Ctec2, activities FPU and CBU

	40°C	50°C	E_a(kJ.mol^{-1})	A (min^{-1})
1/T	3.2E+3	3.1E+3	-	-
FPU	103	128	18.3	6.93E+9
CBU	3796	4465	14.5	5.82E+10

3.1.2 Properties of substrates and suspensions

3.1.2.1 Physical and biochemical properties

The chemical compositions of matrices (FP, PP and SCB) are presented in **Table 3-5**. For all studied substrates, cellulose appears as the main fraction, accounting for 75 % to 99 % by dry weight basis. FP contains no lignin, neither hemicellulose whereas PP and SCB show 19 % and 4.5 % hemicellulose respectively. Both real matrices showed low lignin content (< 2 %)

Table 3-5. Biochemical composition and physical properties of substrates

Matrices	FP	PP	SCB
Composition (carried out by LCPO)			
Cellulose (%)	99.7	75.0	79.9
Hemicellulose (%)	0.00	19.0	4.50
Lignin (%)	0.00	2.00	1.40
Ash (%)	0.30	n.a	n.a
Physical properties			
D(4,3) (µm)	412.4 ± 34.4	206.6 ± 14.6	71.4 ± 1.3
D(v,0.1) (µm)	20.9 ± 0.8	15.1 ± 2.0	9.8 ± 0.3
D(v,0.5) (µm)	169.4 ± 18.8	91.9 ± 7.2	43.5 ± 1.8
D(v,0.9) (µm)	1154 ± 72	597.4 ± 61.6	161.3 ± 3
ρ_{DM} (kg/m^3) at 20°C	1202	1364	1495
ρ_{HM} (kg/m^3) at 20°C	1200	1087	1077
Surface properties (carried out by UW)			
Δ_{GSES}	34.3	27.3	6.5
Δ_{GSE}	-146	-138	-130

LCPO- Laboratoire de Chimie des Polymères Organiques, Université Bordeaux, CNRS, France
UW- Waterloo University, Canada
n.a: not analysed

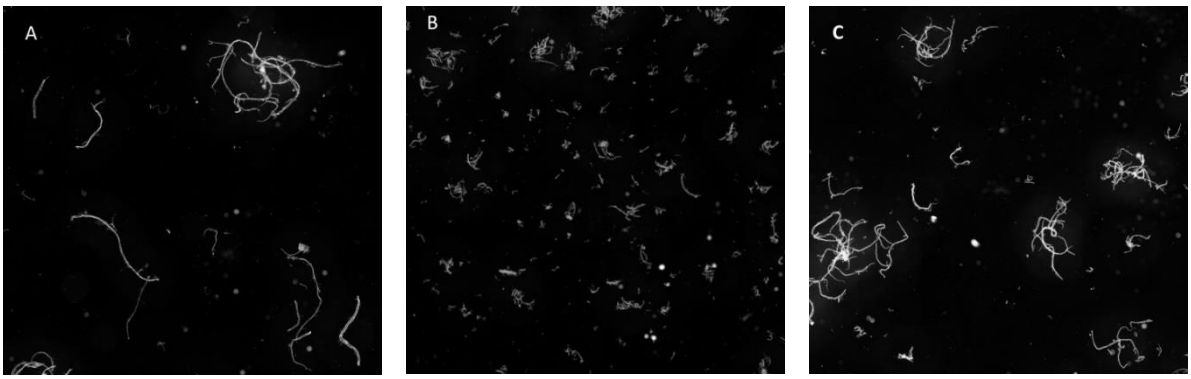

Figure 3-4. Particle morphology of FP (A), SCB (B) and PP (C) observed by microscopy (Morphologi G3S - Malvern Inst), mode dark field, magnification 10x, surface 0.5cm×0.5cm.

Surface tension analysis showed similar magnitude of interfacial interaction free energy (ΔG_{SES}) and hydratation free energy (ΔG_{SE}) for all matrices, indicating similar hydrophilic properties of FP, SCB and PP.

To evaluate the reproducibility of experimental conditions and the differences between FP SCB and PP, morphogranulometry and viscosity were specifically scrutinized. The mopho-granulometric properties were investigated by different analysis: (i) microscopic observation provides a qualitative information about particles shapes and sizes, (ii) diffraction light scattering measurement insists the coarse particle fraction (volume distribution) and (iii) focused beam reflectance measurement highlights the fine particle population (number distribution).

3.1.2.2 Particle morphology

Microscopic observations of FP, SCB and PP suspensions (**Figure 3-4A, B, C**) showed complex mixture of coarse and fine particles with different morphology and ratio. For FP suspensions, microscopy capture indicated a majority of long cellulosic fibers, which were crossed or separated with important ratio between fiber length and diameter. For SCB suspensions, the particle size appeared generally smaller than for FP. It can be explained by a strong pretreatment procedure. A de-structuration mechanism has generated small and short fragmented particles existing as agglomerates or individuals. PP suspension contained several long ramified fibers and small fraction of short fragments. Observed structure of PP suspension was well correlated with the target of industrial process to conserve cellulosic fibers. Qualitatively, proportion of fine particles seems to be highest for SCB suspension; PP and FP show similar magnitude of particle/fiber size.

Volume weighted distributions of sphere equivalent diameter were reported in **Figure 3-5A** for FP, SCB and PP suspensions. Generally, SCB suspension showed mono-modal distribution when FP and PP represented multimodal populations. For FP suspension, the population of coarse particle ($d_{SE} > 224$ µm) accounted for 45.4 % and fine population ($d_{SE} \leq 224$ µm) showed 55.6 % whereas fine particles with $d_{SE} \leq 224$ µm represented 95.6 % of population for SCB. For PP, the fraction of coarse particle ($d_{SE} > 224$ µm) accounted for 31.9 %. The fraction of medium to fine was divided in two sub-populations, 33.3 % of $49 \leq d_{SE} \leq 224$ µm and 34.9 % of $d_{SE} \leq 49$ µm. The volume weighted diameter, $d_v(0.1)$, $d_v(0.5)$, $d_v(0.9)$ corresponding to 10 %, 50 % and 90 % of population and volume weighted mean diameter D(4,3) of three matrices are presented in **Table 3-5**. It is noticeable that, D(4,3) of FP was three folds higher than PP

and 6 folds higher than SCB. Results on DLS confirmed observation on microscope that SCB was the finest population when FP was the largest.

Number weighted distributions of chord length were illustrated in **Figure 3-5B** for FP, SCB and PP. The difference of size range between FP, SCB and PP was noticeable with an expected shift to smaller dimension. All populations ranged between 1 to 200 µm. The mean chord lengths of 25.1 ± 0.5 µm 16.4 ± 0.4 µm and 21.5 ± 2.8 µm were reported for FP, SCB and PP respectively. A slight shoulder was observed for FP. In volume weighted distributions, few coarse fibers may account for a large volume fraction, whereas they will be negligible when considering a number weighted distribution. It is exacerbated with multimodal distributions with high size differences between fine and coarse sub-populations. For example with FP, the 1st population around 49 µm and the 2nd population around 780 µm represented 55.6 % and 45.4 % in volume whereas they stand for 99.98 % and 0.02 % in number assuming a sphere model.

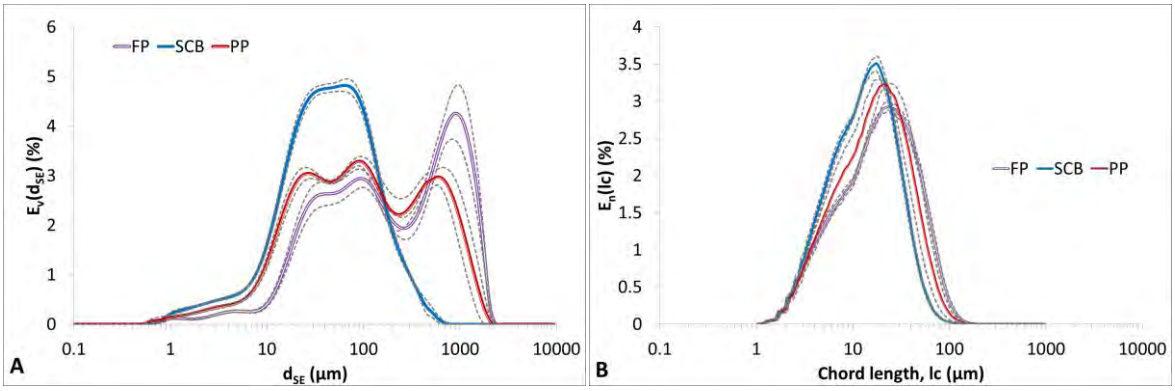

Figure 3-5. Volume distributions of sphere equivalent diameter by DLS measurements (A) and number distribution of chord length by FBRM (B) for FP, SCBand PP (dotted lines represented average deviation issued from at least 6 experiments).

3.1.2.3 Substrate hydration properties

As presented in **Figure 2-15**, a pre-shear and suspending step was necessary prior to the enzymatic hydrolysis. It allows the stabilization and homogenization of suspension before enzymes were added. For FP and SCB suspension at 1.5 and 3 % w/v respectively (**Figure 3-6A**), the stabilization states were obtained after around 2 h of pre-shear at 100 rpm (indicated by red points). Suspension showed good homogeneous level with nearly constant value of torque. In contrast, PP suspension reported very slow and strong hydration effect (**Figure 3-6B**). Even after 36 h of mixing at constant rate (100 rpm), the stabilization state of PP suspension was not established. Measured torque clearly exhibited a rising trends at two different velocities before and after 6 h. Considering the complex structure of PP suspension with broad size spreading and multimodal distribution, the hydration stage of PP is possible to be significant longer than FP and SCB. The pre-shear step for experiments with PP was extended to slightly more than 12 h corresponding to the phrase with less than 1 % variation in torque per hour.

For PP suspension, it was also reported that the evolution of viscosity during suspending step strongly depended on the pH. The raw PP suspended in water showed a pH superior than 8. If the automatic regulation of pH is enabled (set point pH = 4.8 ± 0.2) from the beginning of suspending step, the suspension viscosity reached only around 14000 µN.m after 12 h (data not shown). However, the pH did not significantly affected suspension viscosity of SCB and FP. In order to keep a common experimental protocol for all substrate, the pH regulation was only performed before enzyme adding for batch hydrolysis. As for fed-batch hydrolysis, pH regulation was enabled from the start of experiment.

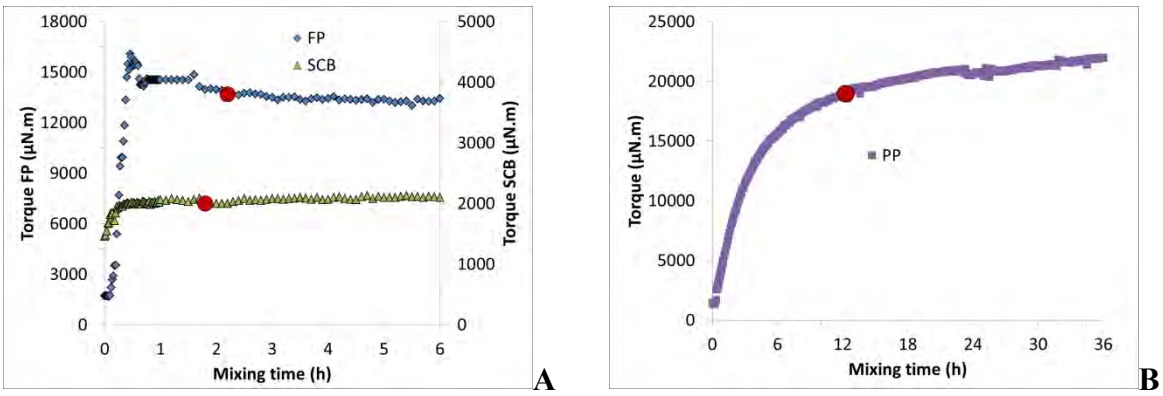

Figure 3-6. Monitoring of torque during agitation of FP 1.5 %w/v, SCB 3 %w/v and PP 3 %w/v at 40 °C, 100 rpm, pH 4.8.

3.1.2.4 Viscosity of suspensions

On-line viscometry was established by varying the rotation frequency and results are illustrated in **Figure 3-7.** For all substrates and concentrations, a decrease in suspension viscosity when increasing mixing rate is observed, translating a shear thinning behavior. Our results are in agreement with others author, the same observation was also reported on various lignocellulosic suspensions. Viamajala, McMillan et al. (2009) observed a significant decrease in viscosity on pretreated corn stove suspension (from 10 to 32.5 %w/w) for increasing shear rate. Nguyen, Anne-Archard et al. (2013) stated the shear thinning properties of several lignocellulosic suspension including hard wood and soft wood paper pulp as well as filter paper. Rosgaard, Andric et al. (2007) reported the decrease in viscosity with increasing shear rates of pretreated barley straw slurries.

Figure 3-8 illustrates the relationship between suspension viscosity versus substrate concentration (gdm/L) at a given mixing rate (100 rpm equivalent to $\dot{\gamma} = 65\ s^{-1}$ in laminar flow). An increase in viscosity was recorded for all substrates but at different magnitude. Viscosity ranking was established indicating: $\mu_{FP} > \mu_{PP} > \mu_{SCB}$ whatever concentration was. For example, at 15 gdm/L (equivalent to Φ_V = 0.0125, 0.01 and 0.011 vol/vol for FP, SCB and PP respectively), the viscosity of suspension were nearly 0.2Pa.s for FP and less than 0.01 Pa.s for both PP and SCB. Differences can be related to several assumptions such as particle size and morphological properties and associated distributions. As reported in **Table 3-5**, the mean volume diameter D(4,3) of FP is significant higher than for PP and SCB. The particle size distribution of FP showed coarser population than for PP and SCB. At a given concentration if the fiber length grows, the interaction probability between particles increases, especially due to entanglement generating a rising viscosity. Microscopy, DLS and FBRM sustain these assumptions. Similar relationship between suspension viscosity and particle size was revealed from the literature. Dasari and Berson (Dasari and Berson 2007) reported that the smaller size particles result in lower viscosity at the same substrate concentration of sawdust. Viamajala et al. (Viamajala, McMillan et al. 2009) stated higher viscosity of pretreated corn stove slurries of 20 mesh (0.841 mm) compared to 80 mesh (0.177 mm).

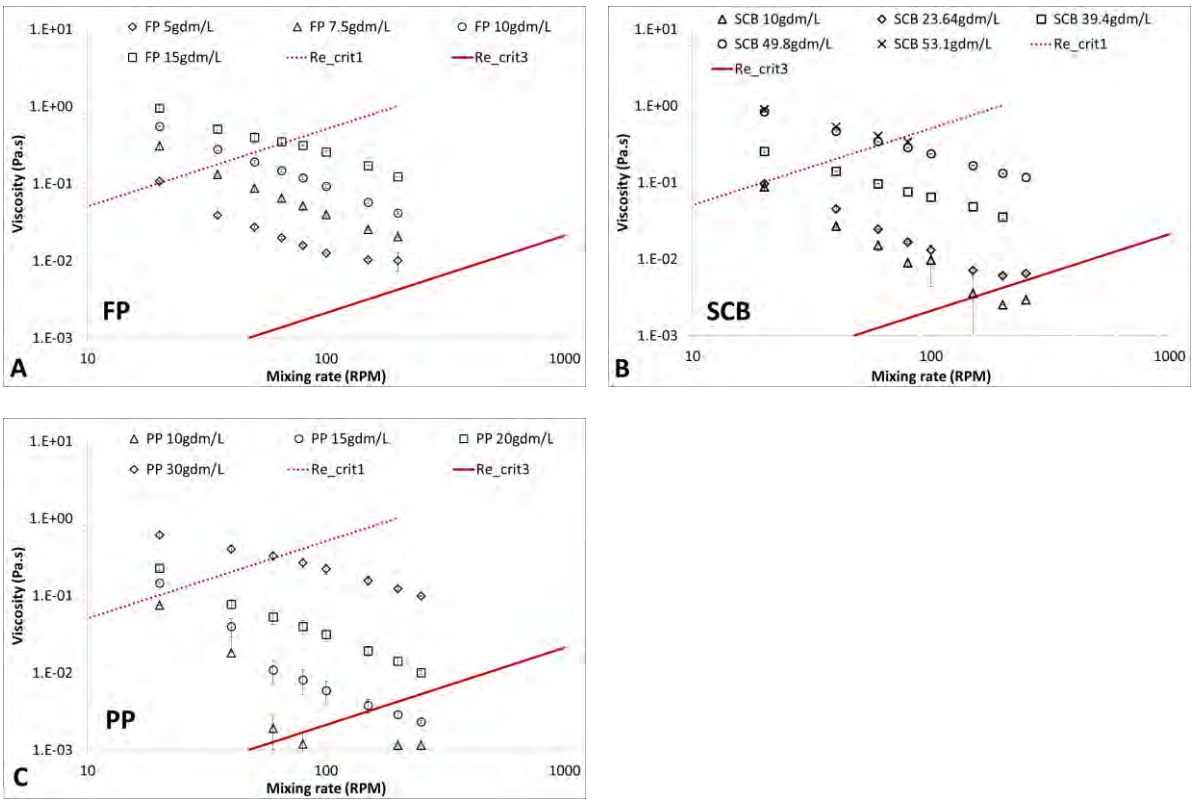

Figure 3-7. In-situ viscosity versus mixing rate of FP(A), SCB(B) and PP(C) suspension at different substrate concentrations. Each point represents an average value from 2 measures. Re_{crit1} and Re_{crit3} illustrated the change from laminar to transition and from transition to turbulent regime.

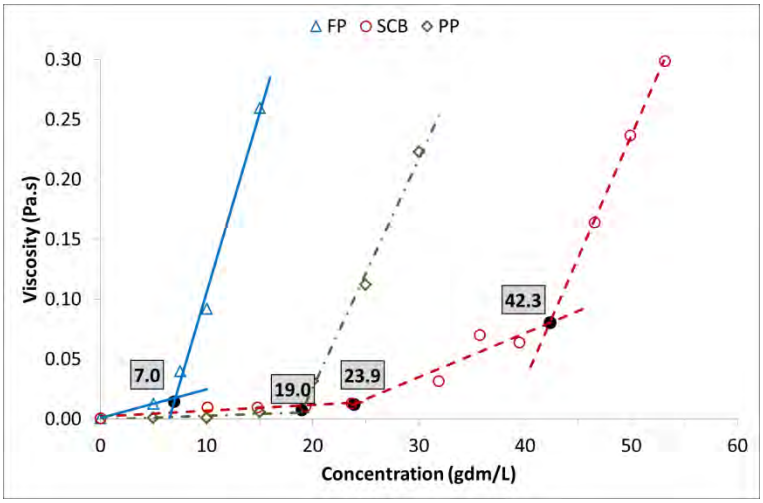

Figure 3-8. In-situ viscosity versus substrate concentration of FP, PP and SCB at 100 rpm.

Critical concentrations were recognized when applying linear regression into experimental data as proposed in **Figure 3-8**. For FP, the viscosity was slightly increased when concentration rose from 0 up to 7gdm/L. Beyond this point, a small growth in concentration led to the sharp rise in suspension viscosity: around 8 folds increased in viscosity for two folds increased in substrate concentration from 5 gdm/L to 10 gdm/L (equivalent to Φ_V = 0.00416 and 0.00832 vol/vol respectively). Similar trends with lower magnitude were observed for PP and SCB suspensions. Critical concentrations indicating the end diluted regime were found at 19.0 and

23.9 gdm/L for PP and SCB respectively. Unlikely FP and PP, a second critical concentration was clearly defined for SCB at 42.3 gdm/L. The viscosity curve of SCB exhibited three behaviors corresponding to dilute, semi-dilute and concentrated regime. During enzymatic hydrolysis, mixing is an important factor which affects the mass, heat and momentum transfers. Energy consumption for mixing strongly depends on suspension viscosity (Fan, South et al. 2003). This critical concentration pointed out the substrate concentration range in which viscosity has to be maintained to stay in a range of low energy consumption. For fed-batch and continuous process, the knowledge about critical concentrations of material will be a guideline to calculate the feeding rate of substrate.

From experimental data, the modeling of suspension viscosity is considered. Several models to describe suspension viscosity were reported (Breuil, Mayers et al. 1986). In present work, the relationship between viscosity and either suspension concentration (equivalent in volume fraction) or applied shear rate were investigated following Krieger-Dougherty (Krieger and Dougherty 1959), Simha (Krieger and Dougherty 1959) and Power-law models.

For the viscosity – particle volume fraction relationship, Albert Einstein reported the linear equation for single hard sphere in a liquid at diluted condition as

$$\mu = \mu_s \cdot (1 + 2.5\Phi_v) \qquad \textit{Eq. 3-1}$$

Where μ is the suspension viscosity, μ_s is the viscosity of solvent and Φ_v the volume fraction of particle present in suspension. The value 2.5 is often termed the intrinsic viscosity [μ] which is dimensionless and depends on nature of material. The ratio of suspension viscosity to solvent viscosity is the relative viscosity μ_{rel}. As the suspension concentration increase, particles in far closer proximity to other neighbors, interaction between particles is enhanced. Subsequently, suspension viscosity rise quickly with volume fraction. In this situation, a semi-empirical model developed by Irvin Krieger and Thomas Dougherty is the most used to describe the relationship between particle volume fraction and suspension viscosity (Krieger and Dougherty 1959).

$$\frac{\mu}{\mu_s} = \left(1 - \frac{\Phi_v}{\Phi_{v\,max}}\right)^{-[\mu]\Phi_{vmax}} \qquad \textit{Eq. 3-2}$$

In this equation, Φ_{vmax} is the maximum packing fraction or volume fraction. It strongly depends on the particle size distribution. In order to apply Krieger-Dougherty relationship, two parameters: intrinsic viscosity [μ] and maximal volume fraction $\Phi_{v\,max}$need to be determined. Several value of [μ] and $\Phi_{v\,max}$ for different particle shapes from sphere to rod are reported in the literature (Barnes, Hutton et al. 1989). However, there are no recommended values for complex lignocellulosic suspension. Theoretically at diluted condition, the identification of [μ] can be based on Einstein equation (**Eq. 3-1**) by plotting $\mu_{rel} - 1$ versus particle volume fraction Φ_v. This should yield a linear relationship with slop equal to [μ]. The $\Phi_{v\,max}$ is obtained from experimental relationship $\mu = f(\Phi_v)$. An alternative approach to determine [μ] and $\Phi_{v\,max}$ by directly fitting to experimental data (μ versus Φ_v) using Microsoft excel "solver" tool was proposed (Roberts, Barnes et al. 2001) This method compares the experimental values against fitted values for constantly changing input values of Φ_{vmax} and [μ] then determines the combination that gives the smallest residual or smallest difference between the measured and the fitted values provided by the model.

In present case, the determination of maximal packing fraction by experimental approach was forbidden due to the complexity of substrate. The [μ] and $\Phi_{v\,max}$ of were adjusted by the least squares method of μ using Microsoft excel "solver" tool. With [μ] = 171.2 and $\Phi_{v\,max}$ = 0.88 (**Figure 3-9B** the dotted line), the dependence of suspension viscosity measured at 100

rpm was well fitted with **Eq. 3-2**. Value of R^2 is equal to 0.977. However, this model indicates a value of $\Phi_{v\,max}$equal to 0.88, which seems to be an unreal packing fraction regarding physical properties of SCB (dry matter content 76.7 %).

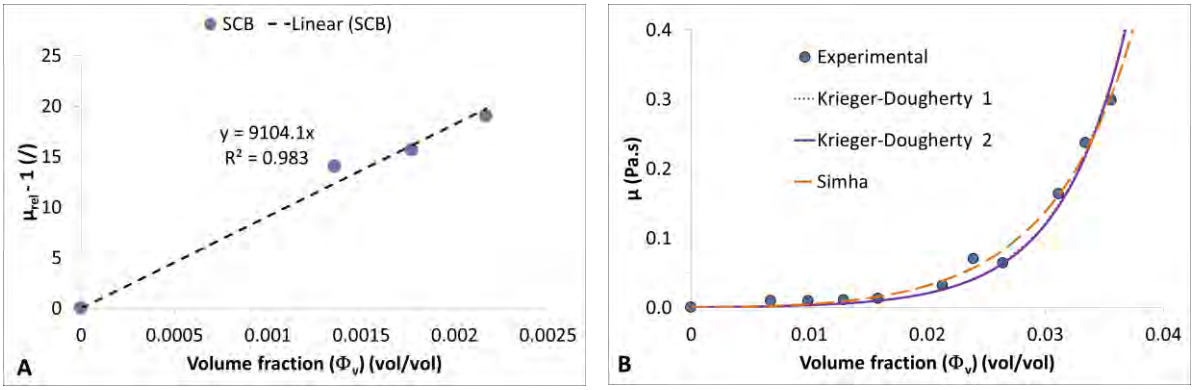

Figure 3-9. Identification of [μ] by Einstein equation (A).and proposed viscosity models (B) for SCB suspension at 100 rpm.

The second possibility of Krieger-Dougherty relationship was also proposed by calculating [u] through Einstein equation at diluted regime (**Figure 3-9A**). The linear plot of μ_{rel}-1 = f(Φ_v) reported the intrinsic viscosity [μ] equal to 9104.1. However, it was unable to find a value of $\Phi_{v\,max}$ in the interval (0;1) that corresponds with this value of [μ]. Although, since [μ] is determined in a dilute regime, there may exist a question of validity regarding its application to higher concentration regime, especially due to the differences in particle properties when Einstein equation was established for hard sphere suspension. For soft particle and taking into account the particle deformation, an effective volume fraction was then introduced as $\Phi_{v-eff} = k_v \cdot C_m$ where C_m is the substrate concentration (g/L) and k_v is a coefficient ($L.g^{-1}$). The original Krieger-Dougherty relation can be written as

$$\frac{\mu}{\mu_s} = \left(1 - \frac{\Phi_{v-eff}}{\Phi_{v\,max-eff}}\right)^{-[\mu]\Phi_{vmax-eff}} \qquad \textit{Eq. 3-3}$$

Whith [μ] = 9104.1 identified from Einstein relation, the **Eq. 3-3** was fitted well with experimental data at $\Phi_{v\,max-eff}$ = 0.02 and k = $1.26 \cdot 10^{-5}$ ($L.g^{-1}$). Value of R^2 is equal to 0.927.

For the concentrated regimes, the Simha's cellular model is reported with good ability to describe the rheological behavior of concentrated suspension (Barnes, Hutton et al. 1989). The relation between suspension viscosity and volume fraction should satisfy

$$\lim_{\Phi_v \to \Phi_{vmax}} \frac{\mu}{\mu_s} = 1 + \frac{54}{5} f^3 \frac{\Phi_v^2}{\left(1 - \frac{\Phi_v}{\Phi_{vmax}}\right)^3} \qquad \textit{Eq. 3-4}$$

Where f is a semi-empirical parameter and $\Phi_{v\,max}$ is the maximum packing fraction. **Eq. 3-4** was adjusted to experimental data using root mean square method of μ. The best solution was found at f = 15.87 and $\Phi_{v\,max}$ = 0.07 (**Figure 3-9B** the dash line) indicating R^2 = 0.991. The value of maximum volume fraction obtained with Simha model was in the same order of magnitude with $\Phi_{v\,max-eff}$ from Krieger-Dougherty model 2. Both models showed good prediction ability compared to experimental data.

For the viscosity – shear rate relationship, power law model $\mu = k \cdot \dot{\gamma}^{n-1}$ is used. Theoretically, the application of this equation is restricted in laminar regime, which allows an

equivalent shear rate can be deduced from mixing rate following Metzner-Otto concept. In this work, this limit was extended in early on transitional (Re < 100). The power law parameters n (flow behavior index) and k (flow consistency index) were identified by linear plotting $\ln(\mu) = A.\ln(\dot{\gamma}) + B$ with A equal to (n-1) and B correspond to ln(k). Due to the flow regime of tested suspension, this investigation is only enabled for highest concentrations of each substrate. The results are presented in **Table 3-6**.

Table 3-6. Power law parameters of suspensions

	n (/)	k (Pa.s^n)	R^2
FP 15gdm/L	0.42 ± 0.04	3.09 ± 1.17	0.989
SCB 49.9gdm/L	0.22 ± 0.02	5.96 ± 1.07	0.996
SCB 53.1gdm/L	0.29 ± 0.02	5.44 ± 1.07	0.996
PP 30gdm/L	0.43 ± 0.08	2.63 ± 1.29	0.930

At laminar pure (Re < 42) and even at the beginning of transitional regime (Re < 100), the linear regression showed good value of R^2 (superior than 0.93 for all suspensions). Subsequently at Re superior than 100 (data not shown), obtained results are significantly less accurate, value of. R^2 was less than 0.8 that do not ensure reliable calculation. Generally for all matrices, observed value of flow behavior index was ranged from around 0.22 to nearly 0.43, reflecting shear-thinning or pseudo-plastic properties. Same conclusions were also reported by other authors on several lignocellulosic biomasses. Both Dunaway, Dasari et al. (2010) and Pimenova and Hanley (2004) stated that pretreated corn stove slurries exhibited pseudo-plastic behavior. The magnitude of n and k for PP suspension obtained from this work seems to be in the similar order of magnitude with reported value in the literature. Nguyen (2014) studied the power law parameters in relation to substrate concentration of Whatman paper and hardwood paper pulp. Their results reveal n = 0.285 and k = 3.24 for hard wood paper pulp suspension at 30 gdm/L. However, similar range of n for other lignocellulosic suspension were reported by Wiman, Palqvist et al. (2011) (0.4 - 0.15 for spruce pulp).

For SCB suspension, the power law indexes were slightly different between the substrate concentrations 49.4 and 53.1 gdm/L. With small variation in concentration, this result indicated the accurate of measurement systems rather than an evolution of power law parameters versus substrate concentration.

Through magnitude of n, it seems that FP and PP suspension possessed weaker non-Newtonian properties than SCB suspension. The comparison between FP and PP suspensions was hard to be establish due to the difference in substrate concentrations .Even when the relationship between n and concentration of lignocellulosic suspension was mentioned in the literature, it existed controversial statements. Wiman, Palqvist et al. (2011) stated that water insoluble content in pretreated spruce (from 4 to 12 % w/w) did not change significantly n. In contrast, Pimenova and Hanley (2004) reported opposite tendency on corn stove suspension, power law index fell from 0.91 to 0.005 when increasing concentration from 5 % to 30 %.

3.1.3 Conclusion

Through physical and biochemical characterizations, three substrates were described. The promising feedstock for bioprocess could be considered from several criteria. In term of composition, FP seems to be the most favorable with nearly 99 % cellulose, PP and SCB showed same potential with approximately similar composition of cellulose and lignin. With nearly 20 % of hemicellulosic fraction, PP is the most complex substrate. However, considering the role of particle size, SCB presented an extra advantage comparing to FP and PP. Following

a pretreatment step, SCB contained in majority fine particles and short fiber fragments that allow increasing specific surface for enzyme binding. PP and FP presented multimodal particle size distribution, with a considerable proportion of coarse and long fibers. SCB was expected to be quicker and easier hydrolyzed by enzymes than the others two substrates.

Toward the goal of working at high dry matter content in order to achieve a viable economic, the physical aspects such as mass, heat transfer during reaction, enzyme/substrate homogenizations and required energy for mixing become non-negligible. These scientific questions are directly linked to suspension viscosity. It is evident that, high viscosity cause rise in energy for mixing, inspire limitation of transfers. Therefore, SCB shows it second advantage with low dependency of suspension viscosity in substrate concentration.

Highlights for enzymes and substrates characterization

- Ctec2 showed good thermo-stability under working conditions (40ºC, pH 4.8). Activities loss were negligible at T = 40 ºC, pH 4.8
- Volume weighted distribution indicated that sugarcane bagasse was "mono-modal" (10 to 160 µm) whereas paper pulp (15 to 600 µm) and filter paper (20 to 1150 µm) had multimodal distributions.
- Optical morpho-granulometry described the particle shape of three substrates. For SCB suspension, fine fragments dispersed with big agglomerates. For PP and FP, a considerable proportion of coarse fibers were reported.
- Impact of substrate loading on suspension viscosity was described and modeled using Power law equation.
- Particle size and shape analyses enabled to explain the suspension viscosities.
- Critical concentrations (C^*) corresponding to regime changes were 6.9, 19.0 and 23.9 gdm/L for filter paper, paper pulp and sugarcane bagasse, respectively.
- Lignocellulosic suspensions behaved as non-Newtonian shear-thinning fluids.
- Krieger Dougherty and Simha models showed excellent ability to describe the relationship between suspension viscosity and substrate loading.

3.2 R&D: ENZYMATIC HYDROLYSIS AT SEMI-DILUTE REGIME

In order to enables the enzymatic hydrolysis at high dry matter condition with high efficiency in term of yield and energy consumption, the mechanisms of reaction as well as limitation factors need to be identified and investigated. The semi-dilute condition was then considered due to several advantages. Firstly at semi-dilute condition, all tested substrates already showed non-Newtonian behavior, which allows the characterization of rheological properties during hydrolysis. Secondly, it enables a simple enzymatic reaction without end product inhibition, neither transfer limitations (mass, heat, enzyme). Thus, semi-dilute condition appeared to be the best operating setup for observation of phenomenon, and for investigation of enzymatic mechanisms.

This chapter will begin by traditional biochemical approach investigating the glucose and xylose conversion yields, describing reaction rate as well as considering kinetics models. This will then be completed by in and ex-situ viscometry measurements in order to better describe the phenomenon during enzymatic hydrolysis. The relationship between biochemical and rheological parameters will be also discussed. Finally, the analysis of particle size distribution will present the last shard to completing the picture of hydrolysis mechanisms.

3.2.1 Biochemical analysis

The biochemical analysis during enzymatic hydrolysis included the dosage of dry matter content and hydrolysis products. From raw data, the hydrolysis yields were calculated for each substrate. The modeling using first and second order equations was also investigated and presented hereafter.

3.2.1.1 Hydrolysis yield

Figure 3-10 and **Figure 3-11** shows the time evolution of the produced sugar concentration and the corresponding yields from enzymatic hydrolysis of FP, SCB and PP. For all tested matrices and in according with E/S ratios, glucose and xylose concentrations increased with the increase in hydrolysis time.

At 25 FPU/g cellulose, the hydrolysis rates of glucose were maximums at the initial stage whatever substrate and they gradually decreased as time increased. In these experiments at low solid loading (1.5-3 %w/v) and high enzyme dosage (25 FPU/g cellulose), the slowdown of the hydrolysis rate during enzymatic reaction was caused by the decrease in hydrolysable substrate rather than enzyme deactivation or product inhibition. The final glucose productions (at 24 h) were 8.7, 22.7 and 23.7 g/L for FP, SCB and PP respectively. At 3 FPU/g cellulose, the first stage of maximum hydrolysis rate was not clearly observed. Glucose concentrations rose gradually up to 24 h for all substrate, reached 4.5, 5.1 and 12.5 g/L for FP, SCB and PP respectively. Similar tendency was reported for the lowest E/S ratio (0.3 FPU/g cellulose) with final concentration of glucose < 2 g/L for all substrate.

Same evolution tendency was observed for glucose conversion yield with an increasing trend by time. Interestingly on PP, glucose and xylose yield were almost identical at both 0.3 and 3 FPU/g cellulose **Figure 3-11B**. In the structure of lignocellulosic substrate, cellulose fibers exist in complex matrix with hemicellulose and lignin. The enzymatic action on one fraction might favorite the attack on the other. This result suggests that cellulosic and hemi-cellulosic fractions are hydrolyzed proportionally or at least, there was some link between them. On switch grass under moderate pretreatment conditions, Pryor, Karki et al. (2012) stated an improve in glucose yield by adding hemicellulase activities. However, similar effect was not observed for switch grass at following mildest pretreatment conditions.

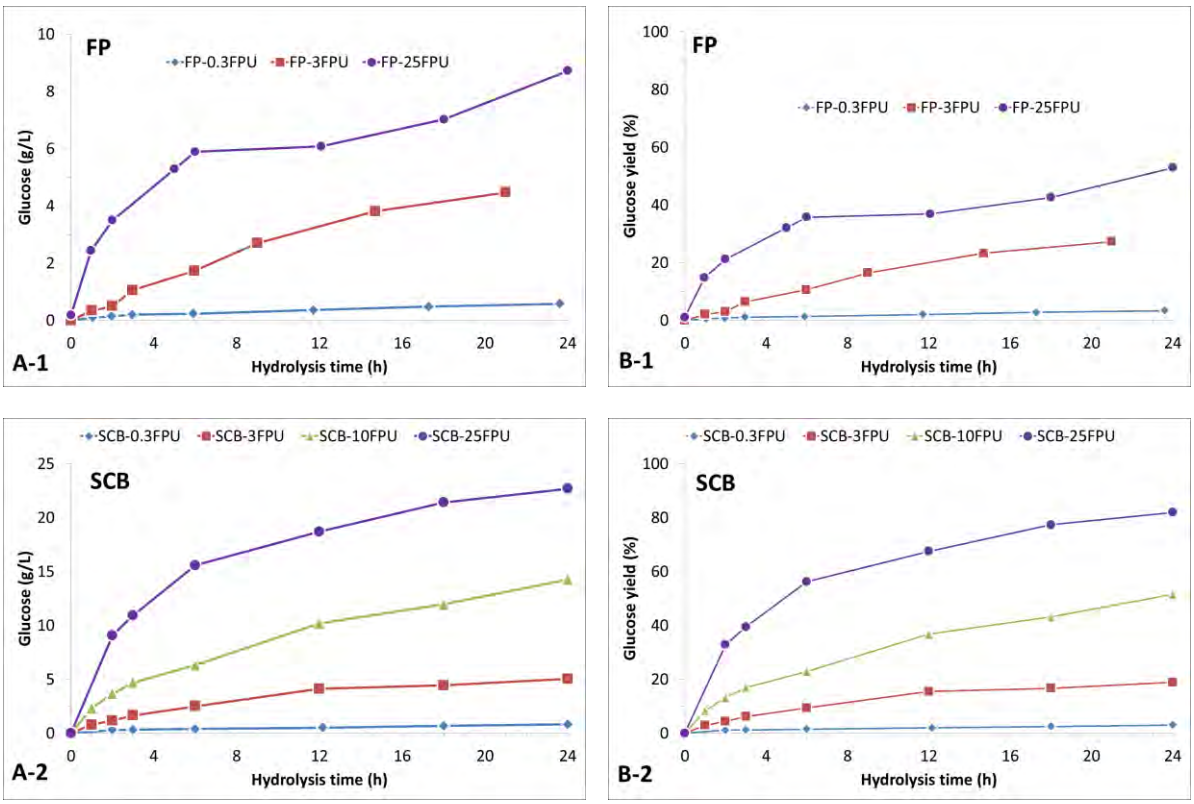

Figure 3-10. Glucose concentration (A) and bioconversion yield (B) as a function of hydrolysis time at difference E/S ratios for three matrices FP (1), SCB (2), enzyme Ctec2.

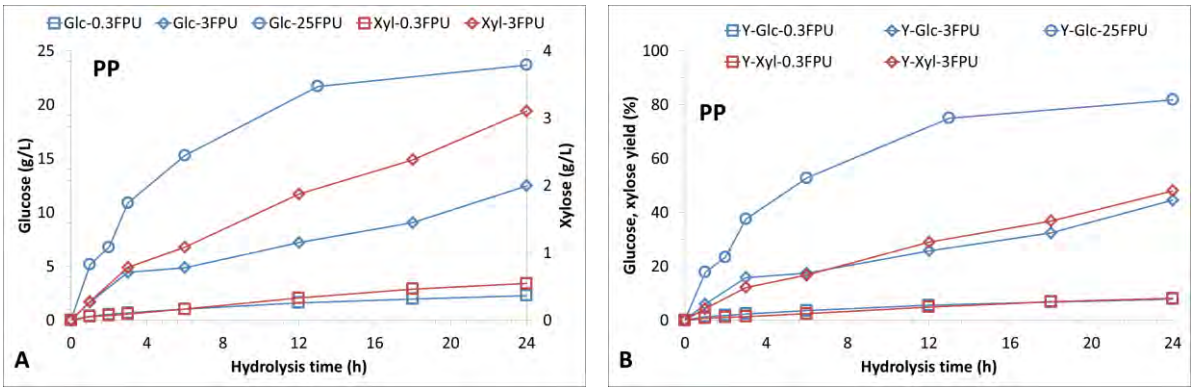

Figure 3-11. Glucose, xylose concentration (A) and bioconversion yield (B) as a function of hydrolysis time at difference E/S ratio for PP, enzyme Ctec2.

At high enzyme loading (25 FPU/g cellulose), both PP and SCB reported similar hydrolysis yields of around 80 %. The over dose of enzyme might overcast the impact of substrate complexity on glucose yield, leading to maximum possible bioconversion rate. At lower enzyme loading, an exacerbation of this relationship could be obtained. Despite the complexity in chemical composition and the large particle size previously stated (see **Table 3-5** and **Figure 3-5**), it is noticeable that at 3 FPU/g cellulose, PP was the most accessible by enzyme among three substrates, better than SCB and FP (44.6 % glucose conversion yield versus 19.1 % for SCB and 28 % for FP). Following the last assumption that the actions of hemicellulase can boost cellulase efficiency and considering the chemical composition of PP, it is well correlated when same dose of Ctec2 (3 FPU/g cellulose) resulted in higher yield for this substrate than for SCB neither FP. In this case, it seems that the complexity in particle size distribution did not

significantly affect bioconversion rate as expected. The contribution of PSD on glucose conversion yield will be deeply focused in the next chapter **§3.2.3** to fully enlighten this scientific question.

3.2.1.2 Initial reaction rate

From biochemical results, it is possible to compare the initial reaction rate between substrate and at different enzyme loading dose. Through the literature, Michaelis and Menten equation is the most used to describe kinetic of reaction. It requires a set of experiment at various substrate concentrations. Unfortunately for this study, it is unable to adopt M&M equation due to the fact that our experiments were carried out at fixed substrate loading. However, traditional model which describe the relationship between reaction rate (V_r) and enzyme dose ($[E_0]$) can be applied (**Eq. 3-5**)

$$V_r = k \cdot [E_0] \qquad \textit{Eq. 3-5}$$

By definition, the reaction rate can be described by the variation of product concentration by time as

$$V_t = \frac{dP}{dt} \qquad \textit{Eq. 3-6}$$

Where P is the product concentration (glucose for the hydrolysis of cellulose), t is the reaction time.

The initial reaction rate V_0 for the first 1h of hydrolysis can be deduced from **Eq. 3-5** and **Eq. 3-6**

$$V_0 = \frac{dG}{dt} = k \cdot [E_0] \qquad \textit{Eq. 3-7}$$

The linear plot of $^{dG}/_{dt}$ versus $[E_0]$ for each matrix will give corresponding value of k which translates the dependency of reaction rate in enzyme dose. This interpretation is illustrated in **Figure 3-12** for FP, PP and SCB under a range of E/S ratio from 0.3 to 25 FPU/g cellulose. All curves were forced to pass through zero point due to the fact that no production of glucose at no enzyme loading. Generally, it clearly reflects the difference in enzyme accessibility of substrates. First, the **Eq. 3-5** showed excellent correlation for FP and SCB with coefficient k equals to 0.09 and 0.2 respectively. The calculation showed R squared value superior than 0.99 for these substrates. As for PP, the point 3 FPU/g cellulose was seems to be slightly out of general tendency. The value of k for PP was 0.21 with an R squared equals to 0.9. From this interpretation, two things can be pointed out.

Firstly, the slop of curves for FP, PP and SCB, or in other word the magnitude of k clearly presents two different trends. The dependency of reaction rate in enzyme loading was more pronounced for PP and SCB compared to FP. Value of k for FP was approximately two fold smaller than that of PP and SCB. The last two witnessed nearly identical value of k translating the same reaction rate at the beginning of hydrolysis. This result is in good agreement with the hydrolysis yields of FP, which is always lower than that of SCB and PP.

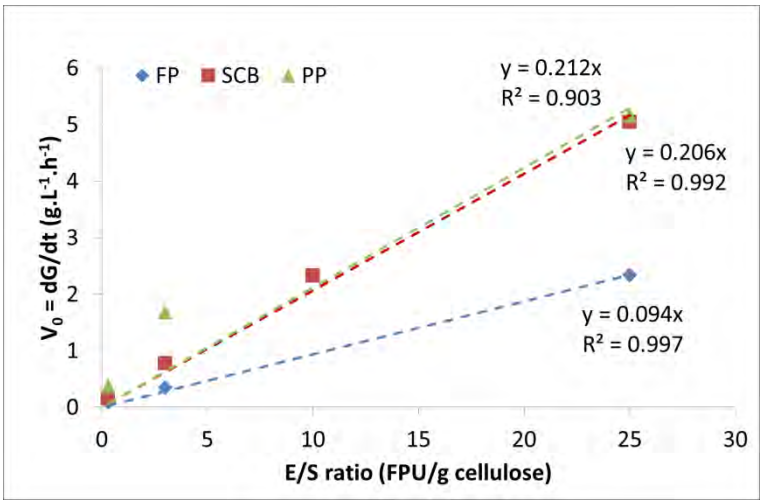

Figure 3-12. Initial reaction rate (V_0) versus E/S ratio of Ctec2 for FP, SCB and PP.

Secondly at **§3.2.1.1** when discussing on the higher glucose conversion yield of PP compared to SCB at 3 FPU/g cellulose, a hypothesis on the contribution of hemicellulase activities was opened. Taking in to consideration the **Figure 3-12**, the analysis of reaction rate brought an additional element of discussion. It was observed that the experimental point corresponding to 3 FPU/g cellulose of PP was located beyond the point of SCB whereas they were super imposed at 25 FPU/g cellulose. This observation is in good agreement with glucose conversion yields at 24h of two substrates. It suggests that for PP, the linearity of **Eq. 3-7** might not extend up to 25 FPU/g cellulose and the enzyme saturation point might be found at lower value. This assumption also explains the value of R squared for PP which was significant lower than that of SCB and PP. Consequently, the "true" reaction rate of PP must be higher than SCB or equivalent with $k_{PP} > k_{SCB}$. It needs to be verified by carrying out complementary experiment at a secondary enzyme loading dose (for example 10 FPU/g cellulose) for PP suspension

3.2.1.3 Kinetic modeling of glucose production

The kinetic modeling of enzymatic reaction has been investigated since many years (Kadam, Rydholm et al. 2004, Yao, Wang et al. 2011, Gupta, Kumar et al. 2012, Ruiz, Vicente et al. 2012, Carvalho, Sousa et al. 2013, Neto, Dos Reis Garcia et al. 2013, Wanderley, Martín et al. 2013). Through the literature review, first and second order as well as Michaelis & Menten equation has been generally used to correlate enzymatic hydrolysis yield. In this study, the enzymatic reactions were carried out at constant substrate concentration that does not allow the application of Michaelis & Menten equation. Kinetic models of first and second orders were applied for enzymatic hydrolysis experiments using Ctec2 at differences E/S ratio. The relationship between substrate conversion and hydrolysis time can be illustrated as below

$$-\frac{dS}{dt} = k \cdot S^{\propto} \qquad \textit{Eq. 3-8}$$

Where S is substrate concentration (fraction hydrolysable), k is the kinetic constant and α is the model order (/). For α equal to 1 (first order) and 2 (second order), **Eq. 3-11** can be resolved as

For α = 1

$$S = (S_0 - S_\infty) \cdot e^{-k_{bio-1}t} + S_\infty \qquad \textit{Eq. 3-9}$$

For α = 2 *Eq. 3-10*

$$S = \frac{(S_0 - S_\infty)}{(S_0 - S_\infty) \cdot k_{bio-2} \cdot t + 1} + S_\infty$$

S_0 and S_∞ indicate the total substrate concentration and the recalcitrant fraction of substrate respectively. The subtraction of S_∞ from S_0 gives the hydrolysable fraction $S = S_0 - S_\infty$. For FP, PP and SCB, only cellulose was considered as hydrolysable fraction for the modeling of glucose production. The constant k was calculated following **Eq. 3-9** or **Eq. 3-10** in each case and represented in **Table 3-7** with R squared value. The plot of predicted versus experimental values of glucose concentrations was illustrated in **Figure 3-13**, **Figure 3-14** and **Figure 3-15** for FP, PP and SCB respectively. It was observed that the rate constant (k) of both first and second order models for enzymatic hydrolysis increases with the increase in enzyme loading at given substrate concentration. For all tested substrate, maximum rate constant was obtained when the hydrolysis was performed at maximum enzyme loading ratios (25 FPU/g cellulose). This is in agreement with biochemical knowledge when k translates the rate of substrate solubilization by time.

For FP suspension, the second order equation seems to be more correlated with the experiment data than the first order equation. Excellent R squared equal to 0.99 was obtained at 3 FPU/g cellulose with this model. However, both first and second order model showed large root mean square error between experimental and predicted value for 25 FPU/g cellulose. It can be explained by two experimental points at 12 h and 18 h which were out of overall trend. At 0.3 FPU/g cellulose, both model provided almost linear relation between glucose production and hydrolysis time with very low value of k (inferior than 0.0015).

For PP suspension, the value of k_{bio-1} and k_{bio-2} were relatively low, indicating very weak effect of substrate concentration. The glucose production trend at 0.3 FPU/g cellulose was almost linear. At 3 FPU/g cellulose, both model showed good correlation with experimental data, value of R squared were 0.93. Interestedly at 25 FPU/g cellulose, first order model reported better prediction ability than second order model with R squared equal to 0.98.

For SCB suspension, the second order showed better correlation with experimental data. Except for the lowest enzyme loading 0.3 FPU/g cellulose, good R squared values (superior than 0.91) were reported for experiments at > 3 FPU/g cellulose with second order model. Similarly with FP, the time-dependency of glucose production at 0.3 FPU/g cellulose exhibited roughly two different trends: a sharp increase between 0h and 1 h followed by a slight and almost linear evolution, explaining the poor R squared for both model. It is noticeable that the evolution of rate constant k_{bio-2} for SCB at 3, 10 and 25 FPU/g cellulose reported an exponential relation with enzyme loading ratios with R squared equals to 0.979.

Table 3-7. Identified kinetics parameters for glucose production of batch hydrolysis

Substrate	FP			SCB				PP		
E/S ratio	0.3	3	25	0.3	3	10	25	0.3	3	25
k_{bio-1} (h^{-1})	0.002	0.015	0.031	0.001	0.012	0.031	0.083	0.004	0.029	0.15
R^2	0.83	0.96	**0.45**	0.66	**0.86**	0.91	**0.82**	0.83	0.93	0.98
k_{bio-2} (h^{-1})	9.9E-5	0.001	0.006	0.0001	0.001	0.004	0.028	0.0005	0.005	0.038
R^2	0.84	0.99	**0.73**	0.67	0.91	0.99	0.93	0.90	0.93	**0.75**

k_{bio1} and k_{bio2} are rate constants of first and second order model respectively

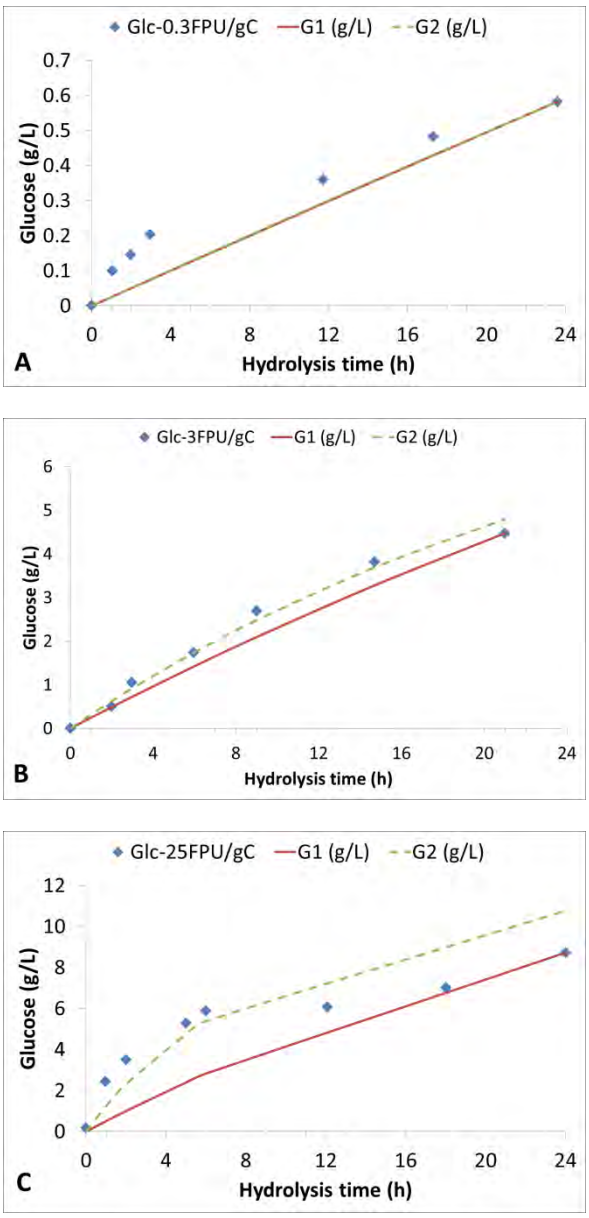

Figure 3-13. Predicted versus experimental values of glucose concentration released during the enzymatic hydrolysis of FP at 0.3 (A), 3 (B), 25 (C) FPU/g cellulose and 1.5 %w/v solid loading. G1: first order model, G2: second order model.

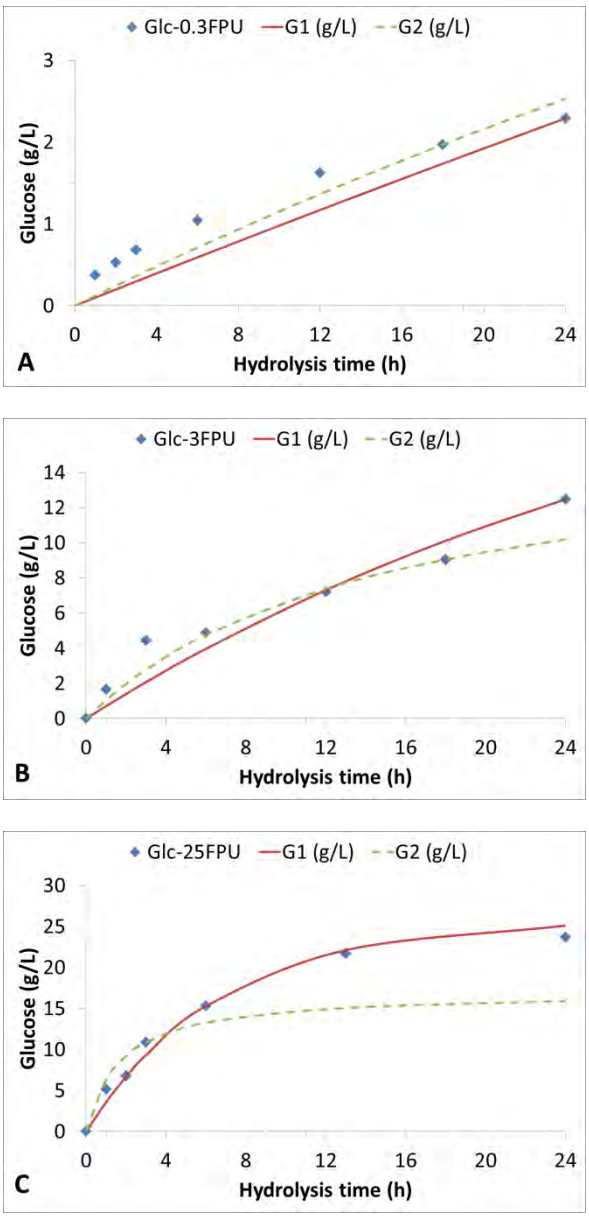

Figure 3-14. Predicted versus experimental values of glucose concentration released during the enzymatic hydrolysis of PP at 0.3 (A), 3 (B) and 25 (C) FPU/g cellulose and 1.5 %w/v solid loading. G1: first order model, G2: second order model.

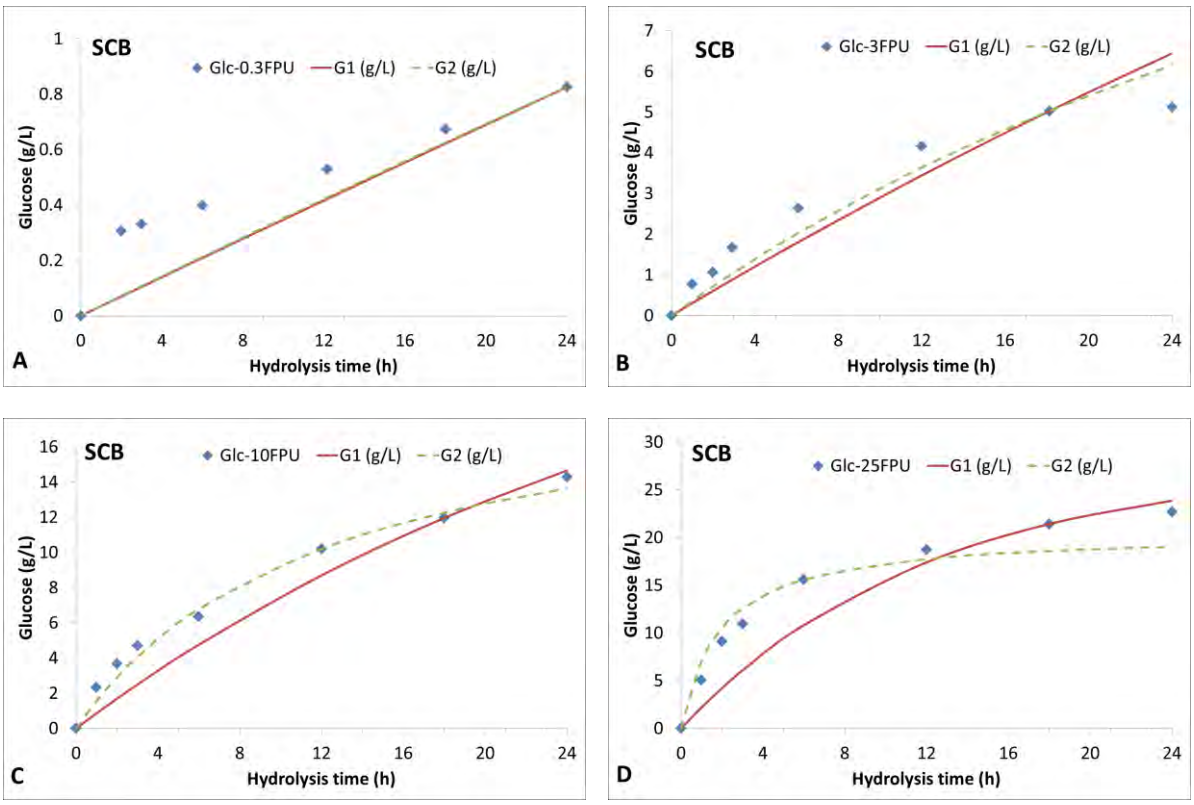

Figure 3-15. Predicted versus experimental values of glucose concentration released during the enzymatic hydrolysis of SCB at 0.3 (A), 3 (B), 10 (C) and 25 (D) FPU/g cellulose and 3 %w/v solid loading. G1: first order model, G2: second order model.

3.2.2 Suspension *in-* and *ex-situ* viscometry

3.2.2.1 In-situ viscosity

The time-viscosity curves of FP, PP and SCB suspensions during hydrolysis for various Ctec2 ratios and with G1, G2+G3 and G1+G2+G3 at E/S ratios equivalent to 0.3 FPU of Ctec2 per g cellulose are reported in **Figure 3-16** and **Figure 3-17**. These curves demonstrate the ability to finely quantify in-situ viscosity during bio-catalysis even for low values (SCB). The reference curves (none activity) shows the absence of significant change in viscosity over 24 h except with PP. With enzyme activities, the curves fulfil a dose-effect response but in a non-linear mode. However, the evolution and the curve shapes strongly differ between FP, PP and SCB considering cocktail and pure activities. These trends and differences are exacerbated with the lowest E/S ratios.

With FP suspensions (**Figure 3-16A**), a monotone decrease in viscosity was observed. At 25 FPU/g cellulose, FP suspension was liquefied in a short time (< 0.37 h); the viscosity collapses from 75 %. At 3 FPU/g cellulose, the viscosity decreased drastically from 0.25 Pa.s to 0.063 Pa.s after 1.57h (reduction by 75 %). When hydrolysis was carried on, the suspension viscosity quickly reached the supernatant (water) viscosity. Turbulent flow regime was then fully established and the estimation of in-situ viscosity was poorly reliable. A steady state power mixing number (Np) restricts the determination of viscosity for mixing Reynolds superior to 3.10^4. The same limitation during ex-situ rheometry due to a shift in turbulent flow at high shear rates was encountered by Rosgaard et al. 2007 (Rosgaard, Andric et al. 2007) with steam-pretreated barley straw. At 0.3 FPU/g cellulose, the viscosity decline is slower and longer, the time needed for 75 % reduction in viscosity was nearly 22h.

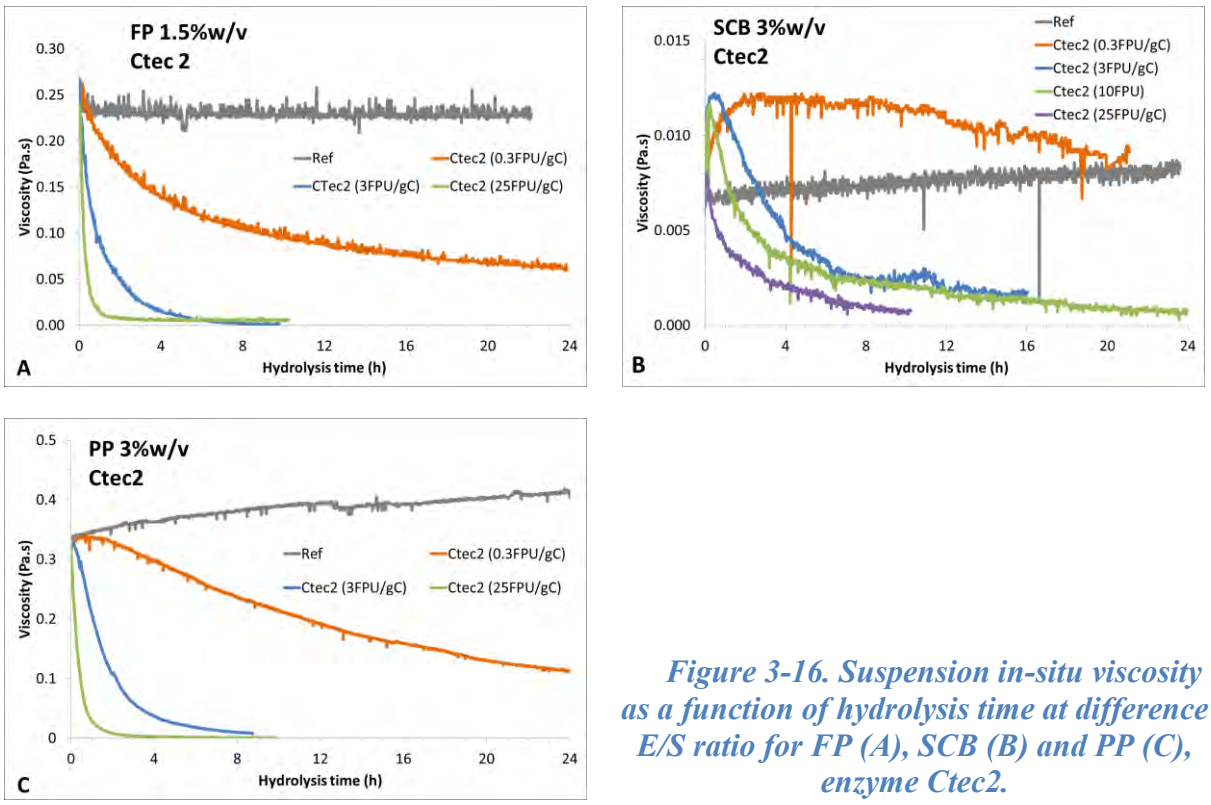

Figure 3-16. Suspension in-situ viscosity as a function of hydrolysis time at difference E/S ratio for FP (A), SCB (B) and PP (C), enzyme Ctec2.

Considering enzymes preparations from pure activities (equivalent to Ctec2 at 0.3 FPU/g cellulose), a decrease in viscosity by more than 50 % after 11.9 h was recognized in presence of endo-glucanase activity (G1). This decrease was then followed by a gentle decline until the end of hydrolysis, reached approximately 60 % reduction in viscosity at 24h. For the mixture (G1+G2+G3) with similar activities profile of endo and exo-glucanase as Ctec2, the reduction in viscosity was similar compared to G1. As expected, the mixture of β-glucosidase (G3) and exo-glucosidase (G2) had almost no effect on the suspension viscosity: only 9 % of viscosity reduction was observed with FP up to 24h. Therefore, the liquefaction efficiency was not affected with or without adding of β-glucosidase and exo-glucanase. Experimental results were well fitted with theory, endo-glucanase activity cleaves randomly 1,4-β-D-glycosidic linkages, breaks down cellulose fibers into shorter polysaccharides and oligosaccharides and rarely up to mono-saccharide. It possesses a more pronounced effect on the viscosity than the exo-glucanase or β-glucosidase. Similar conclusion was also reported by Szijártó et al.(Szijártó, Siika-aho et al. 2011). On hydrothermal pretreated wheat straw using purified enzymes from *Trichoderma ressei*, endo-glucanase was the main enzyme which took responsibility for the viscosity reduction. More than 80 % reduction in viscosity was obtained through hydrolysis by 1377 nkat/g substrate of endo-glucanase alone. On **Figure 3-16B**, the differences in viscosity reduction between Ctec2 and either G1 or mixture (G1+G2+G3) were likely to link with auxiliary activities that may present in Ctec2.

With PP (**Figure 3-16C**), the viscosity of reference experiment represented a gradual increase up to 12.5 % in 24 h. This phenomenon can be explained by hydratation and swelling effect of PP in suspension under mechanical agitation. Similar with FP, a decrease in suspension viscosity depending on E/S ratios was reported under enzymatic catalyst of PP. The time for 75 % reduction in viscosity were 0.51 and 2.4h for enzyme loading 25 and 3 FPU/g cellulose respectively. At 0.3 FPU/g cellulose, it seems that the evolution of viscosity was delayed in the first 1h and subsequently followed by a gradual decrease up to 75 % after 25 h (point extra-poled). It is reported that the liquefaction rate of PP suspension was significant slower than FP

whatever E/S ratio of Ctec2. Working on same substrate PP but using another lignocellulase cocktail (Acellerase 1500), Nguyen (Nguyen 2014) reported the time for 75 % fall in viscosity as 3.2 and 23 h for enzyme loading 28.5 and 5.7 FPU/g cellulose respectively.

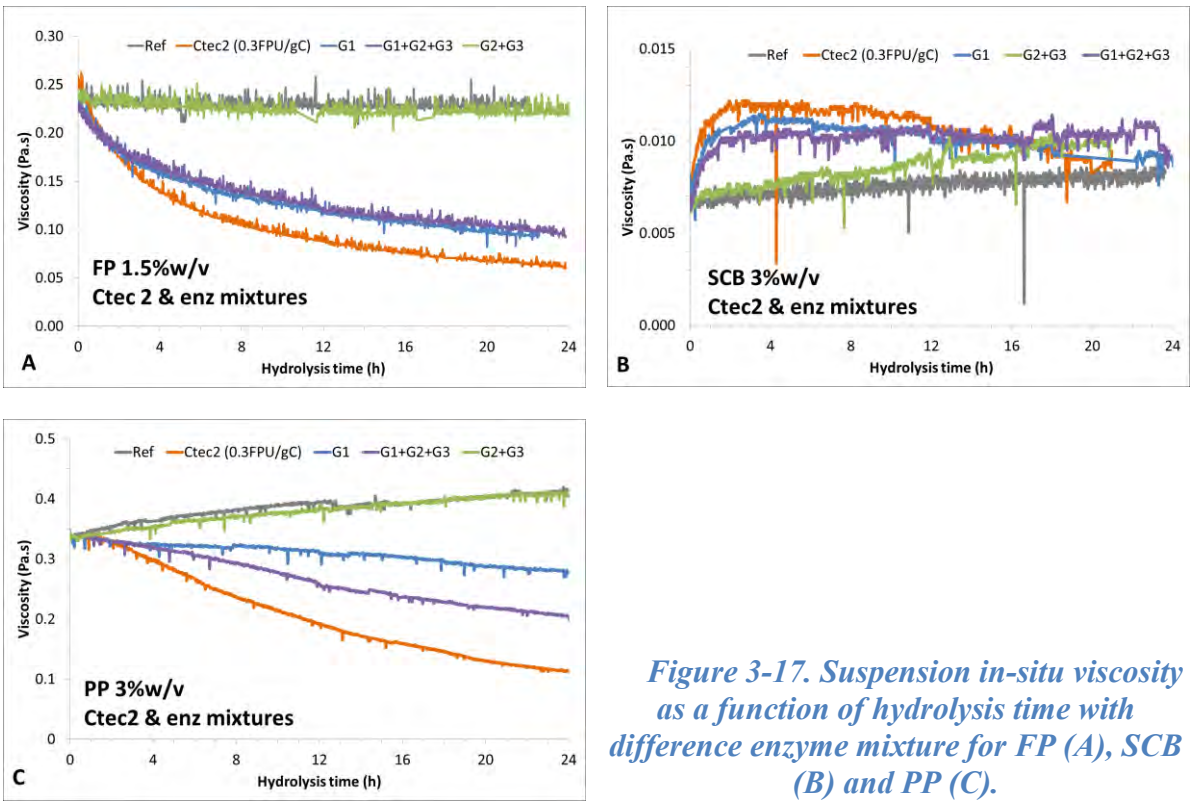

Figure 3-17. Suspension in-situ viscosity as a function of hydrolysis time with difference enzyme mixture for FP (A), SCB (B) and PP (C).

For pure activities (equivalent to Ctec2 at 0.3 FPU/g cellulose **Figure 3-17A**), the observed phenomenon of viscosity showed an addition witness for previous conclusion on FP. As expected, the mixture of G2+G3 has almost no effect on liquefaction. It time dependence viscosity curve is almost super imposed with the reference. For G1, the reduction in viscosity was clearly observed compared to the reference. Interestingly, the mixture G1+G2+G3 reported significant improvement in liquefaction efficiency than G1 alone whereas on FP, these experiments showed nearly identical viscosity curves. Into tie between biochemical analysis (glucose, xylose yields **§3.2.1**) and physical observation, this improvement can be explained by synergy of G1 and G2+G3, boosting mixtures capacity. It is important to notice that Ctec2, one again, showed stronger effect than the mixture G1+G2+G3 on viscosity. In addition with auxiliary enzyme presenting in Ctec2, the action of hemicellulose activities is possible to raise liquefaction efficiency. This assumption is supported by the biochemical analysis, indicating 8.1 % xylose conversion yield at 0.3 FPU/g cellulose.

With SCB suspension (**Figure 3-17B**), the shape of viscosity curves strongly differ and exhibit an initial overtakinging before decrease. From viscosity curve of reference experiment (no enzyme added), a slight and linear increase by 19 % after 24 h was reported. At 0.3 FPU/g cellulose, the viscosity rose to 0.0122 Pa.s after 3h and then followed a progressive decrease until 24 h but it remained higher than initial value. By increasing the enzyme loading from 0.3 to 3 FPU/g cellulose, similar tendency was recognized. The viscosity showed a sharp climb in the first 27 min and reached a maximal value of approximately 0.0122 Pa.s. From this point, it evolution reported an opposite decreasing trend, reached 75 % reduction compared to initial value at 8 h. Beyond 16 h, the poor precision for viscosity determination stands as a limiting factor to discuss absolute value (Re_{Mixing} > 30000). At 10 FPU/g cellulose, viscosity overtakinging occurred with almost same magnitude (maximal value ~ 0.0116 Pa.s) but over a

shorter duration (t = 13 min). It followed by a rapid decrease to 75 % at 7.9 h to 0.0025 Pa.s followed up to 8 h. At 25 FPU/g cellulose, the suspension viscosity quickly collapsed from 0.008 Pa.s over 10 h, without any observable overtakinging. 75 % reduction in viscosity was recognized after 3.7 hours. Surprisingly for three enzyme/substrates ratios (0.3, 3 and 10 FPU/g cellulose), the maximal viscosities were identical (~0.012 Pa.s) with different hydrolysis time. From literature, viscosity of lignocelellulosic suspension at fixed condition (mixing rate, temperature, pH) may be affected by either substrate concentration or particle size and shape distribution (Giesekus 1983, Dasari and Berson 2007). In present case, at 0.3, 3 and 10 FPU/g cellulose, the glucose conversion yield at overtakinging points were insignificant and equal to 1.2 %, 2.9 % and 1.9 % respectively. Therefore, the evolutions of viscosity may be resulted from a change in particle size/shape.

Considering enzymes mixtures from pure activities (equivalent to Ctec2 at 0.3 FPU/g cellulose (**Figure 3-17C**), the hydrolysis by (G1+G2+G3) and G1 produced almost superimposed viscosity pattern. In the first 4 h, these viscosities were identical with a sharp growth of nearly three folds compared to initial value, then followed by a steady state. For (G2+G3), the viscosity presented a gradual climb, which was identical with referent experiment, reached approximately 0.011 Pa.s after 24 h. For Ctec2, the overtaking step was slightly shorter, reached a viscosity of 0.012 Pa.s after 2 h hydrolysis. The tendency in viscosity was then turned to a gradual decrease until the end. The role of G2+G3 on suspension viscosity is confirmed again on SCB.

3.2.2.2 Rheological behavior during enzymatic hydrolysis

From the current literature, there are no works investigating the behavior and consistency index of real lignocellulosic suspension during enzymatic hydrolysis by in-situ methods. Published research only investigates the flow behavior and consistency index of raw suspension (Viamajala, McMillan et al. 2009, Nguyen, Anne-Archard et al. 2013, Zhang, Zhang et al. 2014). In order to complete this knowledge and to better understand the behavior of lignocellulosic suspension, in-situ viscosity at different mixing rates and calculation of power-law index were carried out.

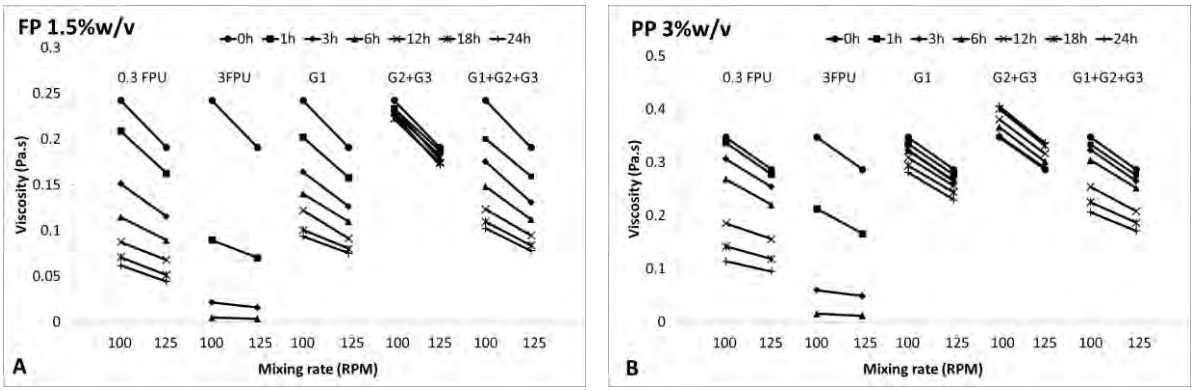

Figure 3-18. Suspension in-situ viscosity at 100 and 125 rpm of FP 1.5 % w/v (A) and PP 3 %w/v (B) as a function time for Ctec2(0.3 and 3 FPU/g cellulose) and for G1, G2+G3 and G1+G2+G3.

For both substrates at 25 FPU/g cellulose, the flow regime quickly changes from laminar/transition into turbulent regime (Re > 10000), which not allows the investigation of shear thinning property neither flow behavior index. Similar investigation is also not suitable for SCB due to low magnitude of viscosity. At 3 FPU/g cellulose, these interpretations was partially performed in the first stage when Reynolds number was still in the reliable range (Re < 642) For all others experiments at low enzyme loading, Reynolds number was located in the

interval of 80 to well under 351 and 169 for FP and PP respectively. These conditions allow calculating the flow behavior index, n using **Eq. 2-41** (see §**2.4.3.2.2**).

Figure 3-18A, B illustrates the evolution of FP and PP suspension viscosities during hydrolysis at 100 and 125 rpm. Clearly, the time evolution of viscosity at all tested single up to mixture activities were in accordant with previous results (see **Figure 3-16A, C** and **Figure 3-17A, C**). The loss in shear thinning property is observed in parallel with the decreasing trend in viscosity except for the mixture G2+G3. For FP, the attenuation of shear thinning is well observed at 3 FPU/g cellulose. The slope of viscosity curve decreased rapidly early on then undergoes a steady fall. At 6h, viscosity at 100 and 125 rpm reported almost similar value, suspension behavior is nearly Newtonian. Similar attenuation trend of shear thinning property but at slower kinetic and smaller magnitude is reported at 0.3 FPU/g cellulose, G1 and mixture G1+G2+G3. For PP, the phenomenon observed at 3 FPU/g cellulose and G2+G3 mixture was identical as FP. However, G1 and the mixture G1+G2+G3 seem to not significantly affect non-Newtonian property of suspension. The experiment at 0.3 FPU/g cellulose also presented weaker evolution of viscosity slop than for FP. The complexity of material is possible to explain this difference.

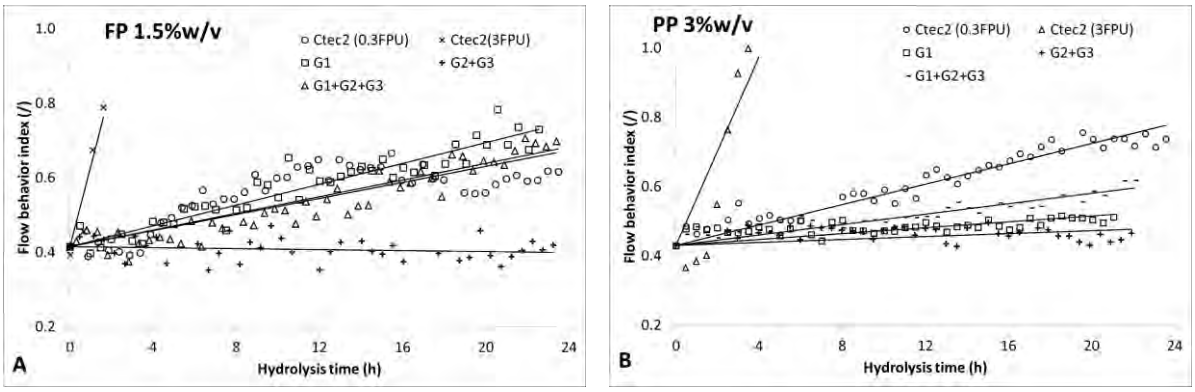

Figure 3-19. Evolution of flow behavior index (n) of FP 1.5 % w/v (A) and PP 3 %w/v (B) as a function of time for Ctec2 (0.3 and 3 FPU/g cellulose) and with G1, G2+G3 and G1+G2+G3.

Figure 3-19 provides information about flow behavior index (power law index) during hydrolysis of FP and PP by different activities. Initial flow behavior indexes at 0.415 and 0.429 were recognized for FP and PP in agreement with initial suspension characterization (shear-thinning or pseudo plastic properties). Same conclusions were also reported by other authors on several lignocellulosic biomasses. Both Dunaway, Dasari et al. (2010) and Pimenova and Hanley (2004) stated that pretreated corn stove slurries exhibited pseudo-plastic behavior. Dasari and Berson (2007) have noted the shear-thinning properties of sawdust slurries at different particle size ranges. A general increase in flow behavior index is noticeable whatever operating conditions, except for G2+G3. The increase in n translates a loss of non-Newtonian properties of suspensions undergoing enzymatic hydrolysis. However the deviation magnitudes are strongly different between activities.

For PP at 0.3 FPU/g cellulose, flow behavior index reported a gradually rise, started at 0.415 and ended at well under 0.8 at the end of experiment. For the mixture G1+G2+G3 and G1 single, these numbers reached nearly 0.6 and 0.5 respectively up to 24 h. In addition, the slop of power law index curve is strongly dependent on enzyme loading, as showed in **Figure 3-19** for 0.3 and 3 FPU/g cellulose. Experimental data confirmed the dominant role of endo-

glucanase for the evolution of flow properties. Exo-glucanase and β-glucosidase had almost no effect. Synergy of enzyme activities on rheological properties is demonstrated on PP.

3.2.2.3 Ex-situ viscosity

The viscoelastic behavior was examined through amplitude sweep oscillation measurement as the hydrolysis reaction proceeded. The storage modulus (elastic modulus) G' and the lost modulus (viscous modulus) G" were plotted versus applied shear stress τ (Pa) in **Figure 3-20** for FP and SCB suspension. Clearly, all curves showed very similar trend with G' and G" were nearly constant in certain shear stress range depending on hydrolysis time. At shear stress beyond this point, the drops in both G' and G" were reported indicating the breakdown of material structure and hence the yield stress (τ_0) of suspension. It is important to note that, an increasing trends for both G' and G" were witnessed during the first 2 h hydrolysis (**Figure 3-20)**. This was then followed by a decreasing trend till the end of hydrolysis. For FP suspension, the yield stresses were located in a wide range from 10^2 to 10^{-2} Pa while these values for SCB suspension varied between 10^{-2} and 1 Pa. Despite the large different in initial yield stress of FP and SCB, this value for both suspension reached same order of magnitude after 24 h hydrolysis at 3 FPU/g cellulose. This observation reflected a similar level of destructuration for FP and SCB particles whatever their initial states. Consequently, the comparison between ex-situ rheometry and in-situ viscometry was presented in **Figure 3-21**. τ_0 (Pa) indicates the yield stress of suspension, defined by 20 % drop in G" when increasing shear stress. μ'(Pa.s) is the dynamic viscosity of suspension measured at given frequency (f = 1 Hz). Interestingly, the evolution of yield stress for both FP and SCB suspension correlated with the changes in their in-situ viscosity. Dynamic viscosity (ex-situ) and in-situ viscosity reported very similar trend versus hydrolysis time. The overtaking in suspension viscosity for SCB was also witnessed from ex-situ measurement through evolution of dynamic viscosity μ'. The different in initial suspension viscosities between FP and SCB (**Figure 3-8**) was confirmed on ex-situ measurement. Initial dynamic viscosity of FP was roughly fivefold higher than that of SCB suspension at frequency 1 Hz. Results from ex-situ rheometry sustain and strengthen the conclusion deducing from in-situ viscometry.

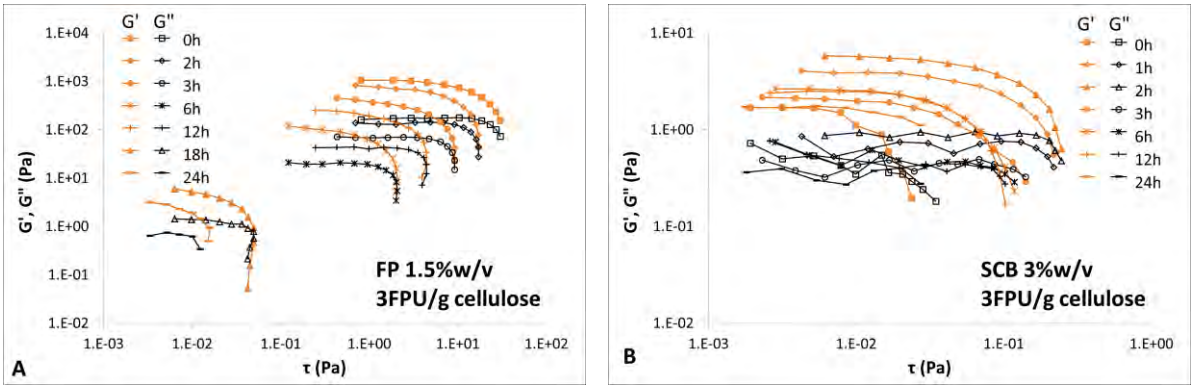

Figure 3-20. Elastic and viscous modulus as a function of the applied shear stress τ for FP andSCB suspension after different hydrolysis time.

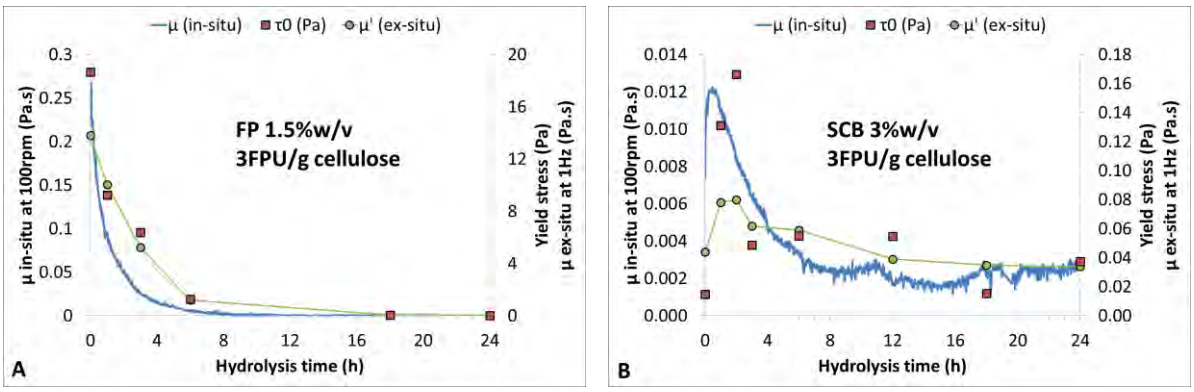

Figure 3-21. Correlation between ex-situ rheometry and in-situ viscometry for FP and SCB at 3 FPU/g cellulose.

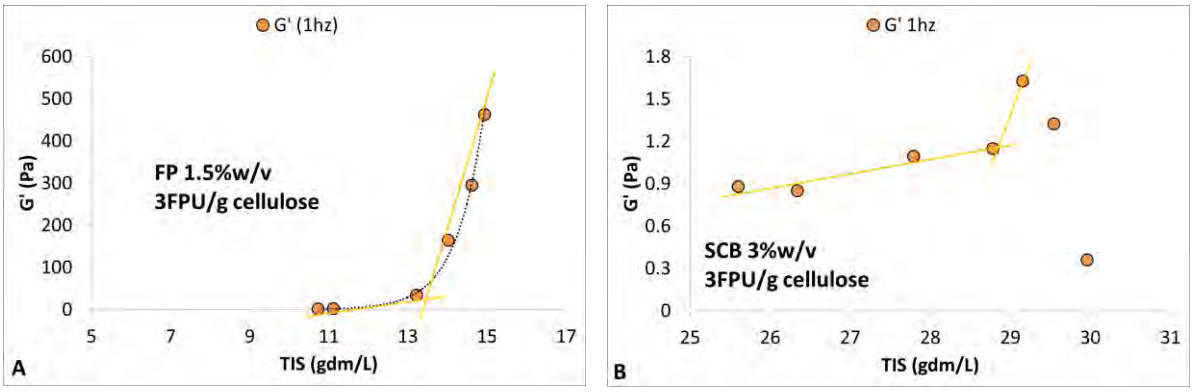

Figure 3-22. Correlation between ex-situ rheometry and biochemitry for FP and SCB at 3 FPU/g cellulose.

The relation between ex-situ rheometry and biochemistry was investigated and illustrated in **Figure 3-22A** and **B**. The variation of total insoluble substrate (TIS) in the suspension during enzymatic digestion was also observed to be reflected by evolution in the rheological parameters. As presented in **§3.2.1** - p106, biochemical analysis attested the existence of solubilization mechanism. The total insoluble concentration in the suspension decreased as the enzymatic digestion progressed. As showed in **Figure 3-22A**, a clear relationship between the elastic modulus G' and the total insoluble substrate was observed. It exhibited roughly two different trends: i) a quasi linear relationship between G' and TIS in the first stage of enzymatic reaction where TIS > 13.5 gdm/L and ii) a nearly independent state of G' whatever TIS at lower than 13.5 gdm/L. The critical point (13.5 gdm/L) corresponded to the hydrolysis time t≈6h where the liquefaction stage was already finished Both in-situ viscometry and ex-situ rheometry reported the viscosity collapse of FP suspension at around 6h (**Figure 3-21A**). The phenomenon can be now explained. Insoluble fraction possessed strong impact on elastic modulus as well as suspension viscosity. In the first stage of hydrolysis, insoluble fraction was attacked mainly through fragmentation mechanism. The broken down of coarse population into finer one led to a reduction in suspension viscosity as well as drop in elastic modulus. When the liquefaction was done, the reduction in suspension viscosity and elastic modulus reached maximal level. Beyond this point, the impact of insoluble fraction on rheological behavior became negligible. Further reduction of insoluble fraction will affect the bioconversion yield rather than rheological properties of suspension. This relationship will be explored more deeply following particle size analysis (see **§3.2.3** - p124). For SCB suspension, similar plot between G' and TIS was tried (**Figure 3-21B**) but no clear assumption can be established. In this graph, the three

rightmost experimental points corresponding to TIS > 29 gdm/L represented the viscosity overtaking period (first 2 h) where suspension viscosity rose significantly (**Figure 3-21B**). Below this point at TIS < 29 gdm/L, the magnitude of evolution in G' versus TIS was not very pronounced but a decreasing trend in G' can be observed as the total insoluble substrate decreased. In this case, the phenomenon was more complex accounted two opposing mechanism liquefaction and overtaking. More analysis is required to create a reliable assumption.

Finally, **Figure 3-23** plots the viscous modulus G" versus elastic modulus G' for all three tested substrate whatever enzyme loading ratios and hydrolysis time. Data were collected from experiments N° 02, 04, 05, 06, 07, 11, 12, 14, 17 and 20 (see **Table 3-1).** Surprisingly, all experimental points were aligned in a unique line. The result suggested that for all lignocellulosic substrate, enzymatic activities have similar impact on the elastic property of the suspension as on the viscous property. Both viscous and elastic moduli were reduced equally during enzymatic hydrolysis.

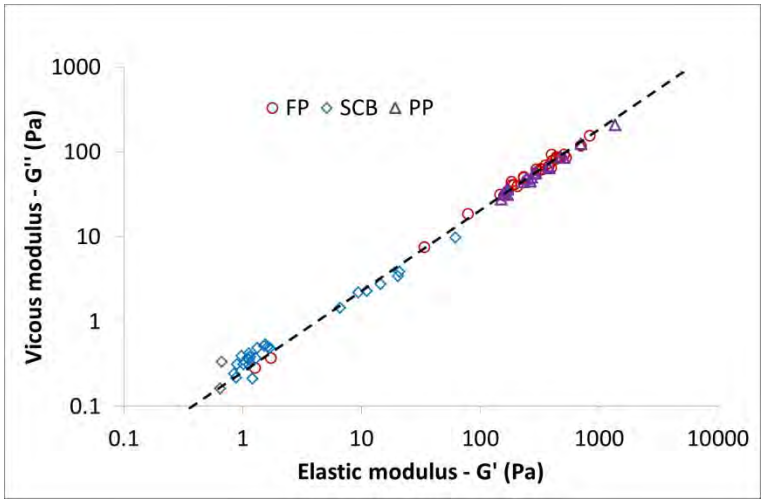

Figure 3-23. Relationship between G' and G" during enzymatic hydrolysis of PP, SCB and PP suspension. Various E/S ratios and substrate concentration.

3.2.2.4 In-situ viscosity modeling

The kinetics of enzymatic hydrolysis of lignocellulosic suspension has been investigated since many years. Most of published works were focusing on bio-chemical approach where hydrolysis yields or glucose productions stand as two main targets. For rheological approach, the time dependency of suspension viscosity can be modeled. Two kinetics models were used in the present work. **Eq. 3-11** illustrates the viscosity reduction in a power relationship where μ is the viscosity (Pa.s), k is the kinetic constant ($Pa^{1-n}.s^{-n}$) and n is the model order (/). The viscosity μ is defined as the subtraction of measured viscosity, μ_m, from solvent viscosity, μ_s which corresponds to the viscosity of water ($\mu = \mu_m - \mu_s$). On the other hand, the research of Geddes, Peterson et al. (2010) reported the excellent ability of exponential equation (**Eq. 3-12**) for viscosity prediction of sugarcane bagasse suspension versus hydrolysis time. This model is the particular case of **Eq. 3-11** when *n* equals to 1 (first order model), the coefficient A is correspond to $\mu_0 - \mu_s$ and B reflecting μ_s. Parameters of the two models were adjusted by least squares method of μ using solver tool (Microsoft Excel ®).

$$-\frac{d\mu}{dt} = k_{visco-1} \cdot \mu^n \qquad \textit{Eq. 3-11}$$

$$\mu = A \cdot e^{-k_{visco-2} \cdot t} + B$$
$$\leftrightarrow \mu = (\mu_0 - \mu_s) \cdot e^{-k_{visco-2} \cdot t} + \mu_s \qquad \textit{Eq. 3-12}$$

The plots of predicted versus experimental values are presented in **Figure 3-24**. The parameters of two models on FP and PP were summarized in **Table 3-8**. Generally, both models accurately described the time dependence of suspension viscosity for FP and PP as values of R squared were superior than 0.93 for all experiments, except for FP 0.3 FPU/g cellulose. For PP, the coefficient $k_{visco-1}$ showed an increasing trend with enzyme loading while the model order, n, fluctuated around 1. As the variation of n between experiments was fairly small, value of $k_{visco-1}$ indicates the dependency of viscosity reduction rate on enzyme loading ratios. This also explained why first order model showed very good predictions values compared to experimental ones. Similar results were reported for FP at 3 and 25 FPU/g cellulose, both first order and order n models indicated good R squared values. The higher value of k was observed for higher enzyme loading ratio. However for FP at enzyme loading 0.3 FPU/g cellulose, the model order n was equal to 2.8, leading to an unexpected value of k.

Table 3-8. Parameters of viscosity modeling for FP and PP at different enzyme loadings.

Substrate	FP 1.5 %w/v			PP 3 %w/v		
FPU/g cellulose	0.3	3	25	0.3	3	25
Kinetics model order n						
$k_{visco-1}$	**3.15**	1.91	4.73	0.04	0.91	3.09
n	**2.79**	1.33	1.17	0.89	1.24	1.13
R^2	0.999	0.995	0.985	0.980	0.968	0.998
Kinetics model 1st order						
$k_{visco-2}$	0.09	0.98	3.42	0.05	0.51	2.52
R^2	**0.666**	0.977	0.956	0.986	0.987	0.997

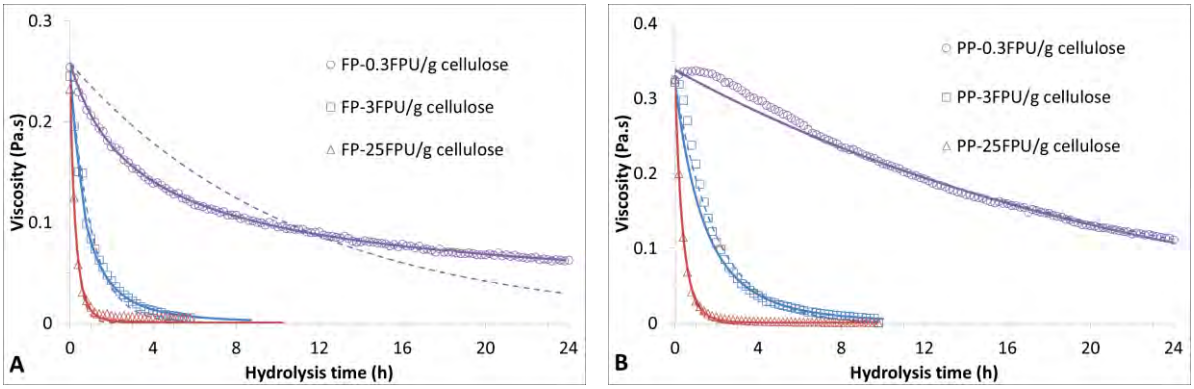

Figure 3-24. Predicted and experimental value of suspension viscosity at different enzyme loading for FP 1.5 %w/v (A) and PP 3%w/v (B). Predicted curves were plotted in full line for order n equation and dash line for first order equation. Experimental data were simplified to 5 points per hour.

To specifically describe the reduction of suspension viscosity during enzymatic hydrolysis, a dimensionless quantity μ^* was defined as

$$\mu^* = \frac{\mu - \mu_s}{\mu_0 - \mu_s} \qquad \textit{Eq. 3-13}$$

Where μ_s is the viscosity of solvent (in our case, $\mu_s = \mu_{water} = 0.000653$ Pa.s at T = 40 °C), μ_0 is the initial viscosity of suspension before enzyme adding. The dimensionless viscosity μ^* vary from 1 to 0 translating the normalized reduction of suspension viscosity compared to initial value. The time for 75 % reduction in viscosity (corresponding to $\mu^* = 0.25$) is investigated and noted $t_{0.25}$. Through experiments on FP and PP, lower value of $t_{0.25}$ was observed at higher enzyme loading ratio. Generally for enzymatic reaction, increasing enzyme loading within saturation limit directly improve reaction rate, lead to an increase in rate of viscosity reduction. The relationship between enzyme loading and $t_{0.25}$ is illustrated in **Figure 3-25**. It can be represented by an exponential function for each substrate

Filter paper 1.5 %w/v

$$t_{0.25} = 6.17 \cdot [E]^{-1} \qquad \textit{Eq. 3-14}$$

Paper pulp 3 %w/v

$$t_{0.25} = 10.57 \cdot [E]^{-1} \qquad \textit{Eq. 3-15}$$

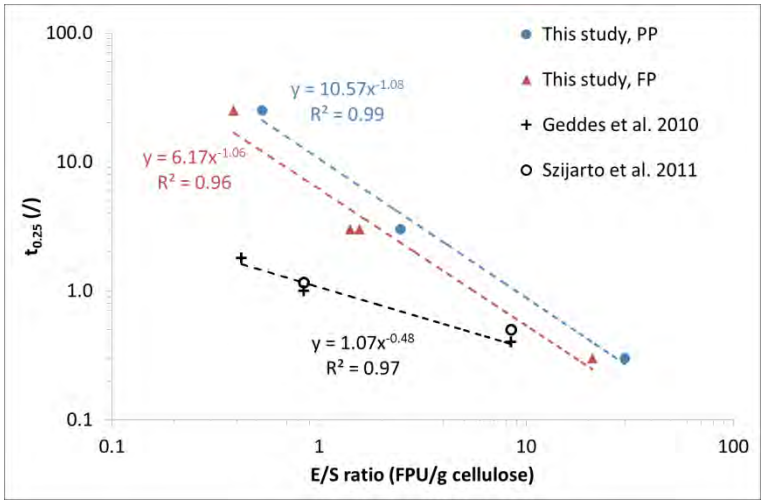

Figure 3-25. Time for 75 % reduction in viscosity in relation to enzyme loading of CTec2 for FP 1.5 %w/v and PP 3 %w/v

For **Eq. 3-14** and **Eq. 3-15**, $[E]$ represents the enzyme loading (FPU/g cellulose) and $t_{0.25}$ (h) was previously defined. The value of $t_{0.25}$ for lowest enzyme loading (0.3 FPU/g cellulose) were obtained by extrapolate from experimental plot $\mu = f(t)$. The R squared values were calculated as 0.964 and 0.987 for FP and PP respectively, indicating good agreement with experimental data. The value of $t_{0.25}$ versus enzyme loading was also exported from the literature and represented in **Figure 3-25**. It is interesting that our results are in the same order of magnitude as collected data on dilute acid pretreated sugarcane bagasse 100 gdm/L (Geddes, Peterson et al. 2010).and hydrothermally treated wheat straw 150 gdm/L (Szijártó, Siika-aho et al. 2011) and several published research (Dasari and Berson 2007, Pereira, Pereira et al. 2011, Palmqvist and Lidén 2012) Surprisingly data collected from Geddes et al. (Geddes, Peterson et al. 2010) also followed a power relationship between $t_{0.25}$ and enzyme dose (**Figure 3-25)**. It is noticeable that the dependency of $t_{0.25}$ in E/S ratio was more pronounced in our research

compared to values from Geddes or Szijarto's work. It may assumed by the fact that our hydrolysis reaction were carried out at semi-dilute condition of substrate that exacerbate the effect of enzyme loading.

Following the interpretation of $t_{0.25}$, the hydrolysis time was normalized following **Eq. 3-16**

$$t^* = \frac{t}{t_{0.25}} \qquad \textit{Eq. 3-16}$$

The dimensionless viscosity-time curves $\mu^* = f(t^*)$ at different enzyme loading ratios are illustrated in **Figure 3-26A** and **Figure 3-26B** for FP and PP. It is observed that all curves are nearly super-imposed. Similar trend was also observed for FP 1.5 %w/v at 0.3, 3 and 25 FPU/g cellulose. This result suggests a similar reaction mechanism for a given substrate whatever enzyme dosage. In contrast the uniqueness viscosity-time curve was not observed for SCB (**Figure 3-26C**). This may due to the overtaking in viscosity during early stage of hydrolysis at low enzyme loading (≤ 10 FPU/g cellulose).

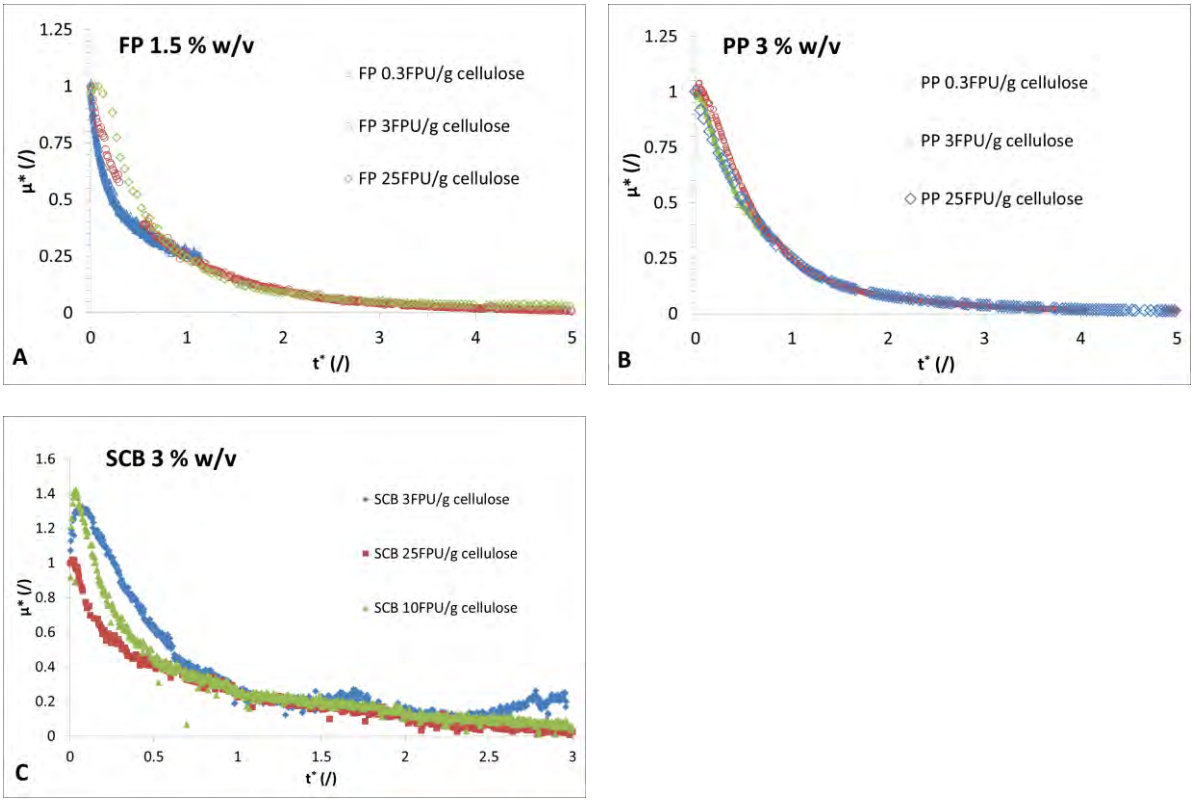

Figure 3-26. Dimensionless viscosity time curves for FP 1.5 %w/v (A), PP 3 % w/v (B) and SCB 3 % w/v at different enzyme loading ratios (FPU/g cellulose).

3.2.2.5 Relationship between rheological and biochemical properties

The relationship between rheological and biochemical during enzymatic hydrolysis was evaluated through two parameters: reduction of suspension viscosity (%) and solubilization yield (%). The reduction of viscosity at time t was calculated by

$$Viscosity\ reduction\ (\%) = \frac{\mu(t) - \mu_s}{\mu_0 - \mu_s} \cdot 100 \qquad \textit{Eq. 3-17}$$

Where μ(t) viscosity measured at t (h), μ_0 initial viscosity at t = 0 h and μ_s viscosity of water at 40 ºC

The solubilization yield of substrate was estimated from hydrolysis rate of glucose and xylose.

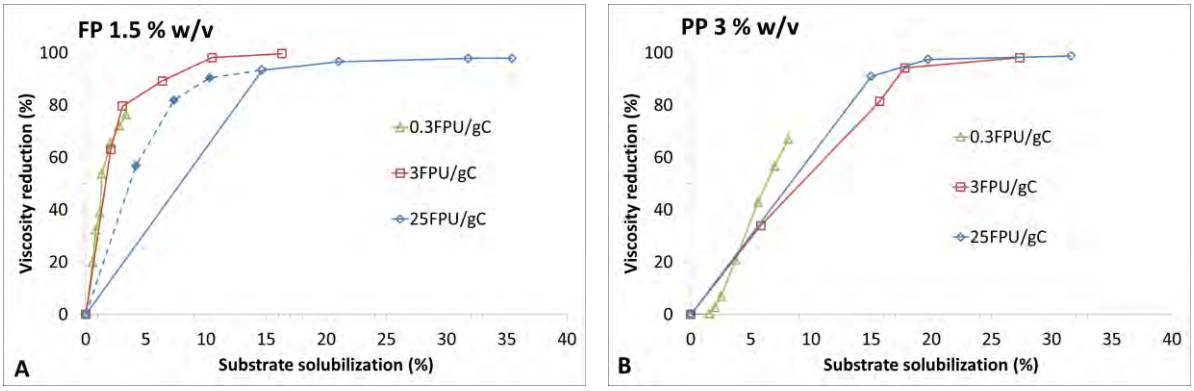

Figure 3-27. In-situ viscosity reduction (%) versus substrate solubilization (%) for FP (A) and PP (B) at difference E/S ratio (0.3, 3, 25 FPU/g cellulose) of Ctec2.

Figure 3-27 illustrated the reduction in suspension viscosity versus the solubilization rate during enzymatic hydrolysis of FP and PP. It was observed that both substrates exhibited similar trend but at different magnitude. For FP at 0.3 and 3 FPU/g cellulose, 75 % reduction of initial viscosity was achieved corresponding to a solubilization rate inferior than 4 %. For the highest E/S ratio (25 FPU/g cellulose), due to the very quick drop in viscosity, the first sampling point at 1 h reported more than 90 % viscosity reduction, corresponding to a solubilization rate of well under 15 %. By interpolate the solubilization curve versus hydrolysis time, three points corresponding to t = 0.25 h, 0.5 h and 0.75 h were added in **Figure 3-27A** (filled diamond with dash line). The reduction of 75 % suspension viscosity was deduced at the solubilization rate equal to approximately 7 %. Previously in **Figure 3-17A**, the experiment with G1 demonstrated that FP suspension can be partially liquefied without any solubilization. A viscosity reduction of 60.7 % after 24 h hydrolysis was achieved for FP using endo-glucanase alone without any solubilization. Experimental results on FP suggest that this suspension can be liquefied without solubilization. Once Ctec2 was added in suspension, the kinetic of liquefaction was progressed first at rate depending on amount of enzyme loading. The solubilization started later when suspension was partially liquefied.

For PP suspension, the 75 % reduction in viscosity was achieved at around 10 to 15 % solubilization for all tested enzyme loading from 0.3 to 25 FPU/cellulose (**Figure 3-27B**). These numbers were slightly higher than that of FP. In contrast, significant different between Ctec2 (0.3 FPU/g cellulose) and G1 alone (**Figure 3-17C**) was reported. By extrapolating, the require time for 75 % reduction in suspension viscosity can be estimated and equal to 27.1 h and 105.9 h for Ctec2 and G1 respectively. For PP suspension, exo-glucanase always stands as main activity for the liquefaction of suspension. From the beginning of hydrolysis, the solubilization of PP suspension showed more pronounced effect than for FP suspension.

From rheological theory, suspension viscosity at given condition (T, pH, shear rate) is depend on several parameters such as substrate concentration, particle size and shape distribution. In case of lignocellulosic suspension during enzymatic hydrolysis, the reduction in viscosity can assumed by the evolution in particle size, shape (fragmentation mechanism) or the reduction in substrate concentration (solubilization mechanism). Observed phenomena on FP and PP suggest that an efficient liquefaction do not require a significant solubilization. At tested condition (semi-dilute regime), the change in particle size by fragmentation mechanism was proved as key factor for liquefaction efficiency. High activity of endo-glucanase is then recommended for a rapid and efficient liquefaction. It can be the key point to avoid physical

limitation when working at high dry matter content and fed-batch mode. A mixture of high endo-glucanase activity can help to rapid decrease suspension viscosity, allowing further increase in total solid loading as well as reduce energy for mixing. However, at concentrated regime where suspension viscosity is strongly dependence on substrate concentration, the role of solubilization mechanism might be more and more important. This question will be investigated when discussing on semi-continuous fed-batch hydrolysis at high substrate loading (see **§4.3**)

3.2.3 Particle size distribution and morpho-granulo analysis

The difference of initial size range between three substrates is noticeable with an expected shift to smaller dimension during hydrolysis. Considering the influence of different physical factors on the suspension rheological behavior, the volume weighted particles size distribution (PSD) as well as the particle volume fraction (Φ_v) were specifically scrutinized and discussed. Meantime, the chord number, N_c, and the number weighted chord length distribution of particles, $E_n(l_c)$, will provide specific information about the evolution and contribution of the finest population. DLS and FBRM have been presented in **§3.2.3.1** and **§3.2.3.2** with their specificities and their limitations, in relation to the volume and number weighted distributions which constitute the raw measures. Their complementarity will be used to investigate changes in coarse and fine populations.

3.2.3.1 Diffraction light scattering

In order to allow comparison of particle size, the PSD is weighted by the particle volumetric fraction (Φ_v), then taking into account the reduction of suspended matter by solubilization during the process. In addition, the evolution of volume diameter $d_v(0.9)$, $d_v(0.5)$, $d_v(0.1)$ and mean diameter D(4,3)during enzymatic hydrolysis were also investigated. Finally, the cross between DLS measurement and rheological analysis will be discussed.

3.2.3.1.1 Filter paper suspension

For FP suspensions, **Figure 3-28** and **Figure 3-29** report the evolution of $E_v(d_{SE}) \times \Phi_v$ and volume weighted diameter d_v during enzymatic hydrolysis using Ctec2 (three enzyme/substrate ratios at 0.3, 3 and 25 FPU/g cellulose), G1, G2+G3 and G1+G2+G3 at similar enzyme profile as 0.3FPU Ctec2. As previously reported in **Figure 3-5A**, the initial PSD exhibits a bimodal and large spreading distribution of 54 % fine (d_{SE} < 200 µm) and 46 % coarse (d_{SE} > 200 µm) populations. Results from DLS analysis highlight the fragmentation mechanism on coarse population at all tested dosage of Ctec2. It suggests a transition into fine population at magnitude depending on the amount of enzyme loaded. However, the increase in volume weighted of fine population was not as strong as expected. It may be due to the fact that, DLS measurement based on volume weighted distribution is probably less sensible to fine particles. On the other hand, concomitantly with the increase in fine by fragmentation of coarse population, the solubilization mechanism possibly affects and balances fine population. The evolution of fine population will be scrutinized deeply following number weighted distribution by FBRM (**§3.2.3.2**).

At 25 FPU/g cellulose (**Figure 3-28C**) and after 1 h, $E_v(d_{SE}) \times \Phi_v$ indicated a transition from coarse to fine population. The total volume weighted of coarse population, $\Phi_{v-coarse}$ decreased by 46.3 % from t = 0 h to t = 1 h. Simultaneously, the volume fraction of fine population, Φ_{v-fine}, increased by 9.4 %. These size and volume evolutions correspond to a viscosity collapse by 94.2 % (**Figure 3-16A**). Beyond 1 h, in parallel with the decrease in coarse population, a significant reduction of fine particle fraction by 45.3 % was observed comparing 1 h and 24 h. However, nearly no change in suspension viscosity was reported during this

period. The reduction of total particle volume fraction was correlated to substrate solubilization as indicated by the increase in glucose yield from 14.8 % (t = 1 h) to 53.0 % (t = 24 h).

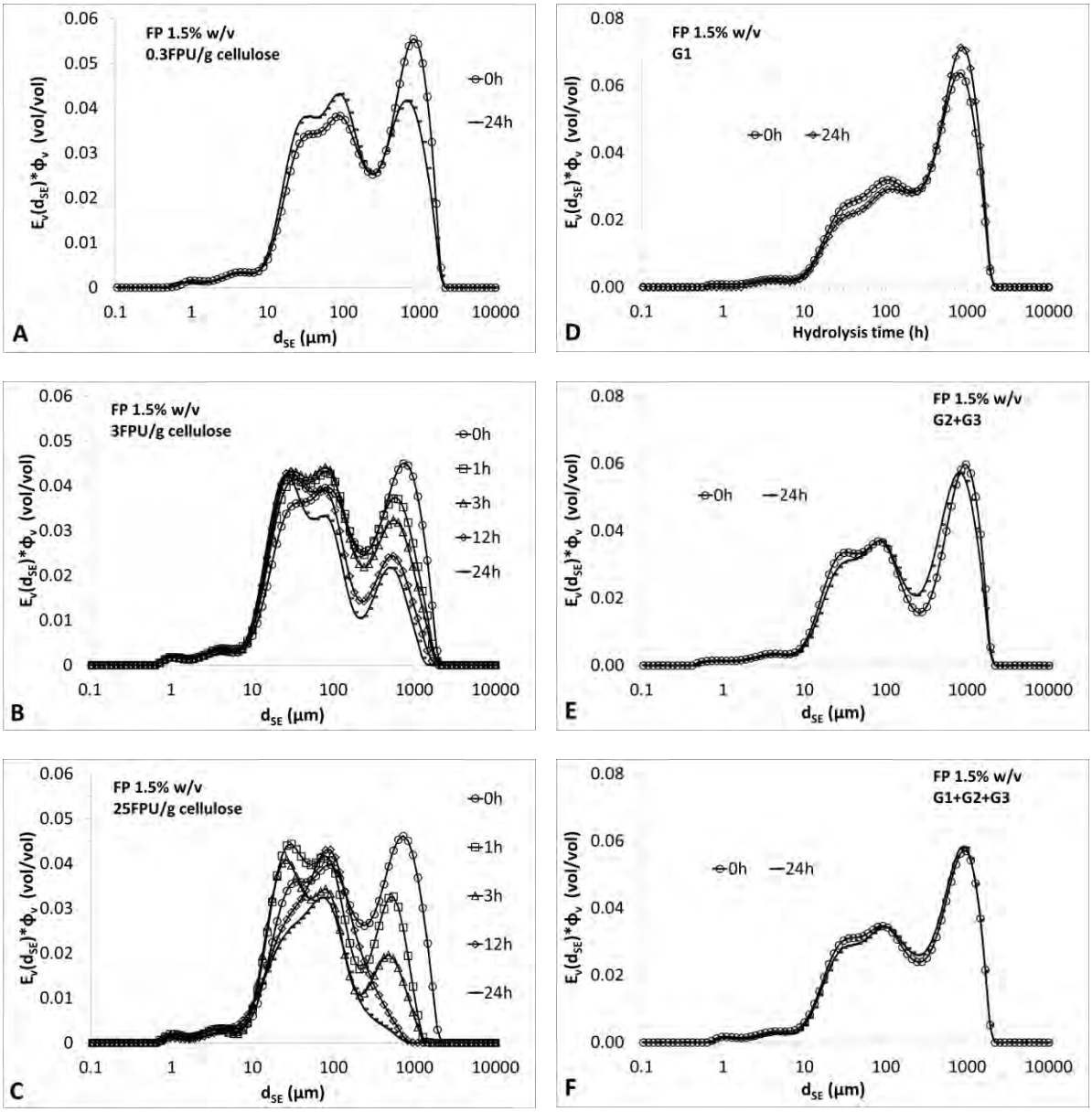

Figure 3-28. Particle size distribution weighted by particle volumetric fraction during hydrolysis of FP suspensions at different enzyme loadings from pure to cocktail activities.

Figure 3-29C presents the evolution of volume weighted diameter corresponding to < 10 %, < 50 %, < 90 % of population and the mean diameter D(4,3)during enzymatic hydrolysis of FP at 25 FPU/g cellulose Ctec2. Clearly, a decreasing trend was observed indicating the reduction in particle size mainly happened with the fraction of coarse population. A drastic fall was observed for $d_v(0.9)$ and D(4,3) in the first 1 h corresponding to the collapse of suspension viscosity (**Figure 3-16A**) and the decrease in $\Phi_{v-coarse}$. From this point, the tendency was then followed by a slow decrease to a steady state until the end of hydrolysis according to the phrase with minor evolution in suspension viscosity but significant increase in glucose yield. The evolution of $d_v(0.5)$ was found in the similar trend with $d_v(0.9)$ and D(4,3)but at smaller magnitude. For $d_v(0.1)$, almost no evolution was witnessed during 24h hydrolysis. In short, the evolution of volume weighted diameter were in good agreement with evolution of $E_v(d_{SE})$ weighted by Φ_v. Both parameters illustrated the close relationship between suspension

viscosity – fraction of coarse population and glucose conversion yield. It suggested that, fraction of coarse played a determinant role in the suspension viscosity. The reduction of this population by fragmentation mechanism is assumed to explain the collapse in suspension viscosity. In the other hand, this fraction was unlikely to correlate with glucose yield or in other word the solubilization mechanism. This assumption will be verified on other E/S ratio before conclusion.

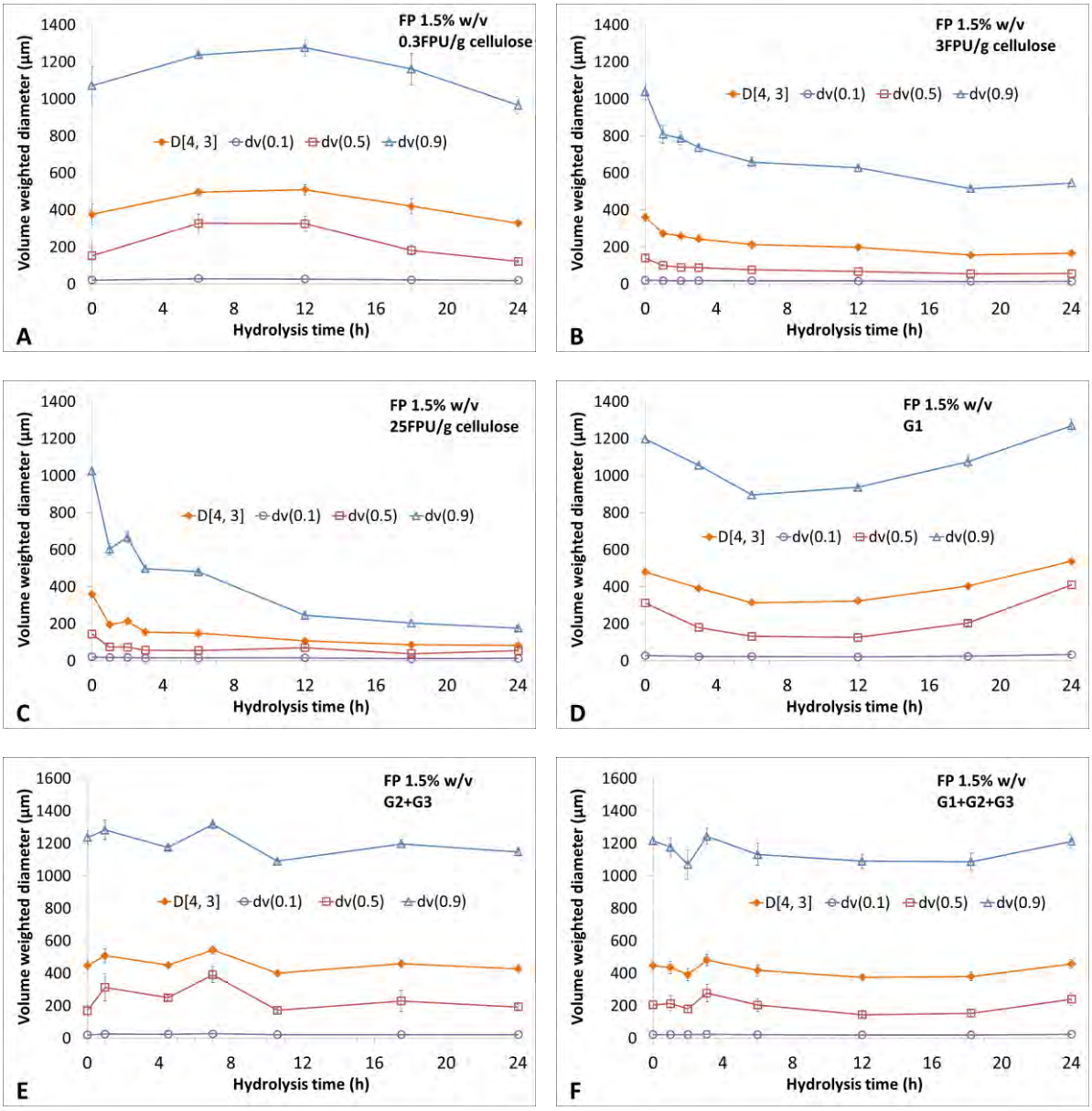

Figure 3-29. Volume weighted diameter during hydrolysis of FP suspensions at different enzyme loadings from pure to cocktail activities.

At 3 FPU/g cellulose (**Figure 3-28B** and **Figure 3-29B**), similar trends as 25 FPU/g cellulose are stated with slower kinetics. Between 0 h and 3h, 38.2 % viscosity reduction is observed corresponding to a 26.5 % decrease in coarse population (from 0.0053 to 0.0043 for $\Phi_{V-coarse}$) whereas a 12.5 % increase in fine population (from 0.0071 to 0.0079 for Φ_{V-fine}). The evolution of volume diameter indicated a noticeable decrease for D[4,3], $d_v(0.9)$ and $d_v(0.5)$ whereas $d_v(0.1)$ was almost unaffected by enzyme activities during this period. At 3 h, the conversion yield of cellulose into glucose remains inferior to 6 % meaning that none significant change in total particle fraction (from 0.0124 to 0.0116 for Φ_V) is observed. Beyond 3 h, the

reduction of coarse and fine populations is demonstrated in association with viscosity reduction up to 75.9 % at 24 h. Meantime, the glucose conversion yield evolves from 5 % (t = 3 h) up to 28.3 % (t = 24 h).

At 0.3 FPU/g cellulose, the time evolutions of parameters were very slow due to the low enzyme loading ratio. To simplify the illustration, **Figure 3-28A** compared the change in $E_v(d_{SE}) \cdot \Phi_v$ between t = 1 h and t = 24 h. **Figure 3-29A** illustrated the evolution of volume weighted diameter versus hydrolysis time. A similar trend of evolution as high enzyme loading was recognized at 0.3 FPU/g cellulose comparing initial and final momentums. A small but significant decrease in volume fraction was observed for the coarse population whereas negligible changes were reported for the fine population. Interpretation of volume diameter only presented the variations of initial value during 24 h hydrolysis without any clear change.

For three experiments with pure and mixed activities G1, G2+G3, G1+G2+G3 at dose equivalent to 0.3 FPU/g cellulose of Ctec2, no significant changes were reported through analysis of $E_v(d_{SE}) \cdot \Phi_v$ (**Figure 3-28D, E, F**) and volume diameters D[4,3], $d_v(0.9)$, $d_v(0.5)$, $d_v(0.1)$ (**Figure 3-29D, E, F**). It is possible that the effect of pure enzyme on FP suspension was too weak to be detected by DLS instrument. Conclusion about pure activities is postponed for the moment and more experiment at higher dose of activities is required for a reliable assumption.

Szijártó, Siika-aho et al. (2011) reported the dominant role of purified endo-glucanase in the liquefaction of pretreated wheat straw slurries. This activity randomly breaks the high DP chains into shorter fragments and causes a quick decrease in suspension viscosity. In our conditions and assuming that initial hydrolysis step is controlled by endo-glucanase activity on coarse population, the evolution of viscosity and PSD weighted by particle volumetric fraction (Φ_V) appeared consistent with this assumption by increasing the number of ending chains. However, granulometry and biochemical mechanisms resulted from a complex balance between coarse and fine populations considering microscopic properties up to biochemical structure. Afterwards the action of exo-glucanase and β-glucosidase became more and more significant, led to an increase in glucose conversion yield and a decrease in the fraction of fine particles.

By hydrolyzing substrate at low enzyme/substrate loadings (0.3 and 3 FPU/g cellulose) the fraction of coarse particles (d_{SE} > 200 µm) was proven to act as the key contributor into viscosity change for FP suspensions. Meantime, fine particles population (d_{SE} < 200 µm) was demonstrated as weakly impacting the suspension viscosity. During enzymatic hydrolysis at diluted condition, the viscosity decreased significantly mainly due to reductions of particle size although morphological aspects could be considered. Working on pretreated spruce chips, Wiman et al. (Wiman, Palqvist et al. 2011) stated the changes in suspension viscosity during enzymatic hydrolysis due to both factors: fiber properties and water insoluble solid content. At higher solid loading condition, the role of biomass concentration may become more pronounced. This assumption will be discussed with the series of hydrolysis at concentrated condition.

3.2.3.1.2 Paper pulp suspension

For PP suspensions, the evolution of $E_v(d_{SE}) \cdot \Phi_v$ and volume weighted diameter d_v during enzymatic hydrolysis with different enzyme profile were presented in **Figure 3-30** and **Figure 3-31**. As represented in **Figure 3-5A**, the initial PSD of PP suspension exhibits a multi-modal and large spreading distribution of 31.9 % coarse (d_{SE} > 224 µm), 33.3 % of medium (224 µm > d_{SE} > 49 µm) and 34.9 % of fine (49 µm > d_{SE}) populations. Results from DLS analysis pointed out the fragmentation mechanism on coarse population at all tested dosage of Ctec2.

Interestingly at medium to high dosage of Ctec2, in parallel with the diminution of coarse population, it was observed that fine population was also significantly reduced. The transition into fine population by fragmentation mechanism cannot compensate the strong solubilization mechanism. This result seems to be in excellent agreement with biochemical analysis showing high bioconversion yields at these enzyme loading ratios. On the other hand, experimental data on pure and mixed activities showed almost no significant changes in PSD during 24 h hydrolysis

At 25 FPU/g cellulose (**Figure 3-30C**) and after 1 h, three phenomena were clearly observed: coarse population showed an important decrease in $E_v(d_{SE}) \cdot \Phi_v$, the peak of fine population was almost faded away while medium population conserved it initial distribution. These evolution correspond to a viscosity collapse by more than 90 % (**Figure 3-16C**) and a hydrolysis yield of 18.5 %. It assumed both fragmentation and solubilization mechanism from the very beginning of enzymatic hydrolysis. It is suggested that reduction in coarse population was responsible for the viscosity drop when evolution of fine population reflected the bioconversion rate. From 1h, the PSD of PP was turned into a bimodal distribution of coarse population d_{SE} > 224 µm and fine population 224 µm > d_{SE}. Both populations were continuously attacked up to 24 h of hydrolysis, ended with a disappearing of coarse population. However, as PP suspension was already liquefied, no significant evolution in viscosity was reported during this period. In contrast, glucose yield gradually increased reaching 81.8 % by 24 h. It was correlated to the decrease in total particle volume fraction comparing 1 h and 24 h.

Figure 3-31C presents the evolution of volume weighted diameter corresponding to < 10 %, < 50 %, < 90 % of population and the mean diameter D(4,3)during enzymatic hydrolysis of PP at 25 FPU/g cellulose Ctec2. Overall trends were in agreement with the evolution of $E_v(d_{SE}) \cdot \Phi_v$. From the beginning to 1h, a stabilization state was observed for all volume diameters. As previously discussed, evolution of $E_v(d_{SE}) \cdot \Phi_v$ pointed out a balance between two mechanisms: the fragmentation of coarse particles and the disappearing of fine particles. The compensation effect of these mechanisms was possible to explain the constant value of D[4,3], $d_v(0.5)$ and $d_v(0.9)$. Beyond 1 h, a decreasing trend was reported until the end of hydrolysis. As fragmentation mechanism lead to an increase in total particle and a decrease in particle size while solubilization mechanism affects these parameters oppositely, obtained results suggest equilibrium between two mechanisms at the early stage of hydrolysis. Then, as the enzymatic reaction progressed, the contribution of fragmentation mechanism seems to be more pronounced than the solubilization one. In this specific case, it is suggested that the fragmentation of coarse population (224 µm > d_{SE}) was required to reach some threshold for a total liquefaction of suspension (> 90 % reduction in viscosity). Consequently, further reduce of particle size will not significantly affects suspension viscosity.

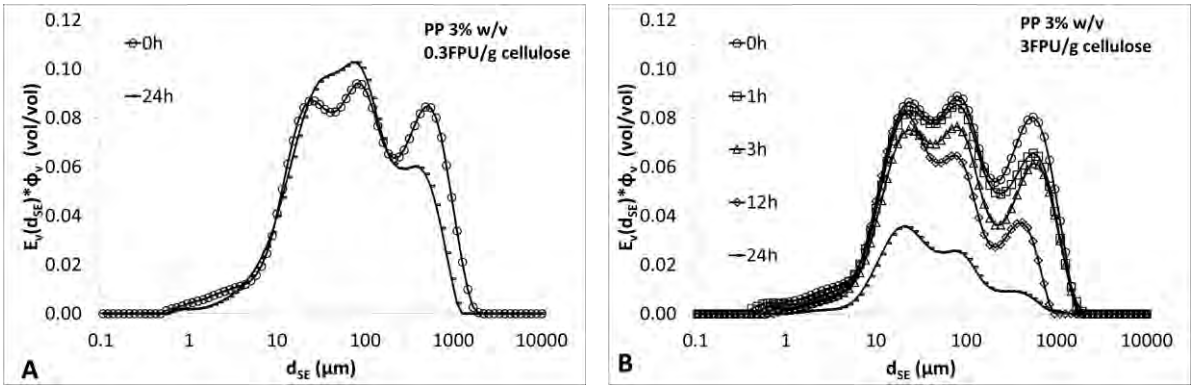

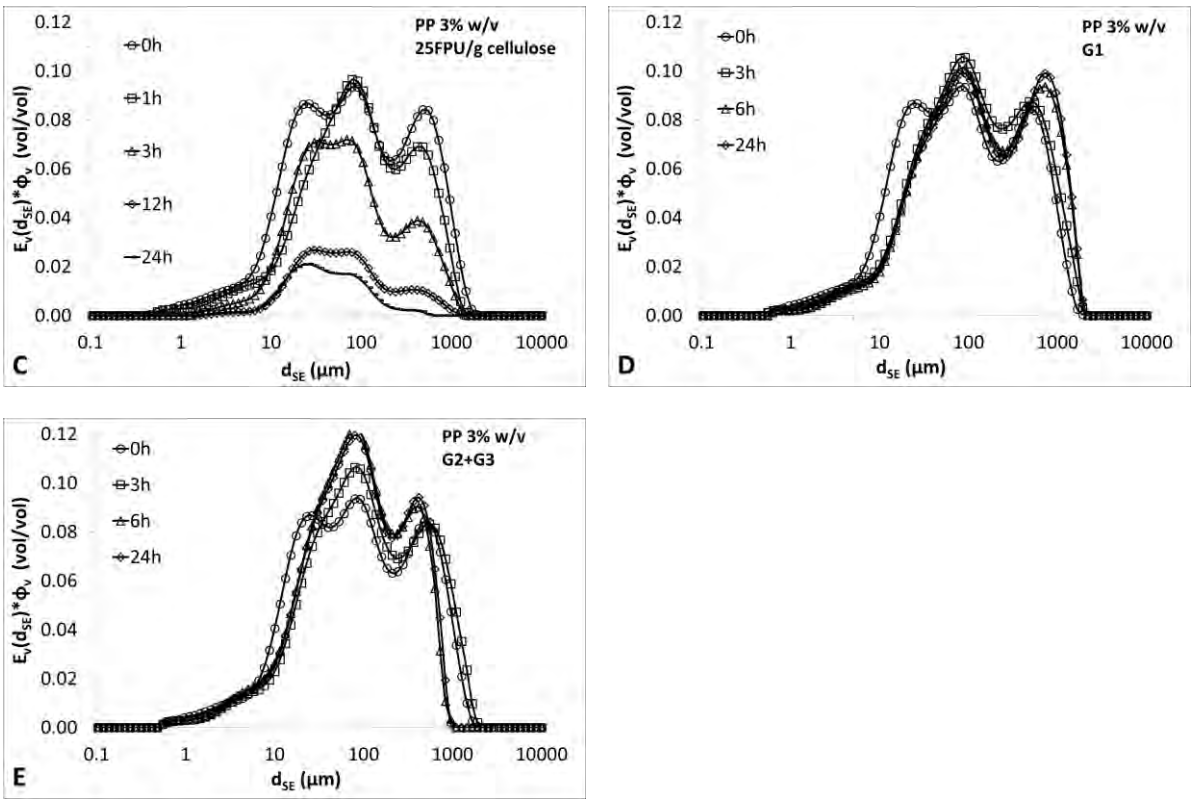

Figure 3-30. Particle size distribution weighted by particle volumetric fraction during hydrolysis of PP suspensions at different enzyme loadings of Ctec2.

At 3 FPU/g cellulose (**Figure 3-30B**), the evolution of $E_v(d_{SE}) \cdot \Phi_v$ for coarse population reported exactly the same trend as 25 FPU/g cellulose but at lower magnitude. The fragmentation was clearly observed after 1 h hydrolysis with a reduction in volume fraction of coarse population by 16.7 %. This reduction was followed until the end of hydrolysis, reached 99.2 % at 24 h. Crossing with rheological band biochemical analysis, the 16.7 % reduction in $E_v(d_{SE}) \cdot \Phi_v$ at 1h corresponded to 44.1 % decrease in suspension viscosity and 7.2 % total hydrolysis yield (glucose + xylose). By contrast, fine population showed nearly no change during the first 1h then followed by a rapid and steady decrease until 24 h. **Figure 3-31B** illustrated the evolution in volume diameter for 3 FPU/g cellulose on PP. Generally, the tendency of $d_v(0.5)$, $d_v(0.9)$ and mean diameter D(4,3) can be roughly divided into three stages: i) a stabilization state between 0h and 3h, ii) a rapid reduction from 3 h to 6 h and iii) an almost slow decreasing rate beyond 6 h. It can be assumed by the same explication as 25 FPU/g cellulose: a balance between fragmentation and solubilization mechanism for the first 3 h of hydrolysis before fragmentation became predominant, affecting particle diameter.

At 0.3 FPU/g cellulose, the evolution of particle parameters was slow and less significant. For $E_v(d_{SE}) \cdot \Phi_v$, **Figure 3-30A** compares the change between initial (t = 0 h) and final state (t = 24 h), revealed a decrease in the fraction of coarse population by 38.3 % that corresponded to a reduction in suspension viscosity by 67.6 %. The fraction of coarse always stands at predominant role for liquefaction efficiency through enzymatic hydrolysis at various E/S ratios (25, 3 and now 0.3 FPU/g cellulose). Fortunately at this lowest enzyme dose, a phenomenon which has been unobservable at higher enzyme dose was now revealed. In parallel with the decrease in coarse, an increase in the fraction of fine by nearly 4 % was reported at 24 h. It may assumed to the fact that total hydrolysis yield (glucose + xylose yields) at the end of hydrolysis was only 10.2 %, reflecting a weak solubilization mechanism. Meantime, analysis of volume

diameter (**Figure 3-31A**) showed almost constant values except for $d_v(0.9)$ which seems to decreased between 1 h and 2 h then fluctuated until 24 h.

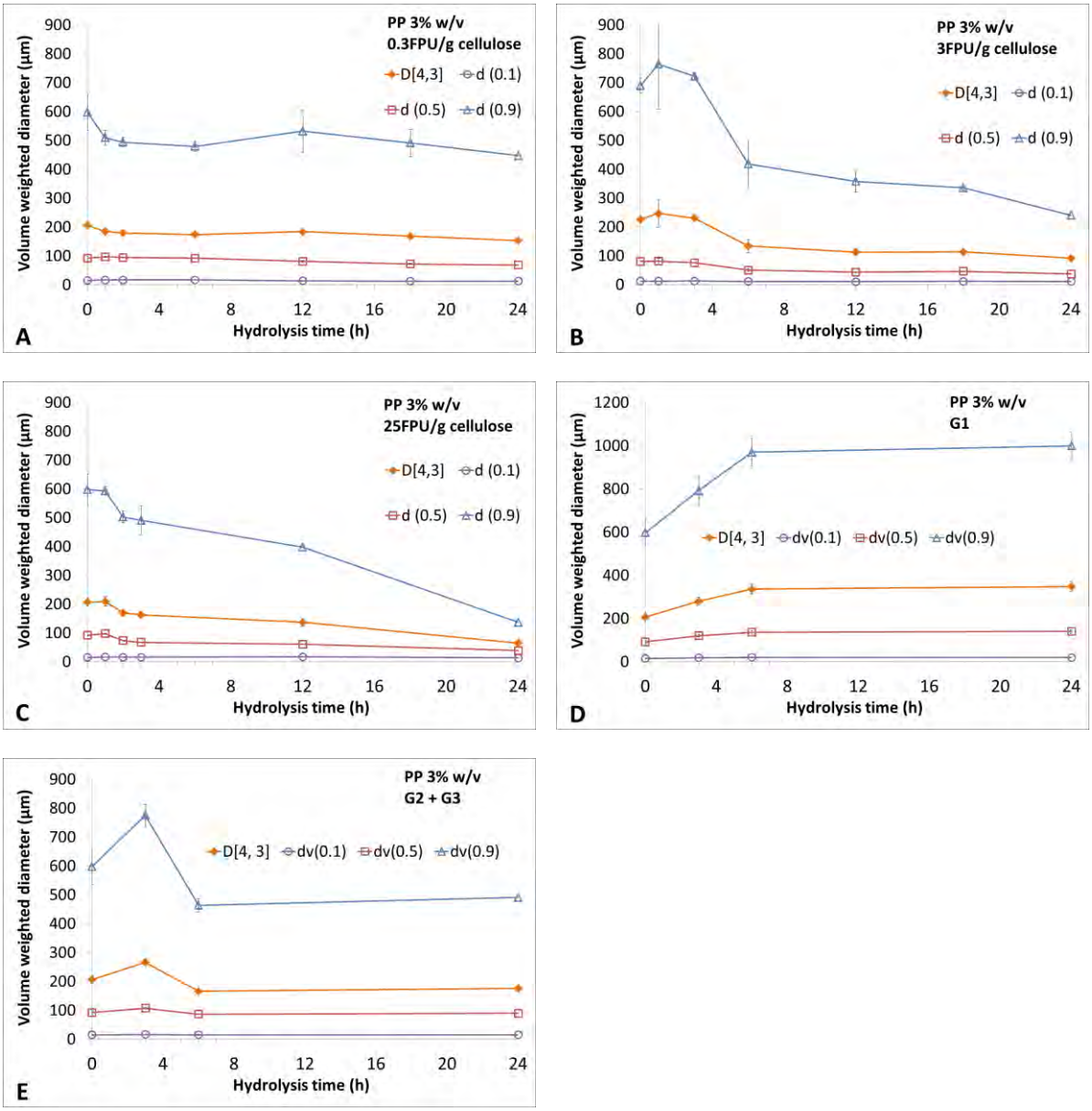

Figure 3-31. Volume weighted diameter during hydrolysis of PP suspensions at different enzyme loadings.

For three experiments with pure and mixed activities G1, G2+G3, G1+G2+G3 at dose equivalent to 0.3 FPU/g cellulose of Ctec2, almost no significant changes were detected through analysis of $E_v(d_{SE}) \cdot \Phi_v$ (**Figure 3-30D, E, F**) and volume diameters D[4,3], $d_v(0.9)$, $d_v(0.5)$, $d_v(0.1)$ (**Figure 3-31D, E, F**). It is important to remind that previously for FP suspension (**§3.2.3.1.1** - p**124**), the hydrolysis under pure and mixed activities also resulted in almost no changes following DLS analysis even at high liquefaction rate. In macro scale, the action of G1 in single or in mixture with G2+G3 was proven to decrease suspension viscosity for both FP 1.5 %w/v and PP 3 %w/v **Figure 3-17A, C**. Unfortunately, these phenomena cannot be characterized under the light of DLS measurement. We supposed that the fragmentation of coarse population always exist during enzymatic reaction as it contributed to reduce the suspension viscosity. However, the changes in particle size were not enough strong to be quantified through DLS measurement. It remains as a scientific question for further researches.

3.2.3.1.3 Sugarcane bagasse suspension

For SCB, the initial population presents a mono-modal distribution of finer size with small spreading compared with FP and PP (**Figure 3-5A**). Considering the curves of **Figure 3-32**,, the evolution of $E_v(d_{SE}) \cdot \Phi_V$ during enzymatic hydrolysis is less pronounced than for others two substrates, but a slight change in particle size was observed despite a reduction of Φ_V. Volume diameters during 24 h hydrolysis at 3 FPU/g cellulose were illustrated in **Figure 3-33**.

At 3 FPU/g cellulose, a slight increase in size in $E_v(d_{SE}) \cdot \Phi_V$ was observed at 1 h and 3 h although the distribution function was weighted by the volume fraction (**Figure 3-32B)**. Corresponding to this shift into larger population, the D[4,3], $d_v(0.9)$ and $d_v(0.5)$ exhibited a rising tendency between 0h and 3h, indicating a rise in average size of particle by volume weighted, mainly due to the change in the fraction of coarse. These evolutions just followed the overtaking in suspension viscosity that previously reported (**Figure 3-16B**). From this point, the evolution of $E_v(d_{SE}) \cdot \Phi_V$ indicated a reduction of particle volume fraction associated to a shift to lower size while particle diameters showed a fluctuation.

At 0.3 FPU/g cellulose, a slight increase in particle size was observed up to 3 h (**Figure 3-32A**). This distribution was nearly identical with those of 3 FPU/g cellulose at 1 h. Beyond 3h, roughly corresponding to the peak in suspension viscosity, the population was significantly more pronounced for coarse particle. For volume weighted diameters (**Figure 3-33A**), values of D[4,3], $d_v(0.9)$ and $d_v(0.5)$ were seems to exhibit a rising trend between 0 h and 3 h, then followed by an almost constant value which were superior than the initial ones. The viscosity overtaking is assumed to be related to particle size evolution. For aggregates corresponding to the biggest particles, the release of fibers from aggregates may contribute to a slight shift of PSD, with a moderate increase in particle number (discussed with CLD) and then an intensification of particle/particle interaction. It is noticeable that the volume fraction as calculated from initial concentration and hydrolysis yield (cf. **§3.2.1.1**) is different from the effective volume fraction of particles which determines the rheological behavior, especially considering the observed aggregates and fibers with SCB. The volume fractions based on dry matter content and effective object volume may exhibit opposite trends.

Moreover, the reason of $E_v(d_{SE}) \cdot \Phi_V$ evolution needs to be contorted and assumptions may be postulated. It is evident that cellulase enzymes are able to break down cellulosic fibers and to solubilize them in order to produce glucose. Basically, this reaction leads to a decrease in particle size. Referring to the granulometry and morphology of pretreated SCB; a considerable number of agglomerates are present. Once enzymes are added into substrate suspension, both agglomerates and individuals particles are attacked at the same time. Biocatalyst actions on agglomerates probably open the structure and extract/separate the fibers from the agglomerates. Then an increase in particle size distribution is realistic. In addition, it leads to a moderate increase in particle number, as well as particle surfaces, in other words, the average distance between particles is reduced and interactions increased. Consequently the interactions particle-to-particle is enhanced and the suspension viscosity rises up. In contrast, the attack of enzymes on individual particles results in a decrease in viscosity due to solubilization mechanism. In the first stage of hydrolysis, the effect on agglomerates is stronger than the solubilization of small individual particles, causing a growth in suspension viscosity. Considering the amount of enzyme/substrate loading, once the de-structuration of agglomerates reaches a threshold where all agglomerates are separated, the suspension viscosity will gradually decrease. An additional phenomenon to explain this overshot in viscosity is linked to particle shape. Giesekus 1983 (Giesekus 1983) studied the dependence of glass fiber suspension viscosity versus length/diameter (L/D) ratios. This research revealed that the relative viscosity rose as the proportion L/D increased or in other words, suspension of longer fibers will possess higher

viscosity than the shorter one. For sugarcane bagasse suspension, the dispersion of agglomerates into individual fibers can be considered as an evolution of particle morphology, from low to high L/D proportion. Thus, the overtaking in viscosity was in agreement with the shift in particle morphology.

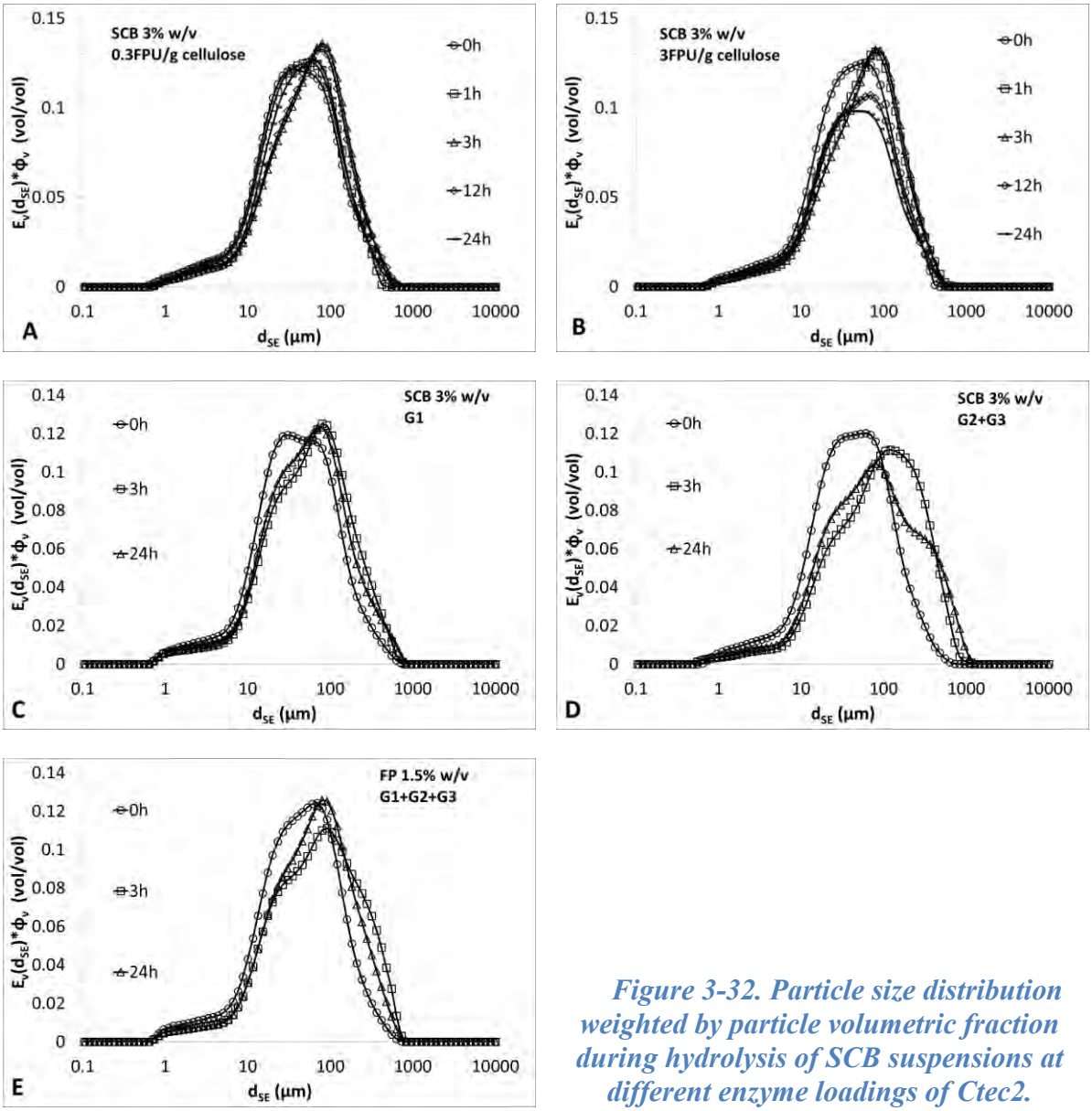

Figure 3-32. Particle size distribution weighted by particle volumetric fraction during hydrolysis of SCB suspensions at different enzyme loadings of Ctec2.

For experiments using pure to mixed activities G1, G2+G3, G1+G2+G3, the evolution in $E_v(d_{SE}) \cdot \Phi_V$ and volume weighted diameters D[4,3], $d_v(0.9)$, $d_v(0.5)$, $d_v(0.1)$ were illustrated by **Figure 3-32C, D, E** and **Figure 3-33C, D, E** respectively.

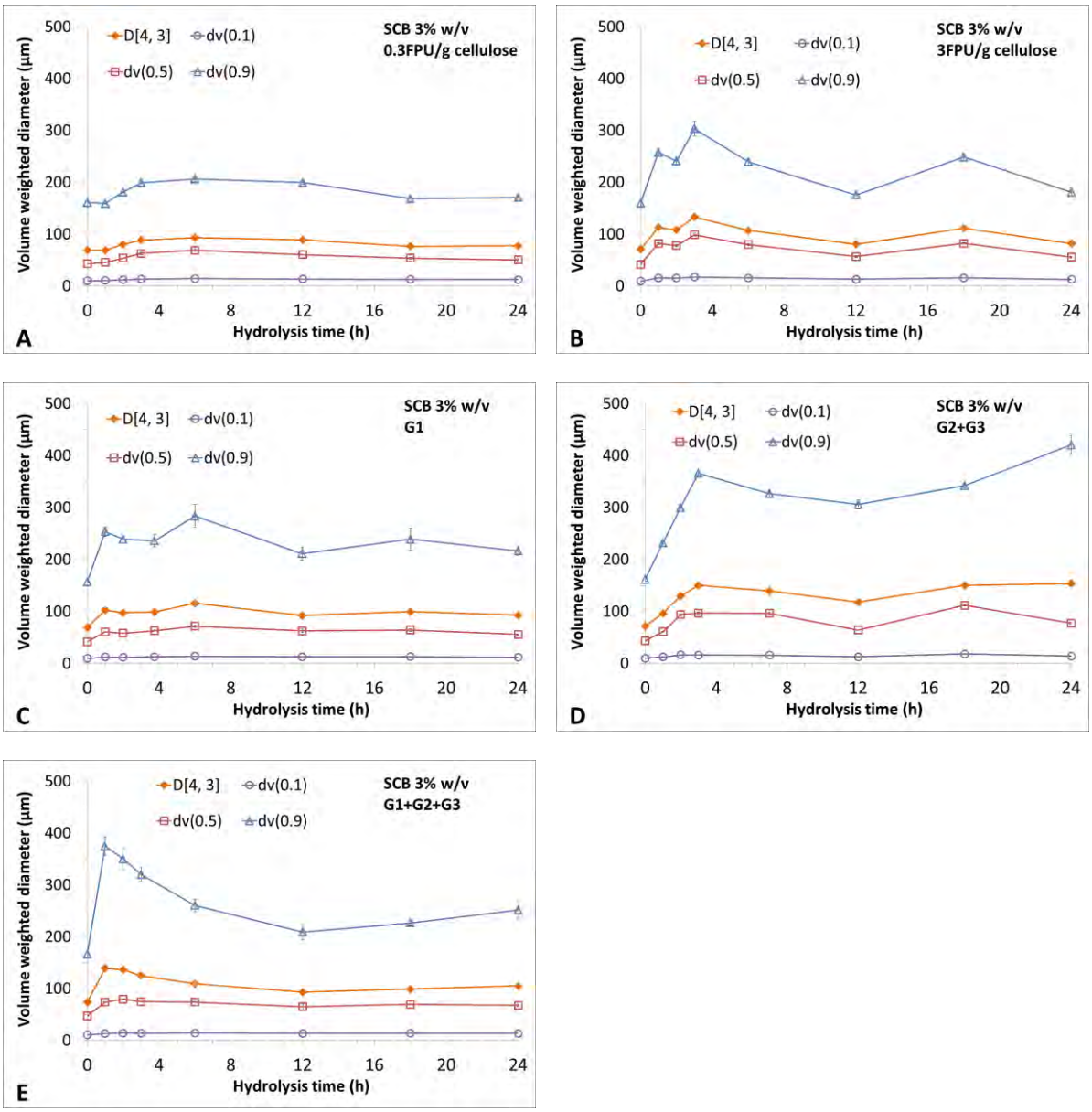

Figure 3-33. Volume weighted diameter during hydrolysis of SCB suspensions at different enzyme loadings.

Experiment using G2+G3 showed almost no significant evolution in $E_v(d_{SE}) \cdot \Phi_V$ during 24h hydrolysis. It is well correlated with biochemical and rheological analysis, reporting no solubilization neither fragmentation mechanisms. The gradual increase in suspension viscosity, which was super imposed with the reference experiment, is likely to link with a simple solvation effect.

As expected, for experiment using G1 alone or in mixture with G2+G3, a slight transition of population from fine to coarse was observed between 0h and 3h. Beyond this point, $E_v(d_{SE}) \cdot \Phi_V$ showed constant distribution. For particle volume diameter, all curves of G1 showed very similar trends; exhibiting a sudden jump in the first hours then followed by a fluctuation until the end of hydrolysis. For the mixture G1+G2+G3, same increasing tendency was witnessed for all curves, then a stable state for D[4,3], $d_v(0.5)$ and $d_v(0.1)$ whereas dv(0.9) tends to decrease between 1h and 12h. The increase in particle diameter in the first stage of hydrolysis for both experiment was in agreement with the evolution of $E_v(d_{SE}) \cdot \Phi_V$. These results sustain

the previous assumption to explain viscosity overtaking by separation mechanism of agglomerates into individual particle under enzymatic activities.

3.2.3.1.4 From DLS to in-situ viscometry

From in-situ viscometry, a reduction in suspension viscosity was quantified during enzymatic hydrolysis of FP and PP. The goal of PSD analysis was to reveal the mechanism of this phenomenon. The first hypothesis to explain viscosity reduction is assumed to a change in concentration regime from semi-dilute to dilute. As previously reported (**Figure 3-8** - p100), substrate concentration (proportional with substrate volume fraction) greatly affects suspension viscosity at semi-dilute and concentrated regime but showed minor impact at diluted regime. During enzymatic hydrolysis, the solubilization of substrate led to a decrease in total volume fraction or in other word substrate concentration. If the concentration drops below critical point, diluted regime is established and suspension viscosity will be nearly independent of substrate concentration. The point corresponding to more than 75 % reduction in viscosity were identified at lower than 14.8 % glucose conversion yield (see **§3.2.1.1** - p106). Clearly, biochemical results rejected this hypothesis.

The second hypothesis was built from DLS results on FP and PP suspensions, declaring the predominant role of the coarse population to suspension viscosity. To deeply investigate this assumption, **Figure 3-34** summarizes the relation between particle size distribution of coarse population ($\Phi^*_{v-coarse}$) and in-situ viscometry (μ*) for FP and PP at different enzyme loading ratios of Ctec2 from 0.3 to 25 FPU/g cellulose. $\Phi^*_{v-coarse}$ is considered as volume fraction of particle which has diameter of sphere equivalent, d_{SE} superior than 224 μm. The value of $\Phi^*_{v-coarse}$ at hydrolysis time t (h) was defined following **Eq. 3-18**, indicating the normalized evolution of the volume fraction of coarse population by time. It varies from 1 (initial state without any modification) to 0 (theoretical final state, totally fragmented to smaller size of d_{SE} < 224 μm) Dimensionless viscosity, μ* was previously defined (**Eq. 3-13** -, p121) translating the reduction of suspension viscosity compared to initial value and solvent (water) viscosity.

$$\Phi^*_{v-coarse} = \frac{\Phi_{v-coarse}(t)}{\Phi_{v-coarse}(t = 0h)} \qquad \textit{Eq. 3-18}$$

For both studied substrates, suspension viscosities showed a correlation with the fraction of coarse population. For FP (**Figure 3-34A**) and at three tested E/S ratios, μ* strongly decreased with the reduction of $\Phi^*_{v-coarse}$. At 3 and 25 FPU/g cellulose, suspension viscosity was strongly reduced as $\Phi^*_{v-coarse}$ decreased up to 40-45 % compared to initial state. Beyond this point, as the suspension was already liquefied, further reduction in $\Phi^*_{v-coarse}$ did not affects suspension viscosity. At lowest enzyme loading ratio, only 20 % reduction in $\Phi^*_{v-coarse}$ was required for an approximately 75 % drop in suspension viscosity. Higher liquefaction rate was not yet achieved due to the slow kinetic at low enzyme dosage and the limit in reaction time to only 24h.

For PP, the complexity of real lignocellulosic substrate might present an impact on reaction kinetic and mechanism. As observed on **Figure 3-34B** for experiments at lowest enzyme loading 0,3 FPU/g cellulose, the tendency of μ* can be roughly divided into two stages: i) an almost constant μ* for $\Phi^*_{v-coarse}$ between ≈ 0.9 and 1; ii) a rapid reduction in μ* for $\Phi^*_{v-coarse}$ below 0.9. At higher enzyme loading 3 FPU/g cellulose, the two stages kinetics was also observed through the point of $\Phi^*_{v-coarse}$ slightly superior than 0.8. It is important to note that, this point was corresponded to the first sampling at 1h of hydrolysis. The initial stage might be shorter due to the increase in enzyme dosage from 0.3 to 3 FPU/g cellulose. At highest enzyme loading ratio (25 FPU/g cellulose), suspension viscosity dropped instantaneously from the first sampling point as $\Phi^*_{v-coarse}$ decreased. The two-stages kinetic were unobservable.

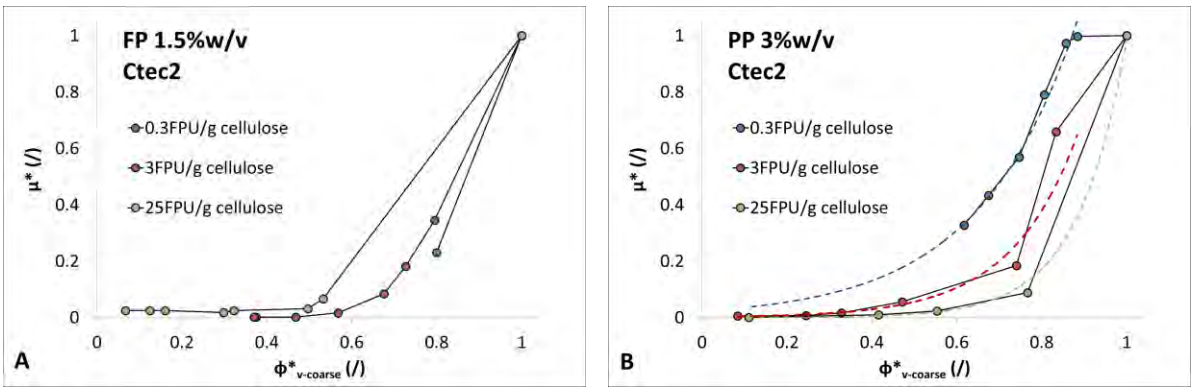

Figure 3-34. Relation between viscosity reduction (μ*) and size reduction of coarse population (224 μm < d_{SE}) for FP (A) and PP (B) at different dose of Ctec2 ranging from 0.3 to 25 FPU/g cellulose

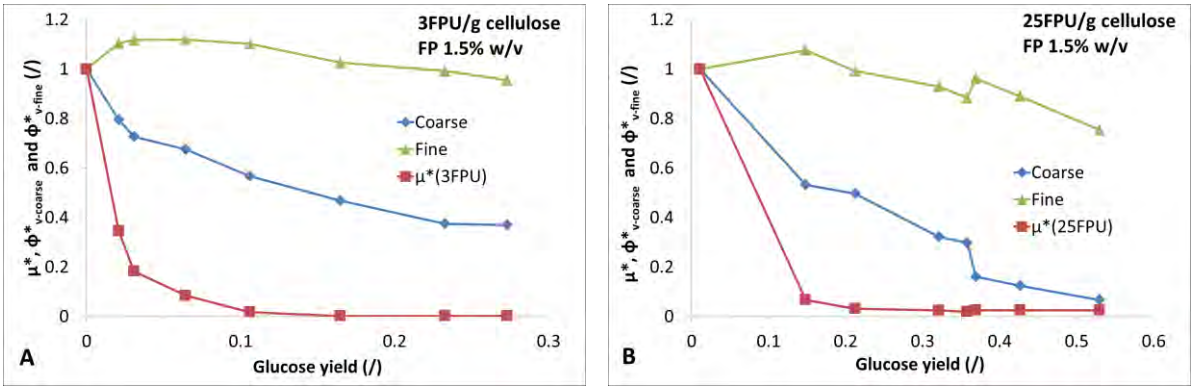

Figure 3-35. Evolution of suspension viscosity and particle populations during enzymatic hydrolysis of FP 1.5 % w/v at 3 (A) and 25 (B) FPU/g cellulose.

As fragmentation mechanism has been well described through investigation of coarse population, the evolution of fine population was expected as indicator of solubilization mechanism. However, this evolution might be oppositely affected by two factors: and increasing trend by fragmentation of coarse and a decreasing trend by direct solubilization of fine. The observation of fine population indicated the equilibrium state between two mechanisms, rather than described the solubilization one. **Figure 3-35** illustrated this equilibrium for FP at two enzyme loading ratios of Ctec2 at 3 and 25 FPU/g cellulose. For glucose yield, the range from 0 to 1 corresponded to 0 % to 100 % bioconversion rate. For both experiments, the enzymatic reaction started at point 0 % glucose yield, 100 % viscosity remaining and 100 % populations remaining. As the hydrolysis progressed, the fraction of fine population was affected by both fragmentation and solubilization mechanisms. In the first stage of hydrolysis, the drastic drop in suspension viscosities and the slow increase in glucose yield indicated stronger mechanism of fragmentation than solubilization. Consequently, Φ^*_{v-fine} increased. Beyond the critical point when suspensions were almost liquefied, the contribution of solubilization mechanism became more and more significant, compensating then overpassing the fragmentation. In this second stage of hydrolysis, fraction of fine population tends to decrease in correlation with the extension of hydrolysis yield. This phenomenon was exacerbated at higher enzyme loading ratio.

Similar equilibrium between fractions of coarse and fine population in relationship with fragmentation and solubilization was also reported for PP through different enzyme loading ratios of Ctec2 from 0.3 to 25 FPU/g cellulose (**Figure 3-35**). The term bioconversion yield

indicated sum of glucose yield and xylose yield. At 0.3 FPU/g cellulose and after 24h, PP suspension was partially liquefied; suspension viscosity reached approximately 30 % of the initial value. Meantime, fraction of coarse population decrease in correlation with the suspension viscosity, reflecting fragmentation mechanism at moderate level. In the other hand, the bioconversion yield of nearly 11 % indicated weak solubilization mechanism. The balance between two mechanism resulted in almost constant volume fraction of fine population (**Figure 3-35A**). By increasing the enzyme loading ratio to 3 and 25 FPU/g cellulose, both fractionation and solubilization presented stronger effect with more pronounced evolution in suspension viscosity, fraction of fine and fraction of coarse population. Even with a nearly total liquefaction level was reached, fractionation mechanism showed weaker effect on fraction of fine compared to solubilization one. This population was dropped significantly in correlation with bioconversion yield.

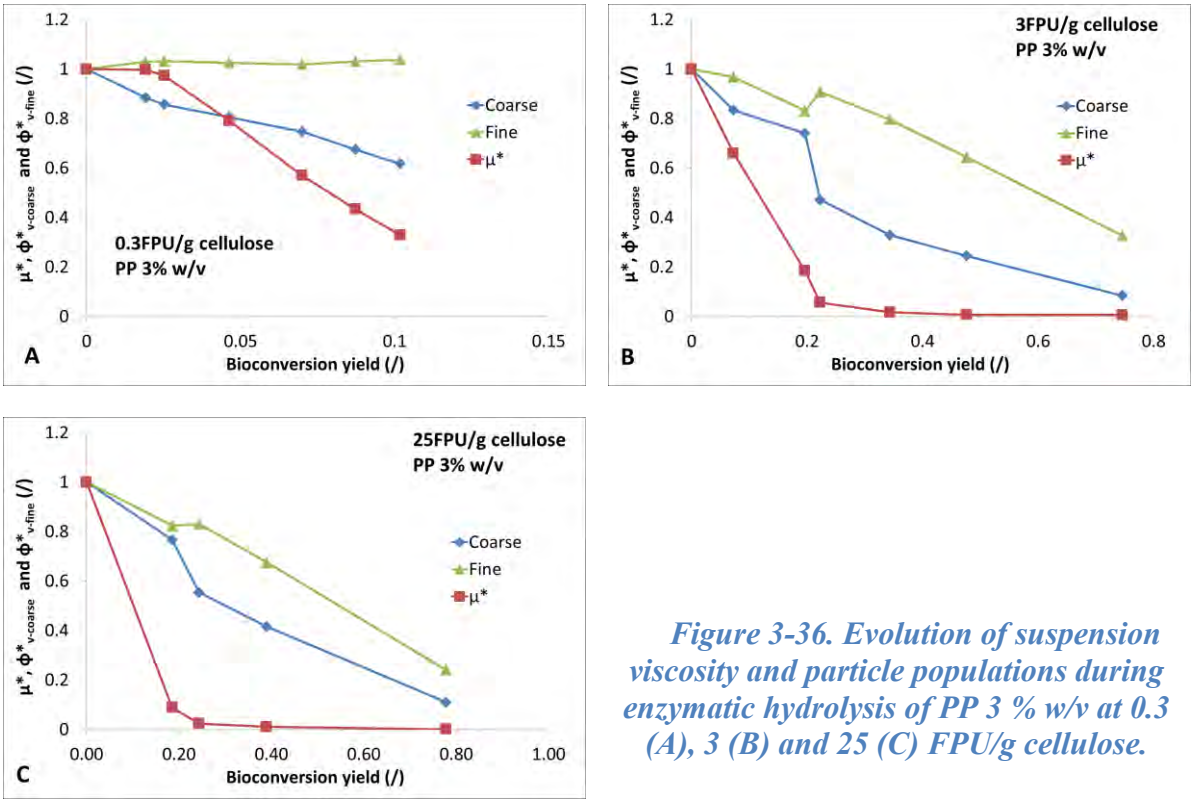

Figure 3-36. Evolution of suspension viscosity and particle populations during enzymatic hydrolysis of PP 3 % w/v at 0.3 (A), 3 (B) and 25 (C) FPU/g cellulose.

For SCB suspension, due to it complex rheological behavior during enzymatic hydrolysis, similar interpretation was postponed for the moment. We aimed first to explain the overtaking in suspension viscosity observed on SCB suspension at low enzyme loading. Then further work is required for more exploration on SCB.

3.2.3.2 Focused beam reflectance

Considering the evolution of fine particles, the in-situ CLD measurements were performed and the normalized quantities defined as the ratio to their initial values. The evolutions of normalized total chord count, N_c^* and normalized mean chord length, l_c^* are reported with FP, PP and SCB for all enzyme/substrate loadings. During enzymatic reaction at given mixing rate, fragmentation and solubilization of particle are two main mechanisms that affect the number of chord counted by FBRM probe. In addition, the reduction of suspension viscosity at certain experiments leads to a change of flow regime (from laminar to transitory and turbulent) which might influence measurement result. Through the literature, there was no publication reporting the role of flow regime on focused beam reflectance measurement. In present work, data

treatment and interpretation were considered under strong assumption that the effect of flow regime on FBRM may not exist or can be negligible.

3.2.3.2.1 Evolution of Nc and lc*.*

For FP, both N_c^* (**Figure 3-37A**) and l_c^* (**Figure 3-38A**) indicated a growing trends whereas reference (none activity) remains almost constant (deviation < 5 %). Small peaks are explained by the mixing rate changes from 100 to 125 rpm every 30 minutes. During 24 h of hydrolysis, a gradual increase in both N_c^* and l_c^* were observed at 0.3 FPU/g cellulose. For the experiment at 3 FPU/g cellulose, there was a quick increasing of N_c^* and mean l_c^* in the first 8 h, following by a stabilization state until the end. At highest enzyme loading, N_c^* and l_c^* witnessed similar growing trend in the first 7 h then exhibited different evolutions. When N_c^* tend to stabilized then fairly decreased at the end of hydrolysis, l_c^* showed a significant decrease from 7 h to 24 h. Considering DLS volume weighted distribution (**Figure 3-5A**), initial FP suspension represents 45.4 % of coarse and 54.6 % of fine particles. Few large fibers are possibly accounting for a considerable volume fraction equivalent to huge number of fine particles. For number weighted distribution obtained by FBRM analysis, the fraction of large size particles is almost invisible whereas is the finest are well described. During enzymatic attack, the fragmentations of large size particles generate a significant growth in number of medium size particles. Meantime, the finest insoluble particles in suspension are solubilized which leads to an increase in l_c^*.

For SCB, N_c^* (**Figure 3-37B** and) and l_c^* (**Figure 3-38B**) exhibit most of the time opposite trends. For reference (none activity), the normalized total chord number shows an increase while mean chord length exhibits a decrease after 24 h. With a constant substrate concentration, the kinetics of agglomerate separation by mechanical agitation will be slow and may justify this phenomenon. At 0.3 FPU/g cellulose, the N_c^* curves overlaps the reference curve. Meantime, l_c^* gradually rises up to 5 % in comparison with the initial value at 24 h. For 3 FPU/g cellulose, both N_c^* and l_c^* curves superpose the reference curves. By increasing enzyme dosage to 10 FPU/g cellulose, a slow rising step of N_c^* was witnessed at 10 h, follows by a moderate decrease until 24 h. In addition, l_c^* curve exhibits a drastic fall from the beginning until the end of hydrolysis. Biochemical analysis (**Figure 3-10**) confirms the existence of a solubilization mechanism at enzyme loading from 3 FPU/g cellulose. It is suggested that there is a balance between four mechanisms: agglomerate separation, fiber fragmentation hydratation and solubilization. At 0.3 FPU/g cellulose, with only 3.1 % glucose yield at 24 h, the effect of solubilization is almost negligible and the fragmentation is not enough to reduce particle size. A swelling effect of substrate by hydratation may be responsible for the slight increase in l_c^*. At higher enzyme loading, the separation of agglomerates and the fragmentation of coarse fibers may explain the rise in chord number as well as the fall in mean chord length in the first stage. Then depending on enzyme dosage, a solubilization mechanism becomes significant and predominant (illustrated by increase in glucose yield), both N_c^* and l_c^* exhibit decreasing trends. The relationship between four mechanisms: separation of agglomerates, fragmentation of coarse fibers, hydratation and solubilization of fine is well established and consistent with enzyme/substrate ratio.

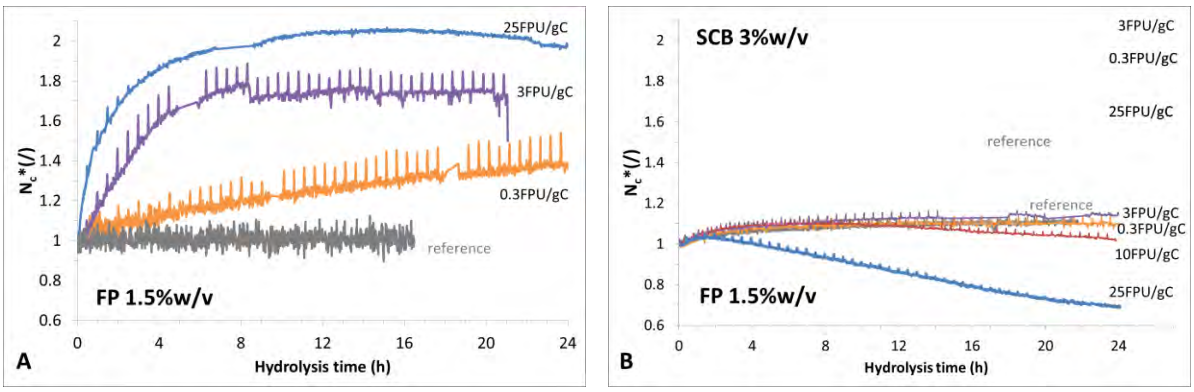

Figure 3-37. Evolution in Nc during enzymatic hydrolysis of FP 1.5 %w/v (A) and SCB 3 %w/v (B) for enzyme/substrate loading ranging from 0.3 up to 25 FPU/g cellulose.*

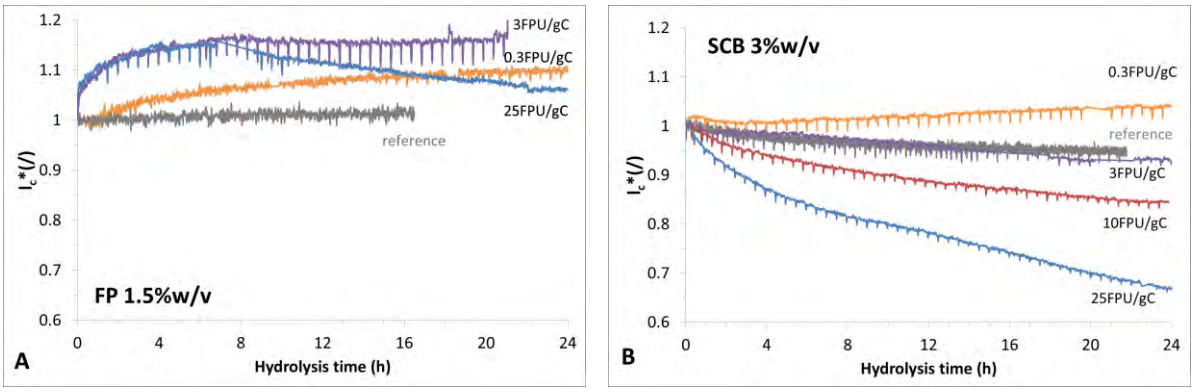

Figure 3-38. Evolution in lc during enzymatic hydrolysis of FP 1.5 %w/v (A) and SCB 3 %w/v (B) for enzyme/substrate loading ranging from 0.3 to 25 FPU/g cellulose.*

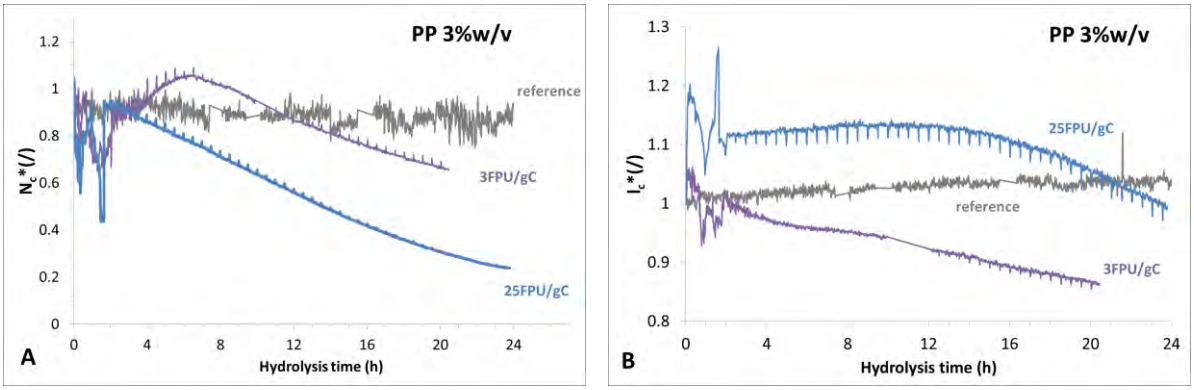

Figure 3-39. Evolution in Nc (A) and lc* (B) during enzymatic hydrolysis of PP 3 %w/v using Ctec2.*

For PP suspension, FBRM encountered several difficulties due to the complexity of substrate. **Figure 3-40** illustrated the N_c^* and l_c^* curves for Ctec2 at enzyme loading 3 and 25 FPU/g cellulose. As observed, FBRM signals were strongly disrupted in the first 2-3h of hydrolysis. This perturbation is explained by the original structure of PP suspension that contains large amount of long ramified fibers. Under mechanical agitation, these fibers were agglomerated and trapped in the strait void between reactor's wall and probes (FBRM, pH, T).

This phenomenon led to a local non-homogeneous state in the measurement zone of FBRM probes and the signal was perturbed.

Fortunately as the enzymatic hydrolysis progressed, coarse fibers were fragmented into shorter one, agglomerates were separated and suspension became fully homogenous with stable flow. For experiment at 3 and 25 FPU/g cellulose, measurement signal from 3 h were proper and may be exploited under restriction. At 25 FPU/g cellulose, it indicated decreasing trend in N_c^* between 3 h and 24 h that corresponded to stronger solubilization than fragmentation mechanism. Rheological analysis (**Figure 3-16C**) reported a constant viscosity near water during this period and biochemical analysis (**Figure 3-11**) showed an increasing bioconversion rate from 54.8 % to 84.9 %. FBRM analysis was in good agreement with rheological and biochemical analysis. For experiment at 3 FPU/g cellulose, an increasing trend up to 8 h in N_c^* was in correlation with the liquefaction period between 0 h and 8 h illustrated in **Figure 3-16C**. Beyond this point, when PP suspension was already liquefied, fragmentation mechanism showed attenuate contribution to N_c when solubilization mechanism became more and more dominant, reducing the N_c^*. In the other hand, the evolution in l_c^* (**Figure 3-40**) reflected exactly the equilibrium between two mechanisms. A constant state of l_c^* was correlated with a balance between fragmentation and solubilization while its decreasing trend translated a stronger effect for solubilization.

The reference experiment without enzyme activities (**Figure 3-40**) was carried out by pre-shearing PP suspension under "free condition" without any probes (pH, T, FBRM) at 40 °C, 100 rpm for 12 h. Subsequently, FBRM probe was carefully added to perform measurement. This experiment provided information about initial chord number and initial mean chord length of PP suspension.

3.2.3.2.2 Evolution in number weighted distribution of chord count.

For a better understanding of the enzymatic attack on finest population, the distribution of non-normalized N_c are reported in for FP (1.5 %w/v) and for SCB (3 %w/v).

For FP (**Figure 3-40**), a significant evolution in particle number is observed for both enzyme loadings. It mainly occurs in the chord length range between 10 µm and 100 µm. At 3 FPU/g cellulose, the reaction slowly starts in the first 1h, and then quickly increases up to 12 h. Focusing on the fraction of 10 µm < l_c < 100 µm, an increase in 7.9 % and 71 % in total count number compared to the initial value is reported at 1h and 12h respectively. At 24h, a slight decrease in chord population is identified. At 25 FPU/g cellulose, the evolution was accentuated, the increase in 48.3 % in chord number was clearly observed after 1h for the fraction of 10 µm < l_c < 100 µm. At 12 h, this fraction shows a sharp increase in 110 % compared to the initial value. Beyond, trends are similar to 3 FPU/g cellulose.

For SCB (**Figure 3-41**), the fraction of chord length ranging from 10 µm to 100 µm was scrutinized in order to be compared with FP. The phenomenon strongly differed with almost none evolution at 3 and 10 FPU/g cellulose. At the highest loading ratio (25 FPU/g cellulose), distribution curves exhibited a sharp evolution. From 0h to 3h, none significant variation was quantified. Nevertheless, a decrease in 30.4 % and 64.2 % were witnessed after 12 h and 24 h respectively. Below 8 µm (corresponding to the finest particle), a constant shoulder was identified.

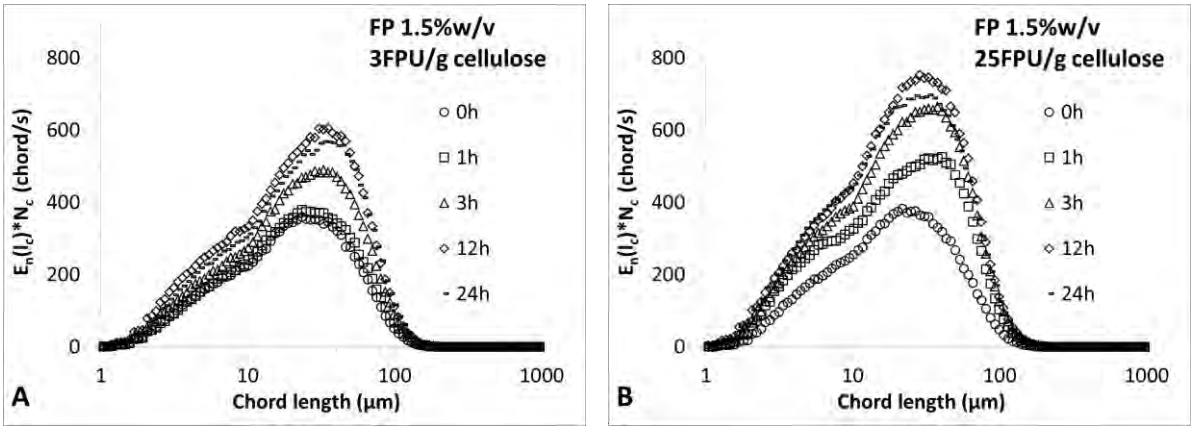

Figure 3-40. Evolution of number weighted chord count distribution (FP suspension, 1.5 %w/v) during hydrolysis with Ctec2 at E/S equal to 3 (A) and 25 (B) FPU/g cellulose

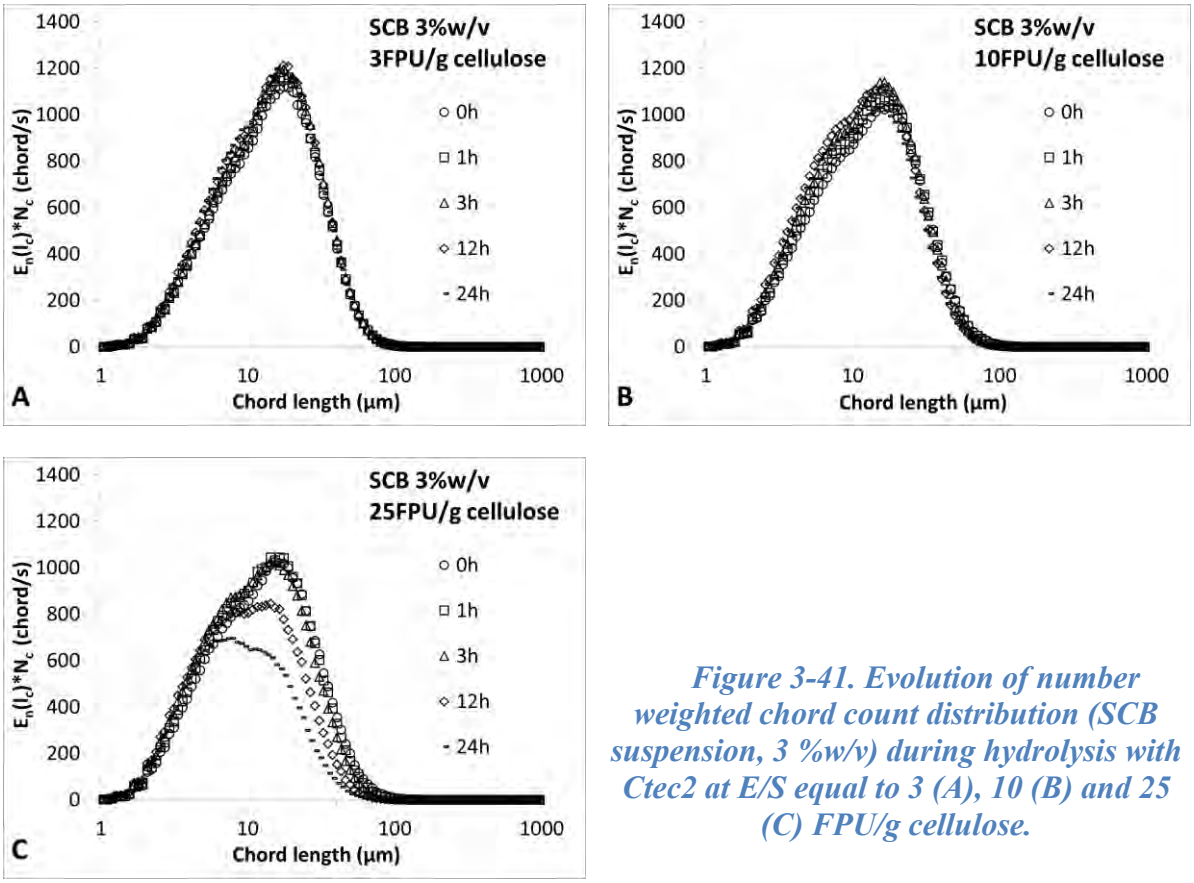

Figure 3-41. Evolution of number weighted chord count distribution (SCB suspension, 3 %w/v) during hydrolysis with Ctec2 at E/S equal to 3 (A), 10 (B) and 25 (C) FPU/g cellulose.

For PP, **Figure 3-42** illustrated the evolution in number distribution of chord count at 3 and 25 FPU/g cellulose. For both graphs, the curves corresponding to t = 0h were adapted from reference experiment due to perturbation of signal in the beginning of hydrolysis at 3 and 25 FPU/g cellulose. Clearly, both experiment showed similar decreasing trends between 0h and 24 h. Focusing on the fraction of 10 µm < l_c < 100 µm, a reduction of 55.2 % and 36.6 % in chord count were reported after 12h for 3 and 25 FPU/g cellulose respectively. The stronger reduction rate for lower enzyme loading can be explained by several assumptions. At higher enzyme loading, the liquefaction rate was almost 4.7 fold quicker than for 3 FPU/g cellulose (**Figure 3-25**), it is possible that particles in suspension were strongly fragmented and their sizes were reduced to under 10 µm. Beyond 12 h, the reduction trends were continued for both enzyme

loading, reached finally 63 % and 78.2 % for 3 and 25 FPU/g cellulose respectively considering the fraction of 10 µm < l_c < 100 µm. These evolutions were well correlated with the bioconversion yields, which were 74.6 and 84.9 % for 3 and 25 FPU/g cellulose, respectively.

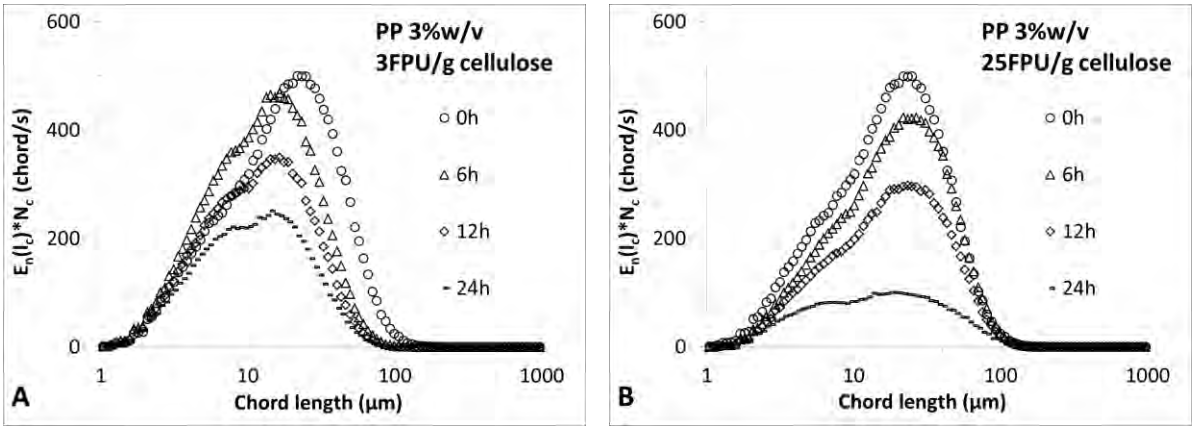

Figure 3-42. Evolution of number weighted chord count distribution (PP suspension, 3 %w/v) during hydrolysis with Ctec2 at E/S equal to 3 (A) and 25 (B) FPU/g cellulose.

With three substrates, the evolution in chord population is linked to the balance and the relative magnitude of two mechanisms: (i) the fragmentation of coarse particles into smaller insoluble particles that cause a rise in total number of chord and (ii) the solubilization of fine particles that leads to a drop in total chord population. The different phenomenon observed between FP, PP and SCB are consistent with their initial morpho-granulometric properties. Biochemical results (see **§3.2.1.1** - p106) confirmed the presence of a solubilization mechanism and sustained the fragmentation mechanism illustrated by PSD and CLD.

At 3 and 25 FPU/g cellulose, the equilibrium between fragmentation and solubilization mechanisms can be roughly divided into two stages: i) the predominant role of fragmentation by endo-glucanse activity when enzymatic reaction stated led to an decrease in viscosity and reduction of coarse population, ii) the balance between two mechanism when suspension was liquefied then solubilization showed more pronounced effect, strongly decreasing fine population as well as raise bioconversion yield. This two stages mechanism is well correlated with substrate properties when both FP and PP contain considerable amount of coarse fibers and broad size spreading. The first stage is then important to reduce particle size alleviating the efficiency of the second stage where particle of smaller size are attacked by endo-glucanase and β-glucosidase. This assumption is in agreement with biochemical knowledge, reporting that the action of endo-glucanse on cellulosic fiber induces better exo-glucanase catalyst by increasing the number of ending chain. It explains why for SCB suspension accounting a narrower size spreading (96 % of fine particle are inferior to 200 µm), two mechanism fragmentation - solubilization appear to be balanced at 3 FPU/g cellulose from the beginning of reaction. When the enzyme loading is increased up to 25 FPU/g cellulose, this equilibrium was maintained during the first 3h, and then solubilization becomes the dominant mechanism.

Firstly, the obtained results suggest that the smallest particles are more accessible to enzymatic hydrolysis. From **§3.2.2.5** - p122, through biochemical and rheological analysis, we suggested that high activity of endo-glucanase is recommended for a rapid and efficient liquefaction. Under the light of particle size analysis or precisely FBRM, this assumption was explained by a two stages machanism from fragmentation to solubilization. It seems that this mechanism is correlated for suspension containing a considerable fraction of coarse population like FP and PP. For substrate that undergo strong pretreatment procedure like SCB, particles size were anteriorly reduced leading to drastic reduction in suspension viscosity at same

substrate loading. The role of the first stage will be relieved because; fragmentation was fully or partially done by pretreatment. Secondly, obtained result insists the role of pretreatment step which create favorite conditions for enzymatic hydrolysis.

3.2.3.3 Optical morpho-granulometry (MG)

In order to provide an additional discussion element, the morphological characterization of particle in suspension was carried out following the protocol described in **§2.4.4.4** - p83. Analysis instrument, Morphologi G3S is a powerful system that allows the observation and characterization of particle size and shape through several morphological parameters. The analysis of lignocellulosic suspension presents a difficulty related to the sample preparation step. For FP and PP suspension, there are a considerable number of long and ramified coarse fibers. In number weighted, these fibers may be negligible whereas considering surface weighted, few coarse fibers may account for large surface. The present of only few fibers during sampling may lead to significant change in final result. SCB suspension which contain narrower size spreading and monomodal distribution appeared as the most suitable substrate for MG analysis. This assumption was well illustrated in **Figure 3-43** where the reproducibility for SCB suspension (from 4 different experiments) was significant better than for FP suspension (from 6 experiments). For PP, due to the complexity of substrate with multimodal size distribution, the MG analysis showed non reliable results. Data from morpho-granulometry analysis will be discussed for only FP and SCB in order to illustrate qualitatively the evolution of particle shape and size and to verify the coherence with established assumption from previous analysis (biochemistry, rheology, DLS, FBRM). The number weighted distribution of aspect ratio (AR) and diameter of circle equivalent (d_{CE}) will be used as indicators for particle shape and size.

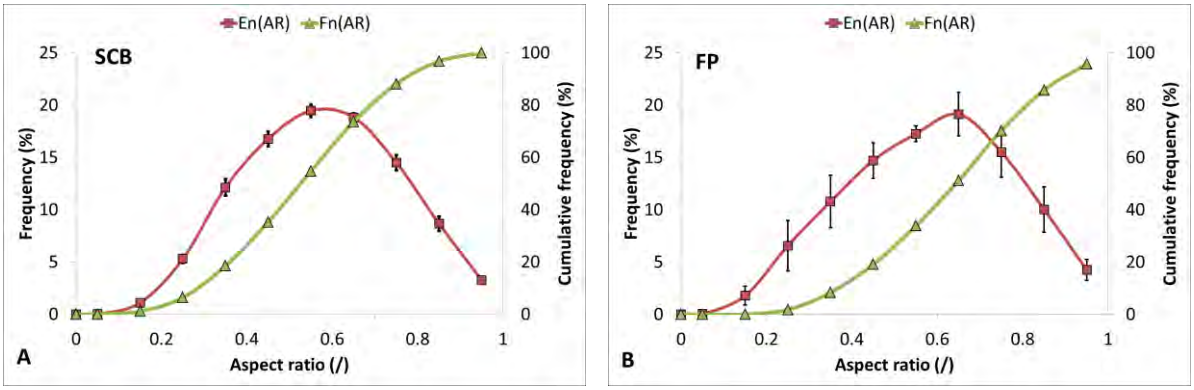

Figure 3-43. Number distribution of aspec ratio (AR) for initial suspension of SCB (A) and FP (B). Error bar shows the average deviation of 4 experiments for SCB and 6 experiments for FP.

Figure 3-43 presents the aspect ratio profiles of SCB and PP suspension at their initial state. The statistical analysis of observed particles was performed under 10 class of aspect ratio from 0 to 1 with linear size band distribution. For SCB suspension, the peak in aspect ratio was located in the range between 0.5 and 0.7 while for FP, aspect ratio was slightly higher. It indicated that FP suspension contains more fibrous particles than SCB suspension.

During enzymatic hydrolysis, particles were attacked and their shape can be changed. **Figure 3-44** presents the evolution in E_n(AR) of FP at enzyme loading 3 and 25 FPU/g cellulose Ctec2. Generally, similar trends were observed with a decrease in number of low aspect ratio (fiber like) up to 12 h, followed by an opposite trend beyond this point. The magnitude of variation was in correlation with enzyme loading ratios. From biochemical, rheological and PSD analysis, the two-stage hydrolysis mechanisms was proposed (see **§3.2.3.1.4** - p134). Results from MG analysis added a description for this assumption. Without considering the fraction of

extreme large fiber that is invisible under number weighted analysis, it seems that the hydrolysis reaction of FP suspension always started by fragmentation of fiber-like particle. Theoretically, the broken of fiber-like particle into shorter one is corresponded to a decrease in suspension viscosity (Giesekus 1983). The trend observed for $E_n(AR)$ was in agreement with the evolution in suspension viscosity previously reported in **Figure 3-16**. For SCB suspension (**Figure 3-44**), the number distribution of aspect ratio, $E_n(AR)$, showed almost no significant changes for both enzyme loading 0.3 and 3 FPU/g cellulose. Results from FBRM also reported very similar trends for the number distribution of chord **Figure 3-41A** and **B**.

The number weighted distribution $E_n(d_{CE})$ was pondered by total number of particle (N) that appeared in the observation surface (1cm × 1cm). **Figure 3-46** represents the evolution of $E_n(d_{CE})\times N$ for FP suspension at 3 FPU/g cellulose of Ctec2. Between 0h and 12h, a strong reduction of 48 % total number of particle was observed, corresponding to a glucose conversion yield of 23.3 %. This reduction was mainly occurred in the fraction of fine population (2 µm < d_{CE} < 10 µm). From 12h to 24h, the reduction trend was significant weaker and reached 59.2 %. Interestingly during this period, the reduction in particle number was mainly observed at very fine particle size of well under 2.5 µm. This evolution was correlated with the glucose conversion yield of 27.3 % at 24h.

Similarly with FP, **Figure 3-47** represents the evolution of $E_n(d_{CE})\cdot N$ for SCB suspension at 3 FPU/g cellulose of Ctec2. Between 0 h and 12 h, a strong reduction of 54.5 % total number of particle was observed, corresponding to a glucose conversion yield of 15.6 %. This reduction was mainly occurred in the fraction of fine population (d_{CE} < 10 µm). From 12 h to 24 h, the reduction trend was significant weaker and reached 76.5 %. Biochemical analysis of this experiment (**Figure 3-10**) showed the glucose conversion yield of 19.1 % at 24 h.

As the fragmentation of one coarse particle can generated large number of fine particle, the evolution in total number of particle in suspension was oppositely affected by two mechanisms as previously discussed (see **§3.2.3.1** and **§3.2.3.2**). The evolution in $E_n(d_{CE})\cdot N$ during hydrolysis is definitively not proportional with the glucose conversion yield. In any case, the reduction in number of particle can only resulted from solubilization mechanism. The decreasing trend in $E_n(d_{CE})\cdot N$ for both FP and SCB suspension were roughly in agreement with hydrolysis yield.

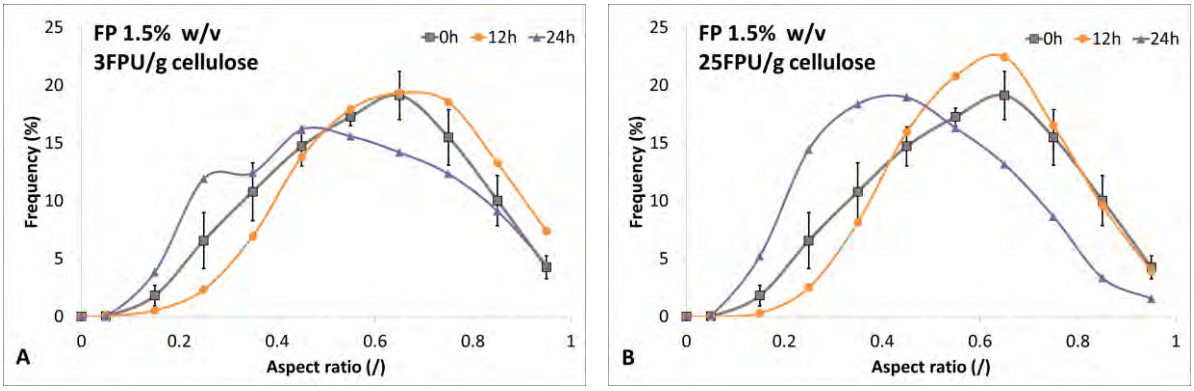

Figure 3-44. Number distribution of aspec ratio (AR) during enzymatic hydrolysis of FP 1.5 %w/v with Ctec2 at E/S equal to 3 (A) and 25 (B) FPU/g cellulose.

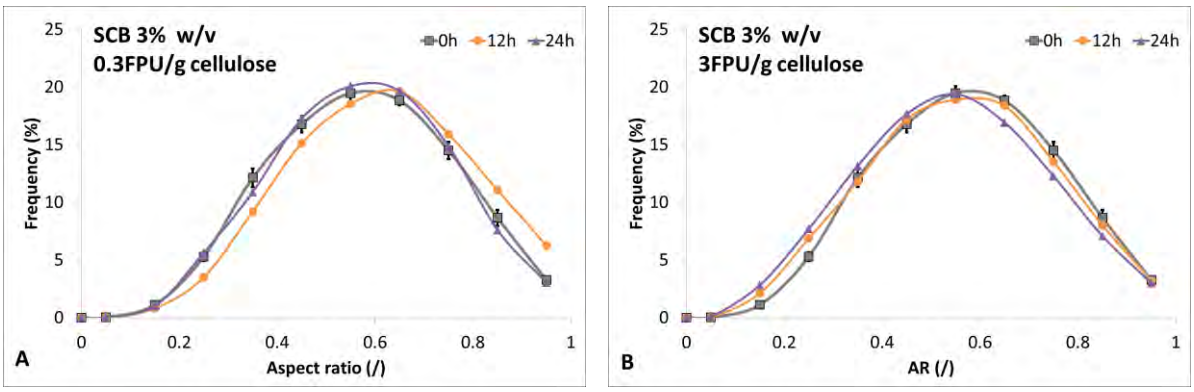

Figure 3-45. Number distribution of aspec ratio (AR) during enzymatic hydrolysis of SCB 3 %w/v with Ctec2 at E/S equal to 0.3 (A) and 3 (B) FPU/g cellulose.

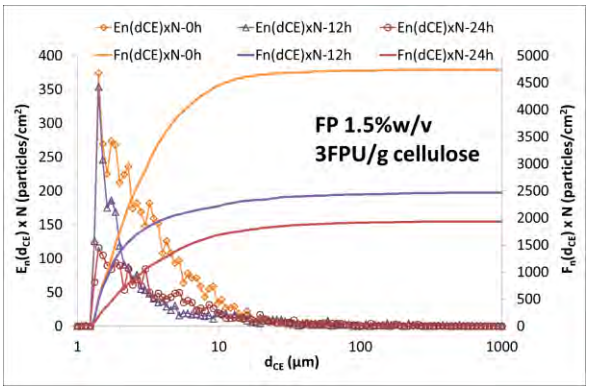

Figure 3-46. Change in $E_n(d_{CE}) \times N$ for FP suspension during enzymatic hydrolysis using Ctec2 at 3 FPU/g cellulose (dilution rate 1/10).

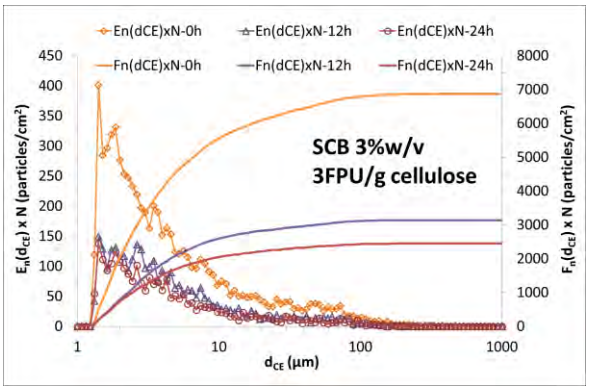

Figure 3-47. Change in $E_n(d_{CE}) \times N$ for SCB suspension during enzymatic hydrolysis using Ctec2 at 3 FPU/g cellulose (dilution rate 1/40).

Highlights for batch hydrolysis

- In-situ viscosity, particle size and chord length distributions of filter paper and sugar cane bagasse during enzymatic hydrolysis were investigated
- Endo-glucanase showed the most important role in the liquefaction of lignocellulosic suspensions whereas exo-glucanase and β-glucosidase showed almost no impact.
- Suspension viscosity was strongly dependence in the fraction of coarse population.
- For PP suspension, synergic actions of exo-glucanase, β-glucosidase and xylanase may improve the liquefaction efficiency.
- Four mechanisms, solvation, particle fragmentation, particle solubilization, and agglomerate separation interact during hydrolysis. Contributions of fragmentation and solubilization mechanisms were pointed out.
- With SCB suspension, viscosity overtakings were observed during the first stage of hydrolysis at low enzyme/substrate ratio (≤ 10 FPU/g cellulose). Phenomenon was quantified and explained by particle size and shape analyses.
- Uniqueness viscosity-time (μ-t) curves were demonstrated with SCB and PP at different operating conditions from batch to fed-batch, from low to high enzyme/substrate ratios.

3.3 R&D: ENZYMATIC HYDROLYSIS AT CONCENTRATED REGIME

In Phd framework, enzymatic hydrolysis at concentrated regime under fed-batch mode stands as the ultimate challenge to be investigated. This part focused on industrial lignocellulosic materials (SCB and PP).Unlikely to semi-dilute regime in batch mode, the experiments in fed-batch were restricted to commercial cocktail Ctec2 and 2 extreme E/S ratios (3 and 25 FPU/g cellulose). Considering feed flowrate, the critical concentration points (C^*) for PP and SCB were previously introduced and identified **Figure 3-8**, Beyond the critical concentration, C^*, a slight increase in substrate concentration may lead to a sharp increase in suspension viscosity. Consequently, it raises the requested energy to ensure an appropriate mixing which is unfavorable to process scale-up and intensification. Fed-batch hydrolyses conducted with concentration inferior to C^* may constitute an issue to maintain low cost and high efficiency process. Moreover, the time ($t_{0.25}$) to reduce suspension viscosity by 75 % was identified in relation with enzyme loading at substrate concentration 30 gdm/L for PP and SCB (**Eq. 3-14** and **Eq. 3-15)**. under batch mode. Thus, a critical substrate feeding rate, Q_s^* (**Eq. 3-19**)can be rationally proposed as the balance between viscosity increase by substrate add and viscosity reduction by hydrolysis kinetics:

$$Q_s^* = V \cdot \frac{C^*}{t_{0.25}} \ (gdm \cdot L^{-1} \cdot h^{-1}) \qquad \textit{Eq. 3-19}$$

In our experimental conditions, the reactor volume is equal to 1.3 L. Q_s^* indicates the upper limit to avoid the concentrated regime. For PP and SCB at enzyme loading ratio 3 and 25 FPU/g cellulose, Q_s^* is equals to 10.1 and 46.6 gdm/h, and 8.9 and 19.4 gdm/h, respectively. In fed-batch mode, favorable (low feeding flowrate and high E/S ratio) and unfavorable (high feeding flowrate and low E/S ratio) were investigated. At 25 FPU/g cellulose, the feeding rates were $Q_s \approx Q_s^*$ and $Q_s \approx 0.5 \cdot Q_s^*$. At low enzyme loading (3 FPU/g cellulose), the feeding rates were two to three time higher than Q_s^*.

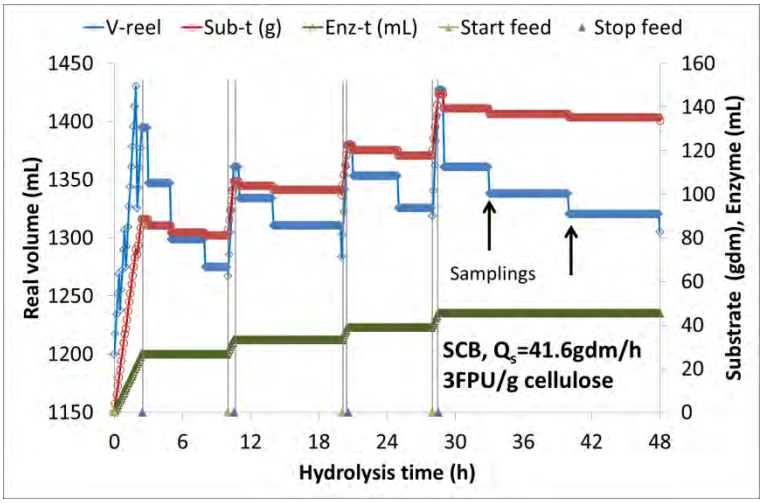

Figure 3-48. Illustration of fed-batch experiments including feeding steps and hydrolysis steps. (V: total volume in reactor (mL), Sub-t (g): total add of substrate (gdm), Enz-t (mL): total add volume of enzyme).

Due to water content of raw materials (> 70 %), total volume in reactor may significantly change during substrate feeding. *In-situ* viscometry is based on the power-consumption curve established with almost a constant volume because torque is affected by concentration and total volume. To overpass this difficulty, the total volume during experiments was controlled in range of 1300 ± 130 mL by adjusting sampling volumes (**Figure 3-48**), corresponding to 10%

tolerance. All experiments started with 1200 mL water in the reactor and sampling volumes were between 2 and 75 mL depending on the real volume. Assuming a homogeneous suspension, the substrate sampling can be estimated from dry matter analysis.

As presented in **§2.5.4** - p88, the enzymatic hydrolysis under fed-batch strategy were controlled by torque monitoring. Regarding system specifications, the SCB and PP feeding was stopped when torque reached the upper limit of around 22 mN.m. The next feeding step started when maximal torque was reduced by 75 %, which corresponding to the 75 % reduction in suspension viscosity. In parallel with the discussion on global phenomena and trends, each stage of fed-batch hydrolysis will be scrutinized specifically. Experiments were divided into feeding (nomenclature Ai) and non-feeding (nomenclature Hi) steps with i indicating the incrementation. . As example, the first feeding stage is named A1 while second non-feeding stage H2 (**Figure 3-49**). In addition, the term "normalized hydrolysis time" for each phase was introduced, taking the first moment of each phase as t = 0 h. It allows comparing the different hydrolysis (non-feeding) phases in fed-batch experiments to batch experiments.

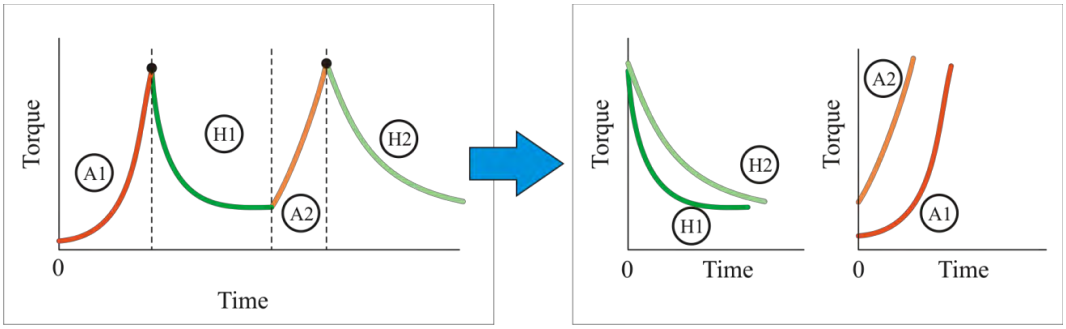

Figure 3-49. Illustration for feeding stages and non feeding stages in one fed-batch hydrolysis.

Similarly with chapter **§3.2**, the results under fed-batch strategy are presented in 3 sub-chapters corresponding to biochemical, viscometry and particle size analysis for SCB and PP. In each sub-chapter, global trends are firstly reported before those specific phenomenons related to each substrate are discussed. For each substrate, three fed-batch experiments were carried out at different feeding rates and enzyme loadings to investigate their impacts on hydrolysis efficiency as well as mechanisms. The detailed operating conditions are presented in **Table 3-9**.

Table 3-9. Fed-batch experiments on SCB & PP.

N°	Substrate	Set point Q_s (ghm/h)	Real Q_s (ghm/h) and equivalent in gdm/h	E/S ratio (FPU/g cellulose)	Final substrate concentration (gdm/L)	Total time (h)
1	SCB	100	100 (23.4)	25	140.0	72
2	SCB	180	180 (41.6)	3	102.4	48
3	SCB	100	100 (23.1)	3	100.4	96
4	PP	180	181 (41.9)	25	99.4	72
5	PP	100	101 (23.5)	25	113.8	96
6	PP	100	115 (27.2)	3	74.7	72

3.3.1 Biochemical analysis

The biochemical analysis consisted in measurement of hydrolysis products (mainly cellobiose, glucose and xylose) by HPLC and dry matter content. From these raw

measurements, hydrolysis yields and mass balance during fed-batch hydrolysis are reported and analyzed.

3.3.1.1 Glucose productions and yields

The **Figure 3-50** illustrates the profile of glucose production through fed-batch hydrolysis of SCB at two enzyme loading ratios of Ctec2 and two feeding rates. The dash lines presents the model equation $[Glc] = k \cdot t$ where $[Glc]$ ($g.L^{-1}$) is the glucose concentration, k ($g.L^{-1}.h^{-1}$) is the coefficient factor reflecting the average production rate and t (h) is the hydrolysis time. In general, increasing trends of glucose concentration were observed for all experiments as the hydrolysis proceeded. In the same way, **Figure 3-51** illustrates the glucose profiles of fed-batch hydrolysis for PP.

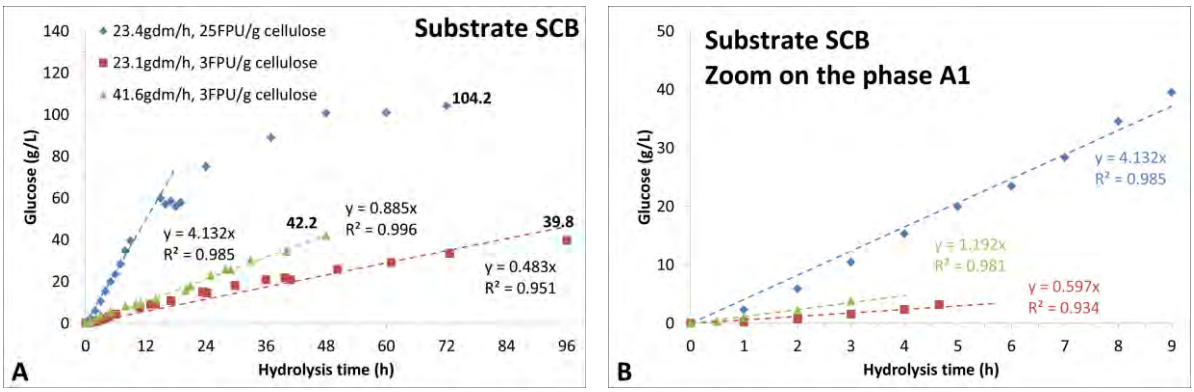

Figure 3-50. Glucose production as a function of time for different feeding rates and enzyme/substrate loadings with SCB. (A: whole experiment, B: focus on A1 step).

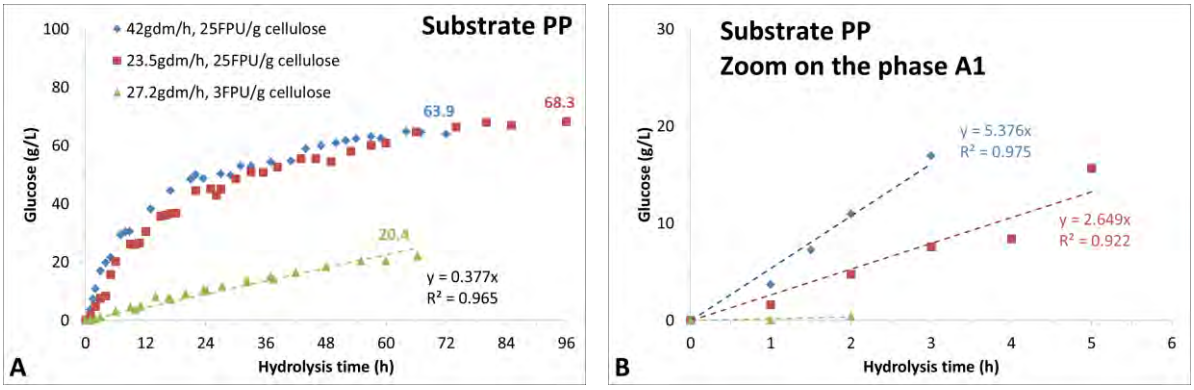

Figure 3-51. Glucose production as a function of time for different feeding rates and enzyme loadings with PP. (A: whole experiment, B: focus on A1 step)

According to these figures, it was reported that for experiments at low enzyme loading (3 FPU/g cellulose), the glucose productions were in proportional relationship with hydrolysis time for both substrates (**Figure 3-50A** and **Figure 3-51B**. The linear regression of $[Glc] = k \cdot t$ gave R^2= 0.996 and 0.951 respectively. Comparing the first stage of hydrolysis at 25 FPU/g cellulose and the experiment at 3 FPU/g cellulose (the blue and red series in **Figure 3-50**), the plot $[Glc] = k \cdot t$ indicated coefficient factor k equal to 4.1 and 0.48 for 25 FPU and 3 FPU, respectively. An 8.3 fold increase in enzyme loading (from 3 to 25 FPU) leads to an 8.4 fold increase in k factor (from 0.48 to 4.1). In the range between 3 and 25 FPU/g cellulose, it seems that k was directly proportional to E/S ratio even if [S] varied in the experiment. For PP suspension at Q_s = 27.2 gdm/h, the same linear regressing showed R^2 = 0.957 for the whole experiment.

In general case of batch hydrolysis of cellulose, the rate of enzymatic reaction decreases as the reaction progressed. It is assumed by the accumulation of end products may negatively affects the reaction rate. Besides, as the enzymatic digestion proceeded, the decrease in substrate concentration lead to a relatively increase of E/S ratio. This may consequently induce an improvement in production rate under no limited substrate condition. For fed-batch hydrolysis and considering only the first feeding stage, there were the evolution of both enzyme and substrate concentrations ([E] and [S]). Under the hypothesis of negligible loss in enzyme activity during this phase, the enzyme concentration must increase. The concentration of substrate, [S], was affected by enzymatic digestion and feeding in opposing ways. The reaction rate can be interpreted following Michaelis & Menten equation:

$$v = k_2 \cdot [E] \cdot \frac{[S]}{[S] + K_m}$$

In case of excess in substrate, [S] >> K_m, the reaction rate will directly dependent of [E]

$$v = k_2 \cdot [E]$$

The results obtained from SCB for the phase A1 (**Figure 3-50B**) seems to be correlated with this assumption. Slopes of two curves representing 3 FPU/g cellulose were close and significantly inferior to that of 25 FPU/g cellulose.

In order to reach similar final substrate loading (≈100 gdm/L), the experiment of SCB at Q_s = 41.6 gdm/L was stopped at 48 h while experiment at Q_s = 23.1 gdm/h was extended to 96 h. Final glucose concentrations of two experiments were reported in the same order of magnitude and equals to 42.2 g/L (for Q_s = 23.1 gdm/h at 48 h) and 39.8 g/L (for Q_s = 41.6 g/L at 96 h).

The experiment at low feeding rate but high enzyme loading ratio for SCB was carried out in order to evaluate the contribution of enzyme loading. At Qs = 23.4 gdm/h and E/S ratio equals to 25 FPU/g cellulose, the glucose production exhibited an increasing trend with clearly three different stages. First stage with linear relationship between glucose and hydrolysis time indicated the maximal enzyme reaction rate in the first 14 h. It corresponds to the evolution of substrate concentration between 0 gdm/L to 86.4 gdm/L. A transitional phase with fluctuation of glucose concentration was corresponded to the second feeding of substrate between t = 15 h and t = 19 h. Third stage at beyond 19 h showed an increasing trend in glucose concentration but with a production rate lower than the first stage. This stage started at glucose concentration superior to 60 g/L and dry matter content was approximately 83 gdm/L. The reduction in production rate for the third stage can be assumed for accumulation of glucose in suspension that affected enzymatic reaction.

For fed-batch hydrolysis of PP (**Figure 3-51B)** the first feeding stage of experiment at 3 FPU/g cellulose was very short (only 2 h) due to the quick increase of suspension viscosity. This do not allows any assumption due to the lack of experimental point. As for two experiments at 25 FPU/g cellulose, linear relationship between $[Glc]$ and hydrolysis time was observed. However, slops of two curves representing $[Glc] = k \cdot t$ at 25 FPU/g cellulose were clearly different. It was observed that values of k were proportional with the feeding rate of PP; twofold increase in k (2.65 versus 5.38) for Q_s from 23.5 to 42 gdm/h.

Focusing on two experiments with PP at enzyme loading 25 FPU/g cellulose (**Figure 3-51A**), the glucose concentration curves exhibited most of the time identical increasing trend despite the different in first feeding stage (**Figure 3-51B**). It is interesting that increasing feeding rate from 23.5 to 42 gdm/h did not affect the glucose production. For the fed-batch using 3 FPU/g cellulose, the glucose concentration exhibited a gradual increase, reached 20.4

g/L by 72 h. The linear relationship between glucose concentration and hydrolysis time was observed for both PP and SCB at low enzyme/substrate ratio (3 FPU/g cellulose).

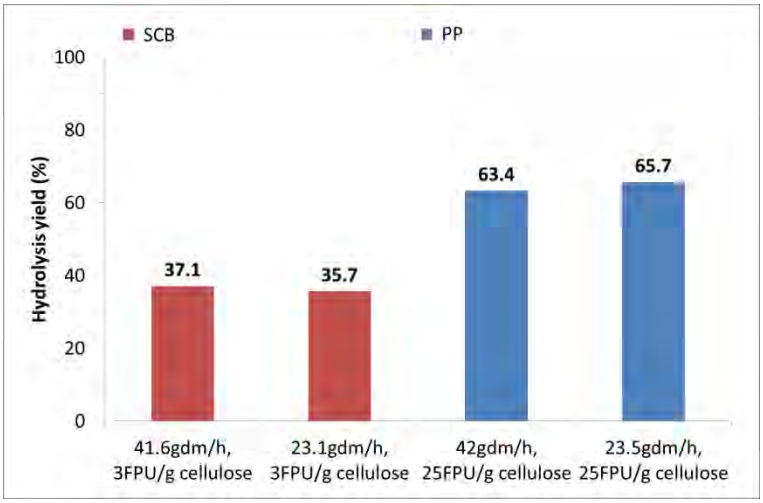

Figure 3-52. Glucose yields of fed-batch hydrolysis conducted with PP and SCB, total sbstrate loading 100 gdm/L.

Figure 3-52 compares the final glucose yield of fed-batch hydrolysis at final substrate loading 100 gdm/L. For all fed-batch hydrolyses, the experiment time were ranged from 48 h to 96 h depending on feeding rates. According to this graph, it was clear that the final glucose yield seems to be proportional with enzyme loading ratio and nearly independent from feeding rate. For SCB at 3 FPU/g cellulose, both low and high feeding rates resulted in 36.4 ± 0.7 % glucose conversion yields. Experiments on PP at 25 FPU/g cellulose showed similar glucose yield (63.4 and 65.7 %) at Q_s = 42 and 23.5 gdm/h. These results confirmed that enzymatic reactions were performed under substrate saturation.

At 3 FPU/g cellulose, the 37.1 and 35.7 % hydrolysis yields were clearly lower than the best yields reported from the literature (Hodge, Karim et al. 2009, Zhao, Dong et al. 2013). It can be explained by the low enzyme loading ratio, which was 3 FPU/g cellulose in our study compared to 10 - 20 FPU/g cellulose reported from literature for fed-batch mode (**Table 1-4**).

For 25 FPU/g cellulose loadings, the glucose conversion yields with FP and SCB were ranged between 63.4 to 67.0 %. Regarding the trend in glucose concentration versus time (**Figure 3-50** and **Figure 3-51**), it seemed that hydrolysis yields can be further increased by lengthening the total hydrolysis time. In addition, the fed-batch hydrolysis based on multiples feeding and non-feeding stages. It was always possible to carry out the fed-batch hydrolysis with more loops to achieve higher solid loading and better glucose production. An alternative solution by increasing the enzyme loading to reach enzyme saturation state may theoretically improve glucose yield. However, the cost for enzyme stands as main drawback at industrial scale and need to be taking into consideration.

3.3.1.2 Cellobiose and xylose

For SCB, cellobiose was accumulated at very low magnitude during fed-batch hydrolysis. HPLC analysis did not found cellobiose in the hydrolysate at 3 FPU/ g cellulose. For the experiment at 25 FPU/g cellulose, cellobiose was accumulated in the first 3 h, reached 1.39 g/L. Beyond, no cellulose was detected in the supernatant. Thus, cellobiose was considered as negligible during fed-batch hydrolysis of SCB (data not shown). Xylose was not found in the hydrolysate of SCB for all experiments. This was in agreement with the applied pretreatment

method and substrate composition of SCB. In this part, the profile of cellobiose and xylose are illustrated in **Figure 3-53** for fed-batch hydrolysis of PP.

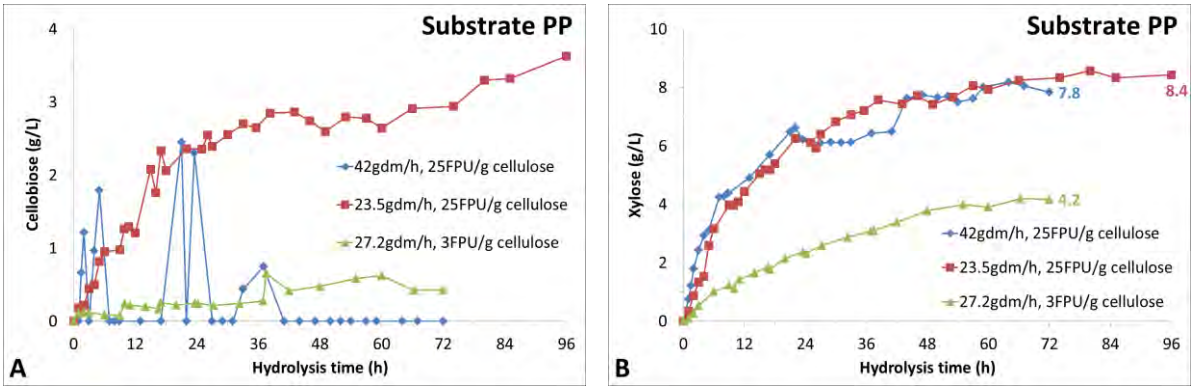

Figure 3-53. Cellobiose (A) and xylose (B) concentrations as a function of time and different feeding rates and E/S ratios with PP.

According to the graph **Figure 3-53A**, the accumulations of cellobiose were negligible for the experiments at lowest enzyme loading (Q_s = 27.2 gdm/h, E/S = 3 FPU/g cellulose). With Q_s = 42 gdm/h, E/S = 25 FPU/g cellulose, some peak of cellobiose were observed corresponding to the feeding phases during experiment. These results corresponded with the performance of commercial cocktail Ctec2 with high ratio of β-glucosidase. Unexpectedly for the experiment at low feeding rate and high enzyme loading (Q_s = 23.5 gdm/h, E/S = 25 FPU/g cellulose), the accumulation of cellobiose was significant. It was observed that cellobiose concentration quickly increased in the first stage, reached 2.06 g/L by 18 h. This was then followed by a gradual rise up to 3.61 g/L cellobiose. This evolution in cellobiose was unfortunately un-explicable considering the glucose production and dry matter content analyses.

As showed in **Figure 3-53B**, the xylose concentrations exhibited similar trend compared to glucose curves (**Figure 3-51A**). It seems that the xylose production was only dependent in enzyme loading ratio. At 3 FPU/g cellulose, the xylose curve exhibited a gradual rise up to 4.2 g/L at 72 h. At 25 FPU/g cellulose, both hydrolysis at Q_s = 23.5 and 42 gdm/h showed similar xylose production curves, reached 7.8 and 8.3 g/L, respectively.

3.3.1.3 Dry matter content and mass balance

Figure 3-54 and **Figure 3-55** showed the profile of dry matter content (DM) for fed-batch hydrolyses of SCB and PP. As expected, an increase of dry matter content during feeding stage was observed while a decrease in non-feeding stage was noticeable.

- *Dry matter content during fed-batch hydrolysis*

At 3 FPU/g cellulose, same values of final residual insoluble content were reported for two feeding rates Q_s = 23.1 gdm/h and Q_s = 41.6 gdm/h. It was in good agreement with HPLC analysis showing nearly identical glucose concentration at the end of these hydrolyses (**Figure 3-50A**). For experiment at Q_s = 23.1 gdm/h and after the first feeding stage (beyond 5 h), the profile of dry matter content showed a nearly stabilization state with fluctuation ranging from 51.4 to 68.8 gdm/L. The enzymatic digestion was nearly capable to compensate and maintain equilibrium in total dry matter with substrate feeding. This stable state of substrate concentration was in good agreement with the linear relationship between glucose production and hydrolysis time (**Figure 3-50A**), indicating constant glucose production rate during the experiment. Similar conclusion can be obtained for the experiment at high feeding rate (Q_s = 41.6 gdm/h).

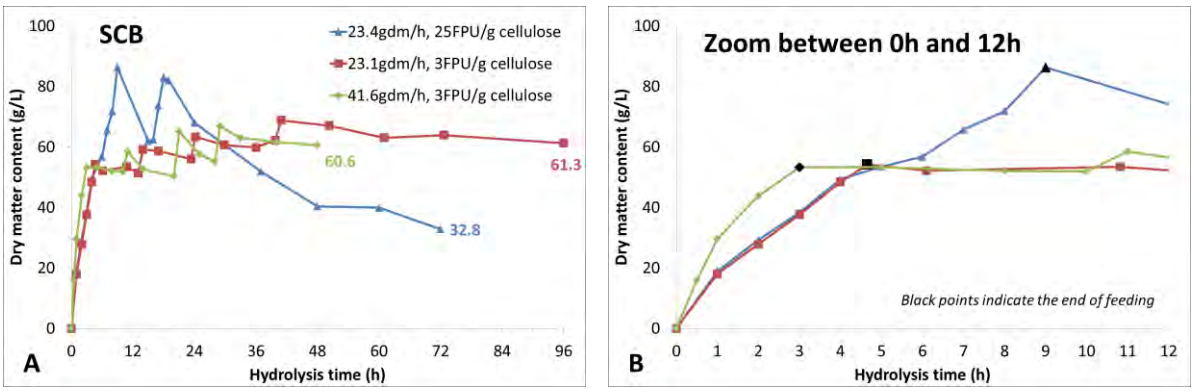

Figure 3-54. Dry matter content as a function of ime for different feeding rates and E/S ratios with SCB (A: whole experiment, B: focus between 0 and 12h)

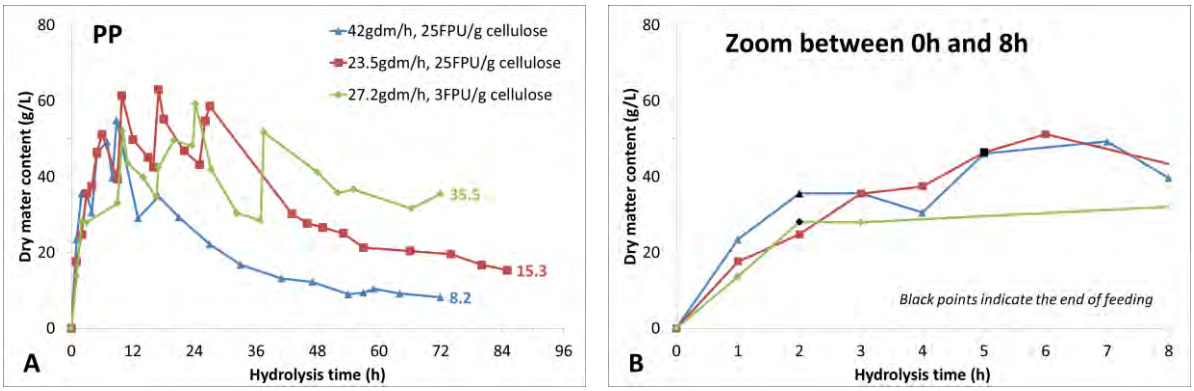

Figure 3-55. Dry matter content as a function of time and different feeding rates and E/S ratiowith PP (A: whole experiment, B: focus between 0 and 8h)

Focusing on the stage A1, at nearly similar feeding rate (≈ 23 gdm/h) and different enzyme loading ratios (3 and 25 FPU/g cellulose), almost identical trends of dry matter content were reported over the 5 first hours (blue and red curves, **Figure 3-54B**). This corresponded to the very different glucose profile (see **Figure 3-50**, blue and red series), which was significantly higher with 25 FPU/g cellulose. These observations can be sustained by the different level of solubilization mechanism during this period. Generally the glucose oligomers and their derivatives with DP > 5 are insoluble in water. The biodegradation of cellulose into glucose oligomers of DP ≤ 5 reflects the solubilization mechanism which is correlated with residual dry matter content. Further digestion of low DP oligomers into glucose indicates the glucose production or in other words, the hydrolysis yield, which is correlated with glucose concentration in liquid phase. At 25 FPU/g cellulose, substrate was degraded until the formation of end product (glucose). At 3 FPU/g cellulose, the enzyme digestion was not reached the same extend as 25 FPU/g cellulose, the substrate can be degraded to soluble oligomers (DP ≤ 5) at same level but further conversion into glucose was not achieved at the same level.

Similar analyses of dry matter content were performed during fed-batch hydrolysis of PP (**Figure 3-55**). Focusing on two experiments at enzyme loading 25 FPU/g cellulose, it was observed that high feeding rate (42 gdm/h) resulted in better solubilization efficiency than low feeding rate (23.5 gdm/h). After 72 h, the dry matter contents were 8.2 and 19.6 gdm/L for 42 and 23.5 gdm/h, respectively. This corresponded to a solubilization rate of 91.8 and 82.7 % for 42 and 23.5 gdm/h, respectively. It is important to note that enzyme was fed in parallel with substrate. By increasing feeding rate, the enzyme and substrate (if not compensated by hydrolysis kinetics) concentrations are increased. This might affect the solubilization and

caused the better solubilization efficiency. However from HPLC analysis, these two experiments showed similar glucose production during hydrolysis (**Figure 3-51A**). These analyses led to an assumption that during the experiment time, the solubilization efficiency did not directly shown the coherence with the glucose production rate. This assumption needs to be confirmed by additional experiments before conclusion can be drawn.

For the experiment at low enzyme loading (3 FPU/g cellulose), the analysis of dry matter content encountered additional difficulties. Due to the slow liquefaction rate, the accumulation of substrate in bioreactor negatively affected the homogeneity of whole slurry and sampling. The analysis of dry matter content was less accurate than for others experiments.

- *Mass balance for fed-batch hydrolyses*

Figure 3-56 interprets two biochemical parameters: the solubilization yield and the glucose yield. Sub_t is the total substrate concentrations which correspond to feeding strategy (gdm/L), Sub_r is the real dry matter (analysis protocol **§0** - p63) and $Sub_{t-yield}$ is the theoretical substrate concentration corresponding to glucose yield calculating from glucose concentration $[Glc]$ (g/L).

$$Sub_{t-yield} = [Glc] \cdot 1.1 \qquad \textit{Eq. 3-20}$$

The difference between Sub_t and Sub_r reflected the amount of substrates which was solubilised. Besides, the difference between Sub_t and $Sub_{t-yield}$ indicated the quantity of substrate (cellulose) which was converted into glucose. It is clearly observed that for all experiments the evolution of both Sub_r and $Sub_{t-yield}$ were correlated with feeding (increasing trend) and non-feeding stage (decreasing trend). For experiment at 23.4 gdm/h and 25 FPU/g cellulose, the substrate profile exhibited clearly two different trends. In the first stage from t = 0h until the end of feeding (t = 13h), the curve of $Sub_r$was nearly overlapped with the one of $Sub_{t-yield}$, reflecting the fully bioconversion of cellulose into glucose. In the 2nd stage (beyond 13h) where all feeding has been done, these two curves tend to be separated and Sub_r was always bellows $Sub_{t-yield}$. It indicated that the bioconversion of cellulose was not fully achieved up to glucose. The offset between two curves translated the fraction of intermediary product accumulating in suspension, theoretically from DP2 to DP5 (soluble glucose oligomers).

For the two experiments at 3 FPU/g cellulose (**Figure 3-56B, C**), similar phenomenon was observed. The curves of Sub_r and $Sub_{t-yield}$ were super-imposed early on then tend to be separated with Sub_r always below $Sub_{t-yield}$ curve. The partial solubilization was exacerbated due to low enzyme loading ratios. Interestingly at the final non-feeding stage, the offset between Sub_r and $Sub_{t-yield}$ seems to be reduced. The analysis of intermediary products (from DP3 to DP5) is then required to strengthen and confirm the extension of solubilization.

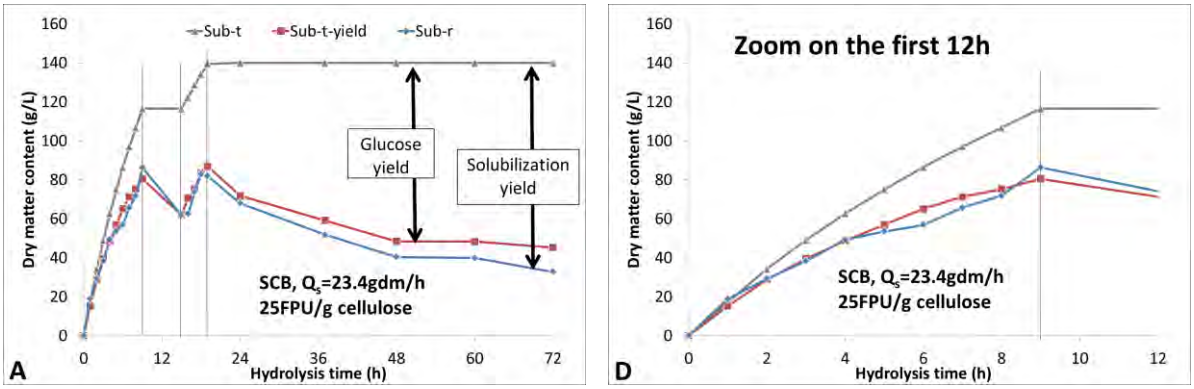

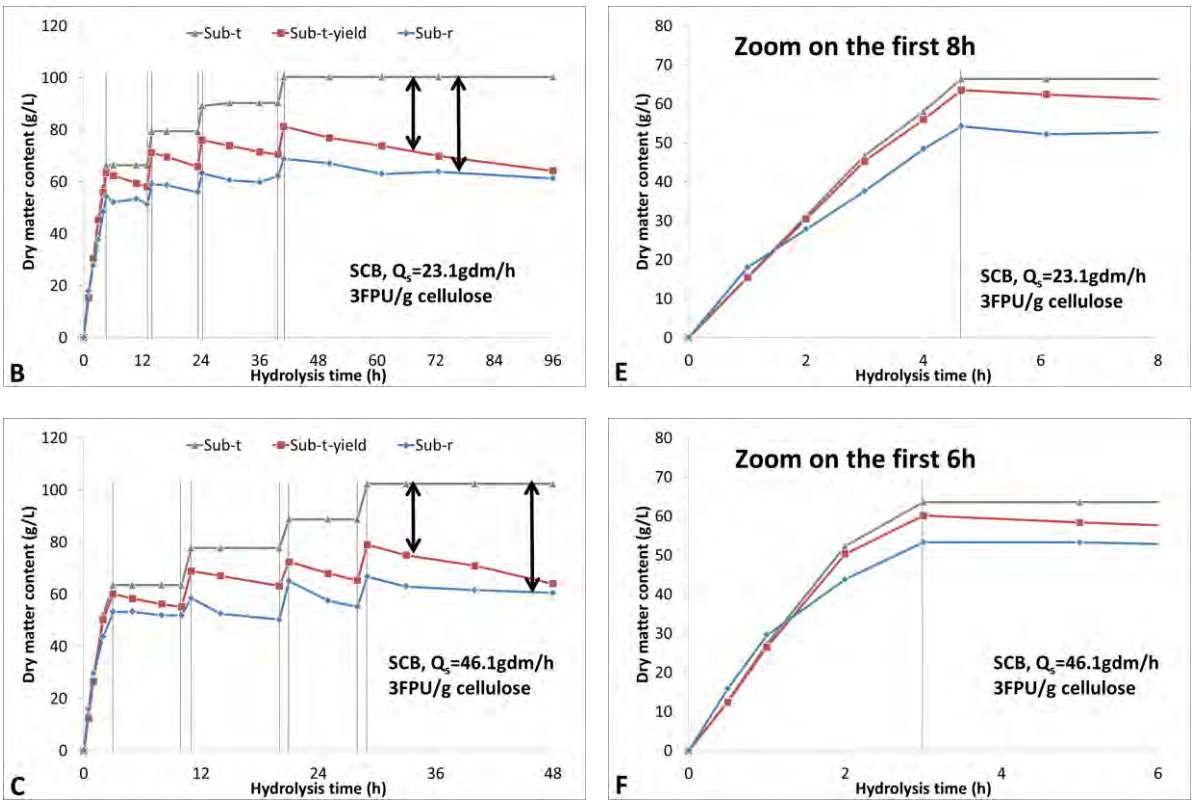

Sub-t: theoretical substrate content calculated from feeding rate
Sub-t-yield: theoretical substrate content corresponds to glucose yield
Sub-r: measured substrate content
Vertical gray line indicates the start or end of feeding stages

Figure 3-56. Substrate balance as a function of time and different feeding rates and E/S ratios during fed-batch mode with SCB(A, C and D: whole experiments, B, D and F: focus on A1)

The mass balances for fed-batch hydrolysis of PP at 25 FPU/g cellulose are presented in **Figure 3-57**. For 3 FPU/g cellulose, data are not considered due to imprecise and fluctuating dry matter contents. Generally, the difference between Sub_t, Sub_r, and $Sub_{t-yield}$ indicated the magnitude of solubilization. With PP, the offset between Sub_r and $Sub_{t-yield}$ for PP was significantly larger than with SCB. This reflected the quantity of substrate that was solubilized but not yet converted into glucose. At low feeding rate (23.5 gdm/h), the solubilization yield was 86.5 % compared to 65.7 % in glucose yield. Nearly 20 % of substrate was only solubilized. This effect was exacerbated for the fed-batch hydrolysis at 42 gdm/h; the solubilization yield was 91.7 % while glucose conversion yield was limited at 63.4 %. The accumulation of soluble fraction in this experiment was equal to 28.3 % of fed quantity. Considering biochemical knowledge about enzymatic action and referring to our obtained results from batch hydrolysis, endo-glucanase was pointed out as the main activity for liquefaction while actions of exo-glucanase and β-glucosidase were responsible for the conversion of oligomers into cellobiose and glucose. An increase of exo-glucanase and β-glucosidase activities in cocktail may consequently lead to an improvement in terms of glucose yield. Besides, this can be achieved by supplement the cocktail with exo-glucanase and β-glucosidase from external sources.

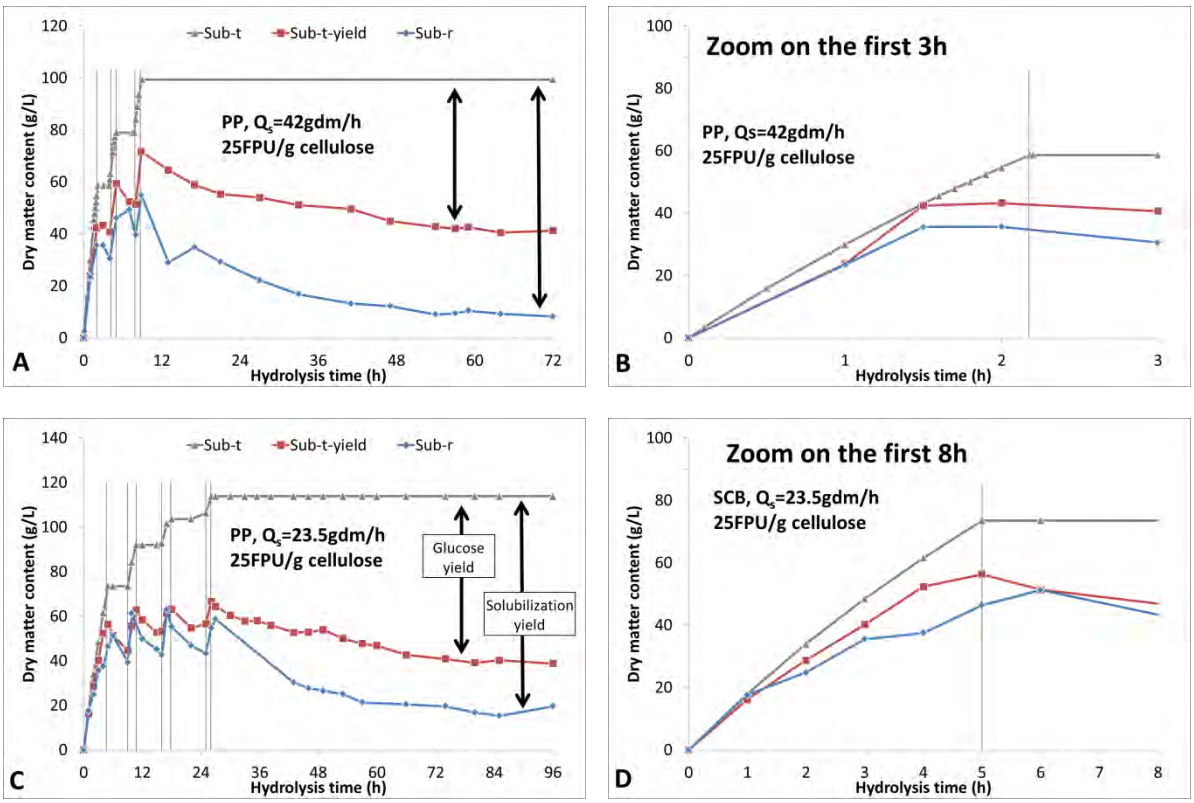

Sub-t: theoretical substrate content calculated from feeding rate
Sub-t-yield: theoretical substrate content corresponds to glucose yield
Sub-r: measured substrate content
Vertical gray line indicates the start or end of feeding stages

Figure 3-57. Substrate balance as a function of time and different feeding rates and E/S ratios during fed-batch mode with PP (A, C: whole experiments, B, D: focus on A1)

3.3.1.4 Kinetics modeling of dry matter content for fed-batch mode

In this part, the modeling of dry matter content during fed-batch hydrolysis at constant feeding rate of both substrate and enzyme was considered separately for feeding and non-feeding phases. For non-feeding phases, taking into consideration the following assumptions: i) enzyme inactivation was negligible during experiment, ii) no effect of end-products inhibition; the power relationship (**Eq. 3-8**) previously used for modeling of batch hydrolysis (**§3.2.1.3**) is now considered.

For the first feeding stage where both enzyme and substrate were fed in the reactor, both enzyme concentration $[E]$ and substrate concentration $[S]$ varied with reaction time. From the literature, there was no standard equation that was reported for this case. In this phase, the increase in $[S]$ by feeding was stronger than its decrease by hydrolyse that led to a substrate saturation condition. Under favourite conditions (no enzyme inhibition by end-product neither irreversible absorption), the reaction rate in this phase may depend only on enzyme concentration, $[E]$. Thus, **Eq. 3-21** was then tested for the modeling of substrate concentration during feeding stage. In this equation, $[E]$ is the concentration of enzyme (FPU/L), $[S]$ is the concentration of substrate (g/L), α is the model order (/) and k_2 indicates the reaction coefficient (h^{-1}).

$$\frac{d[S]}{dt} = -k_2 \cdot [E]^{\alpha} \qquad \textit{Eq. 3-21}$$

For both models, k and k_2 can be adjusted by least squares method of $[S]_{model}$ versus $[S]_{experimental}$ using solver tool (Microsoft Excel ®).

Figure 3-58 represents the modeling for the stages A1 and H2 of fed-batch hydrolysis of SCB at Q_s =23.4 gdm/h and Q_e = 13.5 mL/h (equivalent to the ratio E/S = 25 FPU/g cellulose). Initial volume of reactor V_0 = 1200 mL. These simulations were compared to experimental data from the fed-batch hydrolysis of SCB at same feeding conditions.

For the feeding phase A1, the model (**Eq. 3-21**) fitted well with experimental data for k_2 = 8.47 and α = 1.13 (R^2 = 0.980). This result suggested that our assumptions for feeding stage seem to be correct in this experiment. As the value of α. was nearly 1, the reaction rate ($d[S]/dt$) may be considered as linear proportional with enzyme concentration. For the non-feeding phase, the power relationship (**Eq. 3-8**) accurately predicted suspension dry matter content for k_{bio-4} = 1.41.10^{-5} and α = 2.67 (R^2 = 0.987).

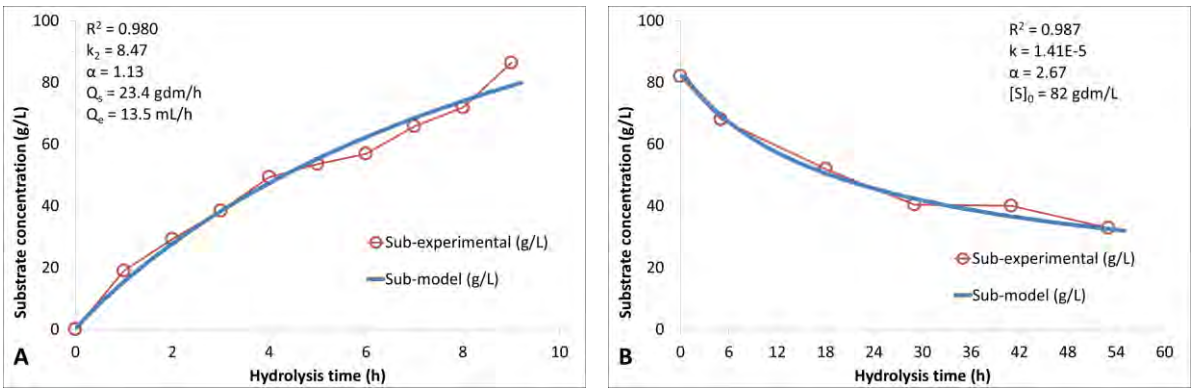

Figure 3-58. Simulation of a feeding stage (A) and non-feeding stage (B) at constant flowrate of substrate and enzyme (Q_s =23.1 gdm/h, Q_e = 13.5 mL/h) compared to fed-batch hydrolysis at the same conditions. Hydrolysis time is normalized.

3.3.2 In-situ viscometry

Figure 3-59 illustrates the in-situ suspension viscosity during fed-batch hydrolysis of SCB and PP at different E/S ratios and feeding rates. In general, suspension viscosity showed an increasing trend during feeding stages and a decreasing trend during non-feeding stages. The feeding stages were well controlled through torque monitoring. The discussion of *in-situ* viscometry is structured in three parts from raw data to viscosity modeling.

- Part 1: description of in-situ viscosity during fed-batch hydrolysis
- Part 2: comparison between measured and theoretical viscosities to highlight impact of fragmentation and solubilization mechanisms
- Part 3: kinetic modeling of suspension viscosity

3.3.2.1 Time evolution of in-situ viscosity

For SCB at 3 FPU/g cellulose, the final viscosity reached nearly same magnitude for two hydrolyses at Q_s equal to 41.6 and 23.1 gdm/h. As suspension viscosity strongly depends on substrate concentration (**Figure 3-8C**), these results were correlated with dry matter contents, which were 60.6 and 61.3 gdm/L for Q_s equal to 41.6 and 23.1 gdm/h respectively (**Figure 3-55A**).

For PP at 25 FPU/g cellulose, the experiment at high feeding rate (Q_s = 42 gdm/h) resulted in better liquefaction efficiency. After three feeding stages, total solid loading reached 100 gdm/L and slurry was liquefied (μ inferior than 25 % of the maximal value) within the first 24 h. At low feeding rate (23.5 gdm/h), four feeding stages were needed to reach approximately final solid loading 113 gdm/L and slurry was liquefied after 48 h. Low feeding rate is not recommended due to the time consuming that will probably lead to more energy consumption. For the experiment at low enzyme loading (3 FPU/g cellulose), suspension viscosity rose very quickly since feeding was started. Consequently, five stages of feeding were required to achieve only 75 gdm/L total solid loading. Further increase in solid loading seemed to be very time consuming mainly due to the slow liquefaction kinetic at low enzyme dosage.

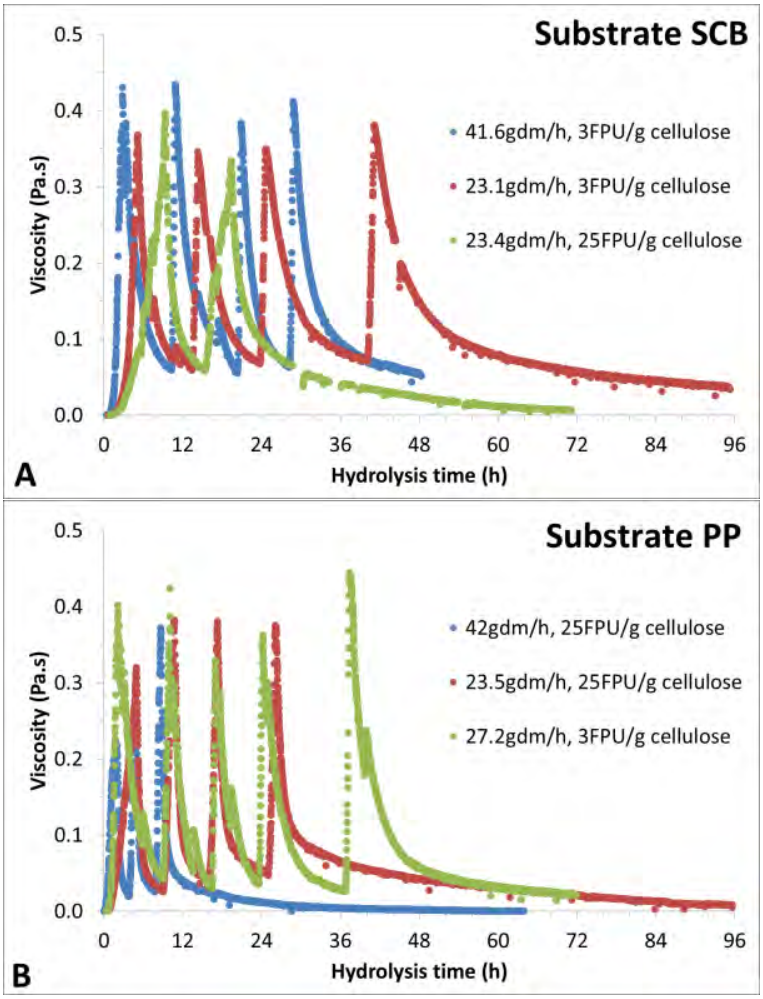

Figure 3-59. In-situ viscosity as a function of time and different feeding rates and E/S ratios with SCB (A) and PP(B).

Due to the complex viscosity profile of fed-batch hydrolysis, it is recommended to analyze the viscometry by separating feeding and non-feeding stage as previously introduced (**Figure 3-49**). In feeding stage (Ai), suspension viscosity was affected by at least three simultaneous factors: i) the substrate increase leads to a viscosity increase, ii) the particle size modification by fragmentation mechanism induces a decrease in μ and iii) the solubilization mechanism, previously shown, has almost no contribution at semi-dilute regime but is expected to interfere at concentrated regime. The viscosity curves (full experiment and zoom on the first feeding stage A1) of three fed-batch hydrolysis were represented in **Figure 3-60**. The μ_{Sub-t} is the theoretical suspension viscosity corresponding to total added substrate concentration, μ_{Sub-DM} is the suspension viscosity corresponding to measured dry matter content and $\mu_{(in-situ)}$ is the

in-situ viscosity. It was clearly observed that the contributions of fragmentation and solubilization mechanisms depend on both enzyme and substrate loading.

3.3.2.2 Comparison between μ_{Sub-DM}, μ_{Sub-t} and $\mu_{(in-situ)}$

For SCB and at low feeding rate and high E/S ratios (23.4 gdm/h, 25 FPU/g cellulose, **Figure 3-60A**), the $\mu_{(in-situ)}$ curves were always below μ_{Sub-DM} ones. The viscosity reduction was achieved through both fragmentation and solubilization. The contribution of fragmentation mechanism is illustrated by the offset between μ_{Sub-DM} and μ_{Sub-t}. As for solubilization mechanism, its contribution corresponds to the offset between μ_{Sub-DM} and $\mu_{(in-situ)}$). During enzymatic hydrolysis, it was observed that the contribution of each mechanism for liquefaction did not remain at the same magnitude. In the first feeding phase (**A1, Figure 3-60D**), both mechanisms showed nearly similar contribution to viscosity reduction and as the enzymatic reaction progressed, the role of solubilization became more and more significant. In the non-feeding phase (H1), the value of suspension viscosity between t = 24 h and t = 48 h was almost stable while dry matter content showed a considerable decrease. The phenomenon was very similar on semi-dilute regime where viscosity become stable and independent of both fragmentation and solubilization once the liquefaction reached some threshold. At this critical point, SCB suspension can be considered as totally liquefied.

At low feeding rate and low enzyme loading ratio (23.1 gdm/h, 3 FPU/g cellulose, **Figure 3-60B**) the contribution of solubilization mechanism seems to be weaker than at high enzyme loading. In particular, the contribution of fragmentation was not observable during the first feeding stage, A1 (**Figure 3-60E**). During this phase, μ_{Sub-DM} and $\mu_{(in-situ)}$ were overlapped reflecting the impact of substrate concentration on suspension viscosity. Both μ_{Sub-DM} and $\mu_{(in-situ)}$ reported a viscosity reduction by approximately 35 % compared to theoretical value μ_{Sub-t}. At low enzyme loading, it was expected that fragmentation mechanism have dominant impact on viscosity reduction. The present of solubilization mechanism was confirmed by the biochemical analysis (see **Figure 3-50**) reporting approximately 3.5 g/L glucose production at t = 4.7 h, equivalent to a bioconversion rate equal to 4.9 %. It is important to note that, at the end of At stage (t = 4.7 h), the total insoluble solid content was 54.3 gdm/L compared to theoretical dry matter content from feeding 64.2 gdm/L. These numbers reported a solubilization rate of 18.8 % (**Figure 3-56**), which was possible to explain the 35 % reduction of viscosity. Comparing with the experiment at high enzyme loading ratio (23.4 gdm/h, 25 FPU/g cellulose), the fragmentation mechanism for 3 FPU/g cellulose was significant weaker and not enough strong to affect the suspension viscosity. It needs to be verified through particle size distribution analysis to explore the evolution in population of coarse particles. From the end of A1 phase (t = 4.7 h) until the end of hydrolysis, similar trends as high enzyme loading were reported; the $\mu_{(in-situ)}$ curve was always below μ_{Sub-DM} one. The trend between t = 4.7 h and t = 96 h illustrated the contribution of both fragmentation and solubilization mechanisms for suspension liquefaction. However from the beginning of the 4th non-feeding stage (H4) until t = 60 h, the viscosity collapse was occurred with a very small evolution in dry matter content. It was suggested that the contribution of fragmentation mechanism was exacerbated during this period. Particle size distribution will be important to validate this assumption (next sub-chapter)

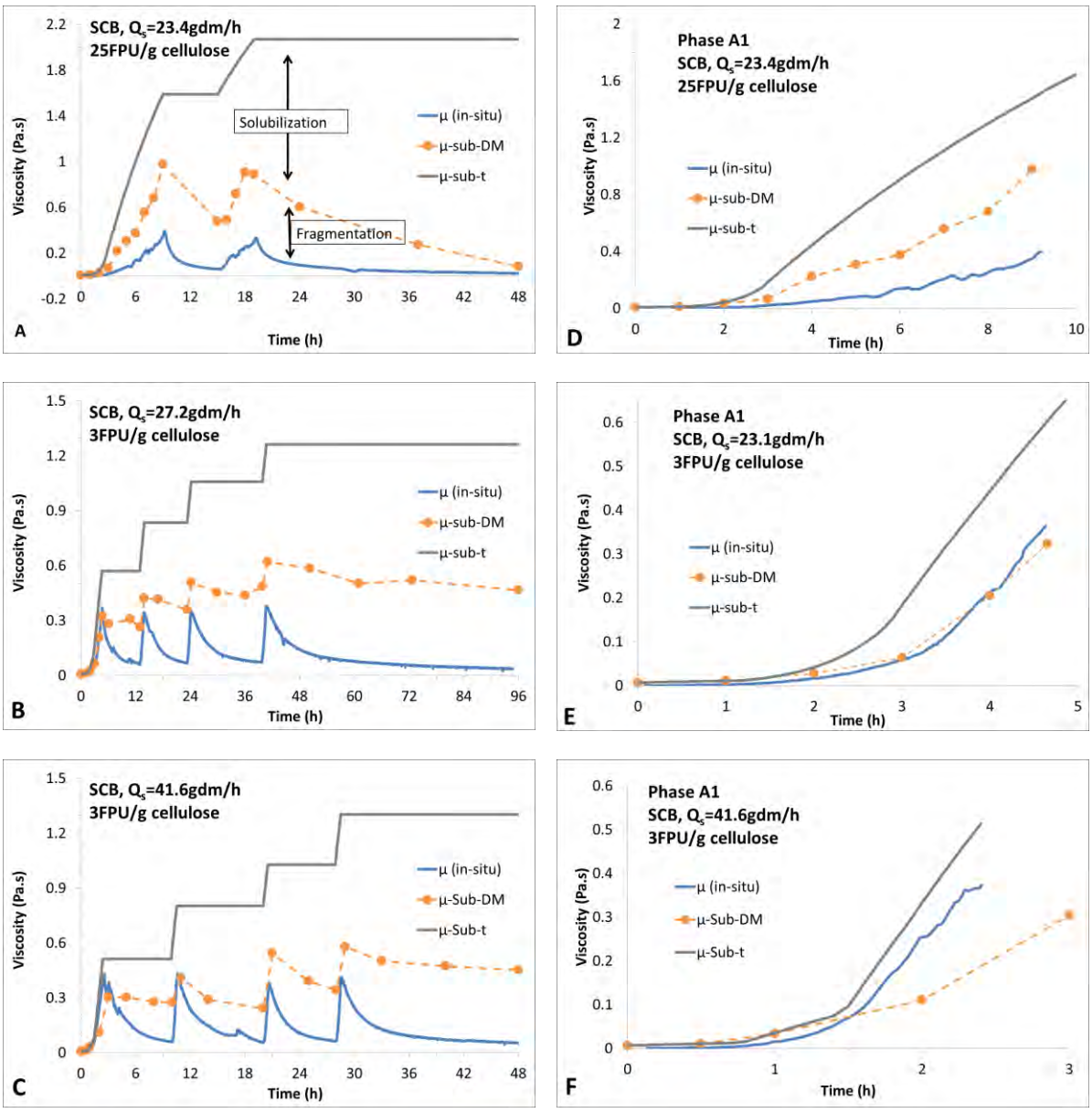

Figure 3-60. Estimated and in-situ viscosities as a function of time and different feeding rates and E/S ratios with SCB. (A, B and C: whole experiments, D, E and F: focus on A1 stage).

At high feeding rate and low E/S ratio (41.6 gdm/h and 3 FPU/g cellulose, **Figure 3-60C**),, the dose-effect relationship was exacerbated; in-situ viscosity, $\mu_{(in-situ)}$, was slightly lower than the theoretical value μ_{Sub-t}. The μ_{Sub-DM} curve was located below $\mu_{(in-situ)}$ during A1 phase (**Figure 3-60F**). The viscosity reduction by both mechanisms was not strong enough to compensate the impact of substrate adding at high feeding rate. It may be explained by the overtakinging phenomenon with SCB which was previously discussed under semi-dilute conditions (**§3.2.2.1**). In the feeding phase (Ai), as the substrate was continuously added in reactor, overtaking phenomenon probably occurred along feeding phase. Suspension viscosity resulted from sum of four opposite contributions:

- Feeding: viscosity increase due to substrate concentration
- Overtaking: viscosity increase generated by the separation of agglomerates,

- Fragmentation: viscosity decrease induced by particle size distribution switching from coarse to fine
- Solubilization: viscosity decrease generated by the solubilization of fine particles.

Viscosities during phase A1 suggested a stronger impact of overtaking and substrate feeding compare to fragmentation and solubilization mechanisms. The phenomenon needs to be discussed under the light of biochemical, rheological and particle size analysis in order to propose an appropriate conclusion. From the end of feeding stage A1, the viscosities patterns showed familiar trend with $\mu_{(in-situ)}$ always inferior to μ_{Sub-DM}.

For PP, similar interpretation was conducted for two fed-batch hydrolysis at Q_s = 25 FPU/g cellulose (**Figure 3-61**). The impact of feeding rate on viscosity was illustrated during the phase A1 (**Figure 3-61C, D**). At 42 gdm/h, the measured viscosity, $\mu_{(in-situ)}$, was nearly similar with the theoretical viscosity deduced from dry matter content, μ_{Sub-DM}. In the opposite at Q_s = 23.5 gdm/h, the $\mu_{(in-situ)}$ curve was located below μ_{Sub-DM} one which indicated the contributions of both fragmentation and solubilization mechanisms.

During the phase A1 (**Figure 3-61D**), the viscosity evolution at Q_s = 23.5 gdm/h (E/S =25 FPU/g cellulose) was very similar to SCB at Q_s =23.4 gdm/h (**Figure 3-60D**). This reflected similar effect of enzyme-to-substrate ratio on both substrates PP and SCB at similar feeding rate. At high feeding rate 42 gdm/h (**Figure 3-61C**), two curves $\mu_{(in-situ)}$ and μ_{Sub-DM} were overlapped that do not allow differing the contribution of fragmentation and solubilization mechanisms. Additional analysis (particle size distribution) is then required to confirm the existence of fractionation effect on coarse particles.

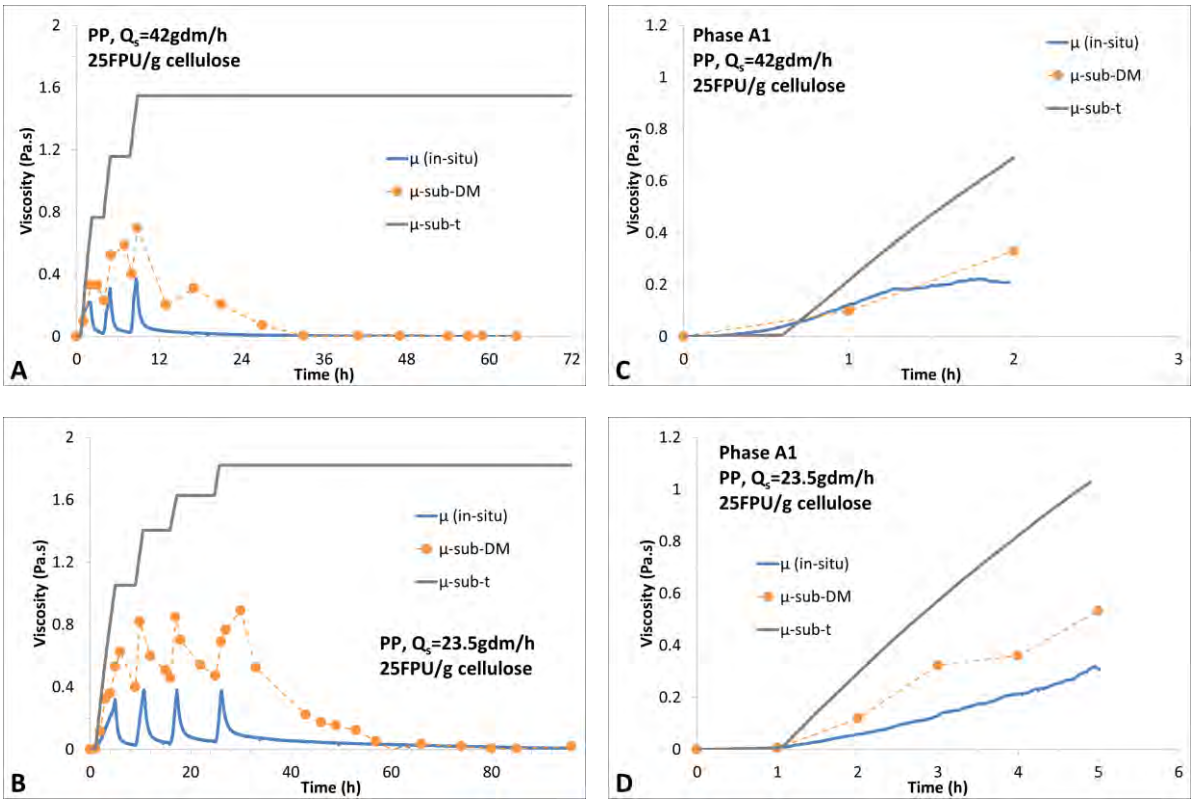

Figure 3-61. Estimated and in-situ viscosities as a function of time and different feeding rates and E/S ratios with PP. (A, B: whole experiments, C, D: focus on A1 stage)

3.3.2.3 Focus and analysis on hydrolysis stage (Hi)

Dimensionless viscosity μ^* (**Eq. 3-13**) and dimensionless hydrolysis time t^* (**Eq. 3-16**) were used again to investigate the liquefaction kinetics. **Figure 3-62A & B** compare the magnitude of viscosity reduction between different non-feeding stages for two fed-batch enzymatic hydrolysis of SCB and PP under similar conditions (Qs = 23.5 gdm/h, E/S = 25 FPU/g cellulose). Illustrations for others fed-batch hydrolysis with SCB and PP are presented in **Appendix 7**. It was clearly observed that, the required time for 75 % viscosity reduction, $t_{0.25}$, increased after each feeding stage. The increasing trend was exacerbated at low feeding rate and high E/S ratios. This observation suggested an accumulation of recalcitrant fraction during fed-batch enzymatic hydrolysis that led to the $t_{0.25}$ increase. .

Previously the dimensionless viscosity-time curves $\mu^* = f(t^*)$ at different enzyme loading ratios for each substrate (FP and PP) were illustrated in **Figure 3-26**. During the non-feeding phase of fed-batch hydrolysis, very similar relationship between μ^* and t^* was observed. All $\mu^* = f(t^*)$ curves during non-feeding stage (Hi) were superimposed, confirming the similar reaction mechanism with SCB and PP whatever E/S ratios and feeding rates were (**Figure 3-62C, D**).

To compare the liquefaction efficiency between batch and fed-batch strategy, **Figure 3-63** reported $t_{0.25}$ as a function of and initial dry matter content with SCB and PP. For fed-batch strategy, the $t_{0.25}$ values were calculated separately for each non-feeding stage (H1 to H3) considering the theoretical dry matter content at the beginning of the phase. In general, fed-batch strategy alleviated the liquefaction rate by decreasing required time for 75 % viscosity reduction at given substrate concentration whatever tested E/S ratio.

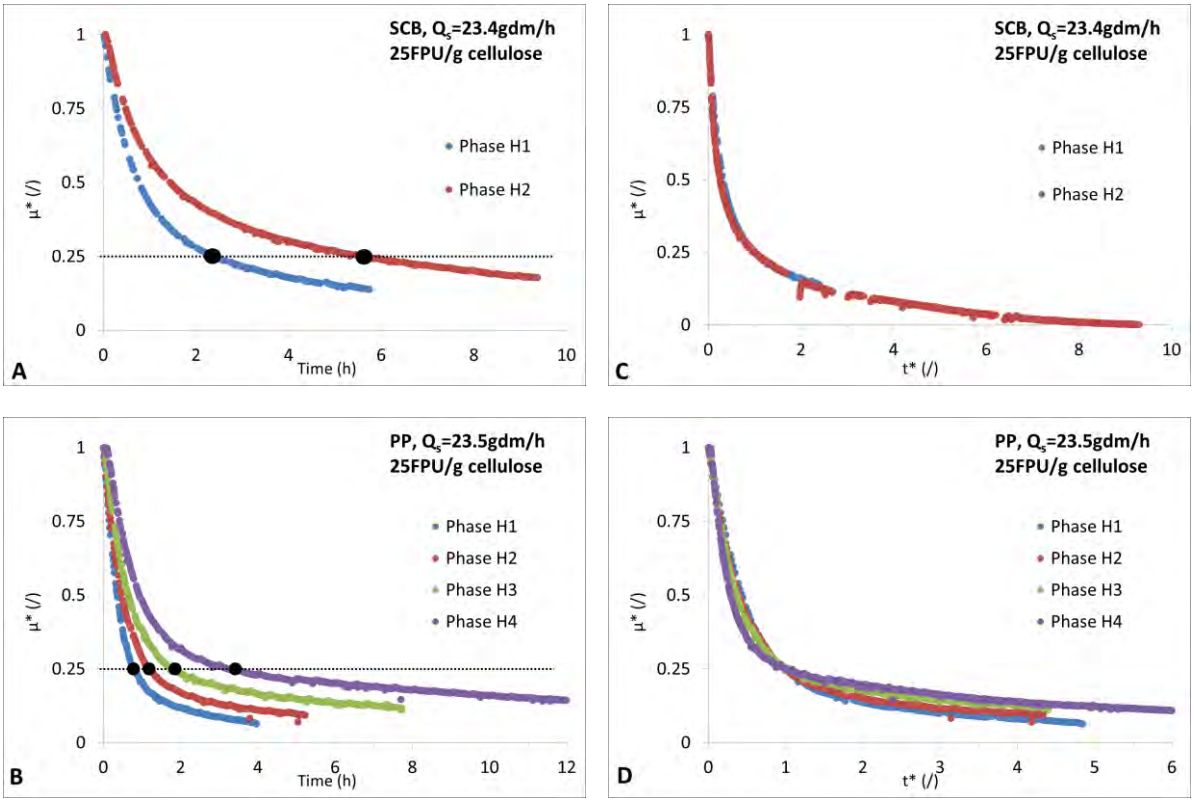

Figure 3-62. Dimensionless viscosities, μ as a function of time (A, B) and normalized time, t*(C, D) with SCB (A,C) and PP (B, D) during non-feeding stages (Hi). Black dots (●) indicate the 75 % viscosity reduction (Qs= 23.5gdm/h, E/S=25 FPU/g cellulose).*

For example, with batch hydrolysis at 3 FPU/g cellulose, $t_{0.25}$ was equal to 6.5 h for a suspension of 30 gdm/L for SCB. In fed-batch strategy, similar $t_{0.25}$ values were reported for substrate concentrations equal to 80 and around 110 gdm/L at low and high feeding rates. At high enzyme loading ratio (25 FPU/g cellulose), this effect was exacerbated. An increase by 4-folds in substrate concentrations (from 30 to 115 gdm/L) was observed for $t_{0.25}$ = 3 h between batch and fed-batch hydrolysis.

Similar trend was observed for PP comparing batch and fed-batch hydrolysis. The time needed for 75 % viscosity reduction was 2.5 h for batch hydrolysis at 30 gdm/L and 3 FPU/g cellulose. Considering fed-batch hydrolysis, duration 2.5 h was enough to liquefy a suspension of concentration around 45 gdm/L

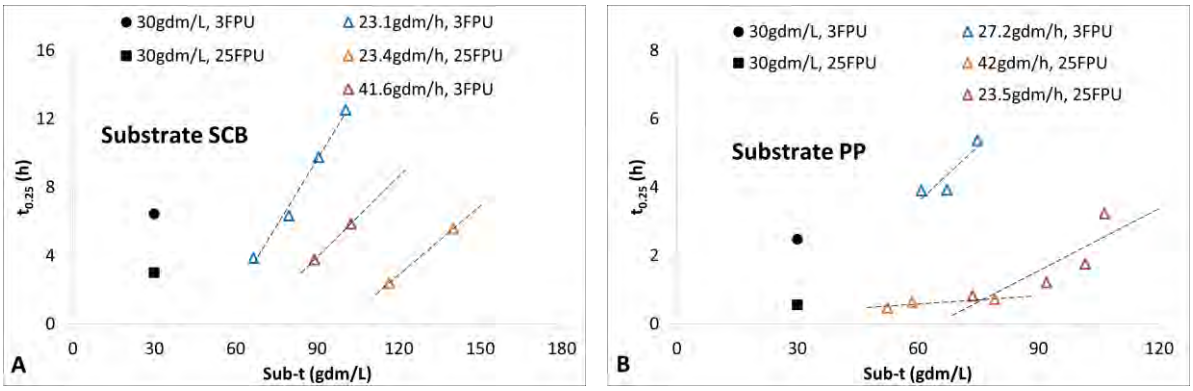

Figure 3-63. Time for 75 % viscosity reduction as a function of initial substrate concentration for batch and fed-batch hydrolysis with SCB (A) and PP (B).

3.3.2.4 In-situ viscosity modeling

Fed-batch hydrolysis may be simplified by considering successive feeding and non-feeding stages. Each non-feeding stage (Hi) can be assimilated to individual batch stage. Previously the viscosity modeling of batch hydrolysis was performed (**§3.2.2.4**) using order n equation (**Eq. 3-11**). Through three different enzyme-to-substrate ratios, there were no common value of reaction order; n was ranged between 0.9 and 1.3. In the specific case when n equals to 1, the 1st kinetic model showed goof ability to accurately predict suspension viscosity. Besides, the coefficient $k_{visco-1}$ and $k_{visco-2}$ seemed to be in proportion with E/S ratio.

$$\frac{d(\mu - \mu_s)}{dt} = k_{visco-3} \cdot (\mu - \mu_s)^{n'} \qquad \textit{Eq. 3-22}$$

In the same way, two models (1st order and order n' kinetics) were used in fed-batch strategy (**Eq. 3-22**). The viscosity μ is defined as the difference between suspension and solvent (water) viscosities, $\mu_{m-}\ \mu_s$, which corresponds to the variation potential, $k_{visco-3}$ is the kinetic constant ($Pa^{1-n}.s^{-n}$) and n' is the model order (/). Besides, a particular case of **Eq. 3-22,** when n' equals to 1 leading to the exponential equation (1st order kinetics). In this model, $k_{visco-4}$ is the only coefficient to be determined. Parameters of the two models were adjusted by least squares method of μ using solver tool (Microsoft Excel ®).

For the feeding stage, it was observed through 6 fed-batch experiments that except for the first stage (A1) where the plot of *in-situ* viscosity *versus* time showed a concave curve, all others feeding stages witnessed a linear relationship with time. The viscosity modeling for feeding stages was then performed by considering the linear increase from μ_{start} to μ_{fin} (measured viscosity at the beginning and at the end of feeding stage).

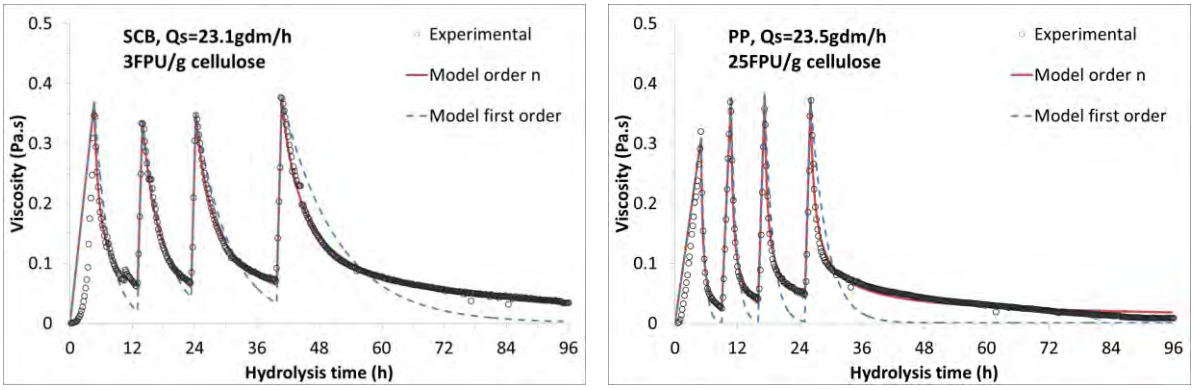

Figure 3-64. In-situ viscosity modeling as afunction of time for SCB, Qs= 23.1 gdm/h, E/S=3 FPU/g cellulose (A) and PP, Qs= 23.5 gdm/h, E/S=25 FPU/g cellulose. Experimental data were limited to 1 point per 12 minutes to facilitate reading

The plots of predicted versus experimental values are presented in **Figure 3-64** for the fed-batch hydrolysis of SCB at Q_s = 23.1 gdm/h, E/S ratio 3 FPU/g cellulose (A) and for PP at Q_s = 23.5 gdm/h, E/S ratio 25 FPU/g cellulose. The parameters of best fitted models were summarized in **Table 3-10** and compared with batch modeling.

Table 3-10. Identified kinetics parameters for in-situviscosity of fed-batch hydrolysis compared with batch

			Model order n			Model 1st order	
	μ_0 (Pa.s)	$t_{0.25}$ (h)	$k_{visco-3}$ ($Pa^{1-n}.s^{-n}$)	n' (/)	R^2	$k_{visco-4}$ (s^{-1})	R^2
SCB, Q_s = 23.1 gdm/h, E/S ratio 3 FPU/g cellulose							
Phase H1	0.37	3.85	3.50	2.36	0.991	0.35	0.753
Phase H2	0.34	3.25	0.50	1.50	0.994	0.22	0.969
Phase H3	0.35	10.5	0.73	1.94	0.993	0.15	0.897
Phase H4	0.38	12.2	0.75	2.17	0.997	0.09	0.829
PP, Q_s = 23.5 gdm/h, E/S ratio 25 FPU/g cellulose							
Phase H1	0.31	0.87	7.12	1.85	0.990	1.41	0.863
Phase H2	0.37	1.29	5.64	2.03	0.989	0.96	0.762
Phase H3	0.38	1.48	6.67	2.36	0.986	0.65	0.640
Phase H4	0.38	2.83	5.64	2.60	0.978	0.32	0.509
PP, 30 gdm/L, 25 FPU/g cellulose (batch)							
	0.32	0.53	3.09	1.13	0.998	2.52	0.997

Generally, the model order n accurately described the time dependence of suspension viscosity as values of $R^2 > 0.99$ for all non-feeding stages. A common value of n was not observed for different non-feeding stages. It was observed that n dispersed around 2 for both SCB and PP while for batch hydrolysis, this value was around 1. This explained why the 1st order kinetic model can accurately predict viscosity of batch hydrolysis but it was no longer adapted for fed-batch hydrolysis. The 1st order model was less accurate than the order n model with R^2 ranged from 0.51 and 0.97 for different feeding stages. According to the **Figure 3-64**, it seemed that 1st order model usually failed to predict low viscosity value. Both coefficient k and n showed an increasing trend with non-feeding stage except for the phase H1 of SCB. As expected for the feeding stage A1, the linear plot of $\mu = f(t)$ was not able to follow experimental

points. However for the next three feeding stages, this plot was perfectly fitted with all measured data points. This can be explained by the quick increase in substrate concentration in a short time that led to a linear increase of suspension viscosity. This short time period did not allow observing the impact of enzymatic actions on suspension viscosity.

3.3.2.5 Energy consumption for mixing

The energy consumption was estimated from measured torque and mixing rate using **Eq. 2-26**. Results were presented in **Figure 3-65** for SCB and PP at different feeding rates.

For fed-batch hydrolysis of SCB, it was observed that higher E/S ratio led to lower energy consumption for mixing at low feeding rates ($Q_s \approx 23.5$ gdm/h). At t = 48 h, the cumulative energy consumption at 25 FPU/ g cellulose was 8.2 kJ compared to approximately 13 kJ for the experiment at 3 FPU/ g cellulose. This result was correlated with the viscosity profile of these experiments during fed-batch hydrolysis (**Figure 3-59**). In the opposite, the role of feeding rate was nearly negligible at 3 FPU/g cellulose. Two experiments at 41.6 and 23.1 gdm/h showed nearly similar cumulated energy consumption curves. The phenomenon can be explained by the low dependency of suspension viscosity on substrate concentration for SCB as previously reported (**Figure 3-8**).

Opposite phenomenon was observed for fed-batch hydrolysis of PP; at 25 FPU/g cellulose, the experiment at high feeding rate (42 gdm/h) showed nearly twofold less energy consumption compared to low feeding rate (27.2 gdm/h). This demonstrated the dominant role of feeding rate on energy consumption. The result was in coherence with the rheological properties of PP with strong dependency of suspension viscosity on substrate concentration (**Figure 3-8)**. Besides at low feeding rate (23.5 and 27.2 gdm/h), similar energy consumption profiles were reported despite the 8 times different in E/S ratio (3 *versus* 25 FPU/g cellulose) in the first 36h of hydrolysis. This can be explained by the fact that at 3 FPU/g cellulose, the liquefaction was significant weaker compared to 25 FPU/g cellulose. As the process was controlled by maximal torque monitoring, it led to a shorter feeding stage and longer non-feeding stage. Consequently, the cumulative quantity of substrate fed at t = 36 h was only 67.3 g/L for this experiment compared to 113 g/L at 25 FPU/g cellulose.

Through the fed-batch hydrolysis of SCB and PP, it was proven that substrate properties had strong impact on energy consumption for mixing. The low suspension viscosity of SCB at given substrate concentration induce weak impact of feeding rate on energy consumption. In opposite, for the substrate that had strong viscosity-concentration relationship like PP, the high feeding rate is not recommended.

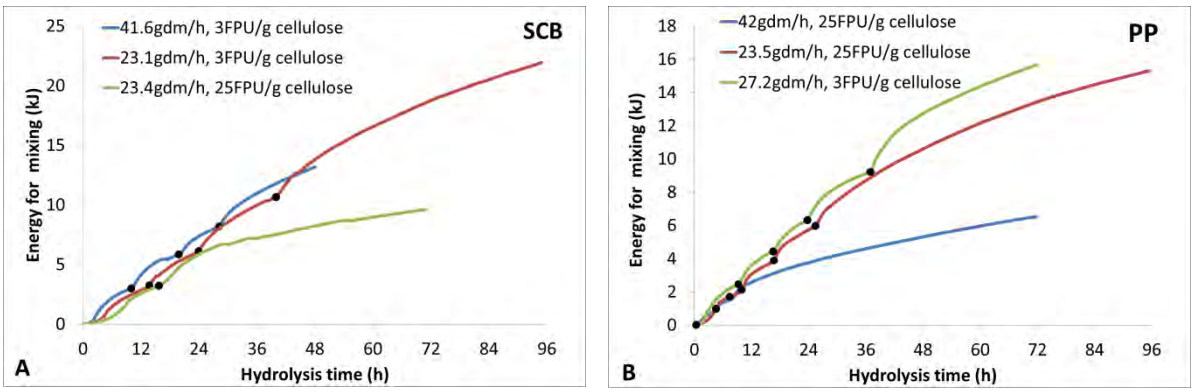

Figure 3-65. Cumulated energy consumption for mixing for fed-batch hydrolysis of SCB (A) and PP (B) as a function of differents time, feeding rates and E/S ratios. Black dots (●) indicate the start of feeding stages.

In order to evaluate the process efficiency in term of energy, **Figure 3-66** compares the energy consumption per 1 g of glucose released at total substrate loading 100 gdm/L. According to this graph for both SCB and PP, it was observed that higher feeding rate led to lower energy consumption at same E/S ratio (3 FPU/g cellulose for SCB and 25 FPU/g cellulose for PP). From the previous discussion (**§3.3.1.3**), higher feeding rate resulted in better solubilization efficiency and consequently lower suspension viscosity. As the energy consumption for mixing depends on suspension viscosity, it was in good coherence when low suspension viscosity led to low energy consumption. Obtained results from biochemical and physical analysis were in good agreement.

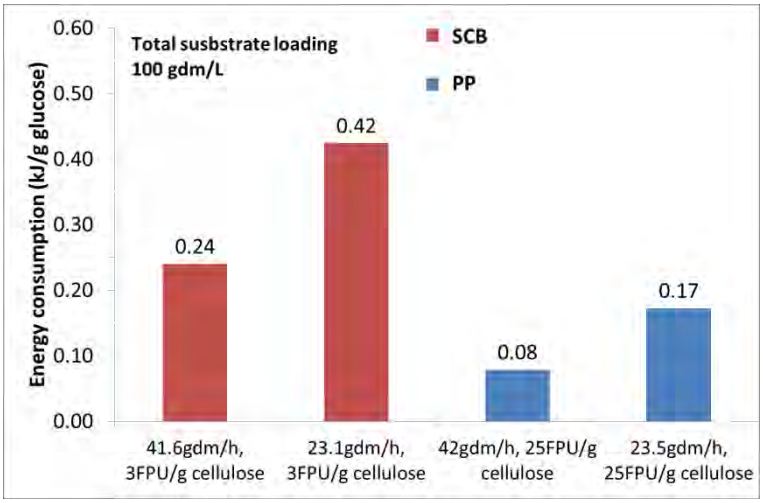

Figure 3-66. Energy consumption during fed-batch hydrolysis of SCB and PP at final substrate loading 100 gdm/L.

3.3.3 Evolution in particle size and morphology

In our fed-batch strategy including feeding and non-feeding stages, the evolution of particle morphology is probably the most complex information to interpret. In a similar way to batch mode, an insight about particle size and morphology is reported through three analytical methods: diffraction light scattering (DLS), optical morphogranulometry (MG) and *in-situ* focused beam reflectance measurement (FBRM).

MG qualitatively illustrated particle morphology and their evolution. The DLS reported Ev(d_{SE}) which focused on the fraction of coarse population. FBRM reported En(lc) which highlighted the fraction of fine population with two indicators: total chord count (N_c) and mean chord length (lc).

3.3.3.1 Morpho granulometry

Morpho-granulometry provides information about particle size, shape and particle opacity. In fed-batch hydrolysis, due to evolution of substrate concentration and internal age of particles, the amount and age of observed particles strongly evolved. **Figure 3-67** illustrated standardized observations of SCB suspension during fed-batch hydrolysis at Q_s = 25 gdm/h and E/S ratio = 25 FPU/g cellulose. These microscopic observations were performed under dark field conditions which allowed recognizing the finest particles. For a better visual, only 25 % of observed area was presented in these figures. A constant dilution rate equal to 1/10 was applied in order to observe the impact of feeding and solubilization mechanism. Between t = 1 h and t = 9 h (phase A1), the increase in particle number was clearly observed. SCB suspension contained both fine particles and coarse fibers which were individual or in agglomerates. From t = 9 h to t = 15 h (phase H1), most of the coarse fibers were disappeared, suspension contained

the majority of smaller fragments. Also, agglomerates were rarely found in the observation area. This observation was correlated with the viscosity collapse (**Figure 3-59**) and the reduction in the fraction of coarse population (**Figure 3-69 – H1**). From t = 15 h to t = 19 h when the second feeding was performed, the increase in number of particle was clearly observed. This was then followed by the decrease trend until t = 72 h. At the end of hydrolysis, few coarse particles were observed. They were likely the recalcitrant fraction, which is the most resistant to enzymatic digestion. For others fed-batch experiments of SCB, the optical observation of suspensions can be found in **Appendix 8** and **Appendix 9**.

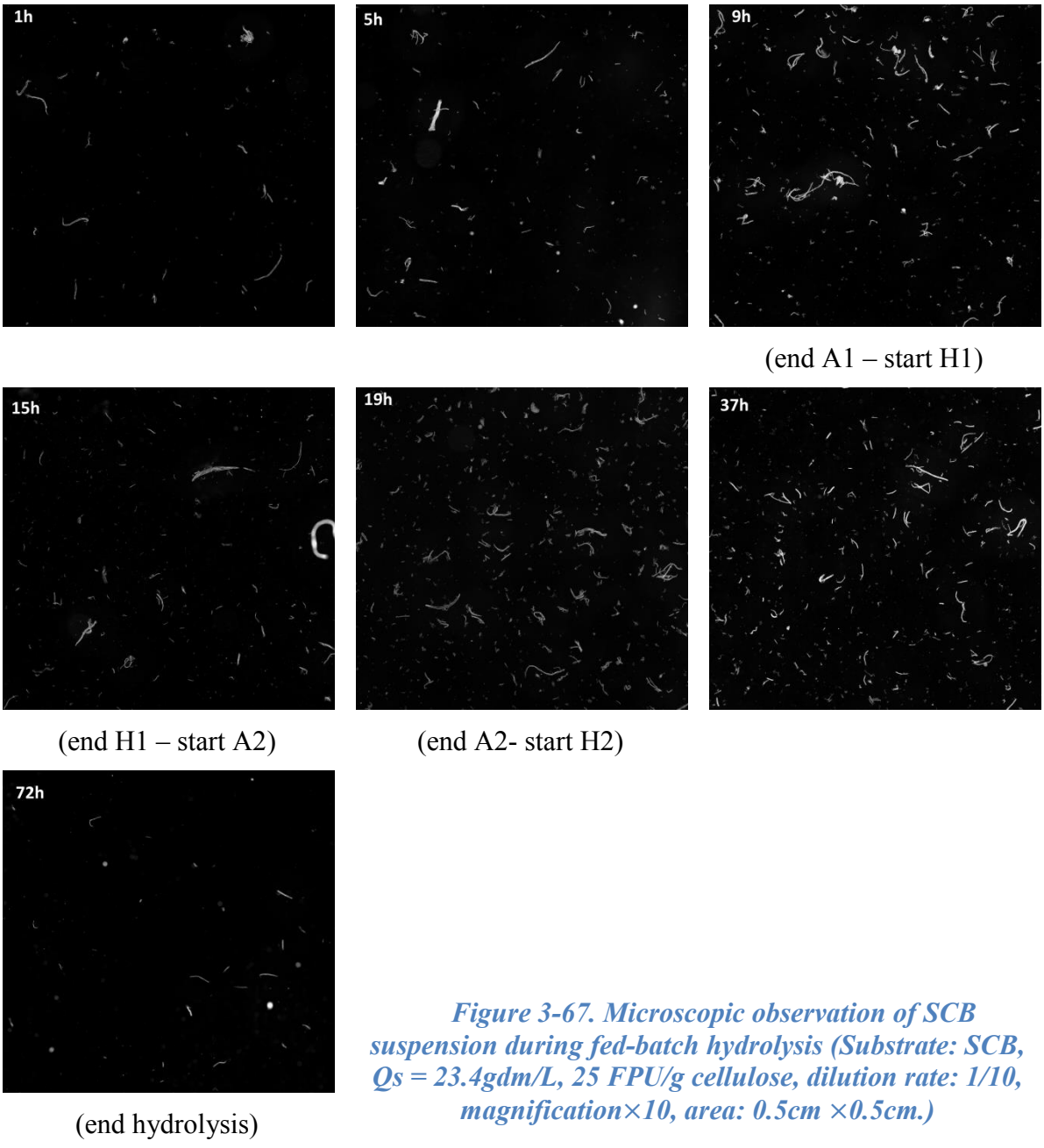

Figure 3-67. Microscopic observation of SCB suspension during fed-batch hydrolysis (Substrate: SCB, Qs = 23.4gdm/L, 25 FPU/g cellulose, dilution rate: 1/10, magnification×10, area: 0.5cm ×0.5cm.)

3.3.3.2 Focus on fine population: En(l_c)

As previously described, FBRM sensor enables on-line tracking of particle chord length and chord count during enzymatic hydrolysis. However operating conditions (mixing rate, suspension viscosity) which affect flow pattern may also influence the count number. Unlikely batch hydrolysis at semi-dilute condition, during fed-batch enzymatic hydrolysis, the strong

variation in suspension viscosity restricted the interpretation of total chord number. The only reliable parameter was particle mean chord length, which was interpreted and illustrated in **Figure 3-68** as a function of hydrolysis time.

It is important to remind that, mean chord length was affected by several factors and mechanisms during fed-batch hydrolysis:

- The fragmentation of coarse fibers leads to an increase in total chord number and consequently a decrease in mean chord length.
- The solubilization of fine particle leads to an increase in mean chord length.
- The feeding of substrate, in particular, can affect the mean chord length by two opposing ways. If the fresh substrate had higher mean chord length than that of the slurry, feeding will raise the suspension mean chord length and *vice versa*.

In our case, the effect of feeding was corresponded to the first possibility for fed-batch hydrolysis of both SCB and PP. It can be observed that l_c exhibited an increasing trend during feeding stage and a decreasing trend during non-feeding stage. The increasing trend of l_c during feeding stage indicated an increase in particle size corresponding to the impact of added substrate. In the other hand, the decreasing trend of l_c during non-feeding stage reflected the impact of fragmentation mechanism.

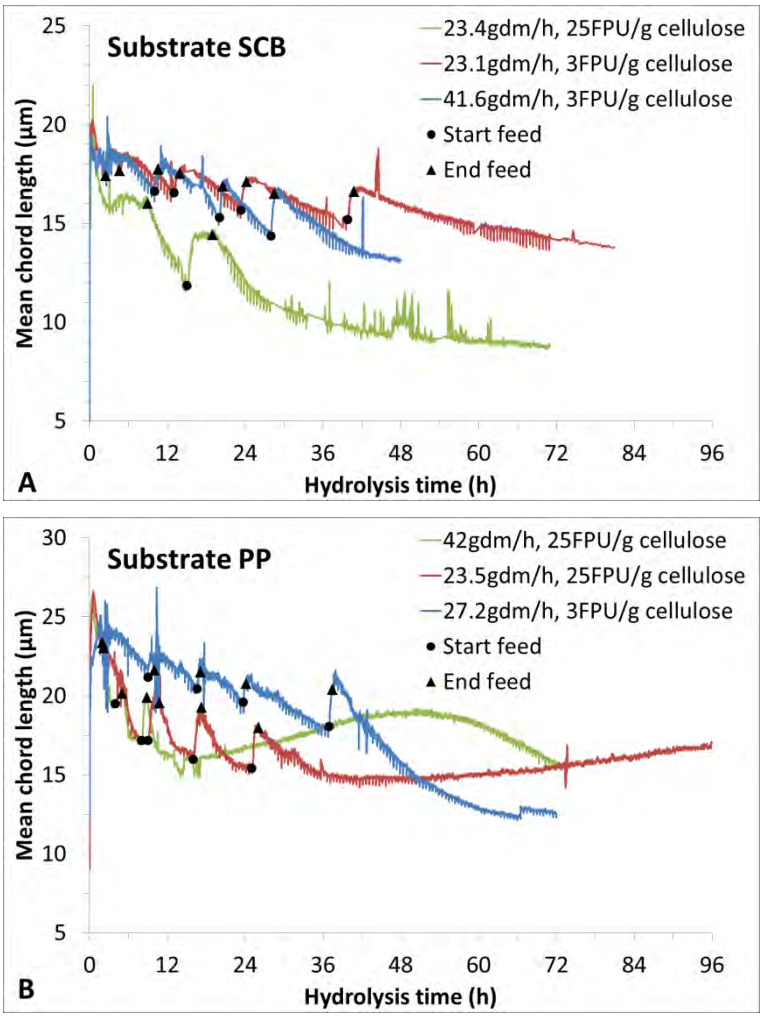

Figure 3-68. Suspension mean chord length as a function of hydrolysis time for SCB (A) and PP (B) at different feeding rates and E/S ratios.

Focusing on the fed-batch hydrolysis at Q_s = 23.4 gdm/L and enzyme loading ratio 25 FPU/g cellulose, the drop rate of l_c in phase H1 was very similar as the first 6 h of the phase H2. Rheological analysis reported approximately 75 % viscosity reduction at these points (**Figure 3-59**). It is suggested that the fragmentation of coarse population which is observed through DLS measurement (**Figure 3-69**) was responsible for the drastic drop in l_c. Then for the phase H2, l_c seems to be stabilized between t = 36 h and t = 72 h corresponding to the period with small variation in both suspension viscosity and fraction of coarse population. This stabilization can be explained by the strong impact of solubilization mechanism at the end of hydrolysis that maintains equilibrium with fragmentation mechanism.

Interestingly for PP suspension, an increasing trend in l_c was observed for Qs = 23.5 gdm/h, 25 FPU/g cellulose from t = 42 h till the end of hydrolysis (**Figure 3-68B**). This increase in l_c can be only explained by a dominant effect of solubilization mechanisms compared to the fragmentation one. From dry matter content analysis (**Figure 3-57**), this experiment witnessed a strong decrease between t = 26 h and t = 60 h then the decreasing trends became weaker until t = 96 h. The effect of solubilization mechanism was then demonstrated. Besides, the suspension viscosity within the period t = 48 h to t = 96 h was nearly stable (**Figure 3-59B**), reflecting no significant fragmentation of coarse population. Both ex-situ biochemical and in-situ viscometry analyses were in good agreement with FBRM result. Similar evolution of l_c was also reported for Qs = 42 gdm/h, 25 FPU/g cellulose from t = 16 h to t = 48 h before the regular decreasing trend took place.

3.3.3.3 Focus on coarse population: Ev(d_{SE})

The evolution of $E_v(d_{SE}) \cdot \Phi_v$ were illustrated for SCB at high enzyme loading (25 FPU/g cellulose) and low feeding rate (Q_s = 25 gdm/h) in **Figure 3-69**. The trends of $E_v(d_{SE}) \cdot \Phi_v$ curves were in agreement with viscosity profile during enzymatic digestion. The changes mainly occurred for particles size between 10 and 200 µm. An increasing of 4.6 folds in $E_v(d_{SE}) \cdot \Phi_v$ for the fraction of 10 < d_{SE} < 200 µm between t = 1 h and t = 9 h was reported (**Figure 3-69** phase **A1**). It corresponded to the evolution in substrate concentration from 27.9 gdm/L (t = 1 h) to 86.3 gdm/L (t = 9h). From 9 h to 15 h, $E_v(d_{SE}) \cdot \Phi_v$ witnessed a significant decrease, the population of coarse particle were strongly reduced while fine population seems to be fairly affected by enzymatic digestion. The evolution in particle size distribution of coarse population corresponded with the viscosity collapse (**Figure 3-59** phase **H1**). This was in good agreement with the last conclusion from semi-dilute experiment, stating that the fraction of coarse particle was determinant of suspension viscosity. In the other hand, biochemical analysis proved the solubilization mechanism during the first feeding stage (**Figure 3-50**). Consequently, the stable state of fine population reflected an equilibrium between two mechanisms: solubilization and fragmentation. Beyond 15 h, very similar trends were observed with an increase in $E_v(d_{SE}) \cdot \Phi_v$ during feeding stage and a decrease during non-feeding stage. The changes were principally occurred in the coarse size population.

It was observed that only during the first feeding stage (A1), the evolution in $E_v(d_{SE}) \cdot \Phi_v$ was more pronounced for fine population than for coarse population (**Figure 3-69** phase **A1)**. It can be assumed for the strong fragmentation at the beginning of enzymatic digestion led to an increase in population of fine. For both experiments at 3 FPU/g cellulose at Q_s = 23.1 and 42 gdm/L (**Appendix 10** and **Appendix 11**), the evolution in $E_v(d_{SE}) \cdot \Phi_v$ was clearly less pronounced compared to 25 FPU/g cellulose. However, it always showed similar increasing or decreasing trend corresponding to feeding or non-feeding stage and in good agreement with the evolution in total dry matter content.

For fed-batch hydrolysis of PP, similar interpretation of $E_v(d_{SE}) \cdot \Phi_v$ was performed strengthening the assumption drawn from experiments with SCB. Detailed profiles of $E_v(d_{SE}) \cdot \Phi_v$ for PP can be found in **Appendix 12** and **Appendix 13**.

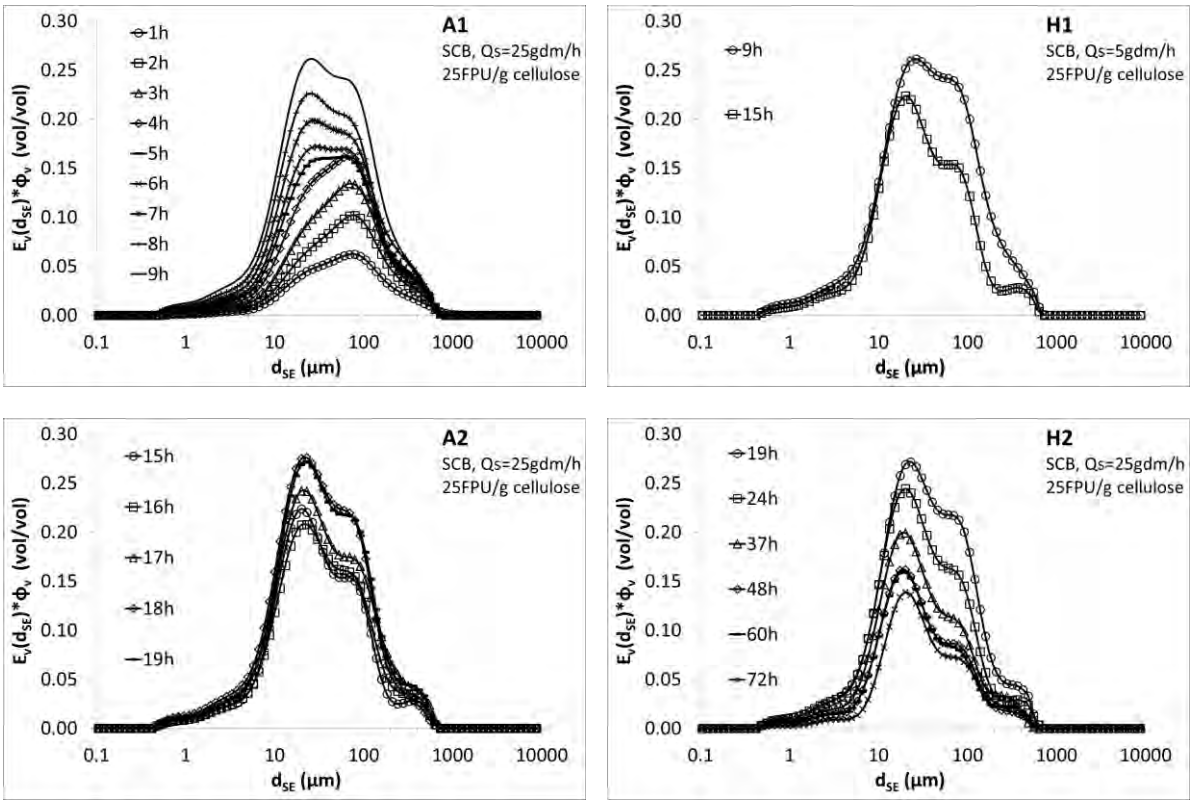

Figure 3-69. Evolution of distribution functions pondered by particle volume fraction, $E_v(d_{SE}) \times \Phi_v$ as a function of feeding and non-feeding stages during fed-batch hydrolysis of SCB (Qs = 23.4 gdm/L, 25 FPU/g cellulose)

Through PSD analysis, the objective was to explain the observed phenomenon from rheological standpoint (**Figure 3-60**) when the suspension viscosity cannot be explained by only biochemical analysis (dry matter content). For all experiments, results from DLS measurement confirmed the evolution of substrate concentration in correlation with the viscosity reduction during the first feeding stage. For the experiments at low enzyme loading (3 FPU/g cellulose) and in final non-feeding stage (H4), in-situ measurement showed a strong reduction in suspension viscosity by more than 90 % while substrate concentration fairly decreased during this period. From DLS measurement, an evolution in PSD for coarse population was observed, showing a decreasing trend. As coarse particles was demonstrated to be the predominant factor affecting suspension viscosity during enzymatic hydrolysis at semi-dilute condition, the observed phenomenon from rheological and biochemical aspects (suspension viscosity and dry matter content) were in good agreement with DLS results (evolution of coarse population). The drop in viscosity during phase H4 was principally determined by the fragmentation of coarse population rather than the solubilization mechanism.

The evolutions in volume weighted diameters during fed-batch hydrolysis were illustrated in **Figure 3-70** for SCB at different feeding rates and enzyme loading ratios. Except for some fluctuation due to substrate feeding, the evolution of $d_v(0.9)$, $d_v(0.5)$, and d(4,3) reported very similar trends, exhibited a strong decrease in the first stage of hydrolysis then followed by a steady state until the end of experiment.

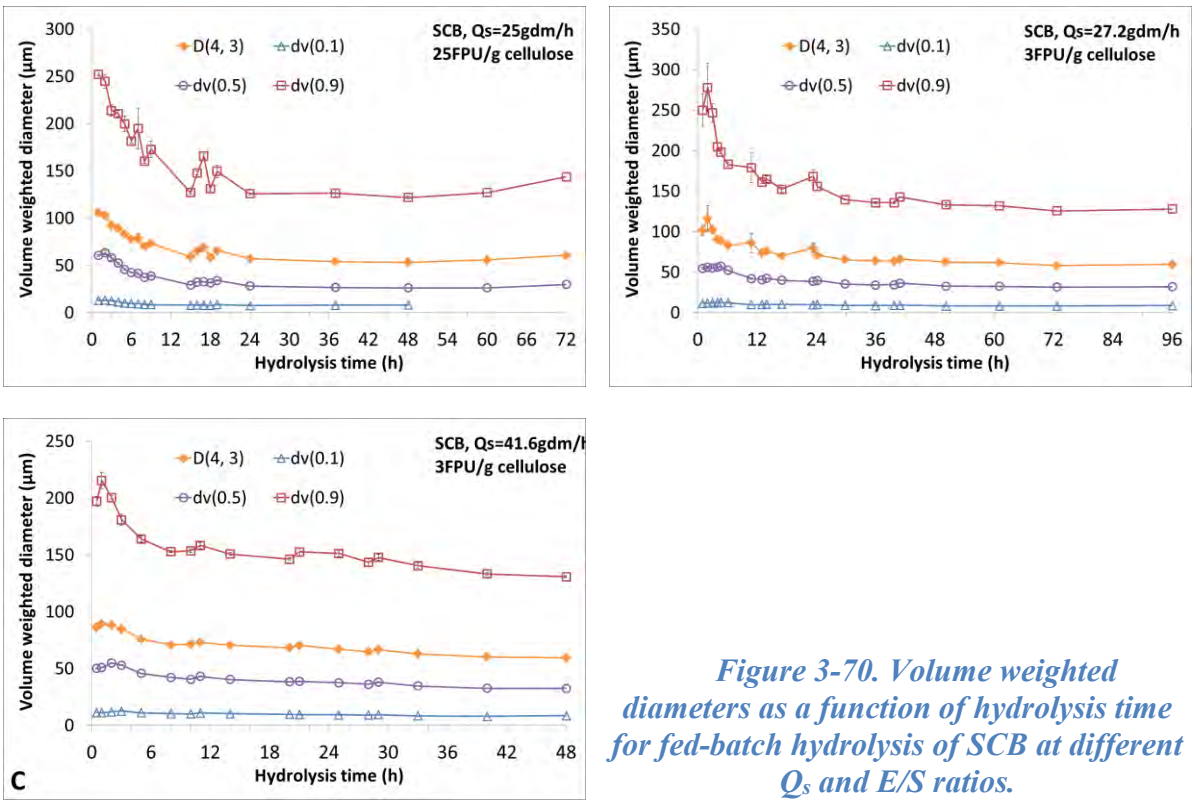

Figure 3-70. Volume weighted diameters as a function of hydrolysis time for fed-batch hydrolysis of SCB at different Q_s and E/S ratios.

At low feeding rate and low enzyme loading ratio (3 FPU/g cellulose), an increase in $d_v(0.9)$, $d_v(0.5)$, and d(4,3) were observed between t = 1 h and t = 2 h. Beyond t = 2 h until the end of feeding stage A1, these volume weighted parameters exhibited a quick decreasing trend. In contrast, at high enzyme loading ratio (25 FPU/g cellulose), only the decreasing trend was observed during the first feeding stage (A1). Observed results from these two feeding stages reflected the impact of enzyme loading on particle size modification. At high enzyme loading, the substrate adding was not enough strong to compensate the enzymatic digestion, resulted in a decrease in $d_v(0.9)$, $d_v(0.5)$, and d(4,3). At low enzyme loading and similar feeding rate, the increase in $d_v(0.9)$, $d_v(0.5)$, and d(4,3) between t = 1 h and t = 2 h indicated the weaker impact of enzymatic digestion.

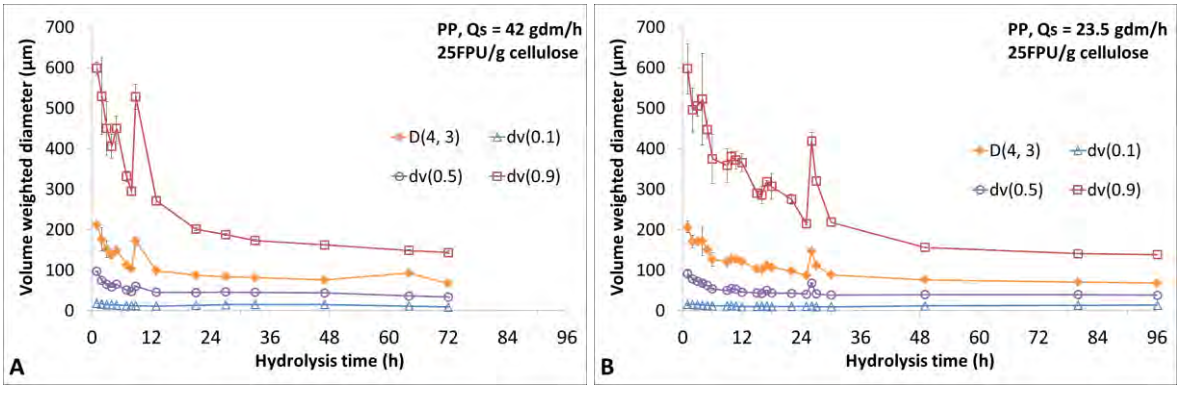

Figure 3-71. Volume weighted diameters as a function of hydrolysis time for fed-batch hydrolysis of PP at different Q_s and E/S ratios.

For PP, **Figure 3-71** illustrates the evolution in $d_v(0.9)$, $d_v(0.5)$, $d_v(0.1)$ and d(4,3) during fed-batch hydrolysis at E/S ratio equals to 25 FPU/g cellulose and different feeding rate (Q_s = 23.5 and 42 gdm/h). Similar strong decreasing trends were observed for $d_v(0.9)$, $d_v(0.5)$, and

d(4,3) during the first 24 h following by a nearly steady state. Except for two large peaks corresponding to feeding at nearly 12 h (**Figure 3-71A**) and after 24 h (**Figure 3-71B**), the rate of size reduction for coarse particles, $d_v(0.9)$, seemed to be quicker at higher feeding rate (42 gdm/h). This was in agreement with the viscosity profile that previously described (**Figure 3-59B**).

Highlights for fed-batch hydrolysis

- Glucose production during fed-batch hydrolysis was only affected by enzyme to substrate ratio.
- Final glucose yield reached superior than 65% for both PP and SCB through fed-batch hydrolysis.
- Both fragmentation and solubilization mechanisms contribute to the liquefaction at concentrated regime.
- Accumulation of recalcitrant fraction leads to the growth in liquefaction time during fed-batch hydrolysis
- Uniqueness viscosity – time curves were demonstrated through different non-feeding stages of fed-batch hydrolyses of SCB and PP
- Suspension viscosity during fed-batch hydrolysis was modelled using order n equation with good accurate.
- A rational definition of the critical feeding rate for fed-batch hydrolysis was proposed and validated for of SCB and PP at Qs ranged from 23 to 42 gdm/h (final substrate concentration 74 to 140 gdm/L).
- Energy consumption for mixing strongly depends on enzyme loading ratio for SCB while for PP, feeding rate plays the more important role.

4 CONCLUSIONS AND PERSPECTIVES

In this final chapter, a short summary of scientific context and challenges is firstly reminded. Afterwards, the research strategy and scientific goals are briefly summed up. Then, the main elements related to materials & method, substrates & enzymes characterizations, semi-dilute batch and concentrated fed-batch hydrolyses are reported. Finally, some perspectives are shortly discussed.

- Scientific context

In recent years, studies to substitute the energy from fossil sources have been taken. Second generation biofuels are a promising solution as they can reduce greenhouse gas emissions; open a way to valorize agriculture and industrial by-products without the concern of food security. The feedstock for 2nd generation biofuels is lignocellulose material, which is the most abundant resource in the world. Thus, the efficient and sustainable use of biomass resources, which is of paramount importance, can be enhanced by the application of biorefinery concept.

The biorefinery is the integral upstream, midstream and downstream processing of biomass into a wide range of products. Several steps are required such as pretreatments (mechanical, thermochemical, biological…), enzymatic or chemical conversions and microbial conversions (fermentation both aerobic, anaerobic). In order to achieve a viable economy, the process must be performed at high substrate concentration and large (industrial) scale. In addition, substrates should be compatible with a realistic industrial scale (feedstock quantity, limited territory between production and transformation, compatibility with pretreatment and bioprocess). Beyond, these specifications introduce several challenges related to life science and bioprocess engineering (substrate pretreatment, enzyme design, selection and identification, physical and biochemical knowledge of substrates, identification of robust and efficient strains, downstream process, and scale up strategy…). Among these challenges, the physical aspects (mass, heat and momentum transfers within bioreactor, energy consumption and reactor and impeller designs) in relation with substrate hydrolysis constitute our scientific interest. These issues can comfort conventional biochemical approach. Thus, the development of rheological and morphological methodology to characterize the enzymatic hydrolysis may contribute to understand bioprocess efficiency (bio-kinetics, mixing and transfers).

- Scientific questions

In this thesis, investigations were conducted on lignocellulose hydrolysis with a special focus on the physical aspects involved in transfers limitations which become increasingly acute as substrate concentration increases. This was addressed through analysis of the rheological and morpho-granulometry study of complex lignocellulosic substrates during enzymatic digestion. Selected substrates were industrial realistic feedstock in France (paper pulp) and in Vietnam (sugarcane bagasse) and a cellulose reference (filter paper). Hydrolysis mechanisms were scrutinized with single activity enzymes and a lignocellulolytic cocktail from semi-dilute batch up to concentrated fed-batch conditions. In this framework, the scientific questions were:

- How do the rheological behaviors and the morphological properties of suspensions impact the transfer limitations and the hydrolysis efficiency?
- Which mechanisms act during the degradation of substrates?
- What are the impacts of biochemical composition and physical structure of substrates?
- Can the contribution of single activity enzymes be quantified by a physical approach?
- How to define in a rational way the feeding conditions (substrate & enzymes) to control and optimize fed-batch process?

- Experimental setup & analyses

Considering materials, home-designed reactor and impellers were developed and integrated in a multi-instrumented setup including specific sensors and actuators such as viscometer, focused beam reflectance, Archimedean pump; Biostat-B ... It allowed to carry out enzymatic hydrolysis under well controlled conditions and to follow the real-time changes in suspension viscosity and chord length distribution via *in-situ* measurements. In addition, several *ex-situ* physical and biochemical analyses were realized. This experimental setup was supervised by specific software named *Pilote_HTMS*. It performed multiple functions such as: (i) the process control during enzymatic hydrolysis, (ii) the feeding of substrate and enzymes, (iii) the data acquisition and graphical plotting of parameters during experiment.

- Research strategy

PhD overview (**Figure 4-1**) considers four principal branches: bibliography, materials, experiments and analysis. Considering our scientific aims, the three lignocellulosic substrates (filter paper – FP, paper pulp – PP and sugarcane bagasse – SCB) represent different levels of biochemical and physical complexity. In a preliminary step, the hydrodynamic identification of experimental setup was realized (power consumption curve, identification of geometrical parameters). Then the substrates and their suspensions were characterized by their physical properties such as density, particle size distribution and morphology, suspension viscosity. In the same way, enzyme activities and their thermostability were investigated.

In a second step, the enzymatic hydrolysis in batch mode was scrutinized under semi dilute condition (1.5 to 3 %w/v). This choice allowed introduction of particle-particle interactions which are implied in transfer limitations, but without the highest complexity of high dry matter contents. This controlled complexity enabled further exploration of the physical limitations during hydrolysis of cellulosic substrates. Enzyme to substrate ratio was varied from low (0.3FPU/g cellulose) to high level (25 FPU/g cellulose). The composition of enzyme mixture was also investigated from single (endo-glucanase or endo-xylanase alone), double (exo-glucanase + β-glucosidase) and triple (endo-glucanase + exo-glucanase + β-glucosidase) activities to cocktail (Cellic Ctec 2, Multifect Xylanase) of activities.

In the third step, the fed-batch hydrolysis of industrial lignocellulosic substrates (PP and SCB) using commercial cocktail (Ctec2) was carried out up to 100 gdm/L and 140 gdm/L respectively. The goal was here to evaluate the hydrolysis efficiency at different enzyme loading (3 and 25 FPU/g cellulose) and substrate feeding rate (100 and 180 ghm/h).

- Main results

The main results are presented in agreement with scientific strategy in three parts: i) characterization of materials, ii) batch hydrolysis in semi-dilute condition and iii) fed-batch hydrolysis up to concentrated condition.

FP exhibited the simplest composition with 99 % cellulose and 1 % of impurity. SCB mainly contained cellulose (~ 80 %) and almost no hemicellulose (< 5 %). PP was the most complex substrate which accounted 75 % cellulose and 19 % hemicellulose. In term of morphology, SCB appeared as the most suitable substrate with a “monomodal” particle size distribution and the finest population. In contrast, FP and PP included coarse fibers which were ramified and fine fragments with broad size range distributions. Rheological properties of suspensions differed between materials (FP, SCB and PP) due to the differences in their particle size distribution (PSD) and morphology. Suspensions containing large and ramified fibers generated high viscosity (the case of FP and PP). Furthermore, the *in-* and *ex-situ* particle size analysis revealed the impact of particle distribution on viscosity. Suspension of “monomodal” size distribution (case of SCB) showed lower viscosity than that of multimodal size distribution

(case of FP and PP). The concentration dependency of viscosity was established for the three lignocellulosic materials. The viscosity versus concentration curves allowed identifying the critical concentration points which indicated the change between dilute, semi-dilute and concentrated regimes. These concentrations were **7.0**, **19.0** and **23.9** gdm/L for FP, PP and SCB, respectively. Obtained results confirmed the non-Newtonian shear-thinning properties with all substrates. Krieger-Dougherty and Simha equations accurately modeled the relationship between viscosity and substrate concentration.

From nearly thirty experiments (semi-dilute batch hydrolysis), several conclusions were drawn. Considering single enzyme activities, as expected, endo-glucanase showed the most important role in the liquefaction of lignocellulosic suspensions whereas exo-glucanase and β-glucosidase showed almost no impact. Viscosity collapses were observed for FP and PP whereas an overtaking was reported for SCB in the early stages of hydrolysis. With FP and SCB, the enzymatic digestion using endo-glucanase alone showed similar liquefaction efficiency as a mixture of the three single activities. On the opposite for PP, the synergistic action of multiple enzyme activities was confirmed by rheological approach. Adding exo-glucanase and β-glucosidase significantly improved liquefaction efficiency of PP suspension. Commercial cocktail (Ctec2) always showed better liquefaction efficiency and hydrolysis yield compared with the mixture of three single activities.

During hydrolysis with cocktail and endo-glucanase, suspension viscosity was strongly dependent on the fraction of coarse population. Once this fraction was fragmented into smaller particles, the suspension viscosity quickly collapsed. The fragmentation mechanism was considered as responsible for the decrease in viscosity or in other word the liquefaction of the slurry. Besides, the solubilization of fine particles did not influenced suspension viscosity. In addition with fragmentation and solubilization, others mechanisms were hydration and agglomerate separation (specifically for SCB suspension). The hydration mechanisms appeared since substrate was in contact with water. This induces a swelling effect and consequently caused a rise in suspension viscosity with different magnitudes for each substrate.

The monitoring of power law index during enzymatic reaction was demonstrated and a loss of non-Newtonian behavior of suspension was recognized as the hydrolysis progressed. The viscosity-time relation during hydrolysis was accurately described through first order kinetics and a unique dimensionless representation was obtained. Our results suggest first order equations to predict the time for a 75 % reduction in suspension viscosity of FP and PP at given enzyme loading of Ctec2 from 0.3 to 25 FPU/g cellulose. Furthermore the present study leads to the identification of a unique dimensionless viscosity-time curve for FP and PP in the range of concentration and E/S ratios studied.

It is interesting to observe the viscosity overtaking for SCB suspension at enzyme loading ≤ 10FPU/g cellulose. During this overtaking, agglomerates were separated into smaller fragments and two assumptions were considered:

- Once agglomerates were separated, the total number of particle markedly increased that enhanced the particle – particle interactions.
- The separation of agglomerates into fragments may be considered as a shift in particles morphology from sphere-like into fiber-like form.

Supplementary experiments on SCB are then recommended before any strong conclusion can be stated. Furthermore, the overtaking may existed on other lignocellulosic material(s) at very low enzyme dosage; i.e PP. Future research may deal with this scientific question in order to deeply explore the overtaking mechanisms.

Through batch hydrolysis and rheological behaviors of suspensions SCB and PP, the critical feeding rates (Q*) were proposed from $t_{0.25}$ (time for 75 % reduction in viscosity) and C* (critical concentration) for substrate. It indicated the threshold of feeding rate, where substrate concentration may be maintained inferior to C* during fed-batch process. In fed-batch experiments, in order to avoid quick limitations, the feed flowrates were significantly lower than Q*.

Through fed-batch hydrolysis, final substrate concentration was brought up to 100 - 140 gdm/L depending on substrates and operating conditions. Overall cellulose to glucose conversion yield reached more than 63 % at 25 FPU/g cellulose for both PP and SCB. The highest yield of 67.0 % was witnessed with SCB using 25 FPU/g cellulose Ctec2 and $Q_s \approx .Q^*/3$ (23.4 gdm/h). This yield is still modest comparing to batch hydrolysis mode. However, higher hydrolysis yield might be achieved by extending the total hydrolysis time.

Unlikely the semi dilute regime, suspension viscosity was strongly affected by both fragmentation and solubilization at concentrated condition. Experiments on SCB at 25 FPU/g cellulose and 23.4 gdm/h sustained this assumption. The predominant role of coarse population on suspension viscosity was confirmed at concentrated regime. In addition, after each substrate fed, there was an increase in $t_{0.25}$. This suggested an "accumulation" of recalcitrant fraction generating an increase in viscosity as hydrolysis progressed.

In conclusion, fed-batch strategy helps to control transfers (mixing efficiency and biokinetics) to alleviate the total solid loading and consequently the glucose concentration. It is important to note that, the experimental substrate feeding rates were always lower than critical feeding rate. However, the original target (to maintain real concentration inferior than critical one) was not achieved. Even at feeding rate $Q \approx Q^*$, real solid concentration quickly overpassed C* after only few hours. Once real substrate concentration reached some threshold, the feeding was forced to stop due to high torque. This led to imagine a fed-batch process controlled by torque monitoring. Then the feeding flowrate will be regulated by the torque enabling to maintain appropriate mixing condition and to control mixing power. When upper limit of suspension torque is achieved, the feeding stops and re-starts when > 75 % reduction in torque is recognized. This strategy need to be considered and optimized in future researches.

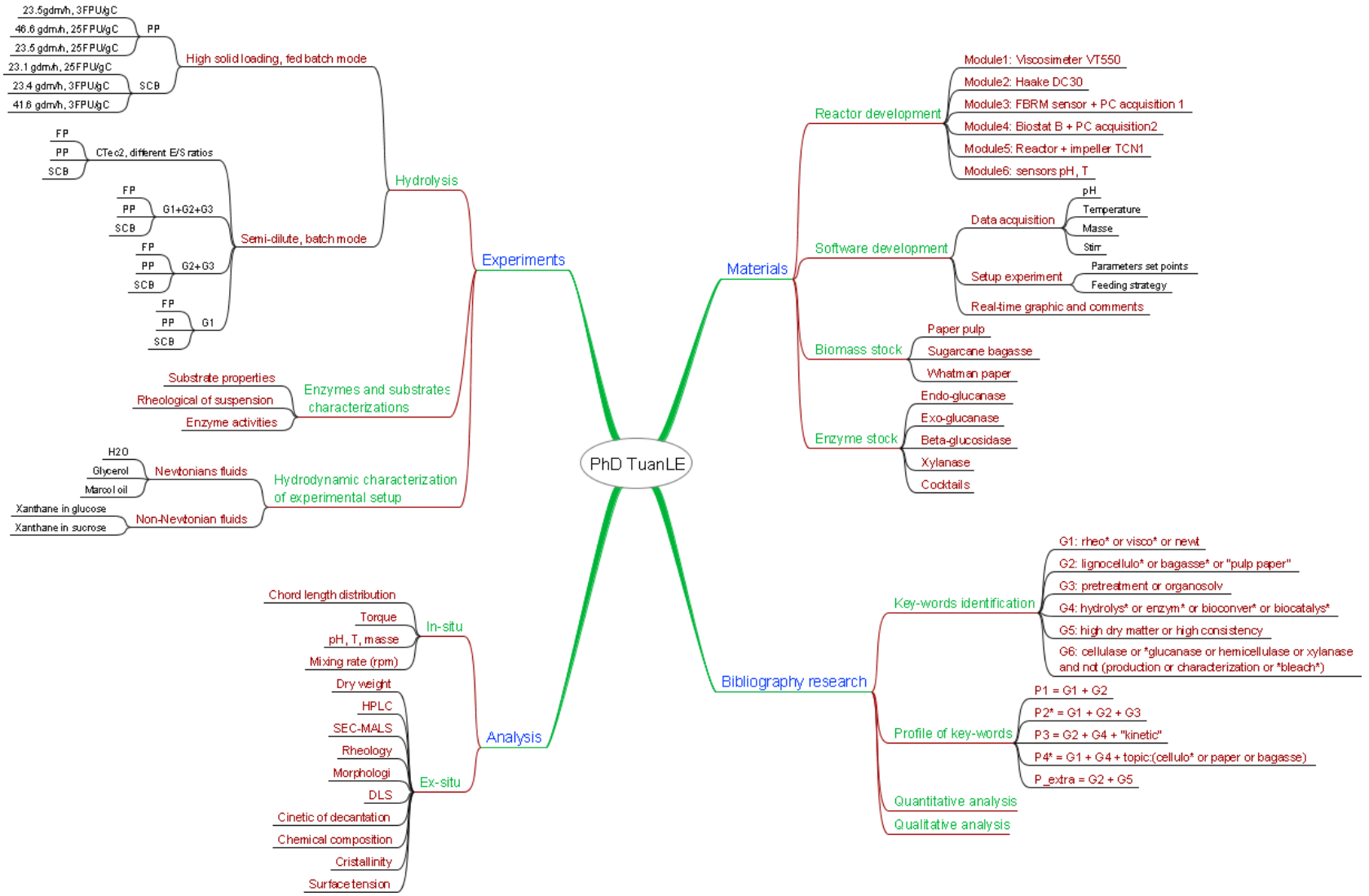

Figure 4-1. Tree diagram presentingdifferent tasks of this PhD

5 APPENDIX

Appendix 1. Enzyme specification sheet, E-Celan

CELLULASE (*endo*-ß-GLUCANASE) from *A. niger* (Lot 130501a)

E-CELAN **06/13**

(EC 3.2.1.4) 4-beta-D-glucan 4-glucanohydrolase
CAZy: GH Family 12

PROPERTIES

1. ELECTROPHORETIC PURITY:

- Single band on SDS-gel electrophoresis (MW = 27,000)
- Single major band on isoelectric focusing (pI = 4.55)

2. SPECIFIC ACTIVITY AND LEVEL OF OTHER ACTIVITIES:

Substrate	Enzyme Measured	Specific Activity (U/mg protein)
CM-Cellulose 4M	*endo*-1,4-ß-Glucanase	82
Barley ß-Glucan	*endo*-1,4-ß-Glucanase	118
Konjac Glucomannan	*endo*-1,4-ß-Glucanase	0.09
Xyloglucan (Tamarind)	*endo*-1,4-ß-Glucanase	0.02
Carob Galactomannan	*endo*-1,4-ß-Mannanase	< 0.015
CM-Pachyman	*endo*-1,3-ß-Glucanase	< 0.01
Starch	*endo*-1,4-α-Glucanase	< 0.03
p-NP-α-Glucoside	α-Glucosidase	< 0.001
p-NP-ß-Glucoside	ß-Glucosidase	< 0.001
p-NP-ß-Xyloside	ß-Xylosidase	< 0.0002

All activities are at pH 4.5 and 40°C. Glycosidase activities were measured using the appropriate *p*-Nitrophenyl glycoside (at 10mM). *endo*-Glycanases were determined with the appropriate substrate (at 10mg/mL) and using the Nelson/Somogyi reducing-sugar procedure.

3. PHYSICOCHEMICAL PROPERTIES:

pH Optima:	4.5
pH Stability:	4.0 - 10.0
Temperature Optima:	60°C
Temperature Stability:	< 50°C

4. STORAGE CONDITIONS:

The crystalline enzyme is supplied in 3.2 M ammonium sulphate plus in 0.02% sodium azide and should be stored at 4°C. On dissolving in buffer or water, the enzyme should be stored in the frozen state between use.

Appendix 2. Enzyme specification sheet, Multifect Xylanase

Genencor International®
Innovative by Nature®

Multifect® Xylanase

Genencor® Xylanase

Product Information

DESCRIPTION

Multifect® Xylanase is derived from a genetically modified strain of *Trichoderma reesei*. A typical application area for Multifect® Xylanase is animal feed.

TYPICAL CHARACTERISTICS

Activity:	8,000 GXU/ml (minimum)
Appearance:	Amber liquid
pH:	4.8 - 5.2
Grade:	Food grade, Kosher
Specific gravity:	1.08 - 1.18 g/ml

Unit Definition

The activity of Multifect® Xylanase is expressed in GXU/ml. The GXU is based on the release of Remazol Brilliant Blue-dyed birch wood xylan at pH 4.5, 30°C (86°F) in 10 minutes, using a xylanase reference standard.

pH Dependency

The pH range for the enzyme activity of Genencor Multifect® Xylanase is approximately 3.5 to 6.5, with an optimum performance at pH 5.0. The exact pH optimum will depend on process variables, including temperature, time, substrate nature and concentration.

Temperature Dependency

The activity of Multifect® Xylanase is effective in the temperature range of 50°C (120°F) to 60°C (140°F), with an optimum performance at 55°C (130°F). The exact temperature optimum will depend on many process variables, such as pH, time, substrate concentration and nature.

BIOCHEMICAL PARAMETERS

Enzyme type:	Xylanase
Molecular Weight:	21 kDa approx.
IEP:	9.0
Side Activities:	Low cellulase side activity, virtually no protease, lipase or amylase side-activities

APPLICATION RECOMMENDATIONS

Multifect® Xylanase degrades non-carbohydrates, specifically xylan polymers. Dispersion of the enzyme is important when used in dry or highly viscous substrates.

DOSAGE

A typical Multifect® Xylanase dosage rate of 25 - 75 ppm is recommended as a starting point for the optimization of enzyme dosage.

REGULATORY STATUS

This product meets or exceeds the **J**oint FAO/WHO **E**xpert **C**ommittee on **F**ood **A**dditives (**JECFA**) and the **F**ood **C**hemicals **C**odex (**FCC**) specifications for enzyme preparations used in food and is **GRAS** (**G**enerally **R**ecognized **A**s **S**afe) in the United States.

STORAGE & STABILITY

Multifect® Xylanase will meet the declared activity of 8,000 GXU/ml upon arrival at the customer's plant.

Genencor® enzymes can be safely stored in unopened and sealed original containers. Enzyme containers should be stored below 20°C (70°F), preferentially refrigerated and sheltered against direct sunlight.

For more information on the storage of this product, please contact your Genencor International® representative.

PACKAGING

Multifect® Xylanase is available in various packaging sizes. Please contact Genencor International® for detailed information.

Please note that some Genencor® products are sold in full pallet loads only.

SAFETY & ENZYME HANDLING

Inhalation of enzyme dust and mists should be avoided. In case of contact with the skin or eyes, promptly rinse with water for at least 15 minutes.

For detailed handling information, please refer to the appropriate Material Safety Data Sheet, the Enzyme Technical Association (ETA) handbook *Working Safely With Enzymes*, and the Association of Manufacturers of Fermentation Enzyme Products (Amfep) handbook *Guide to the Safe Handling of Microbial Enzyme Preparations*. All are available from Genencor International®.

Genencor® enzymes

the right tools

Appendix 3. Temperature and pH optima of Ctec2 (adapted from Novozymes enzyme specifications sheet)

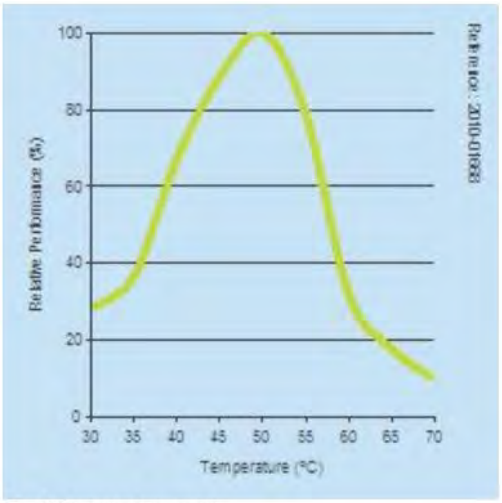

Fig. 1. Temperature curve

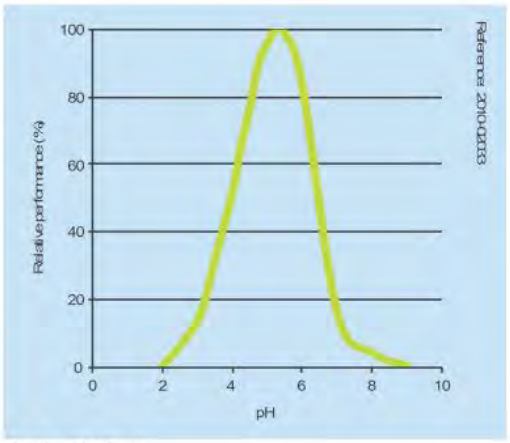

Fig. 2. pH curve

Appendix 4. Characterization of bioreactor

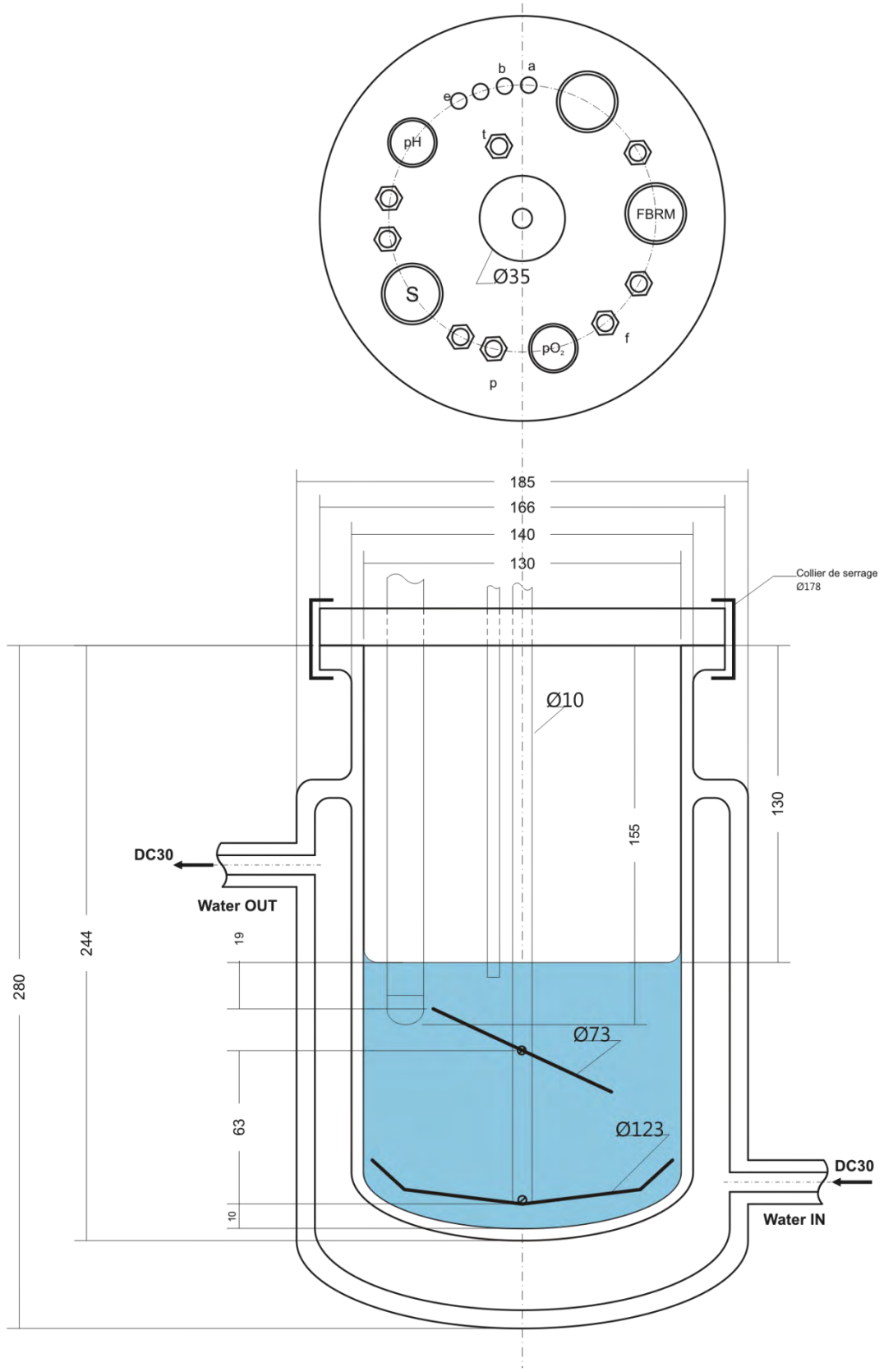

Appendix 5. Photo of the experimental setup

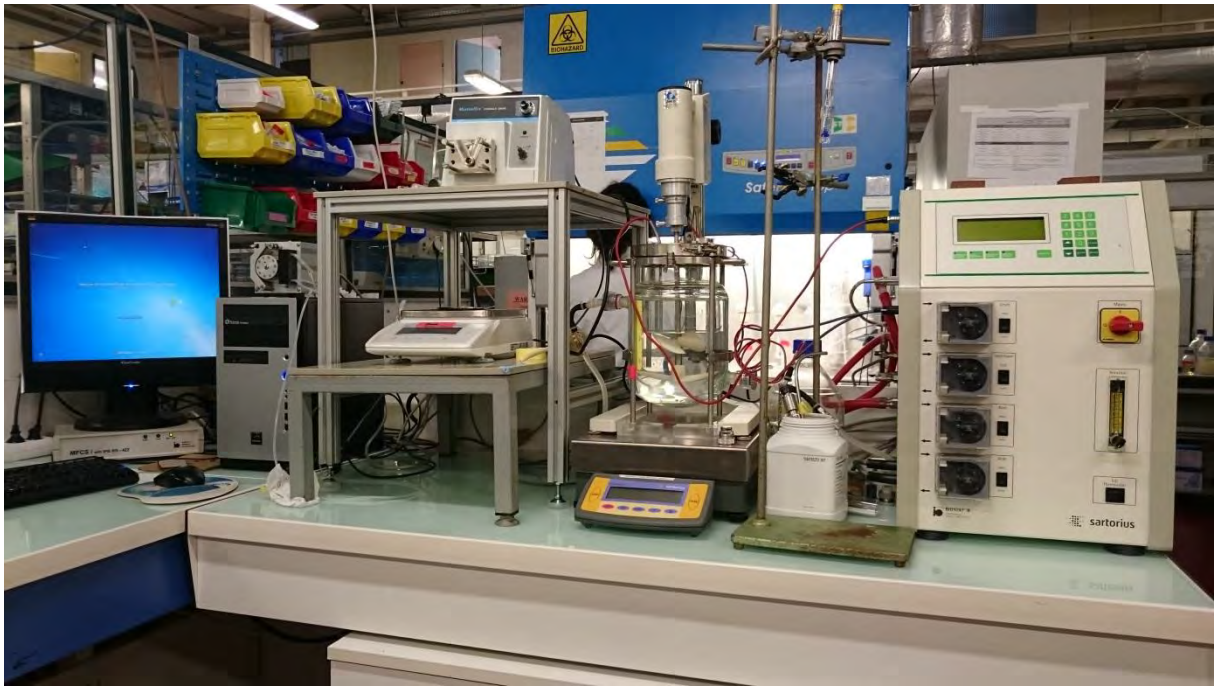

Appendix 6. Archmedean srew pump for substrate feeding: pump hopper, pump head, Achimedean screw and others disassembly parts

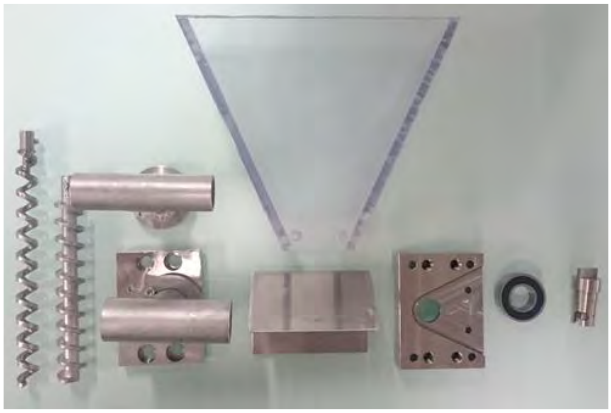

Appendix 7. Dimensionless viscosities μ* as a function of normalized time and t* for fed-batch hydrolysis of SCB and PP. The black dot (●) indicates the point that corresponds to 75 % viscosity reduction.

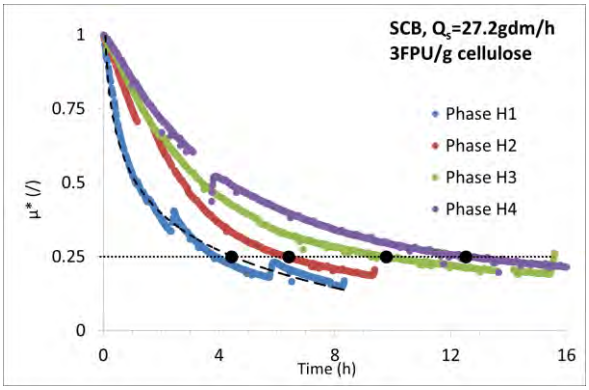

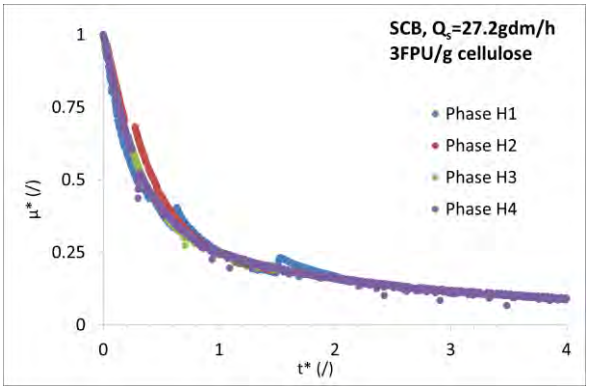

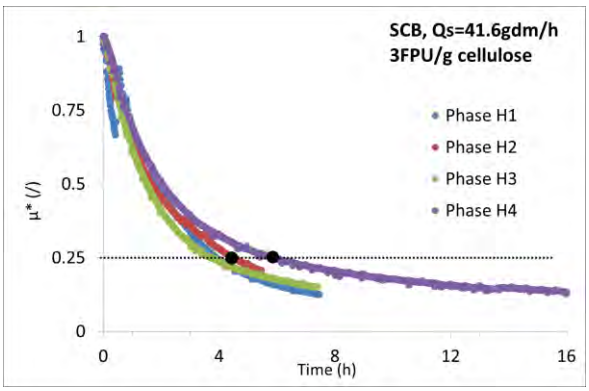

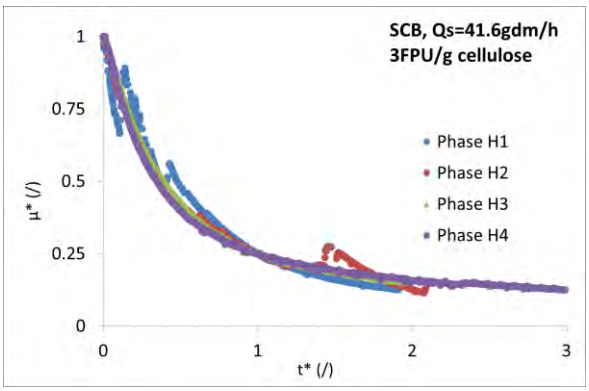

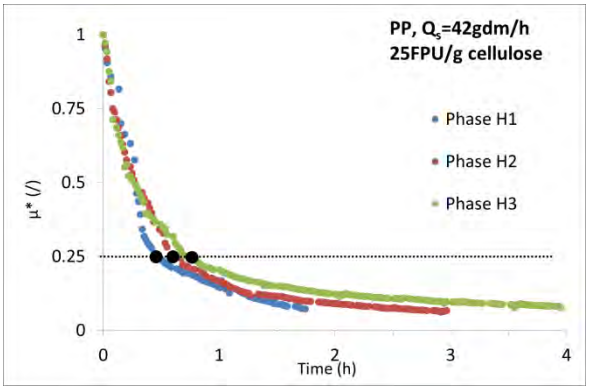

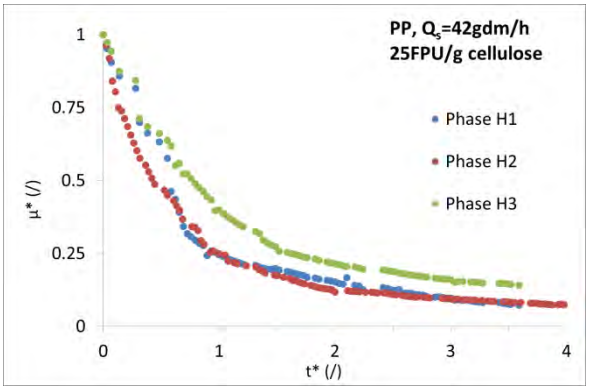

Appendix 8. Microscopic observation of SCB suspension during fed-batch hydrolysis (Substrate: SCB, Qs = 23.1 gdm/L, 3 FPU/g cellulose, dilution rate: 1/10, magnification×10, area: 0.5cm ×0.5cm).

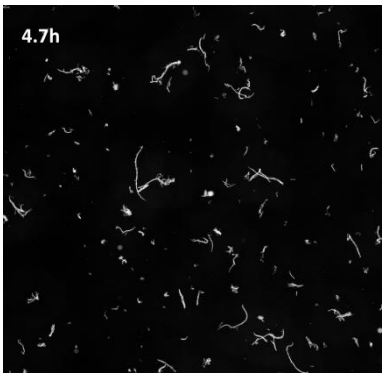

(end A1)

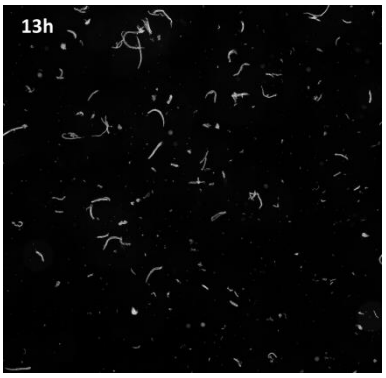

(end H1 – start A2)

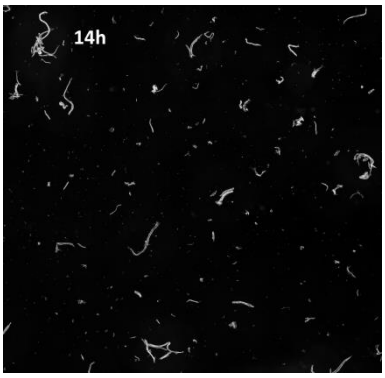

(end A2 – start H2)

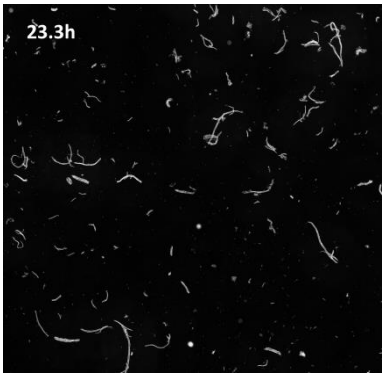

(end H2 – start A3)

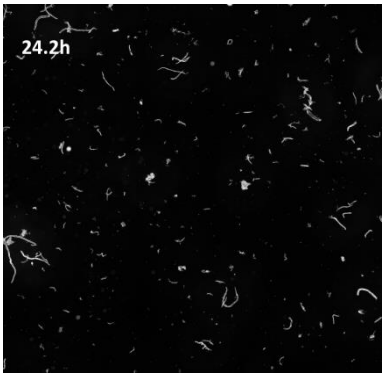

(end A3- start H3)

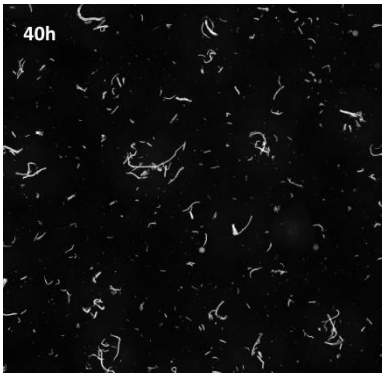

(end H3- start A4)

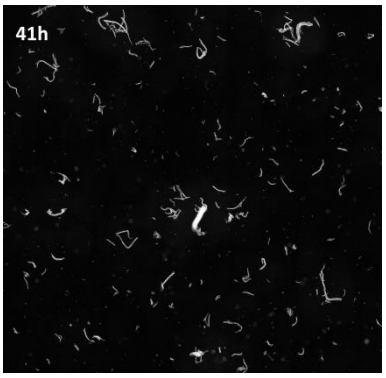

(end A4 – start H4)

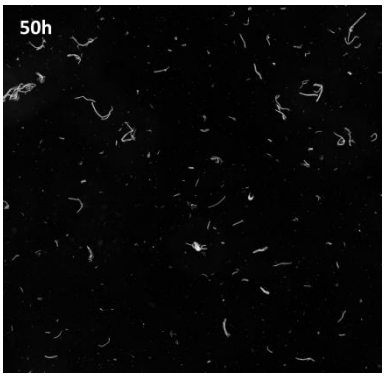

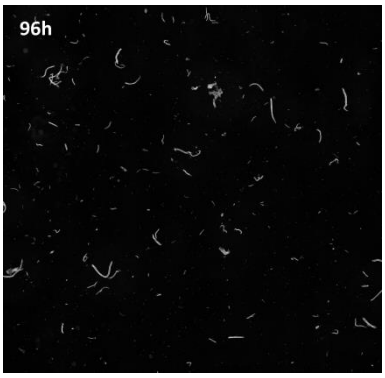

(end hydrolysis)

Appendix 9. Microscopic observation of SCB suspension during fed-batch hydrolysis (Substrate: SCB, Qs = 42 gdm/L, 3 FPU/g cellulose, dilution rate: 1/10, magnification×10, area: 0.5cm ×0.5cm).

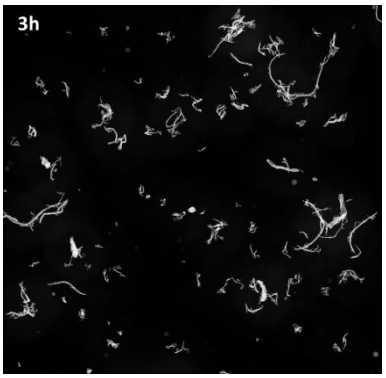

(end A1)

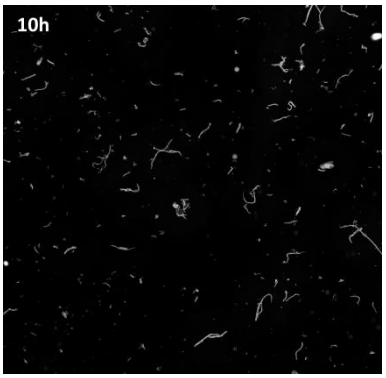

(end H1 – start A2)

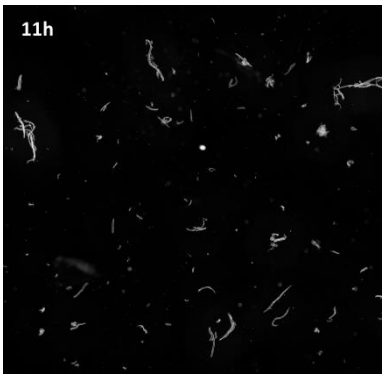

(end A2 – start H2)

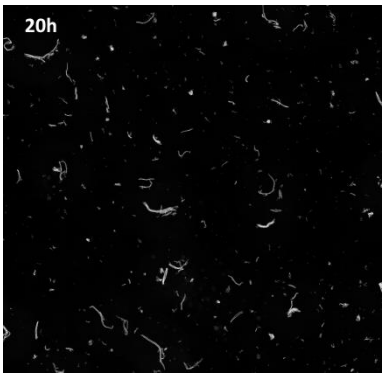

(end H2 – start A3)

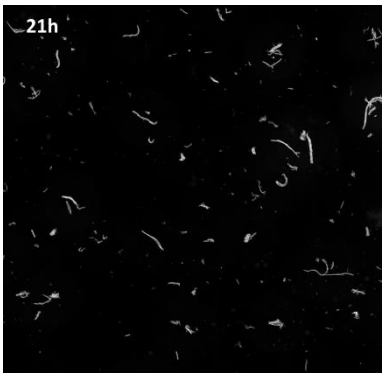

(end A3- start H3)

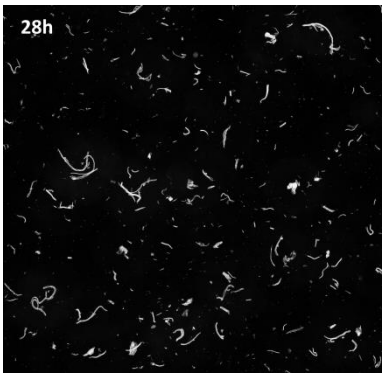

(end H3- start A4)

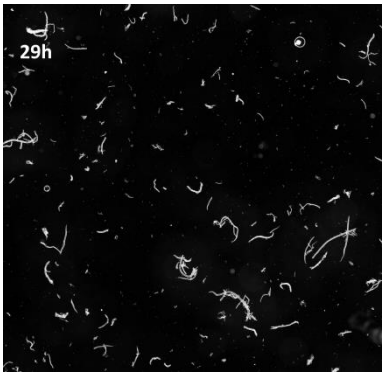

(end A4 – start H4)

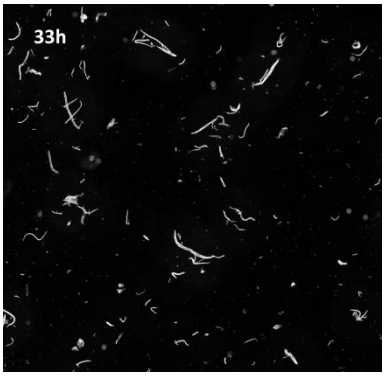

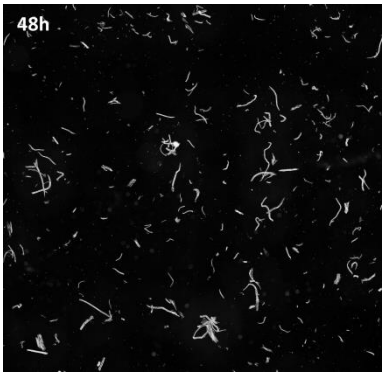

(end hydrolysis)

Appendix 10. Evolution of distribution functions pondered by particle volume fraction, $E_v(d_{SE}) \times \Phi_v$ as a function of feeding and non-feeding stages, $E_v(d_{SE}) \times \Phi_v$ during fed-batch hydrolysis of SCB (Qs = 23.1 gdm/L, 3 FPU/g cellulose)

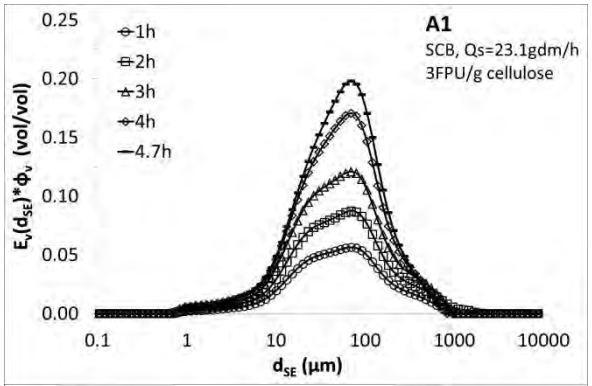

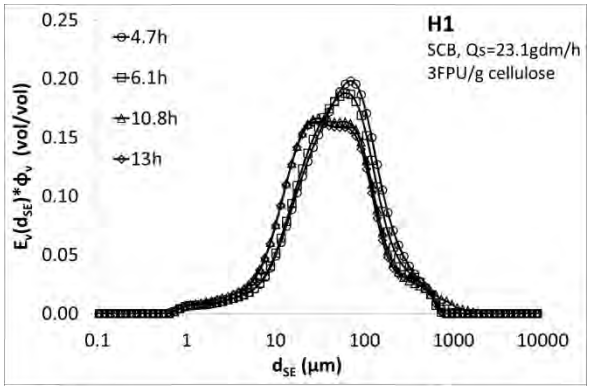

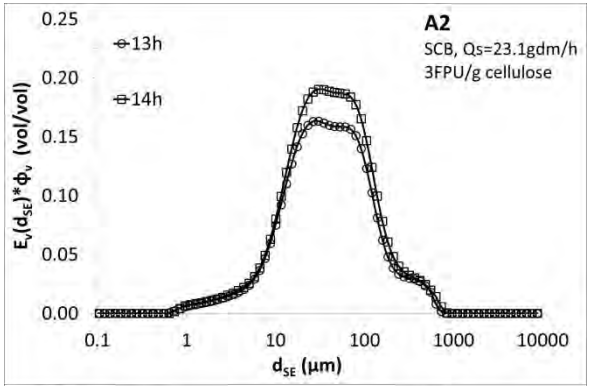

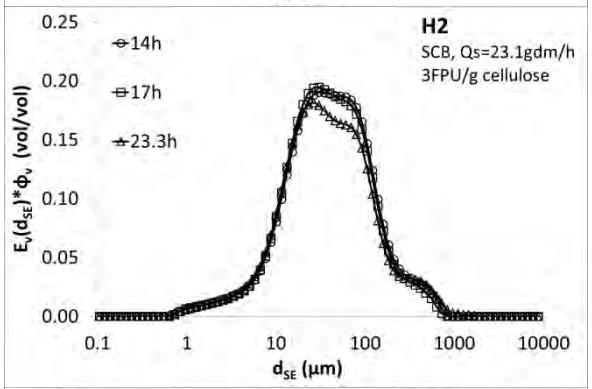

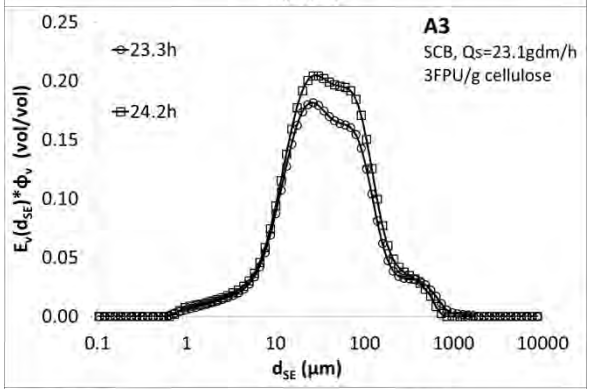

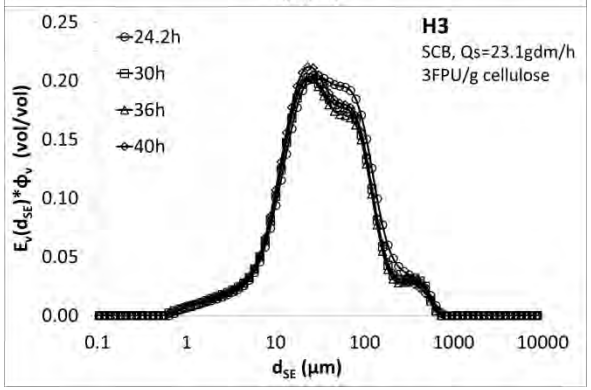

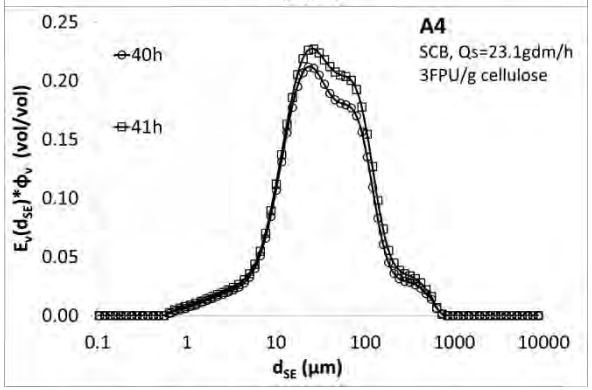

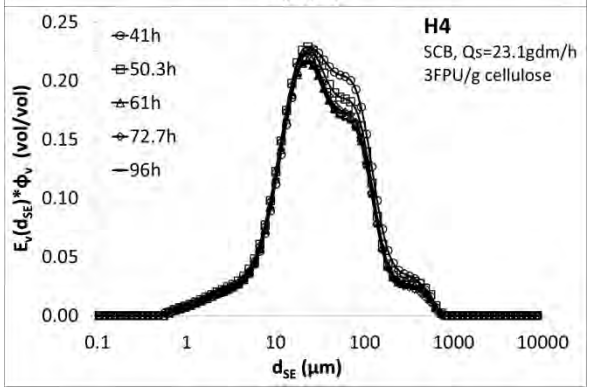

Appendix 11. Evolution of distribution functions pondered by particle volume fraction, $E_v(d_{SE}) \times \Phi_v$ as a function of feeding and non-feeding stages, $E_v(d_{SE}) \times \Phi_v$ during fed-batch hydrolysis of SCB (Qs = 41.6gdm/L, 3 FPU/g cellulose).

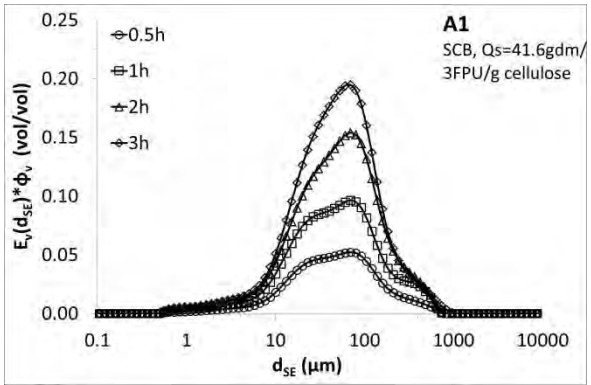

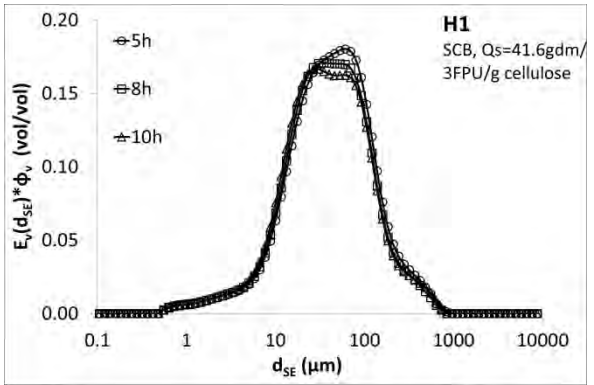

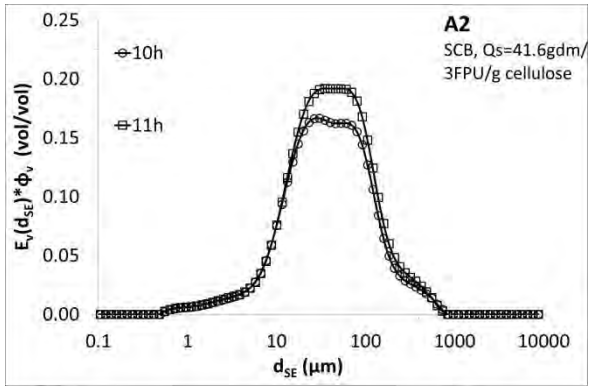

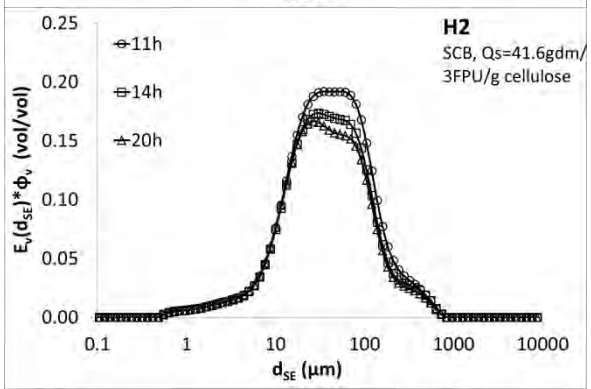

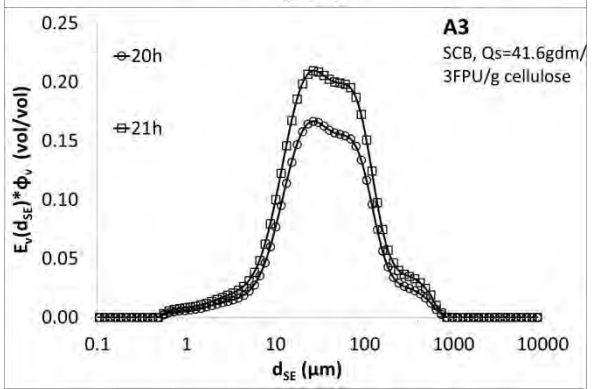

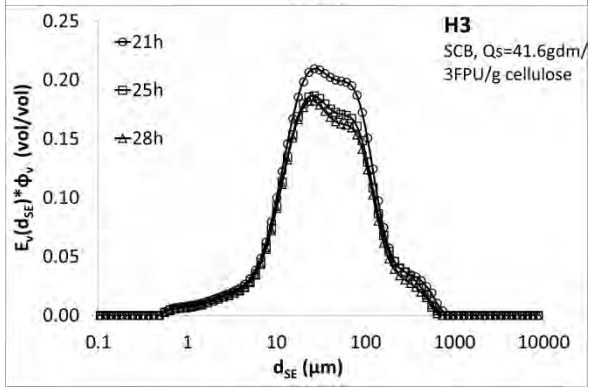

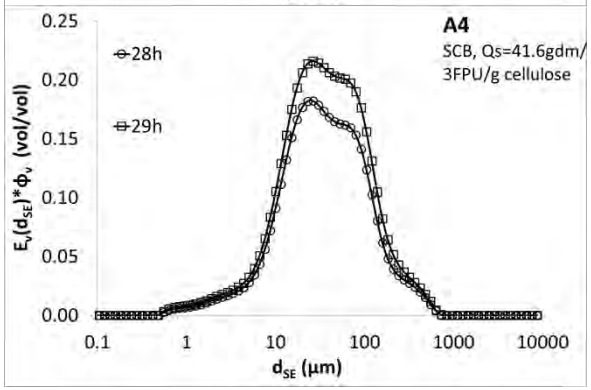

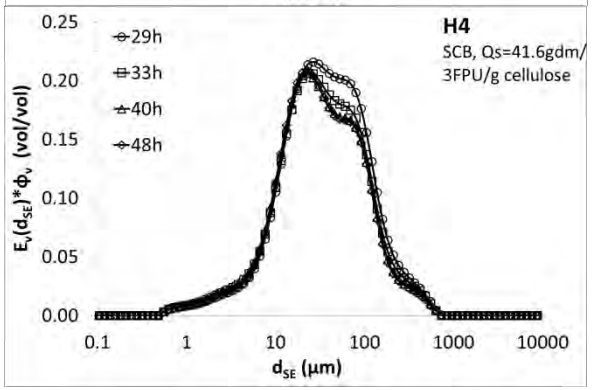

Appendix 12. Evolution of distribution functions pondered by particle volume fraction, $E_v(d_{SE}) \times \Phi_v$ as a function of feeding and non-feeding stages, $E_v(d_{SE}) \times \Phi_v$ during fed-batch hydrolysis of PP (Qs = 42 gdm/L, 25 FPU/g cellulose)

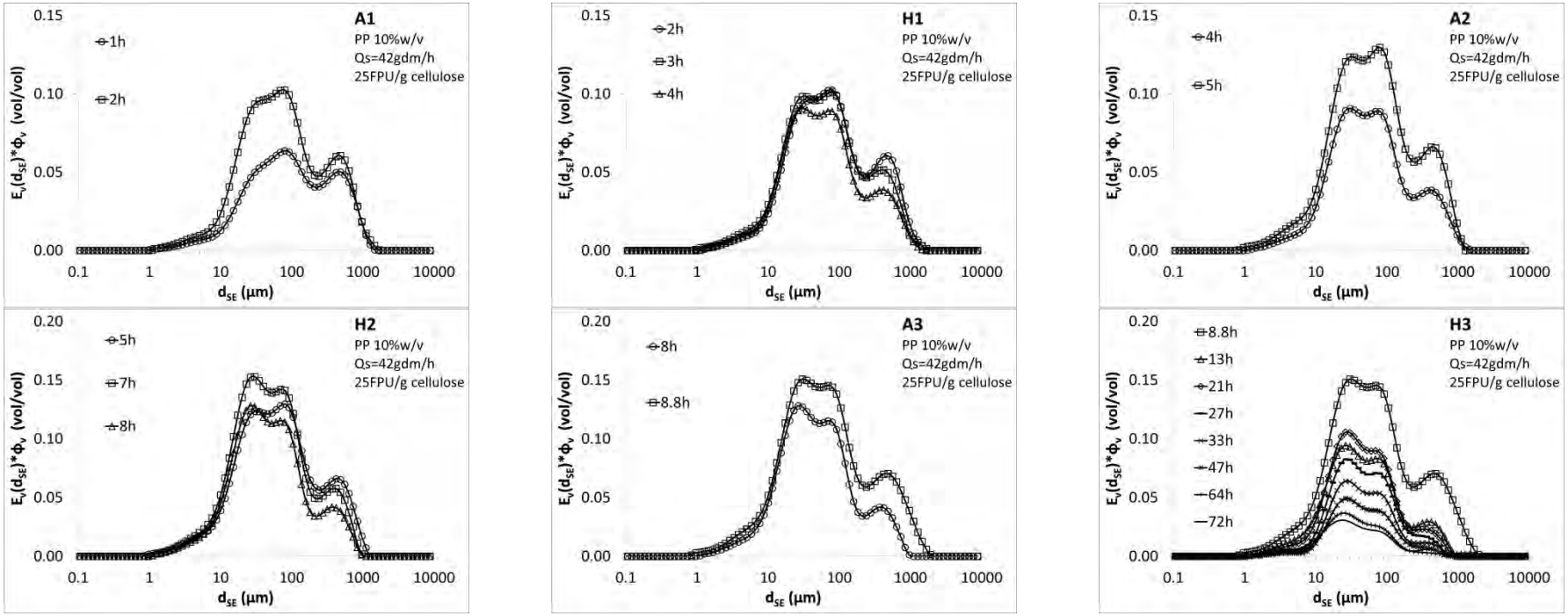

Appendix 13. Evolution of distribution functions pondered by particle volume fraction, $E_v(d_{SE}) \times \Phi_v$ as a function of feeding and non-feeding stages, $E_v(d_{SE}) \times \Phi_v$ during fed-batch hydrolysis of PP (Qs = 23.1 gdm/L, 3 FPU/g cellulose)

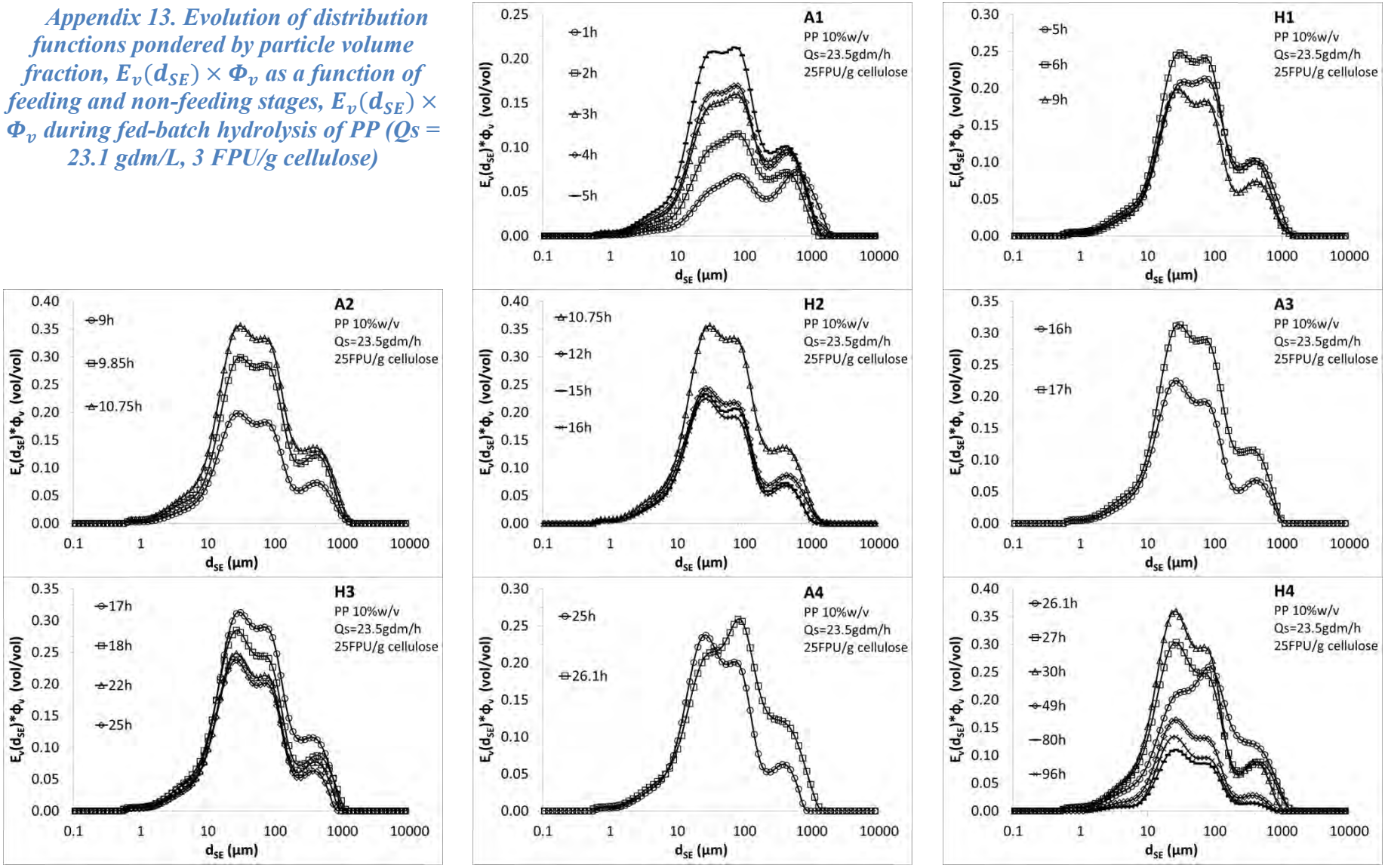

REFERENCES

Ballesteros, M., J. M. Oliva, P. Manzanares, M. J. Negro and I. Ballesteros (2002). "Ethanol production from paper material using a simultaneous saccharification and fermentation system in a fed-batch basis." World Journal of Microbiology & Biotechnology **18**(6): 559-561.

Barnes, H. A., J. F. Hutton and K. Walters (1989). An Introduction to Rheology, Elsevier Science Pub Co.

Bell, G., S. Schuck, G. Jungmeier, M. Wellisch, C. Felby, H. Jørgensen, H. Stichnothe, M. Clancy, I. D. Bari, S. Kimura, R. v. Ree, E. d. Jong, B. Annevelink, K. Kwant, K. Torr and J. J. Spaeth (2014). IEA bioenergy Task 42 biorefining: sustainable and synergetic processing of biomass into marketable foo& feed ingredients, chemicals, materials and energy (fuels, power, heat). R. v. Ree and A. v. Zeeland. Netherlands, International Energy Agency

Bradford, M. M. (1976). "A rapid and sensitive method for the quantitation of microgram quantities of protein utilizing the principle of protein-dye binding." Analytical biochemistry **72**: 248-254.

Breuil, C., P. Mayers and J. N. Saddler (1986). "Substrate conditions that influence the assays used for determining the beta-glucosidase activity of cellulolytic microorganisms." Biotechnol Bioeng **28**(11): 1653-1656.

Brown, R. M. (1999). "Cellulose structure and biosynthesis." Pure & Applied Chemistry **71**: 767-775.

Cao, Y. and H. Tan (2002). "Effects of cellulase on the modification of cellulose." Carbohydrate Research **337**(14): 1291-1296.

Cara, C., M. Moya, I. Ballesteros, M. J. Negro, A. González and E. Ruiz (2007). "Influence of solid loading on enzymatic hydrolysis of steam exploded or liquid hot water pretreated olive tree biomass." Process Biochemistry **42**(6): 1003-1009.

Cardona, M. J., E. J. Tozzi, N. Karuna, T. Jeoh, R. L. Powell and M. J. McCarthy (2015). "A process for energy-efficient high-solids fed-batch enzymatic liquefaction of cellulosic biomass." Bioresource Technology **198**: 488-496.

Carvalho, M. L., R. Sousa, U. F. Rodriguez-Zuniga, C. A. G. Suarez, D. S. Rodrigues, R. C. Giordano and R. L. C. Giordano (2013). "Kinetic study of the enzymatic hydrolysis of sugarcane bagasse." Brazilian Journal of Chemical Engineering **30**(3): 437-447.

Caspeta, L., M. A. Caro-Bermudez, T. Ponce-Noyola and A. Martinez (2014). "Enzymatic hydrolysis at high-solids loadings for the conversion of agave bagasse to fuel ethanol." Applied Energy **113**: 277-286.

Churchill, S. W. (1977). "Friction factor equation spans all fluid flow regimes." Chemical Engineering Science **84**: 91-92.

Clarke, B. (1967). "Rheology of coarse settling suspensions." Transactions of the Institution of Chemical Engineers **45**: 251-256.

Correa, L. J., A. C. Badino and A. J. Cruz (2016). "Power consumption evaluation of different fed-batch strategies for enzymatic hydrolysis of sugarcane bagasse." Bioprocess Biosyst Eng **39**(5): 825-833.

Correa, L. J., A. C. Badino and A. J. Cruz (2016a). "Mixing design for enzymatic hydrolysis of sugarcane bagasse: methodology for selection of impeller configuration." Bioprocess Biosyst Eng **39**(2): 285-294.

Dasari, R. K. and R. E. Berson (2007). "The effect of particle size on hydrolysis reaction rates and rheological properties in cellulosic slurries." Applied Biochemistry and Biotechnology **137**: 289-299.

Davies, G. and B. Henrissat (1995). "Structures and mechanisms of glycosyl hydrolases." Structure **3**(9): 853-859.

Davis, R., L. Tao, C. Scarlata, E. C. D. Tan, J. Ross, J. Lukas and D. Sexton (2015). Process design and economics for the conversion of lignocellulosic biomass to hydrocarbons: Dilute-acid and enzymatic deconstruction of biomass to sugars and catalytic conversion of sugars to hydrocarbons, National Renewable Energy Laboratory.

De Bari, I., F. Liuzzi, A. Villone and G. Braccio (2013). "Hydrolysis of concentrated suspensions of steam pretreated Arundo donax." Applied Energy **102**(0): 179-189.

De Bari, I., E. Viola, D. Barisano and G. Braccio (2002). "Ethanol production at flask and pilot scale from concentrated slurries of steam-exploded aspen." Industrial & Engineering Chemistry Research **41**(7).

Derakhshandeh, B., S. G. Hatzikiriakos and C. P. J. Bennington (2010). "Rheology of pulp suspensions using ultrasonic Doppler velocimetry." Rheologica Acta **49**(11-12): 1127-1140.

Dibble, C. J., T. A. Shatova, J. L. Jorgenson and J. J. Stickel (2011). "Particle morphology characterization and manipulation in biomass slurries and the effect on rheological properties and enzymatic conversion." Biotechnology Progress **27**(6): 1751-1759.

Dunaway, K. W., R. K. Dasari, N. G. Bennett and R. Eric Berson (2010). "Characterization of changes in viscosity and insoluble solids content during enzymatic saccharification of pretreated corn stover slurries." Bioresource Technology **101**(10): 3575-3582.

Ehrhardt, M. R., T. O. Monz, T. W. Root, R. K. Connelly, C. T. Scott and D. J. Klingenberg (2010). "Rheology of dilute acid hydrolyzed corn stover at high solids concentration." Appl Biochem Biotechnol **160**(4): 1102-1115.

Elwyn T. Reese, A. H. M., Frederick W. Parrish (1968). "Glucosidases and exo-glucanases." Canadian Journal of Microbiology **46**(1): 25-34.

Fan, Z., C. South, K. Lyford, J. Munsie, P. van Walsum and L. Lynd (2003). "Conversion of paper sludge to ethanol in a semicontinuous solids-fed reactor." Bioprocess and Biosystems Engineering **26**(2): 93-101.

Fengel, D. and G. Wegener (1983). Wood: Chemistry, Ultrastructure, Reactions, Walter De Gruyter Inc.

Gardner, K. H. and J. Blackwell (1974). "The structure of native cellulose." Biopolymers **13**(10): 1975-2001.

Geddes, C. C., J. J. Peterson, M. T. Mullinnix, S. A. Svoronos, K. T. Shanmugam and L. O. Ingram (2010). "Optimizing cellulase usage for improved mixing and rheological properties of acid-pretreated sugarcane bagasse." Bioresource Technology **101**(23): 9128-9136.

Ghose, T. K. (1987). "Measurement of cellulase activities." Pure and applied chemistry **59**: 257-268.

Ghose, T. K. and V. S. Bisaria (1987). "Measurement of hemicellulase activities. Part 1: xylanases." Pure and applied chemistry **59**: 1739-1752.

Gibbs, R. D. (1958). "The maule reaction, lignins and the relationship between woody plants." The Physiology of Forest Trees: 269-312.

Giesekus, H. (1983). "Disperse systems: dependence of rheological properties on the type of flow with implications for food rheology." Physical properties of foods/edited by R Jowitt et al., Applied Science Publishers, Chap. 13.

Giovanni, D. N., S. Eleonora, S. Giulio and P. Fabio (2011). Advances in the Development of Bioethanol: A Review.

Gottschalk, L. M. F., R. A. Oliveira and E. P. d. S. Bon (2010). "Cellulases, xylanases, β-glucosidase and ferulic acid esterase produced by Trichoderma and Aspergillus act synergistically in the hydrolysis of sugarcane bagasse." Biochemical Engineering Journal **51**(1–2): 72-78.

Goyal, A., B. Ghosh and D. Eveleigh (1991). "Characteristics of fungal cellulases." Bioresource Technology **36**(1): 37-50.

Gupta, R., S. Kumar, J. Gomes and R. C. Kuhad (2012). "Kinetic study of batch and fed-batch enzymatic saccharification of pretreated substrate and subsequent fermentation to ethanol." Biotechnology for Biofuels **5**(16).

Himmel, M. E., S.-Y. Ding, D. K. Johnson, W. S. Adney, M. R. Nimlos, J. W. Brady and T. D. Foust (2007). "Biomass recalcitrance: Engineering plants and enzymes for biofuels production." Science **315**(5813): 804-807.

Hồ, S. T. (2006). Hemicellulose. The chemistry of wood and cellulose. Hanoi, Publishers of scientific and technical. **2:** 30-81.

Hodge, D. B., M. N. Karim, D. J. Schell and J. D. McMillan (2008). "Soluble and insoluble solids contributions to high-solids enzymatic hydrolysis of lignocellulose." Bioresource Technology **99**(18): 8940-8948.

Hodge, D. B., M. N. Karim, D. J. Schell and J. D. McMillan (2009). "Model-Based Fed-Batch for High-Solids Enzymatic Cellulose Hydrolysis." Applied Biochemistry and Biotechnology **152**(1): 88-107.

Hou, W., L. Zhang, J. Zhang and J. Bao (2016). "Rheology evolution and CFD modeling of lignocellulose biomass during extremely high solids content pretreatment." Biochemical Engineering Journal **105, Part B**: 412-419.

Jahangiri, M., M. R. Golkar-Narenji, N. Montazerin and S. Savarmand (2001). "Investigation of the viscoelastic effect on the metzner and otto coefficient through LDA velocity measurements." Chinese Journal of Chemical Engineering **9**(1): 77-83.

Jørgensen, H., J. Vibe-Pedersen, J. Larsen and C. Felby (2007). "Liquefaction of lignocellulose at high-solids concentrations." Biotechnology and Bioengineering **96**(5): 862-870.

Joseleau, J. P., J. Comtat and K. Ruel (1992). Chemical structure of xylans and their interaction in the plant cell walls. Xylan and xylanases,. J. Visser, G. Beldman, M. A. K.-v. Someren and A. G. J. Voragen. Amsterdam, Science Publishers**:** 1-15.

Kadam, K. L., E. C. Rydholm and J. D. McMillan (2004). "Development and validation of a kinetic model for enzymatic saccharification of lignocellulosic biomass." Biotechnology Progress **20**(3): 698-705.

Kim, S. and B. E. Dale (2004). "Global potential bioethanol production from wasted crops and crop residues." Biomass and Bioenergy **26**(4): 361-375.

Knutsen, J. S. and M. W. Liberatore (2009). "Rheology of high-solids biomass slurries for biorefinery applications." Journal of Rheology **53**(4): 877-892.

Knutsen, J. S. and M. W. Liberatore (2010). "Rheology modification and enzyme kinetics of high solids cellulosic slurries." Energy and Fuels **24**(5): 3267-3274.

Krieger, I. and T. Dougherty (1959). "A Mechanism for Non-Newtonian Flow in Suspensions of Rigid Spheres." Transactions of the Society of Rheology **3**: 137-152.

Kristensen, J. B., C. Felby and H. Jorgensen (2009). "Yield-determining factors in high-solids enzymatic hydrolysis of lignocellulose." Biotechnology for Biofuels **2**.

Kuhad, R., A. Singh and K.-E. Eriksson (1997). Microorganisms and enzymes involved in the degradation of plant fiber cell walls. Biotechnology in the Pulp and Paper Industry. K. E. L. Eriksson, W. Babel, H. W. Blanch et al., Springer Berlin Heidelberg. **57:** 45-125.

Leonowicz, A., A. Matuszewska, J. Luterek, D. Ziegenhagen, M. Wojtaś-Wasilewska, N.-S. Cho, M. Hofrichter and J. Rogalski (1999). "Biodegradation of Lignin by White Rot Fungi." Fungal Genetics and Biology **27**(2–3): 175-185.

Li, M. and D. Wilkinson (2005). "Determination of non-spherical particle size distribution from chord length measurements. Part 1: Theoretical analysis." Chemical Engineering Science **60**(12): 3251-3265.

Liu, Y., J. Xu, Y. Zhang, Z. Yuan and J. Xie (2015). "Optimization of high solids fed-batch saccharification of sugarcane bagasse based on system viscosity changes." Journal of Biotechnology **211**: 5-9.

Lu, Y. F., Y. H. Wang, G. Q. Xu, J. Chu, Y. P. Zhuang and S. L. Zhang (2010). "Influence of high solid concentration on enzymatic hydrolysis and fermentation of steam-exploded corn stover biomass." Applied Biochemistry and Biotechnology **160**(2): 360-369.

Lynd, L. R., P. J. Weimer, W. H. van Zyl and I. S. Pretorius (2002). "Microbial Cellulose Utilization: Fundamentals and Biotechnology." Microbiology and Molecular Biology Reviews **66**(3): 506-577.

Matsakas, L. and P. Christakopoulos (2013). "Fermentation of liquefacted hydrothermally pretreated sweet sorghum bagasse to ethanol at high-solids content." Bioresource Technology **127**: 202-208.

Mesa, L., N. López, C. Cara, E. Castro, E. González and S. I. Mussatto (2016). "Techno-economic evaluation of strategies based on two steps organosolv pretreatment and enzymatic hydrolysis of sugarcane bagasse for ethanol production." Renewable Energy **86**: 270-279.

Metzner, A. B. and R. E. Otto (1957). "Agitation of non-Newtonian fluids." AIChE Journal **3**(1): 3-10.

Miao, Y., J. Y. Chen, X. Jiang and Z. Huang (2012). "Kinetic studies on the product inhibition of enzymatic lignocellulose hydrolysis." Applied Biochemistry and Biotechnology **167**(2): 358-366.

Mosier, N., C. Wyman, B. Dale, R. Elander, Y. Y. Lee, M. Holtzapple and M. Ladisch (2005). "Features of promising technologies for pretreatment of lignocellulosic biomass." Bioresource Technology **96**(6): 673-686.

Nakada, S., D. Saygin and D. Gielen (2014). Global Bioenergy - Supply and demand projections. A working paper for REmap 2030, The International Renewable Energy Agency.

Neto, J. M., D. Dos Reis Garcia, S. M. G. Rueda and A. C. Da Costa (2013). "Study of kinetic parameters in a mechanistic model for enzymatic hydrolysis of sugarcane bagasse subjected to different pretreatments." Bioprocess and Biosystems Engineering **36**(11): 1579-1590.

Nguyen, T.-C., D. Anne-Archard, V. Coma, X. Cameleyre, E. Lombard, C. Binet, A. Nouhen, K. A. To and L. Fillaudeau (2013). "In situ rheometry of concentrated cellulose fibre suspensions and relationships with enzymatic hydrolysis." Bioresource Technology **133**(0): 563-572.

Nguyen, T. C. (2014). In-situ and ex-situ multi-scale physical metrologies to investigate the destructuration mechanisms of lignocellulosic matrices and release kinetics of fermentable cellulosic carbon. PhD, Institut National de Sciences Appliquees Toulouse.

Nguyen, T. C., D. Anne-Archard and L. Fillaudeau (2015). "Rheology of Lignocellulose Suspensions and Impact of Hydrolysis: A Review." Adv Biochem Eng Biotechnol **149**: 325-357.

Novikova, L. N., S. A. Medvedeva, I. V. Volchatova and S. A. Bogatyreva (2002). "Changes in macromolecular characteristics and biological activity of hydrolytic lignin hydrolysate in the course of composting." Applied Biochemistry and Biotechnology **38**: 181-185.

Odier, E. and I. Artraud (1992). Degradation of ligin. Microbial Degradation of Natural Products. G. Winkelmann. New York, VCH Publishers**:** 191-191.

Pallapolu, V. R., Y. Y. Lee, R. J. Garlock, V. Balan, B. E. Dale, Y. Kim, N. S. Mosier, M. R. Ladisch, M. Falls, M. T. Holtzapple, R. Sierra-Ramirez, J. Shi, M. A. Ebrik, T. Redmond, B. Yang, C. E. Wyman, B. S. Donohoe, T. B. Vinzant, R. T. Elander, B. Hames, S. Thomas and R. E. Warner (2011). "Effects of enzyme loading and β-glucosidase supplementation on enzymatic hydrolysis of switchgrass processed by leading pretreatment technologies." Bioresource Technology **102**(24): 11115-11120.

Palmqvist, B. and G. Lidén (2012). "Torque measurements reveal large process differences between materials during high solid enzymatic hydrolysis of pretreated lignocellulose." Biotechnology for Biofuels **5**(1): 1-9.

Pandey, A., C. R. Soccol, P. Nigam and V. T. Soccol (2000). "Biotechnological potential of agro-industrial residues. I: sugarcane bagasse." Bioresource Technology **74**(1): 69-80.

Peng, L. and Y. Chen (2011). "Conversion of paper sludge to ethanol by separate hydrolysis and fermentation (SHF) using Saccharomyces cerevisiae." Biomass and Bioenergy **35**(4): 1600.

Pereira, L. T. C., L. T. C. Pereira, R. S. S. Teixeira, E. P. D. Bon and S. P. Freitas (2011). "Sugarcane bagasse enzymatic hydrolysis: rheological data as criteria for impeller selection." Journal of Industrial Microbiology & Biotechnology **38**(8): 901-907.

Pimenova, N. V. and A. R. Hanley (2004). "Effect of corn stover concentration on rheological characteristics." Applied Biochemistry and Biotechnology **113**: 347-360.

Pimenova, N. V. and T. R. Hanley (2003). "Measurement of rheological properties of corn stover suspensions." Applied Biochemistry and Biotechnology **105**: 383-392.

Prior, B. A. and D. F. Day (2008). "Hydrolysis of ammonia-pretreated sugar cane bagasse with cellulase, β-glucosidase, and hemicellulase preparations." Applied Biochemistry and Biotechnology **146**: 151-164.

Pryor, S. W., B. Karki and N. Nahar (2012). "Effect of hemicellulase addition during enzymatic hydrolysis of switchgrass pretreated by soaking in aqueous ammonia." Bioresource Technology **123**(0): 620-626.

Quemada, D. (2006). Modélisation Rhéologique Structurelle. Dispersions Concentrées et Fluides Complexes, Lavoisier.

Quiroga, A. G., A. Costa and R. Maciel Filho (2010). "Analysis of conversion and operation strategies for enzymatic hydrolysis of lignocellulosic biomass in a series of CSTRs with distributed feeding." Bioprocess Biosyst Eng **33**(8): 901-910.

Rabinovich, M. L., M. S. Melnik and A. V. Bolobova (2002). "Dedicated to the memory of I.V. Berezin and R.V. Feniksova Microbial Cellulases (Review)." Applied Biochemistry and Microbiology **38**(4): 305-322.

Radeva, G., I. Valchev, S. Petrin, E. Valcheva and P. Tsekova (2012). "Kinetic model of enzymatic hydrolysis of steam-exploded wheat straw." Carbohydrate Polymers **87**(2): 1280-1285.

Ramos, L. P., C. Breuil and J. N. Saddler (1992). "Comparison of steam pretreatment of Eucalyptus, Aspen and spruce wood chips and their enzymatic hydrolysis." Applied Biochemistry and Biotechnology **34/35**: 37-47.

Rezania, S., Z. L. Ye and R. E. Berson (2009). "Enzymatic Saccharification and Viscosity of Sawdust Slurries Following Ultrasonic Particle Size Reduction." Applied Biochemistry and Biotechnology **153**(1-2): 103-115.

Rico, M., S. Hugon, M. Bazin, N. L. Scouarnec, A. Mucchielli, D. Marini, P. Liogier, R. Dupont, A. Rodary, N. Petit, F. Fructus and F. Virely (2014). Etudes économiques, prospective: Benchmark européen sur les plateformes chimiques, quels sont les leviers pour améliorer la compétitivité des plateformes françaises?, Pôle interministériel de Prospective et d'Anticipation des Mutations économiques.

Roberts, G. P., H. A. Barnes and C. Mackie (2001). "Using the microsoft excel "solver" tool to perform non-linear curve fitting, using a range of non-Newtonian flow curves as examples." Applied Rheology **11**(2): 271-276.

Rocha, G. J. M., A. R. Gonçalves, B. R. Oliveira, E. G. Olivares and C. E. V. Rossell (2012). "Steam explosion pretreatment reproduction and alkaline delignification reactions performed on a pilot scale with sugarcane bagasse for bioethanol production." Industrial Crops and Products **35**(1): 274-279.

Roche, C., C. Dibble and J. Stickel (2009a). "Laboratory-scale method for enzymatic saccharification of lignocellulosic biomass at high-solids loadings." Biotechnology for Biofuels **2**(1): 1-11.

Roche, C. M., C. J. Dibble, J. S. Knutsen, J. J. Stickel and M. W. Liberatore (2009b). "Particle Concentration and Yield Stress of Biomass Slurries During Enzymatic Hydrolysis at High-Solids Loadings." Biotechnology and Bioengineering **104**(2): 290-300.

Rosgaard, L., P. Andric, K. Dam-Johansen, S. Pedersen and A. S. Meyer (2007). "Effects of substrate loading on enzymatic hydrolysis and viscosity of pretreated barley straw." Applied Biochemistry and Biotechnology **143**(1): 27-40.

Ruiz, H. A., A. A. Vicente and J. A. Teixeira (2012). "Kinetic modeling of enzymatic saccharification using wheat straw pretreated under autohydrolysis and organosolv process." Industrial Crops and Products **36**(1): 100-107.

Samaniuk, J. R., C. T. Scott, T. W. Root and D. J. Klingenberg (2015). "Effects of process variables on the yield stress of rheologically modified biomass." Rheologica Acta **54**(11): 941-949.

Sánchez, J. H., G. C. Quintana and M. E. Fajardo (2015). "Rheology of pulp suspensions of bleached sugarcane bagasse: Effect of consistency and temperature." Tappi Journal **14**(9): 601-606.

Simha, R. (1952). "A treatment of the viscosity of concentrated suspensions." Journal of Applied Physics **23**: 1020-1024.

Singh, R., A. J. Varma, R. Seeta Laxman and M. Rao (2009). "Hydrolysis of cellulose derived from steam exploded bagasse by Penicillium cellulases: Comparison with commercial cellulase." Bioresource Technology **100**(24): 6679-6681.

Soccol, C. R., L. P. d. S. Vandenberghe, A. B. P. Medeiros, S. G. Karp, M. Buckeridge, L. P. Ramos, A. P. Pitarelo, V. Ferreira-Leitão, L. M. F. Gottschalk, M. A. Ferrara, E. P. d. Silva Bon, L. M. P. d. Moraes, J. d. A. Araújo and F. A. G. Torres (2010). "Bioethanol from lignocelluloses: Status and perspectives in Brazil." Bioresource Technology **101**(13): 4820-4825.

Soulies, A., J. Pruvost, J. Legrand, C. Castelain and T. I. Burghelea (2013). "Rheological properties of suspensions of the green microalga Chlorella vulgaris at various volume fractions." Rheo Acta **52**: 589-605.

Szijártó, N., M. Siika-aho, T. Sontag-Strohm and L. Viikari (2011). "Liquefaction of hydrothermally pretreated wheat straw at high-solids content by purified Trichoderma enzymes." Bioresource Technology **102**(2): 1968-1974.

Tanahashi, M., S. Takada, T. Aoki, T. Goto, T. Higuchi and S. Hanai (1982). "Characterization of explosion wood. 1. Structure and physical properties." Wood research **69**: 36-51.

Vallette, P. and C. De Choudens (1987). Le bois, la pêtes, le papier. Centre Technique de l'Industrie des papiers, Cartons et Celluloses.

Van-Soest, P. J. (1963). "Use of detergents in the analysis of fibrous feeds. II. A rapid method for the determination of fiber and lignin." Journal of the A.O.A.C **46**: 829-835.

Várnai, A., L. Huikko, J. Pere, M. Siika-aho and L. Viikari (2011). "Synergistic action of xylanase and mannanase improves the total hydrolysis of softwood." Bioresource Technology **102**(19): 9096-9104.

Viamajala, S., J. D. McMillan, D. J. Schell and R. T. Elander (2009). "Rheology of corn stover slurries at high solids concentrations - Effects of saccharification and particle size." Bioresource Technology **100**(2): 925-934.

Vilotte, O., F. Houllier, P. Mauguin, C. Ronceray, C. Cherbut, H. Guyomard, C. Huyghe, J.-F. Soussana, P. Chemineau, F. Marty and O. L. Gall (2016). Document d'orientation #inra2025, Institut national de la recherche agronomique.

Wanderley, M. C. d. A., C. Martín, G. J. d. M. Rocha and E. R. Gouveia (2013). "Increase in ethanol production from sugarcane bagasse based on combined pretreatments and fed-batch enzymatic hydrolysis." Bioresource Technology **128**(0): 448-453.

Wang, G., W. M. Post, M. A. Mayes, J. T. Frerichs and J. Sindhu (2012). "Parameter estimation for models of ligninolytic and cellulolytic enzyme kinetics." Soil Biology and Biochemistry **48**: 28-38.

Wiman, M., B. Palqvist, E. Tornberg and G. Liden (2011). "Rheological characterization of dilute acid pretreted softwood." Biotechnology and Bioengineering **100**(5): 1031-1041.

Worlitschek, J. and M. Mazzotti (2004). "Model-Based Optimization of Particle Size Distribution in Batch-Cooling Crystallization of Paracetamol." Crystal Growth & Design **4**(5): 891-903.

Wynn, E. J. W. (2003). "Relationship between particle-size and chord-length distributions in focused beam reflectance measurement: stability of direct inversion and weighting." Powder Technology **133**(1–3): 125-133.

Xu, Q., A. Singh and M. E. Himmel (2009). "Review: Perspectives and new directions for the production of bioethanol using consolidated bioprocessing of lignocellulose." Biotechnology and Bioengineering **20**(3): 364-371.

Yang, J., X. Zhang, Q. Yong and S. Yu (2010). "Three-stage enzymatic hydrolysis of steam-exploded corn stover at high substrate concentration." Bioresource Technology **102**(7): 4905-4908.

Yao, M., Z. Wang, Z. Wu and H. Qi (2011). "Evaluating kinetics of enzymatic saccharification of lignocellulose by fractal kinetic analysis." Biotechnology and Bioprocess Engineering **16**(6): 1240-1247.

Z, X. Z., Z. X, G. D. J and S. J. N (2004). "Effects of sugar inhibition on cellulases and beta-glucosidase during enzymatic hydrolysis of softwood substrates." Applied Biochemistry and Biotechnology **113-16**: 1115-1126.

Zhang, L.-P., J. Zhang, C.-H. Li and J. Bao (2014). "Rheological characterization and CFD modeling of corn stover–water mixing system at high solids loading for dilute acid pretreatment." Biochemical Engineering Journal **90**: 324-332.

Zhang, X., W. Qin, M. G. Paice and J. N. Saddler (2009). "High consistency enzymatic hydrolysis of hardwood substrates." Bioresource Technology **100**(23): 5890-5897.

Zhang, Y., Y. Y. Liu, J. L. Xu, Z. H. Yuan, W. Qi, X. S. Zhuang and M. C. He (2012). "High solid and low enzyme loading based saccharification of agricultural biomass." Bioresources **7**(1): 345-353.

Zhao, X. B., L. Dong, L. Chen and D. H. Liu (2013). "Batch and multi-step fed-batch enzymatic saccharification of Formiline-pretreated sugarcane bagasse at high solid loadings for high sugar and ethanol titers." Bioresource Technology **135**: 350-356.